UNIVERSITÉ DU QUÉBEC À TROIS-RIVIÈRES

DISSECTION FONCTIONNELLE ET SPATIALE DE LA BIOSYNTHÈSE DU GALANTHAMINE CHEZ LES AMARYLLIDACÉES : UNE APPROCHE COMBINANT N-MÉTHYLTRANSFÉRASE ET IMAGERIE PAR SPECTROMÉTRIE DE MASSE

FUNCTIONAL AND SPATIAL DISSECTION OF GALANTHAMINE BIOSYNTHESIS IN AMARYLLIDACEAE: A *N*-METHYLTRANSFERASE AND MASS SPECTROMETRY IMAGING APPROACH

THÈSE PRÉSENTÉE
COMME EXIGENCE PARTIELLE

DU DOCTORAT EN BIOLOGIE CELLULAIRE ET MOLÉCULAIRE

PAR
NUWAN SAMEERA LIYANAGE

SEPTEMBRE 2025

UNIVERSITÉ DU QUÉBEC À TROIS-RIVIÈRES
BIOLOGIE CELLULAIRE ET MOLÉCULAIRE (DOCTORAT)

Direction de recherche :

Isabel Desgagné-Penix	
Prénom et nom	directeur de recherche

Jury d'évaluation

Isabel Desgagné-Penix	
Prénom et nom	directeur de recherche

Tagnon Degbedji Missihoun	Membre interne à l'UQTR, Président du jury
Prénom et nom	Fonction du membre de jury

Charles Goulet	Membre externe à l'UQTR
Prénom et nom	Fonction du membre de jury

Vincent Courdavault	Membre externe à l'UQTR
Prénom et nom	Fonction du membre de jury

“නිදහස් අධ්‍යාපනය දිගුකල් වැජඹේවා!”

“Long live free education!”

ACKNOWLEDGEMENTS

As this long and winding PhD adventure finally approaches its conclusion (yes, it's really happening!), I find myself filled with gratitude—and a touch of disbelief—that I've made it to the end. But before closing this chapter, I'd like to take a moment to thank the many wonderful beings—both human and otherwise—who've helped me along the way. Whether through their wisdom, patience, caffeine offerings, emotional support, or just by silently existing and making the world a little less chaotic, your contributions—direct or delightfully indirect—have meant more than words can express.

I owe immense gratitude to my supervisor, Prof. Isabel Desgagné-Penix. Thank you for your constant guidance, for always being available with a listening ear and thoughtful advice, and above all, for your empathy and unwavering support through every twist and turn of this long academic road. Your mentorship, patience, and kindness have been a lighthouse during stormy times.

To my Amma and Appachchi—thank you for everything. For the life you gave me, the values you taught, the kindness and sacrifices, and for tolerating the endless stubbornness of your curious, occasionally chaotic son. Your love and strength are the foundation on which all of this stands. Also to my sister, for your support and constant encouragement through all the ups and downs.

Dr. Natacha Mérindol, from the moment I arrived, your warmth and good energy made me feel right at home. Thank you for taking me under your wing, teaching me so much—from techniques to scientific thinking—helping shape my project and manuscripts, and being a steady presence through all my highs and lows. Thank you also for tolerating my occasional bouts of strong personality and wild ideas—and, of course,

for all your hearty homemade food and garden vegetables that brought extra joy (and nutrition!) to my life. To Prof. Christian Janfelt, thank you for welcoming me into your lab in Copenhagen, for your mentorship, your calm and kind demeanor, and for teaching me from scratch with such generosity and patience. You made my internship a truly enriching and memorable experience.

Manoj Koirala, I don't even know where to start. From day one in the lab, you've been like a brother—teaching me everything from A to Z, constantly challenging me with questions I should probably know, and feeding me delicious Nepali food. I still remember: "Sameera, have you tried momo before? Then let's go to my place tonight." Unforgettable. Sarah-Eve Gélinas, thank you for always being there with technical support, kind words, and the legendary phrase: "You'll be fine, Sameera." It always helped more than you know. To the funding agencies—Canada Research Chair, NSERC, MITACS, UQTR, and all the organizations that supported me financially—thank you! Without your help, none of this would have been possible. And to the professors and collaborators who helped me source plants and materials, you played a huge role in bringing this research to life. I also want to sincerely thank all my co-authors for their valuable contributions to the research papers we worked on together—your insights, collaborations, and critical feedback were instrumental in shaping the scientific outcomes of this thesis.

Fatima Awwad, Elisa Fantino, Maribel Diaz-Garza—thank you for your generous hearts, for being there when I needed someone to talk to (or vent to), and for simply helping me stay sane. To Oscar Martinez Avilla, Snehi Gazal, Arghavan Arjmandi, Nicolas Sene, Vahid Karimzadegan, Bharat Bhusan Mahji, Rohith Grandi, Mélodie Plourde, and every member of the lab—thank you for the debates, experiments, shared

laughs, and occasional frustrations that made this experience so real and unforgettable. A heartfelt thank-you as well to the interns who joined me during this journey, especially Andrey Dias and Maria García Tobón—your enthusiasm, curiosity, and dedication brought fresh energy into the lab and made mentoring a truly rewarding experience. Prof. Hugo Germain and the entire team of professors in the Cellular and Molecular Biology program—thank you for your valuable teaching, guidance, and support throughout the PhD.

A very special thank-you to my Sri Lankan family in Trois-Rivières: Nimalan Ganesarajah, Vasana Dharmadasa, Thilina Uduwaka, Udani Gunasekara, and you, little Theo—you made this place feel like home. Thank you for all the good times, the drunk times, the food, the laughter, and everything in between. Alain Lacroix, you were like a Papa to me here—always looking out for me, checking if I was safe, and making me feel cared for. Thank you for your kindness and laughter. And to Ludgi, Denis, and Kevin—thank you for the friendship, your endless support, and all those wonderful memories: our cooking adventures, late-night talks, spontaneous swims, and even our slightly illegal (but fun!) fruit raids in the neighborhood. To Sebastien Robert, David Chen, Mahesh Liyanage, and Saman Vidanage—you entered my life at different moments and left a lasting mark. Thank you for the joy, comfort, support, and love you've shared with me during both the good and not-so-good times.

And finally, to every single person who crossed paths with me on this journey—family, friends, professors, colleagues, bus drivers, snowplow operators, university staff, hospital workers, and random kind strangers—thank you. Whether you knew it or not, you helped me get here. I'll never forget the impact you had on my life and on this journey.

RÉSUMÉ

Les plantes de la famille des Amaryllidacées sont reconnues pour leur capacité à produire des alcaloïdes structurellement complexes et pharmacologiquement actifs, parmi lesquels la galanthamine se distingue par son importance clinique en tant qu'inhibiteur de l'acétylcholinestérase utilisé dans le traitement symptomatique de la maladie d'Alzheimer. Cependant, sa disponibilité naturelle limitée et la compréhension encore incomplète des processus biosynthétiques impliqués dans sa formation freinent sa production et son utilisation à plus grande échelle. Cette thèse combine des approches enzymatiques et de métabolomique spatiale afin de faire progresser la caractérisation biochimique et spatiale de la biosynthèse de la galanthamine ainsi que d'autres alcaloïdes apparentés chez les espèces d'Amaryllidacées, dans le but de favoriser leur production durable par des applications biotechnologiques futures.

La première partie de cette thèse propose une revue approfondie qui contextualise les connaissances actuelles sur la biosynthèse des alcaloïdes des Amaryllidacées, en mettant en lumière les principaux défis, notamment la découverte limitée de gènes, les faibles rendements en alcaloïdes et la résolution spatiale insuffisante de leur distribution métabolique. Ces lacunes soulignent la nécessité d'approches pluridisciplinaires intégrées pour décrypter les réseaux biosynthétiques et les stratégies de compartimentation métabolique in planta.

Le deuxième chapitre est consacré à l'analyse fonctionnelle d'enzymes apparentées aux coclaurine *N*-méthyltransférases provenant de trois espèces à forte production de galanthamine : *Leucojum aestivum*, *Lycoris radiata,* et *Hippeastrum papilio*. L'enzyme identifiée, *La*NMT1, catalyse la *N*-méthylation de la norgalanthamine, une réaction jusqu'alors non attribuée dans la voie de biosynthèse de la galanthamine. Cette enzyme présente une promiscuité de substrats, en méthylant efficacement d'autres substrats comme la tyramine et la tryptamine, et partage des caractéristiques de séquence conservées avec les *N*-méthyltransférases de la voie des alcaloïdes benzylisoquinoléiques (BIA). Des études de localisation suggèrent une association avec l'interface cytosol–réticulum endoplasmique, indiquant un positionnement stratégique favorisant le transfert de substrats et le flux métabolique. De plus, une analyse d'expression sous stress environnemental a révélé un lien potentiel entre la biosynthèse des alcaloïdes et la réponse aux stress abiotiques, suggérant un rôle physiologique plus large.

Le troisième chapitre utilise l'imagerie par spectrométrie de masse avec désorption/ionisation laser assistée par matrice (MALDI-MSI) pour étudier la distribution spatiale de la galanthamine et d'alcaloïdes apparentés dans *Hippeastrum papilio*. L'étude cartographie l'accumulation tissulaire spécifique à travers les feuilles, les bulbes et les racines, et identifie des schémas distincts de distribution pour les intermédiaires biosynthétiques et les produits finaux. Les alcaloïdes se localisent principalement dans les tissus épidermiques et vasculaires, certains intermédiaires présentant une distribution plus étendue que les produits finaux. Cette distribution non homogène suggère un système biosynthétique décentralisé, impliquant un transport intercellulaire et une éventuelle division du travail biosynthétique entre les tissus. Ces observations remettent en question l'hypothèse d'une biosynthèse spécifique à un organe et soutiennent plutôt l'existence d'un réseau coordonné à l'échelle de plusieurs tissus.
Le dernier chapitre synthétise les données biochimiques et spatiales obtenues, en proposant un modèle intégré de la biosynthèse de la galanthamine chez les plantes d'Amaryllidacées. L'association de l'enzymologie fonctionnelle à une métabolomique spatiale à haute résolution permet de mieux comprendre la nature dynamique et compartimentée de la biosynthèse des alcaloïdes. Ces résultats affinent non seulement notre compréhension du métabolisme spécialisé des plantes, mais ouvrent également de nouvelles perspectives pour l'ingénierie métabolique dans des systèmes hétérologues. En identifiant les enzymes clés, les sites d'action subcellulaires et les schémas d'accumulation tissulaire, ce travail jette les bases d'un développement futur de voies biosynthétiques d'alcaloïdes des Amaryllidacées pour une production pharmaceutique durable.

Mots-clés : Alcaloïdes des Amaryllidacées, Biosynthèse de la galanthamine, Imagerie par spectrométrie de masse, MALDI-MSI, Caractérisation fonctionnelle des enzymes, Distribution spatiale des métabolites, Métabolisme spécialisé végétal, *N*-méthyltransférase (NMT), Voie métabolique des plantes.

ABSTRACT

Plants in the Amaryllidaceae family are recognized for producing structurally complex and pharmacologically active alkaloids, among which galanthamine is clinically significant as an acetylcholinesterase inhibitor used to manage symptoms of Alzheimer's disease. However, limited natural availability and incomplete understanding of the biosynthetic processes underlying its formation continue to restrict its production and broader utilization. This thesis integrates enzymatic, and spatial metabolomics strategies to advance the biochemical and spatial characterization of galanthamine biosynthesis and other related alkaloids in Amaryllidaceae species, with the aim of enabling future biotechnological applications for sustainable production.

In the initial part of this thesis, a comprehensive review contextualizes the current knowledge on Amaryllidaceae alkaloid biosynthesis, addressing key challenges such as limited gene discovery, low alkaloid yield, and inadequate spatial resolution of metabolite distribution. These gaps underscore the need for integrated multi-disciplinary approaches to dissect biosynthetic networks and compartmentalization strategies in planta.

The second chapter focuses on the functional analysis of coclaurine *N*-methyltransferase-like enzymes from three high-galanthamine-producing species: *Leucojum aestivum*, *Lycoris radiata*, and *Hippeastrum papilio*. The identified enzyme, *La*NMT1, catalyzes the *N*-methylation of norgalanthamine, a reaction previously unassigned in the galanthamine pathway. This enzyme exhibits substrate promiscuity, efficiently methylating substrates like tyramine and tryptamine, and demonstrates conserved sequence features with benzylisoquinoline alkaloid (BIA) pathway *N*-methyltransferases. Localization studies indicate its association with the cytosol–endoplasmic reticulum interface, suggesting its strategic positioning for facilitating substrate channeling and metabolic flux. Moreover, expression profiling under environmental stress revealed a possible regulatory link between alkaloid biosynthesis and abiotic response.

The third chapter employs matrix-assisted laser desorption/ionization mass spectrometry imaging (MALDI-MSI) to explore the spatial distribution of galanthamine and related alkaloids in *Hippeastrum papilio*. The study maps tissue-specific accumulation across leaves, bulbs, and

roots and identifies distinct distribution patterns of biosynthetic intermediates and end-products. Alkaloids predominantly localize to epidermal and vascular tissues, with some intermediates showing broader distribution than final products. This non-uniform distribution pattern suggests a decentralized biosynthetic system, involving intercellular transport and possible division of biosynthetic labor among tissues. The findings challenge the assumption that galanthamine biosynthesis is organ-specific and instead support a spatially coordinated network across multiple tissues.

The final chapter synthesizes these biochemical and spatial insights, presenting an integrative model of galanthamine biosynthesis in Amaryllidaceae plants. The combination of functional enzymology with high-resolution spatial metabolomics provides a nuanced understanding of the dynamic and compartmentalized nature of alkaloid biosynthesis. These findings not only refine our conceptual framework for plant specialized metabolism but also create new opportunities for metabolic engineering in heterologous systems. By identifying key enzymes, subcellular sites of action, and tissue-specific accumulation patterns, this work lays a foundation for future efforts to engineer Amaryllidaceae alkaloid biosynthetic pathways for sustainable pharmaceutical production.

Keywords: Amaryllidaceae alkaloids, Enzyme functional characterization, Galanthamine biosynthesis, Mass spectrometry imaging, MALDI-MSI, Metabolite spatial distribution, *N*-methyltransferase (NMT), Plant metabolic pathway, Specialized plant metabolism

TABLE OF CONTENTS

LIST OF TABLES

LIST OF FIGURES

LIST OF ACRONYMS AND ABBREVIATIONS

AA – Amaryllidaceae alkaloids

AKR – Aldo-keto reductase

BIA – Benzylisoquinoline alkaloids

BLAST – Basic Local Alignment Search Tool

CNMT – Coclaurine N-methyltransferase

CYP – Cytochrome P450

DESI – Desorption Electrospray Ionization

HPLC – High Pressure Liquid Chromatography

IPTG – Isopropyl β-D-thiogalactopyranoside

JA – Jasmonic Acid

JAZ – Jasmonate ZIM-domain

LC-MS – Liquid Chromatography Mass Spectrometry

MALDI – Matrix-Assisted Laser Desorption/Ionization

MALDI-MSI – Matrix-Assisted Laser Desorption/Ionization Mass Spectrometry Imaging

MJ – Methyl Jasmonate

MRM – Multiple Reaction Monitoring

MS – Mass Spectrometry

MSI – Mass Spectrometry Imaging

MYB – Myeloblastosis

NAA – 1-Naphthaleneacetic Acid

NBS – Norbelladine Synthase

NMT – N-methyltransferase

NOMT – Norbelladine O-methyltransferase

NR – Noroxomaritidine/Norcraugsodine Reductase

ODD – 2-Oxoglutarate Dependent Dioxygenase

OMT – O-methyltransferase

PCR – Polymerase Chain Reaction

PIA – Phenethylisoquinoline alkaloids

RT-qPCR – Quantitative Reverse Transcription Polymerase Chain Reaction

SAM – S-adenosyl methionine

SDS-PAGE – Sodium Dodecyl Sulfate-Polyacrylamide Gel Electrophoresis

SDR – Short Chain Dehydrogenase/Reductase

TYDC – Tyrosine Decarboxylase

VIGS – Virus-Induced Gene Silencing

CHAPTER I[1]

1. INTRODUCTION

Tens of thousands of years of human civilisation have depended on nature to grant a cure for illnesses and diseases. Amaryllidaceae J. St.-Hil. (*sensu stricto*) is a plant family that has provided beneficial medicinal value worldwide (Jin and Yao, 2019). Various ethnic groups have traditionally used this plant family to treat a range of illnesses, such as mental health issues, cancer, and respiratory and liver problems (Nair and van Staden, 2013). For instance, *Crinum zeylanicum* has been used in Sri Lankan folk medicine to treat rheumatism, snake bites, and ear aches (Jayaweera, 1981; Tsuda *et al.*, 1984). *Zephyranthes fosteri* was used in traditional Aztec medicine to treat 'fatigue' and 'stress' (Centeno-Betanzos *et al.*, 2021). Chinese folk medicine has long utilized *Lycoris radiata* bulbs to treat skin and laryngeal conditions. *Amaryllis belladonna* and *Boophone disticha* have been used in the African continent to treat cancer, inflammation, wounds, and infections (Nair and van Staden, 2013; Wang *et al.*, 2009). The Amaryllidaceae J. St.-Hil., also known as subfamily Amaryllidoideae according to APG III, is a cosmopolitan family of bulbous monocots consisting of approximately 900 species shared by around 75 genera, that thrive mainly in Africa and South America (APG, 2009; Meerow *et al.*, 1999). Their slow-blooming, exquisite flowers render them popular in horticulture. Their ability to produce a unique group of alkaloids called the Amaryllidaceae alkaloids (AAs) may explain

the use of these geophytes in traditional medicine systems around the world.

AAs are basic nitrogen-containing specialised metabolites with a benzopyridine heterocyclic group. More than 650 different AAs have been elucidated so far. They derive from the metabolism of phenylalanine and tyrosine (Desgagné-Penix, 2021; Jayawardena *et al.*, 2024). In the plant, they display defence properties to protect against abiotic or biotic stress, such as predators, targeting their nervous system (Berkov *et al.*, 2020; Nair and van Staden, 2020), or to attract pollinators to promote seed dispersion (Berkov *et al.*, 2020). Therapeutically, AAs exhibit various biological activities, including anti-acetylcholinesterase, antiviral, antibacterial, antifungal, anticancer, and cytotoxic activities (Ding *et al.*, 2017; Hotchandani and Desgagne-Penix, 2017; Ka *et al.*, 2020). This wide range of potential pharmaceutical applications position AAs as attractive candidates for the development of new drugs. One of the main breakthroughs has been the approval of galanthamine as a treatment of mild symptoms of cognitive impairment and Alzheimer's disease in at least 29 countries (Loy and Schneider, 2006; Olin and Schneider, 2002). Galanthamine selectively, reversibly, and competitively inhibits acetylcholinesterase, which leads to improved cognitive function (Olin and Schneider, 2002). Lycorine and their derivatives also attract a lot of attention due to their strong anticancer properties (Roy *et al.*, 2018). Many other AAs, such as cherylline,

crinamine and pancratistatin are effective against multiple viruses, including herpes simplex virus, Rauscher leukaemia virus, coronaviruses, flaviviruses, human immunodeficiency virus, and hepatitis C virus, as reviewed in Jayawardena et al. (2024). Narciclasine, lycorine, and diverse AAs also display antifungal activities through a plethora of mechanisms (Nair and van Staden, 2020). Cripowellin, lycorine, ungeremine and multiple AAs exhibit antibacterial activity, and are studied pharmacologically to overcome antibiotic resistance (Bendaif *et al.*, 2018; Chen *et al.*, 2018; Kianfe *et al.*, 2020). AAs such as crinamine, 8α-ethoxyprecriwelline, epivittatine, lycorine and derivatives are evaluated for their anti-inflammatory activity specific to cyclooxygenese-1 and 2 (Elgorashi *et al.*, 2003; He *et al.*, 2015). Their multifaceted activities highlight the relevance of these plants' metabolites in drug discovery for human health improvement.

The yield of AA of interest is limited and variable in plants grown in the wild, in part due to the diversity of plant metabolic routes and to environmental stresses. In the wild, Amaryllidaceae grow in specific regions, sometimes under singular conditions, and some are classified as endangered species, such as *Eucrosia stricklandii*, a rare Amaryllidaceae from Ecuador, while several *Narcissus* species have already become extinct (Colque *et al.*, 2002; Santos-Gally *et al.*, 2015). In a nutshell, wild plants are not a suitable sustainable source of medicinal compounds. Organic synthesis is a challenging, less

profitable, and not sustainable alternative because of the complexity of the AA structure (Kohelová *et al.*, 2021). Usually, they are extracted directly from Amaryllidaceae harvested from the field or greenhouse, or micropropagated, but the AA yield is low. Much effort is concentrated on developing *in vitro* systems with profitable production of AAs, and in uncovering biosynthetic pathways to acquire the knowledge to carry out metabolic engineering (Koirala *et al.*, 2022), but much remains to be discovered with regard to their biosynthesis and transport in their natural host.

A growing number of research papers have been exploring different aspects of AA biosynthesis, such as enzyme discovery, substrate selectivity, and pathway hypothesis. In this chapter, we will summarise the established biosynthetic steps, examine both *in vivo* and *in vitro* plant studies that helped unravel enzymatic reactions or their regulation, and depict the available multi-omics data. Additionally, we will discuss the latest insights into the pathway characteristics *in planta* and explore modern techniques and tools that can expedite pathway assembly.

1.1. Structural diversity of Amaryllidaceae alkaloids

Ever since lycorine was isolated from *Narcissus pseudonarcissus*, 150 years ago, scientists have identified and determined the structures of hundreds of AAs (Ding *et al.*, 2017; Gerrard, 1877). Each year, several new alkaloids from Amaryllidaceae species are added to the list, making

the puzzle of their biosynthetic route increasingly complex. For instance, in 2023 and 2024, Chaichompoo and colleagues reported 18 new AAs from the bulbs of *Crinum latifolium* and *Crinum* x *amabile* (Chaichompoo *et al.*, 2023, 2024). Experts in the field of AAs have suggested various classification systems for their structure. One of the earliest classifications was introduced by Wildman, based on the presence of different nucleus types, such as pyrrolo [*de*] phenanthridine, dibenzofuran, or [2] benzopyrano [3,4*g*] indole (Wildman, 1960). Later, Ghosal et al. presented a 12-ring system, which is still considered the standard for numbering ring carbons (Ghosal *et al.*, 1985). Several other ring-type classification systems were proposed based on chemical structure analysis or AA biosynthetic origin, including 42 by Berkov et al., 9 by Bastida et al., 18 by Jin, and 9 by Desgagné-Penix (Bastida *et al.*, 2006; Berkov *et al.*, 2020; Desgagné-Penix, 2021; Jin, 2009). These classification systems evolve through the years with the periodic discovery of novel alkaloids. Hence, there is currently no universal classification system for AAs.

1.1.1. Amaryllidaceae alkaloid biosynthesis

Despite divergences in the classification systems of AA complex structures, the general early steps of their biosynthesis, and the precursors involved, namely tyramine and 3,4-dihydroxybenzaldehyde (3,4-DHBA) coming from the phenylpropanoid pathway, are largely

accepted (Desgagné-Penix, 2021; Kilgore and Kutchan, 2016). A tyrosine decarboxylase (TYDC) catalyses decarboxylation of tyrosine into tyramine, as studied in *Narcissus* aff. *pseudonarcissus*, *Lycoris radiata,* and *L*. *aurea* (Hu *et al.*, 2021; Kilgore, 2015; Wang *et al.*, 2019); while a phenylalanine ammonia-lyase (PAL) explored in *L*. *radiata,* and a cinnamic acid 4-hydroxylase (C4H) uncovered in *L*. *radiata* and *L*. *aurea* catalyse important steps of the phenylpropanoid pathway (Li *et al.*, 2018a; Li *et al.*, 2018b). There remain gaps of knowledge in the precursor pathway such as the synthesis of 3,4-DHBA which still waits to be uncovered. Nevertheless, these steps are beyond the scope of this review which focuses on the biosynthesis of AAs, starting from the condensation step.

1.1.2. Early and current evidence for biosynthesis of Amaryllidaceae alkaloids

Analytical techniques such as high pressure liquid chromatography (HPLC), gas chromatography (GC), mass spectrometry (MS), nuclear magnetic resonance (NMR), *in situ* metabolite imaging techniques like matrix-assisted laser desorption/ionization (MALDI), and desorption electrospray ionization (DESI) coupled MS has allowed the detection and the elucidation of AA structures and their localisation *in planta* (Bjarnholt *et al.*, 2014; Mehta *et al.*, 2024). In early studies dating back to the 1950s, radioisotope studies contributed to the identification of precursors and

intermediates, and to the assembly of AA metabolic pathways (Barton and Cohen, 1957). Radioactive or stable isotope labelling, random mutagenesis with ethyl methanesulfonate (EMS) or gamma-radiation induced, gene silencing, and multi-omics techniques all contributed to identify specific genes and enzymes candidates. Their integration is decisive to metabolite pathway elucidation. For instance, this approach has enabled the assembly of the canonical pathway of vincristine and vinblastine from *Catharanthus roseus,* a well-studied medicinal plant, but it took more than 30 years (Qu *et al.*, 2019).

In this chapter, the AA pathway will be divided into three sections: 1.2.2.1 Formation of the initial stable intermediates, 1.2.2.2 Oxidative phenol coupling for diversification of the metabolites, and 1.2.2.3 Downstream pathways.

1.1.2.1. Formation of the initial stable intermediates

1.1.2.1.1. The formation of norbelladine

In the 1960's, the early radioactive isotope labelling studies gave the first insight that tyramine, as the amine group, and 3,4-DHBA as the aldehyde partner, incorporated into multiple AAs like lycorine, haemanthamine and galanthamine (Feinstein, 1967; Suhadolnik *et al.*, 1962, 1963; Wildman *et al.*, 1962). Another radiolabel studies showed that the two precursors combined to yield norbelladine, as scaffold reaction for the biosynthesis of all AAs (Battersby *et al.*, 1961). Hence, to understand AAs

biosynthesis, the formation of norbelladine is the first key reaction to explore. Biochemically, norbelladine is synthesised through a reduction reaction that follows condensation of tyramine and 3,4-DHBA yielding norcraugsodine, a Schiff base (Figure 1.1) (Majhi *et al.*, 2023).

The first enzymatic evidence for the formation of norbelladine was reported by Kilgore and colleagues (Kilgore *et al.*, 2016b). From the transcriptome of *Narcissus* aff. *pseudonarcissus*, they identified and cloned a short chain dehydrogenase (SDR) named noroxomaritidine/norcraugsodine reductase (NR), which is phylogenetically close to a tropinone reductase II from *Datura stramonium* producing tropane alkaloids. Although the major reaction catalysed by that enzyme is related to a downstream pathway step, NR can catalyse the reduction of norcraugsodine to norbelladine, using tyramine and 3,4-DHBA as substrates. Later, Singh et al. identified another candidate for this reaction from *Narcissus pseudonarcissus* transcriptome. Norbelladine synthase (NBS) is an ortholog to norcoclaurine synthase (NCS), a well characterised enzyme that catalyses the first condensation reaction in benzylisoquinoline alkaloid (BIA) pathway via a Pictet–Spengler reaction. NBS from *N. pseudonarcissus* rather commits to a Mannich reaction for the condensation tyramine and 3,4-DHBA (Singh *et al.*, 2018). Orthologous NBS enzymes from *Leucojum aestivum* and *Narcissus papyraceus* were cloned and shown to catalyse the same reaction (Majhi *et al.*, 2023;

Tousignant *et al.*, 2022). Interestingly, norbelladine synthesis yield is increased through the interaction between NBS and NR, that catalyse the condensation and the imine reduction, respectively, possibly through preventing the degradation of the unstable norcraugsodine (Figure 1.1) (Majhi *et al.*, 2023). None of the studies related to NBS or NR provides any information related to enzyme kinetics. This will be necessary for a better biochemical understanding of the reactions. Nonetheless, NBS and NR may be the gateway to the formation of AA, catalysing the first steps in their biosynthesis. Similar to the formation of norcoclaurine in BIA pathway or of 1-phenethylisoquinoline scaffold in phenethylisoquinoline (PIA) alkaloids, the synthesis of norbelladine is the step that establishes the structural features observed in AAs (Beaudoin and Facchini, 2014; Nett *et al.*, 2020).

1.1.2.1.2. *The formation of 4'-O-methylnorbelladine*

Norbelladine 4'-*O*-methylation is another key step of the biosynthesis of AA, because it is required for the subsequent oxidative phenol coupling (Kilgore *et al.*, 2014). 4'-*O*-methylnorbelladine was established as a central intermediate by radio isotope labelling experiments that aimed to uncover the origin of the methylenedioxy group in haemanthamine (Barton *et al.*, 1962a). Mann et al. also provided the first evidence of a norbelladine-*O*-methyltransferase (N*O*MT) that catalysed this reaction, by identifying an analogous enzyme to a catechol *O*-methyltransferase (C*O*MT) partially purified from *Nerine bowdenii* (Mann *et al.*, 1963). This

study established 4'-*O*-methylnorbelladine as the intermediate required for the downstream pathway. Thirty five years later, a study that focused on galanthamine biosynthesis confirmed the catalysis of norbelladine *O*-methylation using crude enzyme extracts from six Amaryllidaceae species, with the recurrent observation that 4'-*O*-methylation was favoured over 3'-*O*-methylation (Eichhorn *et al.*, 1998; Mann *et al.*, 1963).

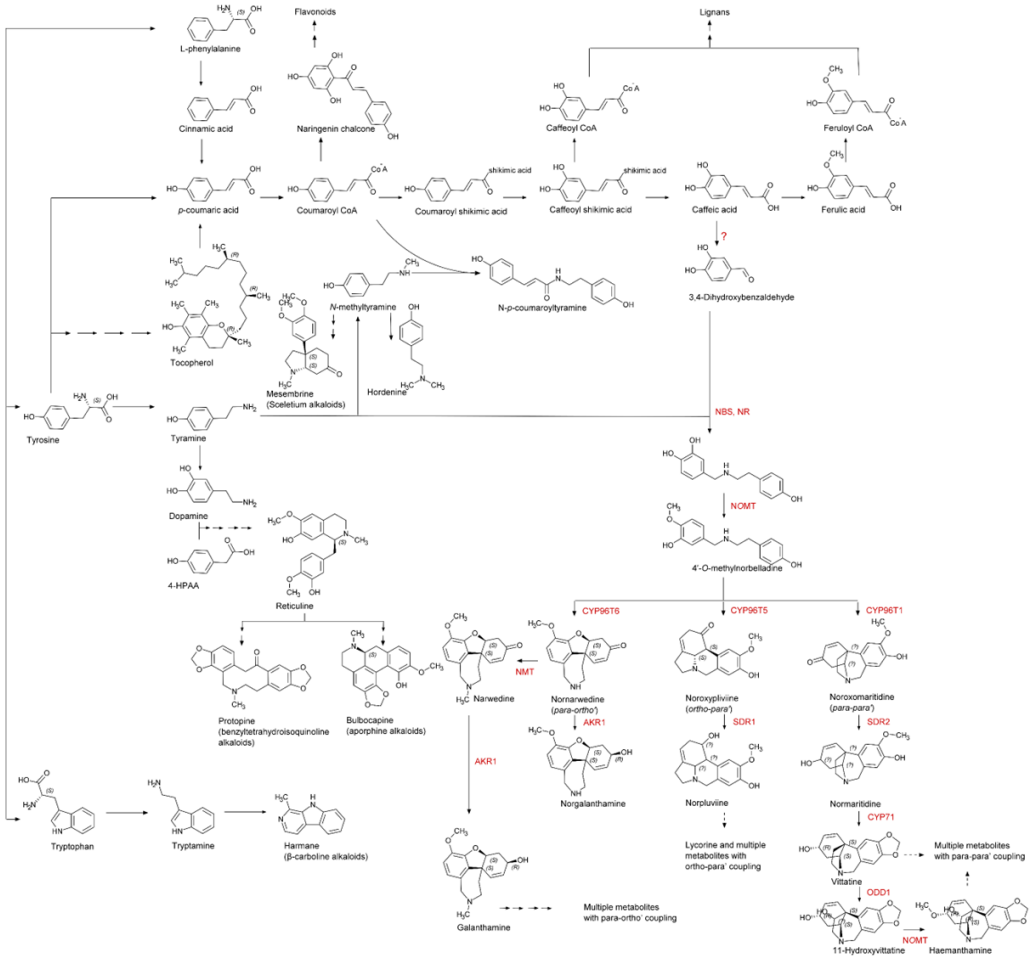

Figure 1.1. Amaryllidaceae metabolic pathways. Enzymatically characterised steps of Amaryllidaceae alkaloid pathway along with other defense-related specialised metabolites and non-Amaryllidaceae alkaloids representatives recorded in the family starting from the three aromatic amino acids. A single arrow represented a single biochemical step while multiple arrows represented multiple steps. Identified enzymes in AA pathway represent in red. Abbreviations are in the text. Although aldo-keto reductase (AKR1) may act upstream of the NMT step in some proposed galanthamine

pathways, Figure 1.1 was limited to previously characterized enzymatic steps before this study. The placement of AKR in relation to NMT remains hypothetical and is therefore not represented.(Liyanage et al. 2025).

The proteins extracted from the leaves of *Clivia miniata* and *Leucojum vernum* demonstrated the best activity (Eichhorn *et al.*, 1998). Sixteen more years, and the first N*O*MT, classified as a class I *O*-methyltransferase, was cloned and a detailed characterisation of the step was performed along the assembly of *Narcissus* aff. *pseudonarcissus* transcriptome (Figure 1.1) (Kilgore *et al.*, 2014). Several orthologs with various substrate specificity and regioselectivity were characterised from *Lycoris radiata*, *L*. *aurea*, and *L*. *longituba* (Hnin *et al.*, 2023; Liu *et al.*, 2024). W50M/A53N/Y186K triple variant of *Galanthus elwesii* N*O*MT showed that the inversion of regioselectivity from 1 : 99 to 94 : 6 (para/meta) can be achieved through specific mutations and coordinating Ni^{2+} instead of Mg^{2+} as the metal ion partner (Su *et al.*, 2022).

1.1.2.1.3. *Norbelladine or 4'-O-methylnorbelladine as key intermediates*

Although early isotope labelling studies established norbelladine as the first intermediate for the downstream pathways, the literature related to N*O*MT promiscuity raises a doubt about the order of the reactions yielding to the formation of norbelladine and its methylated form. Indeed, the first N*O*MT candidate studied in 1963 was shown to methylate dopamine, which is a hydroxylated form of tyramine (Mann *et al.*, 1963).

NOMTs from *L. radiata* and *L. aurea* catalyse the *O*-methylation of 3,4-DHBA and caffeic acid in addition to norbelladine. Hence, other precursors, such as vanillin and isovanillin (the methylated products of 3,4-DHBA) could condense with tyramine to yield 3'-*O*-methylnorbelladine and 4'-*O*-methylnorbelladine, respectively, suggesting a more complex metabolic routes (Li *et al.*, 2019; Sun *et al.*, 2018). Furthermore, *O*-methylation of other norbelladine derivates such as *N*-methylnorbelladine was observed in some of the studies mentioned above (Eichhorn *et al.*, 1998; Kilgore *et al.*, 2014). NR was shown to catalyse of condensation and reduction of isovanillin and tyramine to form 4'-*O*-methylnorbelladine, but a lower yield was observed compared to norbelladine synthesis (Kilgore *et al.*, 2016b). The ability of NBS to catalyse the condensation of methylated precursors, such as vanillin and isovanillin, with tyramine remains to be tested.

1.1.2.2. Oxidative phenol coupling to branch into multiple directions

In plants, phenol coupling is observed in the synthesis of various specialised metabolites including lignans, flavonoids, and alkaloids. It is a key step in the synthesis of AAs. Following this reaction, the basic alkaloid structures undergo further changes to produce a range of distinct alkaloid compounds. Oxidative phenol coupling involves the formation of C-C and C-O bonds primarily catalysed by cytochrome P450 (CYP), with laccases and peroxidases playing a role in some cases.

These enzymatic reactions are highly regio and stereoselective, contributing significantly to the production of specialised metabolites (Hüttel and Müller, 2021). Barton and Cohen were the first to show evidence of phenol oxidation in the formation of AA (Barton and Cohen, 1957). They proved through radio labelled studies that 4'-*O*-methylnorbelladine, not *O*,*N*-dimethylnorbelladine nor *N*-methylnorbelladine, underwent the phenol coupling reaction to synthesise AAs, such as galanthamine and haemanthamine, in *N*. *pseudonarcissus* (Barton and Kirby, 1962; Barton *et al.*, 1963). Depending on the C–C bond formation three types of phenol couplings were suggested, i.e. *para–ortho'*, *ortho–para'*, and *para–para'* (Barton *et al.*, 1962b, 1963; Eichhorn *et al.*, 1998; Fuganti and Mazza, 1971). The formation of these bonds and the details of the biochemical reactions are well described in various literature reviews (Bastida *et al.*, 2006; Jayawardena *et al.*, 2024).

Transcriptome assembly from *N*. aff. *pseudonarcissus* and correlation analysis with N*O*MT lead to the first characterisation of gene candidates categorised under a novel CYP subfamily, named as CYP96T (Kilgore *et al.*, 2016a). Enzymatic characterisation of the candidate CYP96T1 showed that this enzyme catalyse *para–para'* coupling ((10b*S*,4a*R*)- and (10b*R*,4a*S*)-noroxomaritidine) of 4'-*O*-methylnorbelladine as major reaction (Figure 1.1), leading to AAs like crinine, montanine and pretazzetine, and *para–ortho'* phenol coupling (nornarwedine) as minor

reaction, leading to galanthamine (Kilgore *et al.*, 2016a). *In silico* modelling, dynamics and simulations provided an atomic understanding of the C–N coupling, and C–C bond formation that follows a diradical mechanism in the active site of CYP96T1 (Peng *et al.*, 2023).

Recently, Mehta and their colleagues conducted an interesting study that expanded our understanding of CYP96T enzymes in AA biosynthesis(Mehta *et al.*, 2024). They used a combined approach of stable isotope labelling and transcriptome analysis, followed by co-expression analysis, to identify potential genes for the phenol coupling of 4'-*O*-methylnorbelladine. Their research suggests that three different CYP96T types are involved in *para–ortho'*, *ortho–para'*, and *para–para'* phenol couplings. They confirm that CYP96T1 catalyses *para–para'* coupling; and propose that CYP96T6 leads to *para–ortho'* phenol coupling, while CYP96T5 catalyses *ortho–para'* coupling (noroxopluviine) leading to lycorine-type AAs (Figure 1.1). They also present evidence that these enzymes could be modified to alter their regioselectivity, *i.e.* substituting leucine 308 with alanine on the *para–para'* coupling enzyme CYP96T1, yielded the same catalytic capacity as *para–ortho'* oxidative coupling enzyme CYP96T6. If confirmed, these results will shed light on the divergent regioselectivity of CYP96T, and on the means to achieve AAs molecular diversity. To facilitate understanding, an additional schematic has been included (Figure 1.2) highlighting the carbons and atoms involved in the oxidative phenol

coupling reactions, with arrows indicating the positions of bond formation. This visual aid is intended to make the nomenclature more accessible to readers outside the alkaloid field.

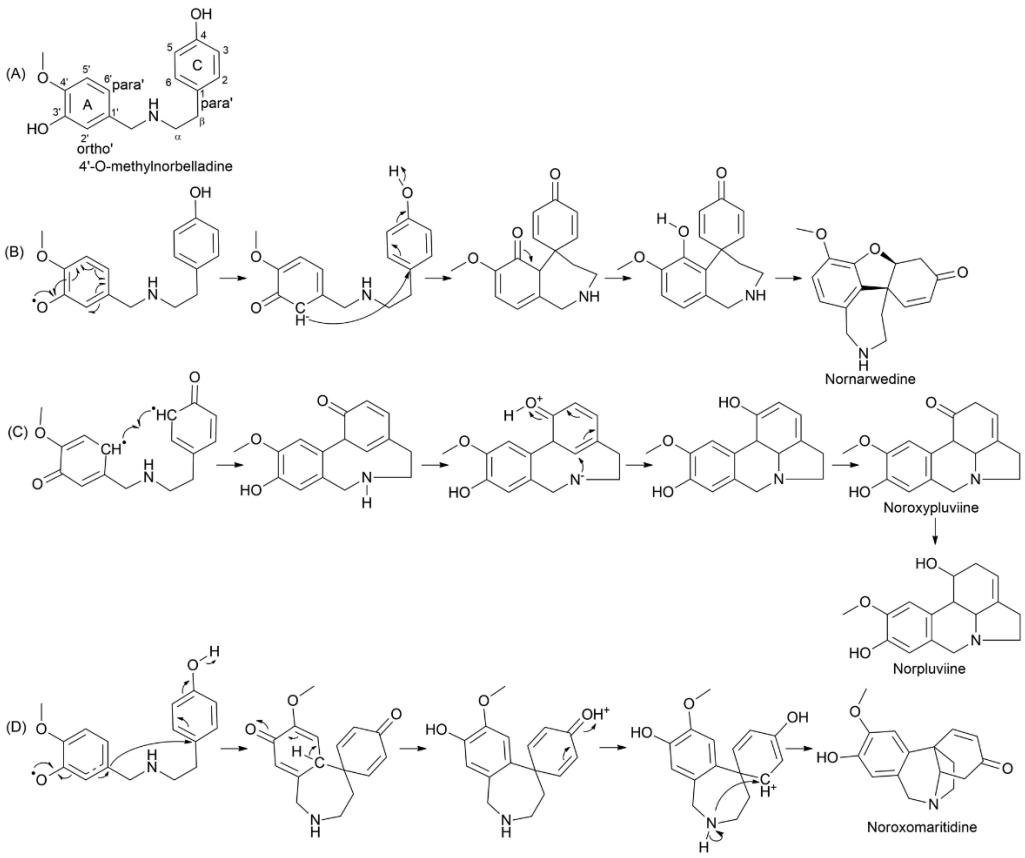

Figure 1.2. Proposed mechanism for the phenol coupling reaction. (A) The structure of 4′-*O*-methylnorbelladine; (B) *para–ortho′* coupling leading to nornarwedine; (C) *ortho–para′* coupling resulting norpluviine; (D) *para–para′* coupling leads to noroxomaritidine.

1.1.2.3. Paths to galanthamine, haemanthamine and lycorine

Intermediate compounds formed by the oxidative phenol couplings undergo further chemical changes, such as hydroxylation, methylation, reduction, oxidation, condensation, and oxygen bridge formation (Kilgore and Kutchan, 2016). Early isotope labelling and organic synthesis has helped build up multiple hypothesis for the synthesis of the intermediate and downstream metabolites, providing the basis to interpret the

biosynthetic path of newly discovered compounds (Barton *et al.*, 1962a; Berkov *et al.*, 2020; Eichhorn *et al.*, 1998). An alternative way has been to compare structures and reactions of the AAs pathway with specialised metabolic pathways from other plant families, as this provides strong hints on the candidate enzymes. For example, enzyme families like aldo–keto reductases (AKRs), SDRs, CYP450 monooxygenases like CYP71, *O*-, *N*-methyltransferases (*O*MT, *N*MT), and 2-oxoglutarate dependent dioxygenases (ODD) are known plant enzymes super families which catalyse multiple biochemical reactions diversifying alkaloids structures (Kilgore and Kutchan, 2016).

The first molecular evidence of enzymes involved in AA downstream pathway comes from studies of NR catalysing noroxomaritidine to oxomaritine, and of vittatine 11-hydroxylase catalysing vittatine to 11-hydroxyvittatine (Kilgore, 2015; Kilgore *et al.*, 2016b). Vittatine 11-hydroxylase is an ODD homologous to an enzyme characterised in *Pisum sativum* that produces gibberellin (Kilgore, 2015). Isotope feeding of multiple tissue sections of *Narcissus* cv. 'Tête-à-Tête', and correlation analysis of the transcriptome suggested the involvement of multiple enzymes, such as SDR, AKR, *O*MT, *N*MT, CYP71, and ODD in the synthesis of haemanthamine and galanthamine from 4'-*O*-methylnorbelladine (Figure 1.1) (Mehta *et al.*, 2024). The *O*MT proposed to catalyse the *O*-methylation of 11-hydroxyvittatine to yield haemanthamine is an ortholog to N4*O*MT, and the *N*MT catalysing

nornarwedine to narwedine is a gamma-tocopherol methyltransferase, homologous to an enzyme involved in colchicine synthesis(Mehta *et al.*, 2024). As the information regarding the transcripts and amino acid sequences is not yet available, it is difficult to discuss further on these enzymes, their mechanism, or their phylogenetic relationships.

1.1.3. Directions for enzyme discovery

On the path to discover novel enzymes, several future directions should be considered, including deepening our knowledge of already characterised steps. Further research should focus on testing and validating experimentally various hypotheses, such as resolving the involvement of multiple precursors in the formation of the first intermediates (Li *et al.*, 2019). Furthermore, it will be important to study substrate specificity and promiscuity of *O*- and *N*-methyltransferases, hydroxylases, and dehydrogenases discovered in the early pathway, in the context of downstream steps.

1.1.3.1. Involvement in defence and in other pathways

The precursor pathway, which consists primarily of the phenylpropanoid pathway and tyramine, is not only responsible for the synthesis of alkaloids in plants, but also contributes to the production of other defence chemicals, such as lignans, flavonoids, and coumarins (Figure 1.1) (de Vries *et al.*, 2021). The phenylpropanoid pathway has multiple functions,

highlighting the versatility of plant metabolic routes and their importance in protecting plants against herbivores and pathogens, helping them adapt to various environmental conditions (Dong and Lin, 2021). Understanding the synchronisation of the production of different classes of specialised metabolites may help discovering promiscuous enzymes which co-evolved in these multiple branches. For example, *C. roseus* 16-hydroxytabersonine-*O*-methyltransferase catalyses the *O*-methylation of both flavonoid and alkaloid synthesis, giving some insights into the evolutionary relationships of multiple pathways related to plant chemical defences (Lemos Cruz *et al.*, 2023).

Not only could there be relationships with non-alkaloid pathways, but also between some major AA groups or with other alkaloids. Cherylline and norbelladine, which do not undergo phenol coupling, could have evolved independently from other AAs groups (Desgagné-Penix, 2021; Jayawardena *et al.*, 2024). Moreover, there are other alkaloid groups reported in the Amaryllidaceae family, such as sceletium, phthalideisoquinoline, benzyltetrahydroisoquinoline, β-carboline, and aporphine alkaloids, also produced by other plant groups, such as *Sceletium*, Papaveraceae and Fumariaceae (Figure 1.1). The elucidated pathways of these multiple non-Amaryllidaceae alkaloid groups may help identify more candidate enzymes associated with the production of AAs.

Studying evolution of plant pathways would contribute to reinforce our

knowledge on AAs biosynthesis *in planta*. There are studies on the evolutionary origin of few alkaloid groups such as BIA in plant kingdom, yet no studies are available for AAs, with the exception of some studies on alkaloid diversity within the family, or within a genus like *Narcissus* (Berkov *et al.*, 2014; Liscombe *et al.*, 2005; Rønsted *et al.*, 2012). By investigating across different plant species, we can also gain new insights, improve our understanding of AA, and provide a broader perspective on alkaloid biosynthesis in plants in general. For instance, as the biosynthesis of norbelladine follows a similar pathway to that of BIA alkaloids and PIA, this suggests a possible shared evolutionary history or convergent evolution.

Recently, transient expression approaches such as agroinfiltration and viral induced gene silencing (VIGS) contributed to the discovery of specialised metabolites biosynthesis pathways, such as colchicine biosynthesis, and to the discovery of a serpentine synthase gene in *C. roseus* (Nett *et al.*, 2020; Yamamoto *et al.*, 2021). In AA biosynthesis, agroinfiltration was only used in one study producing galanthamine and haemanthamine in *Nicotiana benthamiana* (Mehta *et al.*, 2024). Application and establishment of VIGS in Amaryllidaceae plants were conducted in *Narcissus tazetta* for silencing *MYB3* in relation to flavonoid biosynthesis, and in *Lycoris chinensis* for silencing *Cloroplastos Alterados 1 (CLA1)* and *Phytoene Desaturase (PDS)* genes. However, the use of VIGS for characterizing AA biosynthesis has not yet been

reported (Cheng *et al.*, 2023; Zhou *et al.*, 2021).

1.2. Cellular and tissue organisation of the pathway

This section focuses on the molecular regulation and organisation of the pathway. Understanding the mechanisms that regulate metabolite biosynthesis at the plant and cell level is crucial for its advancement. Unlike some other well-studied medicinal plants, there is limited literature available for the Amaryllidaceae family.

1.2.1. Organ-specific expression and subcellular localization of NBS, NR, N4*O*MT and CYP96T

Knowledge of subcellular localisation and organ specific expression of genes and proteins involved in specialised metabolite biosynthesis informs on its spatial organisation and regulation (Watkins and Facchini, 2022). The overall compartmentalisation and regulation of the alkaloid pathways have been well described in some medicinal plants like *P. somniferum* or *C. roseus* (Watkins and Facchini, 2022), showing that there is no common compartmentalisation and regulation to plants. This highlights the need for studies on compartmentalisation in Amaryllidaceae. Enzyme subcellular localisation and gene expression pattern over different tissues and developmental stages have been described in *N. pseudonarcissus*, *L. radiata*, *L. longituba*, and *L. aestivum* (Figure 1.3). *NBS* is expressed mainly in bulbs of *N.*

pseudonarcissus sampled at the floral stage*,* in bulbs and roots of *L. aestivum* and *N*. *papyraceus* of the floral stage, while it is enriched in leaves of *L*. *longituba* sampled at *the* vegetative stage (Li *et al.*, 2020; Majhi *et al.*, 2023; Singh *et al.*, 2018; Tousignant *et al.*, 2022). The expression of *NR,* also involved in norbelladine synthesis*,* is higher in bulbs during the floral stage of *L. aestivum*, *N. papyraceus,* and during the vegetative stage of *L. radiata* (Majhi *et al.*, 2023; Park *et al.*, 2019), but is increased rather in the stem of *N*. *pseudornarcissus* during the floral stage (Singh and Desgagné-Penix, 2017). *N4OMT* was reported as expressed mainly in bulbs of *N*. *pseudonarcissus* and *L*. *radiata* in the vegetative stage*,* in bulbs and flowers of *N*. aff. *pseudonarcissus* at the floral stage, in bulbs and roots of *L*. *longituba* in the vegetative stage (Kilgore *et al.*, 2014; Li *et al.*, 2020; Park *et al.*, 2019; Singh and Desgagné-Penix, 2017). In the case of *CYP96T1*, the highest expression was observed in the floral stems of *N*. *pseudonarcissus* in the floral stage, in roots and bulbs of *L*. *radiata* of floral stage*,* and in bulbs of *L*. *longituba* in the vegetative stage (Li *et al.*, 2020; Park *et al.*, 2019; Singh and Desgagné-Penix, 2017). Overall, these studies suggest that these four key enzymes are often detected in bulbs, although there are differences between species and developmental stages. Mehta et al. (2024) performed a detailed tissue analysis and argued that biosynthesis of AA starts in the bases of mature leave, where they detected expression of most of the genes responsible for AA biosynthesis, starting

from 4'-*O*-methylnorbelladine (NBS and N4*O*MT were not included in that study). They propose that AA biosynthesis, starting from the phenol coupling reaction, primarily occurs in leaf bases. Even though more evidence is needed to prove that hypothesis, this conclusion is consistent with observations from the alkaloid biosynthesis pathway in other plants, such as *Veratrum nigrum* and *Phlegmariurus tetrastichus* (Mehta *et al.*, 2024; Nett *et al.*, 2021).

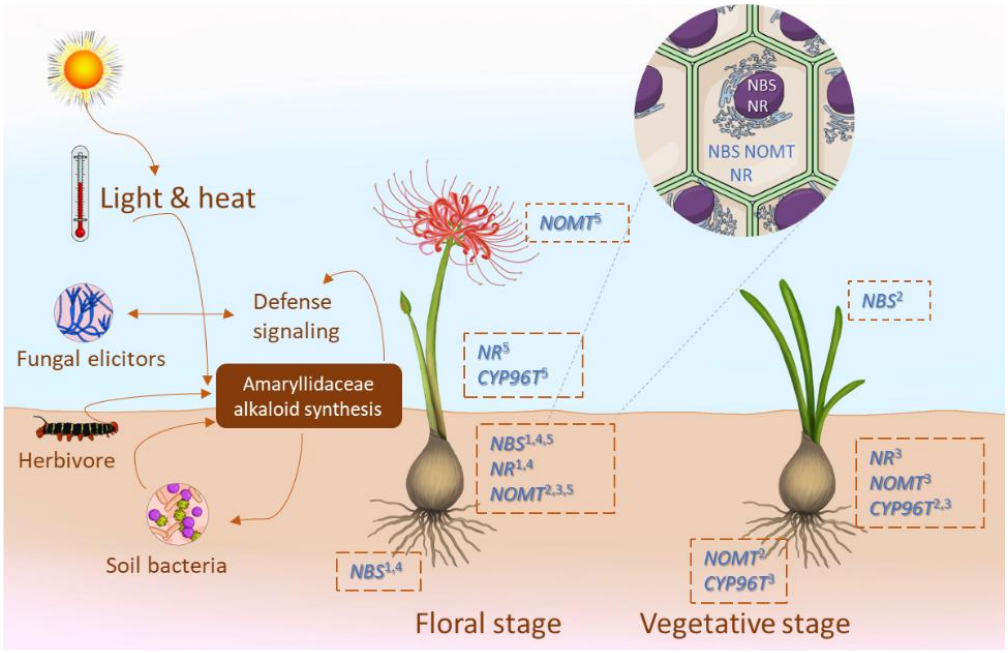

Figure 1.3. A summary of Amaryllidaceae alkaloid metabolism, representing environmental stimuli initiating the biosynthesis, gene expression, and protein expression of genes associated in the AA pathway, accumulation of few AAs at tissue level. 1 *Leucojum aestivum*, 2 *Lycoris longituba*, 3 *Lycoris radiata*, 4 *Narcissus papyraceus*, 5 *Narcissus pseudonarcissus*. Abbreviations are in the text. (Liyanage et al. 2025)

At the cellular level, *L. aestivum* and *N. papyraceus* NBS and NR are localised in the cytoplasm and nucleus (Majhi *et al.*, 2023), while *L. longituba* N4*O*MT is present only in the cytoplasm (Li *et al.*, 2020). CYP96T are membrane-bound proteins that are probably accumulating

in the ER membrane, even though this has not been verified yet. Overall, these findings suggest that biosynthesis of AAs may start in the cytoplasm of leaf bases cells. In BIA pathway of *P*. *somniferum,* NCS and multiple other enzymes like *O*MT were detected mainly in the phloem sieve elements, and NMTs in laticifers from leaves or stems; but gene expression principally happens in the phloem companion cells (Beaudoin and Facchini, 2014). Further studies need to be conducted to explore these aspects regarding AAs.

1.2.2. Accumulation (storage) of alkaloids

Over 20 000 plant exudate latex or mucilage upon physical damage or other interactions with the environment (Cui, 2019; Kekwick, 2002). The role of latex in storage and transport of alkaloids have been brought to light in medicinal plants like *C. roseus* and *P. somniferum* (Beaudoin and Facchini, 2014; Watkins and Facchini, 2022). Plants of Amaryllidaceae secrete mucilage, which can cause skin irritations, when damaged by physical forces (Santucci and Picardo, 1992). In one study, narciclasine was isolated as a functional compound from the mucilage of *N*. *tazetta* which inhibited the seed germination and growth of rice and Chinese cabbage (Bi *et al.*, 1998).In addition to mucilage, vascular tissues, like xylem and phloem, are involved in the transport and storage of precursors, and alkaloids. Some major reactions of alkaloids biosynthesis have been detected inside these vascular elements (Watkins and Facchini, 2022). “Phloem sap”, or most probably mucilage,

analysis of *Hippeastrum papilio* revealed that it was rich in galanthamine (30.2% of TIC), haemanthamine (15.5% of TIC) and 11β-hydroxygalanthamine (3.6% of TIC) (Haist *et al.*, 2024b).

Wang et al. studied the tissue distribution of galanthamine in *L*. *aurea* at vegetative stage using fluorescent signals emitted by galanthamine (Wang *et al.*, 2007). They suggested that AAs may be stored in the apoplast of the tissues, mainly in the cell walls. According to the study, the primary organ of accumulation is leaf scales, and galanthamine is present in the cell walls of vascular bundles, mesophyll cells between vascular bundles, and epidermal cells of mature leaves. Multiple mass spectrometry imaging (MSI) of the leaf cross-sections of *N*. *papyraceus* indicated that lycorine and 11-hydroxyvittatine are primarily found in the vicinity of vascular tissues, supporting the previous research on galanthamine accumulation (Mehta *et al.*, 2024). Furthermore, tissue staining with Dragendorff's reagent of *H*. *papilio* indicated that alkaloids are more concentrated in vascular bundles, vacuoles, and intracellular spaces (Haist *et al.*, 2024b). These studies indicate that AAs may be mainly produced in specialized cell types of vascular tissues, or in their proximity, and stored in the extracellular matrix like the apoplast, highlighting the importance of the cellular transport of AA.

1.2.3. Transport (trafficking) of alkaloids

Takos and Rook suggested that AA glycosides, such as lycorine-1-O-β-

D-glucoside may be the form of transportation of AAs, increasing the solubility and minimising the toxicity (Takos and Rook, 2013). Extracellular transport may be required to protect the plant from the toxicity of the produced specialized metabolites. Different transporters involved in alkaloids trafficking have been characterised in other medicinal plants like *C*. *roseus*, and *Coptis japonica*. They fall under transporters families like ATP-binding cassette (ABC), multidrug and toxic compound extrusion (MATE), and purine uptake permease (PUP) (Shitan *et al.*, 2014). There is only one published transporter related to Amaryllidaceae at the moment (Wang *et al.*, 2021b). The ABC transporter ABCB11 is associated with the plasma membrane and transports lycorine outside of the cell in *L*. *aurea* (Figure 1.2). *In situ* hybridisation technique revealed that this transporter is predominantly expressed in the phloem of leaves and bulbs, as well as in the cortical cells of roots of *L*. *aurea* supporting the hypothesis that AA are produced in leaf bases cells and stored in apoplast (Wang *et al.*, 2021b). A comparative transcriptomic study related to methyl jasmonate (MJ) treatments, known to induce specialised metabolite production, showed changes in the expression level of 138 transporter genes. These transporters include ABC transporters (20, 14.49%), amino acid/peptide/protein transporters (23, 16.67%), and drug transporters (11, 7.97%). These changes could provide indications of AA transporters (Li *et al.*, 2021). In conclusion, further studies that combine the

characterisation of enzymes, transporters, and AA *in planta* will provide a mechanistic understanding that will contribute to enhance metabolic engineering possibilities.

1.3. Insight of AA biosynthesis regulation from *in vitro* culture studies

Fields or greenhouse culture present a simple approach for mass cultivation if not in competition with nutritional crops. It enables the control of environmental factors, such as nitrogen uptake, modulation of storage temperature, light wavelength, potting media, and application of fungicides, which may influence specialised metabolites accumulation (El-Naggar and El-Nasharty, 2009; Lau *et al.*, 2014; Zaragoza-Puchol *et al.*, 2021). However, harvesting from cultivated Amaryllidaceae often leads to a lower yield compared to wild plants (Jin, 2013; Reis *et al.*, 2019) because our knowledge on the biosynthetic pathways' regulation is not complete. As an alternative to field and greenhouse grown plants, *in vitro* culture enables the exploration of the effect of many more factors simultaneously.

1.3.1. Current methods of *in vitro* culture

In vitro culture was used already seventy years ago as a mean of cell-free purified enzymes, from *Nerine bowdenii* flowering bulbs (Mann *et al.*, 1963). The following years were unsparing in different approaches

and innovations. *In vitro* cultivation as a means for production of AAs is rather a long and contamination-prone process whose success depends on the species, the tissue and sample quality, the growth media, the time of acclimatation, and many other unknown factors. The selection of the primary plant material (tissue and clone origin) appears to have a crucial effect on the AA yields (Bogdanova *et al.*, 2009; Georgiev *et al.*, 2020). This emphasizes the need for more efforts on the selection and study of high alkaloid-producing cultivars. It also suggests that AAs are produced by specialised differentiated cells of specific tissues, in response to environmental factors, and that modulation of their production is possible only within this frame.

Biotic and abiotic stresses have been the subject of numerous *in vitro* culture studies (Figure 1.2). The application of fungal elicitors on *L. radiata* plant culture induced the production of AAs precursors (Zhou *et al.*, 2020a). Synthetic bacterial communities applied to *in vitro* cultures *of L. radiata* suggested an interplay between AA production, bacterial endophytes, and fungal pathogens, and illustrated that AA biosynthesis could be better understood in the context of biotic interactions (Erb and Kliebenstein, 2020; Zhou *et al.*, 2023). Interestingly, a study reported a *L. aestivum* endophytic bacterium *Paenibacillus lautus* that was able to produce a wide range of plant hormones simultaneously, induced higher production of AAs by the plant but also endogenously produced its own, such as galanthamine, lycorine, ismine, lycoramine, galanthine,

haemanthamine, homolycorine, 1,2-dihydrochlidanthine, and hippeastrine (Ptak *et al.*, 2022). Others have studied the effect of hormones such as jasmonic acid (JA) and 1-naphthaleneacetic acid (NAA), or specific light waves on different plant tissue (Berkov *et al.*, 2020; Fennell *et al.*, 2003; Kilgore and Kutchan, 2016; Meena *et al.*, 2022; Ptak *et al.*, 2020). Different auxins, picloram, meta-topolin and thidiazuron were shown to regulate the regeneration rate and alkaloid profile in *L. aestivum, R. bifida* and other species (Ptak *et al.*, 2017; Reis *et al.*, 2019). Specific combinations of hormones (6-benzylaminopurine (BAP), kinetin (KIN) and NAA) led to specific AA increase in micropropagated *Caliphruria tenera* plants (Trujillo Chacón *et al.*, 2023). Treatment of *in vitro* culture of *C. x powellii* “Album” with different plant growth regulators (PGRs) led to variable tissue differentiation and growth, and a rather wide range of AAs such as lycorine, crinine and cherylline types (Koirala *et al.*, 2023). In calli culture, light and auxin both modulated the production of many alkaloids, and AA biosynthetic genes *in vitro*, highlighting the delicate balance between stress and growth that must be achieved for calli to produce AA.

All these studies emphasise the importance of discovering the biotic and abiotic elements that are involved in activation of AA biosynthesis partially or completely. Understanding the quality, quantity and timing of the elicitors required to boost AAs production is key to advance the yield range. Contrarily to production for commercial purposes, the elucidation

of biosynthetic pathway does not require that AAs are produced in large amount. It requires subtle differences of production in between samples used in comparative omics studies. In this regard, harvesting samples from *in vitro* culture offers several advantages, such as homogeneous growth, and controlled variables. The concomitant analysis of AA yield, biosynthetic genes, and culture conditions is the foundation knowledge that should be acquired to obtain high yield of AAs in the future.

1.3.2. Elucidation of biosynthetic pathways in *in vitro* culture

There are various environmental factors that can stimulate the production of alkaloids in plants. The previous section provided a non-exhaustive list of environmental stimuli used in *in vitro* culture that affect alkaloid biosynthesis in the Amaryllidaceae family. Transcription factors (TFs) are proteins that bind to specific DNA sequences, such as enhancer or promoter regions, initiating the transcription process that converts DNA to RNA. They coordinate the biosynthesis of specialised metabolites in response to environmental and developmental stimuli in plants (Li *et al.*, 2023b; Ziegler and Facchini, 2008). There are many families of TFs studied in plants such as APETALA2/Ethylene-Responsive Factor (AP2/ERF), WRKY and Basic Helix–Loop–Helix (bHLH) that contribute to alkaloid biosynthesis (Yamada and Sato, 2021). Also in upstream defence signalling, mechanisms like jasmonate signalling modulate the expression of TFs in response to environmental

stresses (Wang *et al.*, 2023). Transcriptome analysis of various tissues of *L*. *longituba* revealed a high percentage of transcription factors (TFs) such as bHLH, AP2/ERF, NAC, and TCP in this galanthamine producing plant (Li *et al.*, 2020). A comparative transcriptomic study showed that MJ treatment was associated with an upregulation of AAs related genes and of many TFs, such as WRKY (26 out of 32), AP2/EF (21 out of 25) and myeloblastosis (MYB) (all 14). As phenylpropanoid and flavonoid related genes were also upregulated in this experiment, the identification of TFs specific to AA synthesis was not possible (Li *et al.*, 2021). Transcriptomic analysis related to floral development and anthocyanins in *L*, *chinensis*, *L*. *longituba*, *L*. *radiata* and *L*. *sprengeri* identified multiple TFs, like MYB, bHLH, AP2/ERF, Cys2–His2 zinc finger (C2H2), NAM, ATAF1/2, and CUC2 (NAC); but this study did not focus on AA synthesis (Wang *et al.*, 2021a; Yang *et al.*, 2021a; Yue *et al.*, 2019; Zhang *et al.*, 2022b). Transcriptomic analysis *N. pseudonarcissus* calli and field grown plants also mentions the identification of different TFs (Ferdausi *et al.*, 2021). None of the identified sequences mentioned in all the literature detailed above are publicly available. Although most of these studies are related to anthocyanin or flavonoid synthesis in Amaryllidaceae plants, a deeper analysis could provide new insight into the AA pathway, as multiple specialized metabolites pathways are interconnected (Figure 1.1). Recently, the heat shock transcription factors (*HST*) expression was characterized in various tissues, flower

developmental stages of *L. radiata*, and studied in response to hormones and abiotic stresses (Wang *et al.*, 2024). The expression of several *HSFs*, especially *LrHSF5*, was associated with plant development and response to abiotic and hormone stresses. The correlation with AAs remains to be characterised further. Interestingly, a recent study on TFs related to MJ treatment in *L*. *aurea* helped identify a MYC transcription factor (*La*MYC2) that upregulated the biosynthesis of lycorine. The study demonstrated the *La*MYC2 binds to the E-box motifs of the promoter region of the *TYDC* gene of *L*. *aurea* involved in the precursor formation of AA biosynthesis (Zhou *et al.*, 2024).

Jasmonate triggers the activation of TFs in response to environmental stresses (Goossens *et al.*, 2017). Jasmonate ZIM domain (JAZ) proteins are key components in the positive regulation of the interaction of JA signalling. In Amaryllidaceae family identification and characterization of JAZ genes have been performed in one study in *L*. *aurea* (Wang *et al.*, 2020). Wang *et al.* cloned and characterized 7 JAZ genes, and showed that the expression of the JAZ genes among tissues varied. Most of them were highly expressed in flowers and JAZ 2, 5,6 were highly expressed in leaves. External MJ treatment upregulated the expression of almost all of the JAZ genes and in protein level, JAZ 11 was expressed in both nucleus and cytoplasm while JAZ 22 and 5 in cytoplasm and JAZ 3,4, 6 and 7 were expressed in the nucleus (Wang *et al.*, 2020). They have not studied the relationship with these JAZ genes with AA synthesis, but all

the data (transcript, protein sequences) are available in public databases for further studies.

Until now, AA biosynthetic genes have been mostly elucidated one gene at a time at the molecular level, based on assumption of candidate genes identified by homology in transcriptomic data from plant or its tissues grown in strictly specific conditions (Majhi *et al.*, 2023; Nguyen and Dang, 2021). This approach, although very useful, limits the discovery of enzymes full potential and of their physiological relevance, as they can indeed be implicated in multiple metabolic pathways and important for their crosstalk.

In vitro culture offers a controlled platform that could help connect alkaloid, terpenoid, and phenolic compound pathways and reveal new ways to optimise AA production, but also understand AAs implication in cellular functions and defence related mechanisms (Muro-Villanueva and Nett, 2023). Understanding the elements that modulate AAs production would help identify specific conditions permissive or restrictive to their accumulation. These conditions and their transcriptomic and metabolomic consequences could be classified into biotic and abiotic elements, stored, and tracked in a database that would help researchers link triggers of AAs production or of precursors, and thus understand new elements in the biosynthesis pathway.

1.4. Available multi-omics information on Amaryllidaceae species

The genes involved in biosynthetic pathway may be organised in gene clusters, as is the case for several well-studied plant species, such as *Zea mays* (2,4-dihydroxy-l,4-benzoxazin-3-one and 2,4-dihydroxy-7-methoxy-l,4-benzoxazin-3-one biosynthesis (Frey *et al.*, 1997)), *Oryza sativa* (momilactones and phytocassanes (Otomo *et al.*, 2004; Shimura *et al.*, 2007)), *Papaver somniferum* (noscapine (Winzer *et al.*, 2012)), *Arabidopsis thaliana* (thalianol and marneral (Field *et al.*, 2011)) and *Solanum* spp. (terpenes (Matsuba *et al.*, 2013)). Unfortunately, the resources that allowed the discovery and characterisation of these gene clusters, such as linkage maps and genome assemblies, are absent for Amaryllidoideae species.

1.4.1. Genomic data

The cost of sequencing the nuclear genome of these species is prohibitive due to the large and complex genomes of members of this subfamily. For instance, their 1C genome size (which indicates the amount of DNA in a haploid nucleus) ranges from 6.03 Gbp in *Chlidanthus fragans* to 80.5 Gbp in *Galanthus lagodechianus* (science, 2019; Zonneveld *et al.*, 2003; Zonneveld *et al.*, 2005)). In comparison, *Zea mays* 1C genome is 2.65 Gbp and *Arabidopsis thaliana* is 157 Mbp (Leitch *et al.*, 2019; Vu *et al.*, 2017). Also, their ploidy levels are so

variable that a same species of the genus *Narcissus* has diploid, triploid and tetraploid cultivars (Sochacki *et al.*, 2022), while the ploidy of the genus *Crinum* varies up to octoploid (Jones and Smith, 1967; Wahkstrøm and Laane, 2009). At present, the only genomes assembled and published in the Amaryllidaceae family are those of garlic (*Allium sativum* (Sun *et al.*, 2020)) and onion (*A. cepa* (Finkers *et al.*, 2021)), both diploid species with genome size 16.24 Gbp and 13.6 Gbp, respectively. However, the Allioideae subfamily does not produce AAs, limiting the interest use of these recent genomic resources for the study of AA biosynthesis.

As for Amaryllidoideae, a nuclear genome assembly for *Narcissus pseudonarcissus* was recently submitted to NCBI Genome database (accession JAVXUK01). However, it may not be the final version, as it consists of 3 138 040 scaffolds, has no complete or partial chromosome, and no publication is associated with it. Also, four Amaryllidaceae genome sequencing datasets are available from the Ruili Botanical Garden (Liu *et al.*, 2019); however, the species from which the datasets originated was not provided. As these samples are part of the “10,000 Plant Genomes Project” (Cheng *et al.*, 2018; Databases, 2017), they should be clearly identified and the assemblies available in the near future. Finally, there are several chloroplast genome assemblies available for this subfamily, and they have been used for phylogenetic studies (Cheng *et al.*, 2022a; Dennehy *et al.*, 2021; Hori *et al.*, 2006; Jin

et al., 2018; Konyves *et al.*, 2021; Zhang *et al.*, 2021).

1.4.2. Transcriptomic and proteomic data

In the absence of genome assemblies, researchers have attempted to reconstruct the AA biosynthetic pathway using transcriptome sequencing combined with metabolomics, or proteomics. Currently, there are transcriptomic data, in the form of raw reads or assembled transcriptomes, for 13 genera of this subfamily, the first one being that of *Lycoris aurea* (Wang *et al.*, 2013). Unfortunately, these data are not always made publicly available (Chang *et al.*, 2011; Song *et al.*, 2019; Wang *et al.*, 2017; Xiang *et al.*, 2022). In other cases, accession numbers or links to their datasets/assemblies are not provided (Ferdausi *et al.*, 2021; Pulman, 2014), or contains mistakes (Ren *et al.*, 2022; Yang *et al.*, 2021b; Yang *et al.*, 2023), complicating the analysis. Park *et al.* (2019) published their transcriptome assembly for *L. radiata* in NCBI SRA, without the raw data, while Yang *et al.* (2021b) reported the use of long- and short-read technology for the generation of a high-quality transcriptome assembly of *Narcissus tazetta*, but neither final assembly nor the raw long-reads were provided. As the use of long-read sequencing is new for Amaryllidoideae species, these datasets and assemblies should be published since they could help transcriptome and, in the future, genome annotations.

All transcriptome studies presented here were done using bulk RNAseq.

In some cases, a single tissue was sampled (Hotchandani *et al.*, 2019; One Thousand Plant Transcriptomes Initiative, 2019; Singh and Desgagné-Penix, 2017; Tousignant *et al.*, 2022; Wang *et al.*, 2018; Xiang *et al.*, 2022). In others, tissue samples were pooled into a single library (Li *et al.*, 2022; Wang *et al.*, 2013; Zhang *et al.*, 2022a). These tactics allowed the identification of several genes in the AA biosynthetic pathway, as well as genes in anthocyanin and phenylpropanoid pathways, and were sufficient for phylogenetic studies (One Thousand Plant Transcriptomes Initiative, 2019; Wang *et al.*, 2018). However, genes weakly expressed in a single tissue or cell-type may have been missed. Coupling the study of multiple tissues and conditions with metabolomics enables co-expression analyses, using known genes of the pathway as bait to pull out new candidates from the transcriptome (Kilgore *et al.*, 2016a; Kilgore *et al.*, 2014; Koirala *et al.*, 2023). This is potentiated by single-cell multi-omics, which was recently used in *C. roseus* and lead to the identification of a new enzyme in the monoterpene indole alkaloid pathway (Li *et al.*, 2023a).

Comparative proteomic studies can help identify candidate enzymes in the biosynthetic pathway by analysing species that differ in their alkaloid composition. Out of the three proteomic studies available for Amaryllidoideae, all of them have analysed *Lycoris* species (Jiang *et al.*, 2021; Ru *et al.*, 2013; Tang *et al.*, 2023), Tang *et al.* (2023) is the only study that focused on alkaloid biosynthesis. By comparing *L. longituba*,

L. *sprengeri* and *L*. *incarnata*, the authors were able to identify candidates for N4*O*MT and for the *N*-methyltransferase that converts norgalanthamine into galanthamine, but the sequences of these enzymes have not been published.

1.4.3. Multi-omics

In upcoming omics research, integrating transcriptomics and proteomics to compare tissues or populations with varying alkaloid contents (as reported for *G. elwesii* (Berkov *et al.*, 2004)) will be essential. It will determine whether the differences in alkaloid content are predominantly influenced by variations in the genes expressed, their expression levels within specific tissues or populations, or if these metabolic distinctions can be attributed to translational or post-translational mechanisms. Once genome sequencing becomes a more affordable avenue in the study of Amaryllidoideae species, transcriptomic and proteomic studies will help improve genome annotations. Omics toolsets offer also a powerful approach to study genetic polymorphism, evolution and single nucleotide polymorphism in homologous genes between Amaryllidaceae species, and their link to present/absent enzymatic reactions and related metabolites (Méteignier *et al.*, 2023; Stander *et al.*, 2022). Then, comparative studies between species with different alkaloid compositions, or accumulating specific alkaloids in different amounts, will facilitate the search for the missing enzymes of the AA biosynthesis

pathway. Furthermore, comparative genomics and phylogenetic analysis will help elucidate the evolutionary relationships between alkaloid biosynthetic pathways in different plant families, aiding in predicting undiscovered enzymes and pathways.

1.5. Importance of prediction tools and databases

1.5.1. Prediction tools of biosynthetic pathways and metabolic routes

Prediction tools, such as Plant Metabolic Network 15, RefMetaPlant, and MetaCyc that forecast metabolic routes are improving the discovery of new pathways in many aspects (Caspi *et al.*, 2020; Hawkins *et al.*, 2021; Shi *et al.*, 2024). The PathPred on Genome Japan tools helps predict pathway by machine learning (Moriya *et al.*, 2010). Prediction deep learning tools could also help to discover uncharacterised plant metabolites. For example, searching for potent therapeutical compounds with similarities to AA could help to suggest undiscovered AAs and identify their value (Sreeraman *et al.*, 2023). A recent article describes a Self-driving Autonomous Machines for Protein Landscape Exploration (SAMPLE) platform designed to combine prediction and experimental automation to engineer proteins with zero human intervention for synthetic biology and pathway elucidation (Rapp *et al.*, 2024). These new platforms provide insight for future scientific discoveries.

1.5.2. Public databases for Amaryllidaceae alkaloids

Many facets of AA biosynthesis are being covered in public database, including a transcription factors database PlantTFDB 4.0 (Jin *et al.*, 2016), gene ontology annotation through Planteome (Cooper *et al.*, 2024), metabolomes through PMhub 1.0 or RefMetaPlant (Shi *et al.*, 2024; Tian *et al.*, 2024), transport through ChannelsDB (Špačková *et al.*, 2024), and many more. However useful, these databases are not sufficient on their own to decipher AA biosynthetic pathway. A common effort of multiple groups integrated into a single database that includes genomes of few reference species, transcriptomic data in different conditions and most importantly AA profiling in all available experiments. To understand the physiological fate of AAs and improve metabolic engineering strategies, data from proteomic analysis, *in vitro* assays and propagation yields results according to various condition should be further included. Such united effort would allow gathering and visualising valuable datasets in one platform, similarly to TAIR for *Arabidopsis*, The Bio-Analytic Resource for Plant Biology BAR and Genevestigator for multiple species (Hruz *et al.*, 2008; Lamesch *et al.*, 2012; Waese and Provart, 2017). Building a network of AA researchers would not only allow cost sharing but also build stronger datasets and exchange of expertise and resources. Furthermore, multi-omic metadata gathered in a single platform along with datasets on biotic and abiotic experiments, phenotyping, chemical profiling would allow faster discovery of AA

enzymes and improve our definition of Amaryllidaceae plants interactions with their environment, a very useful piece of puzzle to add to biosynthetic pathway discovery, and to *in vitro* production for higher AA production.

1.6. Limitations

Knowledge of the complex genetic regulation, transport, and accumulation of AA would solve complex questions around the chronological order in the synthesis and allow further technological advances such as metabolic engineering of *in vitro* tissues or heterologous systems.

The production of Amaryllidaceae alkaloids is a fascinating and intricate process that offers numerous opportunities for exploration and discovery. Studying these pathways not only sheds light on plant biochemistry, but also has implications for pharmacology and potential medicinal uses of these alkaloids. There is still much to uncover regarding the specialised metabolite production in Amaryllidaceae plants, such as identifying new enzymes, improving their activity, and understanding the interconnected pathways. The ongoing research in this area holds the potential to unleash the full potential of these bioactive compounds for medicinal, agricultural, and industrial purposes.

1.7. Problematic, Hypothesis, and Objectives

While extensive research has been conducted on AAs over the past several decades, most studies have focused either on their structural

characterization or on isolated steps within their biosynthetic pathway. Yet, a systems-level understanding of how these steps are coordinated—biochemically and spatially—within the plant remains largely undeveloped. It is increasingly evident that unlocking the full potential of AAs, both scientifically and commercially, requires a shift in perspective: from analyzing individual enzymes in isolation to deciphering how molecular, cellular, and tissue-level processes interact to produce these complex natural products *in planta*.

One of the most conspicuous bottlenecks is the poor resolution of late-stage biosynthetic events. While early enzymes, such as norbelladine synthase and *O*-methyltransferases, have been relatively well characterized, the enzyme responsible for catalyzing the final *N*-methylation in the galanthamine pathway had not been conclusively identified. This gap has persisted despite the commercial value of galanthamine. While coclaurine itself has not been reported in Amaryllidaceae, the structural similarity of the coclaurine N-methyltransferases (CNMTs) from benzylisoquinoline alkaloid pathways suggested that analogous enzymes could function in Amaryllidaceae. This provided the rationale for Hypothesis 1, namely that a CNMT-like enzyme catalyzes the final N-methylation step in galanthamine biosynthesis. Furthermore, metabolic engineering efforts have been hindered by an incomplete understanding of the enzymatic contributors and their spatial organization.

Compounding the biochemical gaps is a broader anatomical and physiological uncertainty—Where exactly in the plant are these alkaloids made? Are they produced in the same tissues in which they accumulate, or do biosynthesis and storage occur in distinct cellular compartments? Traditional alkaloid studies have treated plant tissues as homogeneous units, overlooking the spatial and developmental nuances that likely underpin alkaloid biosynthesis. Without spatial resolution, any attempt to engineer high-yielding production platforms—whether microbial or plant-based—is operating with limited insight. Advances in mass spectrometry imaging (MSI), particularly MALDI-MSI, have demonstrated the power of spatial metabolomics to uncover tissue-specific compartmentalization and intercellular transport in other plant alkaloid pathways, such as benzylisoquinolines and monoterpene indole alkaloids (Bjarnholt *et al.*, 2014; Uzaki *et al.*, 2024). Applying this approach to Amaryllidaceae alkaloids offers the opportunity to test whether galanthamine biosynthesis is decentralized across tissues rather than organ-specific.

From an appliedperspective, this research responds to two pressing needs: (1) improving the biosynthetic understanding required to sustainably produce galanthamine and related alkaloids, and (2) advancing the scientific frontier in spatial metabolomics and integrative biosynthesis in medicinal plants. The pharmaceutical supply chain is already constrained by limited natural sources, and climate instability threatens wild and cultivated populations of alkaloid-producing species.

At the same time, synthetic biology is rapidly emerging as a solution—but requires the foundational enzymology and spatial data this thesis seeks to provide.

To address these interlinked challenges, the following hypotheses were proposed:

H1: A conserved coclaurine N-methyltransferase-like enzyme is responsible for catalyzing the final N-methylation step in galanthamine biosynthesis and that this enzyme is conserved across multiple Amaryllidaceae species.

H2: Galanthamine and other AAs are localized to a specific area, with intermediates and final products localized in specific tissue types across different plant organs.

Correspondingly, the objectives of this thesis are:

Objective 1: To identify, biochemically characterize, and localize the *N*-methyltransferase responsible for converting norgalanthamine to galanthamine in *Leucojum aestivum*, *Lycoris radiata*, and *Hippeastrum papilio*. This transformation had long been proposed based on chemical logic and isotopic labeling studies but lacked a definitive enzymatic assignment (Battersby *et al.*, 1961; Feinstein, 1967; Suhadolnik *et al.*, 1963).

Objective 2: To map the spatial distribution of galanthamine and its

biosynthetic intermediates in *Hippeastrum papilio* using mass spectrometry imaging, and to derive insight into the organization and transport dynamics of alkaloid metabolism within plant tissues.

This research takes a multidimensional approach, merging functional biochemistry with cutting-edge spatial metabolomics to offer an integrative model of alkaloid biosynthesis. In doing so, it not only addresses long-standing knowledge gaps but also lays a practical foundation for future biosynthetic pathway reconstruction and pharmaceutical applications.

1.7.1. Objective 1 – Chapter II: Coclaurine *N*-methyltransferase-like enzymes drive the final biosynthetic reaction of the anti-Alzheimer's drug galanthamine in Amaryllidaceae

The first objective of this research was to identify and functionally characterize the enzyme responsible for the *N*-methylation of norgalanthamine, the final biosynthetic step in the production of galanthamine in Amaryllidaceae species. This transformation had long been proposed based on chemical logic and isotopic labeling studies but lacked a definitive enzymatic assignment.

To address this gap, the experimental approach focused on mining transcriptomic data from three commercially and high-galanthamine-producing species—*Leucojum aestivum*, *Lycoris radiata*, and

Hippeastrum papilio—to identify candidate *N*-methyltransferase genes with homology to known coclaurine *N*-methyltransferases from benzylisoquinoline alkaloid (BIA) pathways. The aim was to isolate full-length coding sequences of the top candidates and express them heterologously for *in vitro* enzymatic assays.

In parallel, structural and phylogenetic analyses were planned to assess evolutionary relationships with *N*-methyltransferases and to evaluate potential substrate-binding residues. Molecular docking was to be used to predict substrate-enzyme interactions and guide site-directed mutagenesis experiments to verify key active site residues. A further objective was to determine the subcellular localization of the identified enzymes to better understand their integration within the biosynthetic machinery of the plant. To this end, eGFP-fusion constructs were designed for transient expression in *Nicotiana benthamiana* to visualize intracellular targeting.

Finally, the study aimed to examine how the expression of these *N*-methyltransferases responds to environmental stress, based on the broader hypothesis that alkaloid biosynthesis may be co-regulated with plant stress responses. Quantitative RT-PCR was planned under different abiotic stress conditions using *in vitro* shoot cultures. Together, these experiments aimed to provide a comprehensive characterization of the terminal *N*-methyltransferase enzyme in galanthamine biosynthesis, encompassing its functional, structural, and regulatory

aspects.

1.7.2. Objective 2 – Chapter III: Dissecting specialized metabolism in space: A MALDI-MSI atlas of Amaryllidaceae alkaloids in *Hippeastrum papilio* (Ravenna) Van Scheepen.

The second objective was to elucidate the spatial architecture of galanthamine and related Amaryllidaceae alkaloid biosynthesis at the tissue and organ levels using mass spectrometry imaging (MSI). While most prior studies inferred biosynthesis based on metabolite extraction from bulk tissues, little was known about the *in situ* distribution of biosynthetic intermediates and end-products within the plant. This lack of spatial resolution impedes pathway reconstruction and limits understanding of metabolic compartmentalization and transport. This objective focused specifically on *Hippeastrum papilio*, a species known for its high galanthamine content. The experimental goal was to prepare anatomically preserved cross-sections of leaves, bulbs, and roots and analyze them using matrix-assisted laser desorption/ionization mass spectrometry imaging (MALDI-MSI). The intention was to localize known alkaloids, including galanthamine, haemanthamine, and structurally related intermediates, within different tissue layers.

Key preparatory objectives included optimizing sample preparation protocols (embedding, cryo-sectioning, and matrix application) to preserve spatial integrity while achieving sufficient ionization of the target

alkaloids. Mass spectrometric acquisition parameters were to be fine-tuned to ensure detection of both low- and high-abundance metabolites with minimal background interference. In addition, unsupervised multivariate statistical tools, including principal component analysis (PCA), were planned to extract chemically distinct spatial features and determine tissue-specific clustering of metabolites. The overarching goal was to integrate this spatial information with existing biochemical knowledge of the galanthamine pathway to infer biosynthetic versus storage regions, and potential intercellular transport routes.

These experiments aimed to provide a detailed metabolite atlas of galanthamine-producing organs, thereby offering new insights into the localization, coordination, and possibly compartmentalized nature of alkaloid biosynthesis in *H. papilio.*

[1] Introduction of this thesis was adapted from our published review article “Liyanage, Nuwan Sameera, et al. "Navigating Amaryllidaceae alkaloids: bridging gaps and charting biosynthetic territories." Journal of experimental botany 76.1 (2025): 16-34.”

CHAPTER II

This chapter explores the characterization of coclaurine *N*-methyltransferase like enzymes for the *N*-methylation steps of alkaloid biosynthesis of Amaryllidaceae plants. The chapter was written in article format and published in the Plant Physiology and Biochemistry journal (https://doi.org/10.1016/j.plaphy.2025.110067.), and the content unavoidably overlaps with other chapters.

Contribution: Nuwan Sameera Liyanage: Conceptualization, Methodology, Experiments, Analysis, Writing- Original draft, Writing- Reviewing and Editing; Basanta Lamichhane: methodology, Sub-cellular localization experiment, Analysis, Writing- Reviewing and Editing; Elisa Fantino: Site-directed mutagenesis experiment, Writing- Reviewing and Editing; Natacha Merindol: Methodology, Supervision, *In silico* analysis (docking), Writing- Reviewing and Editing; Maria Camila García Tobón: Assisting the enzymatic characterization experiments, Writing- Reviewing and Editing; Sarah-Eve Gélinas: methodology, LC-MS, and analysis, Writing- Reviewing and Editing; Isabel Desgagné-Penix: Conceptualization, Methodology, Resources, Supervision, Funding acquisition, Writing- Original draft, Writing- Reviewing and Editing.

2. Coclaurine *N*-methyltransferase-like enzymes drive the final biosynthetic reaction of the anti-Alzheimer's drug galanthamine in Amaryllidaceae

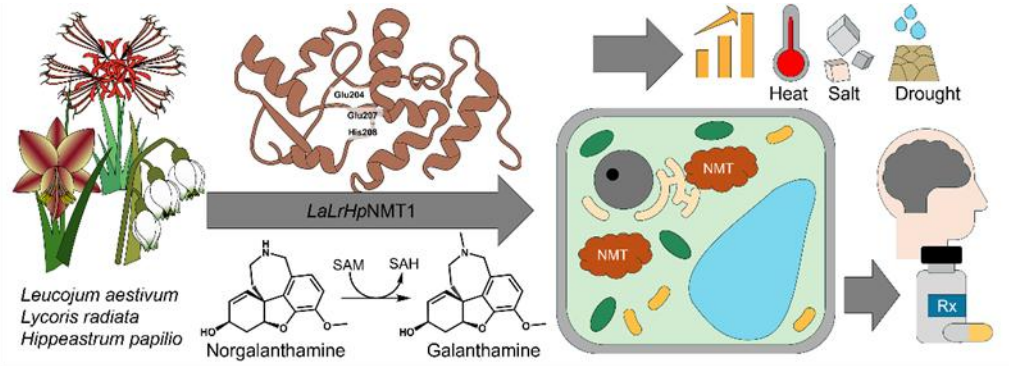

Nuwan Sameera Liyanage[1], Basanta Lamichhane[1], Elisa Fantino[1], Natacha Mérindol[1], Sarah-Eve Gélinas[1], Maria Camila García Tobón[1], and Isabel Desgagné-Penix[1,2,*]

[1]Department of Chemistry, Biochemistry and Physics, Université du Québec à Trois-Rivières, Trois-Rivières, QC, Canada.[2]Plant Biology Research Group, Trois-Rivières, Québec, Canada.

Keywords

Alkaloids; norgalanthamine; specialized metabolism; *Hippeastrum papilio*; *Leucojum aestivum*; *Lycoris radiata*; substrate promiscuity; molecular docking; environmental stress

2.1. Abstract

Galanthamine, an isoquinoline alkaloid used to treat symptoms of Alzheimer's disease, is predominantly extracted from Amaryllidaceae plants, yet its supply remains limited. In this study, we identified, isolated, and characterized *N*-methyltransferases (NMTs) from three galanthamine-producing species: *Leucojum aestivum*, *Lycoris radiata*, and *Hippeastrum papilio*. The transcriptomic analysis identified five unique NMT isoforms, among which *LaLrHp*NMT1, an isoform highly conserved across all three species, exhibited the highest catalytic activity. Phylogenetic and structural analyses revealed that these enzymes share high sequence conservation and maintain the class I methyltransferase Rossmann fold with key catalytic residues, paralleling known NMTs from benzylisoquinoline alkaloid pathways. Flexible docking simulations confirmed that norgalanthamine, a crucial precursor, fits within the enzyme's active site and interacts with conserved residues Glu204 and His208. *In vitro* and *in planta* assays demonstrated that *LaLrHp*NMT1 efficiently catalyzes the *N*-methylation of norgalanthamine to galanthamine. Site-directed mutagenesis confirmed the key role of Glu204 and the participation of Phe residues in substrate stabilization. Additional enzyme assays revealed that *LaLrHp*NMT1 is promiscuous towards various alkaloid intermediates, while subcellular localization using eGFP-tagged constructs exposed a dual distribution in the cytosol and endoplasmic reticulum, suggesting that NMT activity occurs at the

cytosol–ER interface where other biosynthetic enzymes reside. Environmental stress experiments in *H. papilio* shoots culture showed significant upregulation of *NMT* expression under heat and other stress conditions associated with AA levels modulation, indicating a potential link between stress responses and alkaloid biosynthesis. These findings deepen our understanding of galanthamine biosynthesis and provide a foundation for metabolic engineering strategies aimed at improving production yields.

2.2. Introduction

In the 1950s, a Russian scientist identified galanthamine, a plant isoquinoline alkaloid (*aka* Amaryllidaceae alkaloid (AA)) from *Galanthus woronowii*, after observing its traditional use in treating poliomyelitis (Heinrich and Teoh, 2004). Galanthamine's anticholinesterase activity and neuromuscular blocking antagonism led to its approval for Alzheimer's treatment in over 32 countries (Hotchandani and Desgagne-Penix, 2017; Loy and Schneider, 2006; Olin and Schneider, 2002). The Amaryllidoideae subfamily produces over 700 AAs with diverse biological activities, including anti-cancer, anti-viral, anti-inflammatory, and antioxidant(Berkov *et al.*, 2020; Ding *et al.*, 2017; Jayawardena *et al.*, 2024; Ka *et al.*, 2021; Merindol *et al.*, 2024). As galanthamine and other AAs in the pharmaceutical industry are primarily sourced from

plants, understanding the enzymatic steps of their biosynthesis offers biotechnological opportunities to enhance their production.

The biosynthesis of AAs involves complex enzymatic steps, some elucidated and others yet to be uncovered. This process begins with aromatic amino acids, tyrosine, and phenylalanine, which produce precursors leading to norbelladine (Desgagné-Penix, 2021; Jayawardena *et al.*, 2024) (Fig. 2.1.). The enzymes norbelladine synthase (NBS) and noroxomaritidine/norcraugsodine reductase (NR), studied in species such as *Narcissus* spp. and *Leucojum aestivum*, catalyze the condensation of 3,4-dihydroxybenzaldehyde and tyramine to form norbelladine, indicating the start of the main AA biosynthetic pathway (Kilgore *et al.*, 2016b; Majhi *et al.*, 2023; Singh *et al.*, 2018; Tousignant *et al.*, 2022). Norbelladine *O*-methyltransferase (N*O*MT) then methylates norbelladine at specific hydroxyl groups (Kilgore *et al.*, 2014; Koirala *et al.*, 2024; Li *et al.*, 2019). N*O*MT has been examined in various species, including *Narcissus* spp. and *Lycoris* spp., finding species-specific differences in enzyme activity and substrate selectivity (Koirala *et al.*, 2024; Li *et al.*, 2019; Sun *et al.*, 2018; Wang *et al.*, 2024). 4′-*O*-methylnorbelladine, a branchpoint intermediate in the pathway, is then modified by various enzymes, contributing to the structural diversity of AAs. CYP96T1 from *Narcissus pseudonarcissus* predominantly catalyzes *para–para'* coupling, with minor *para–ortho*' phenol coupling (Kilgore *et al.*, 2016a). Additional CYP96T enzymes identified in

Narcissus cv. Tête-à-Tête, *Lycoris aurea,* and *L. aestivum* catalyze diverse phenol coupling reactions (Lamichhane *et al.*, 2025; Liu *et al.*, 2024; Mehta *et al.*, 2024). Nornarwedine, the *para-ortho'* product, undergoes *N*-methylation via tocopherol *N*-methyltransferase (TocoNMT) to yield narwedine, which is reduced to galanthamine by an aldoketo reductase (AKR) (Mehta *et al.*, 2024)(Fig. 2.1). While TocoNMT cannot methylate norgalanthamine to galanthamine (Mehta *et al.*, 2024), radio- and stable-isotope labeling studies suggest multiple biosynthetic routes for galanthamine *in planta* (Eichhorn *et al.*, 1998; Jayawardena *et al.*, 2024). Given the necessity for various *N*-methylation steps in AA biosynthesis (Desgagné-Penix, 2021), additional *N*-methyltransferases likely contribute to these pathways.

N-methyltransferases (NMTs) are enzymes that transfer a methyl group (-CH_3) to specified nitrogen atoms in substrates, typically using *S*-adenosylmethionine (SAM) as the methyl donor, resulting in the formation of *N*-methylated products (Zhou *et al.*, 2020b). This methylation process is crucial for altering and diversifying plant-specialized metabolites, such as alkaloids, by changing their solubility, stability, and biological activity, which can influence endogenous functions and therapeutic potential (Lee *et al.*, 2024). For example, galanthamine exhibits strong anti-acetylcholinesterase inhibitory activity, whereas its demethylated form, norgalanthamine, a bit less (Orhan *et al.*, 2021).

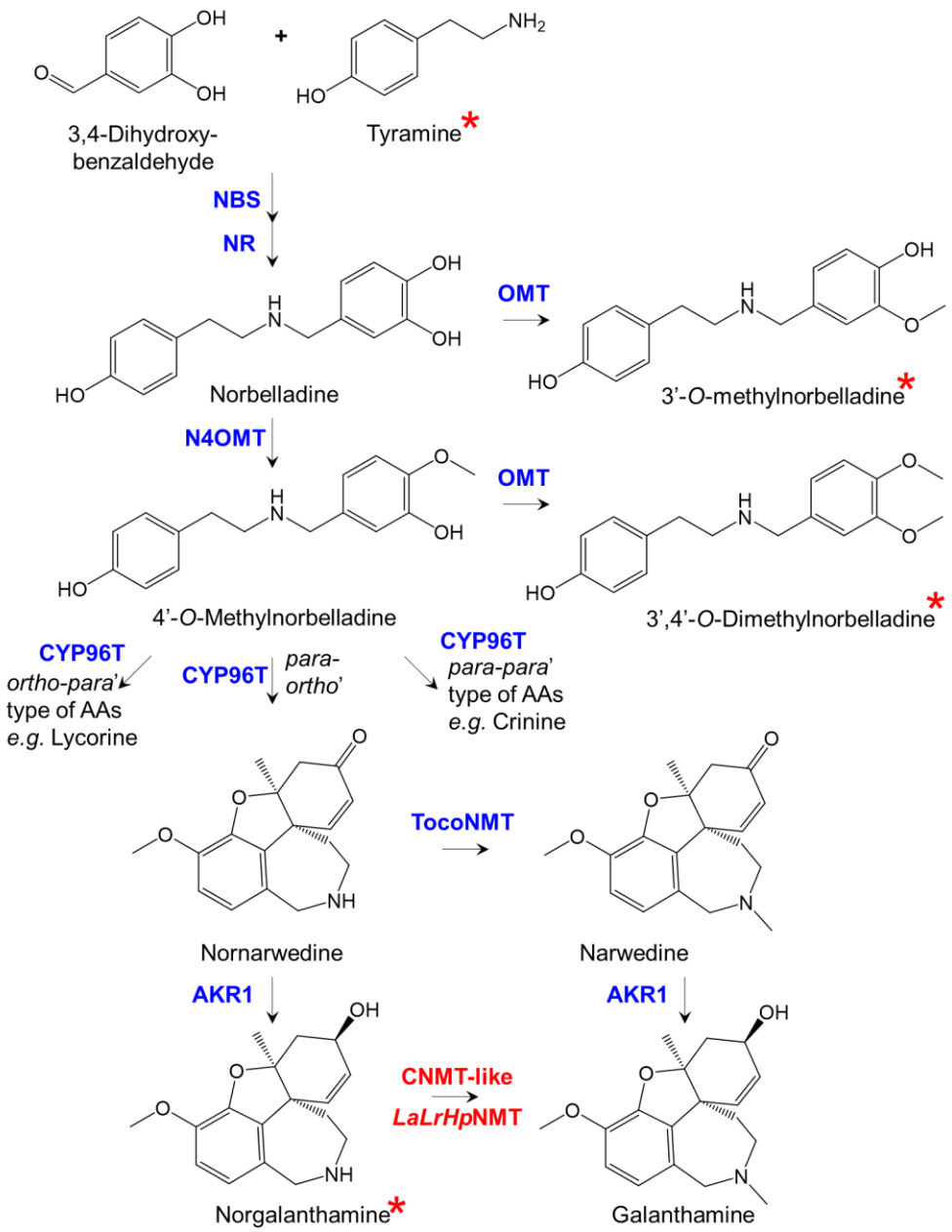

Fig. 2.1. Biosynthetic pathway leading to galanthamine starting from the condensation of tyramine and 3,4-DHBA. All enzymes shown in bold blue have been identified from Amaryllidaceae. Abbreviations are NBS, norbelladine synthase; NR, noroxomaritidine/norcraugsodine reductase; OMT, *O*-methyltransferase; N4*O*MT, norbelladine 4'-*O*-methyltransferase; CYP96T, cytochrome P450 monooxygenase 96T; TocoNMT, tocopherol *N*-methyltransferase; AKR1, Aldoketoreductase1; and CNMT-like *LaLrHp*NMT, coclaurine *N*-methyltransferase-like enzymes (five isoforms) from this study. * represents the substrates accepted by *LaLrHp*NMT1 characterized in this study.

In benzylisoquinoline alkaloid (BIA) biosynthesis, a subclass of isoquinoline alkaloids, multiple NMTs have been identified, including

coclaurine-*N*-methyltransferases (CNMT), reticuline *N*-methyltransferases (RNMT), and tetrahydroxyprotoberberine *N*-methyltransferases (TNMT), each catalyzing specific methylation reactions critical for BIA structural diversity (Lee *et al.*, 2024; Morris and Facchini, 2019).

In this study, we identified, isolated, and characterized CNMT-like NMTs from two commercially galanthamine-producing species, *L. aestivum* and *L. radiata*, and a high galanthamine-producing species, *Hippeastrum papilio*. We compared *CNMT-like NMT* expression levels and galanthamine content across different organs of these three species during the vegetative stage. Additionally, we investigated the subcellular localization of CNMT-like NMTs and analyzed how various stress conditions affect their expression. This study uncovers a new enzyme of the AA pathway and provides new insights into the regulation of *N*-methylation in AA biosynthesis, offering potential strategies for metabolic engineering to enhance galanthamine production.

2.3. Materials and Methods.

2.3.1. Plant materials and growth conditions

Mature bulbs of *L. aestivum* and *H. papilio* were purchased from Florissa (https://florissa.com), and *L. radiata* mature bulbs were bought from a plant nursery in China. Bulbs were planted in plastic pots in autoclaved soil (ARGO MIX G6 potting soil), grown at room temperature with

14h:10h light: dark conditions for 12 months, watered weekly, and fertilized when necessary. Leaves, bulbs, and roots were separated when the plants were in the vegetative stage, flash-frozen in liquid nitrogen, and stored at -80˚C.

In vitro H. papilio shoot cultures were prepared for the stress treatment experiment as follows. After four weeks at 4°C, a mature bulb of *H. papilio* was left at room temperature overnight. After a one-hour heat treatment at 52°C, it was left to rest at room temperature for the night. Then, dead and dried scales were removed before sterilizing the bulb's surface. The bulb was then rinsed with tap water and detergent five times and submerged in 70% ethanol for one minute. After that, the bulb was exposed to commercial bleach that contained 6% sodium hypochlorite for 30 minutes. The bulb was then repeatedly washed in a biological hood using autoclaved water five times. Finally, 2-3 mm size twin-scale explants were obtained with sterilized scalpels and forceps. Murashige and Skoog media supplemented with 3% sucrose, 0.075% plant preservative mixture, 3 $g.L^{-1}$ of Phytagel, and 15 µM benzyl aminopurine (BAP) were used as the basic shoot induction media. Before adding Phytagel and autoclaving, the pH was adjusted to 5.7 ± 0.1. Ten explants were cultivated in each plate under dark conditions at 25°C. Every two weeks, the transplants were subcultured until the shoots appeared and grew to a length of a few centimeters to separate them. The shoots were then separated and cultivated in glass jars with the same media, with 5

μM BAP and 5 μM naphthalene acetic acid (NAA) at 25°C under light conditions (14h:10h light: dark , 100 $\mu Mol.m^{2-1}$). Cultures were maintained for six months until sufficient material was produced. Then, shoots were transferred into 250 mL flasks containing liquid Murashige and Skoog media supplemented with 3% sucrose, 0.075% plant preservative mixture, 5 μM BAP, and 5 μm NAA, as ten shoots per flask, and maintained with the same growth chamber conditions for another two weeks. They were then treated for 0, 6, 24, and 48 hours with 100 μM MeJA, 1 μM coronatine, 400 mM NaCl, 20% PEG-6000 solution (w/v), 500 μM sodium nitroprusside (SNP), or 50 μM $CdCl_2$, individually. Shoot cultures were kept in chambers at 4°C and 35°C for 0, 6, 24, and 48 hours to simulate cold and heat stress. The shoots were then collected, crushed with liquid nitrogen, and stored at -80°C. The experiment was conducted in three replicates.

2.3.2. Chemicals and reagents

Standards of the alkaloids 11-hydroxyvittatine, 9-*O*-demethylhomolycorine, cherylline, flexinine, gigancrinine, gigantelline, gigantellinine, haemanthamine, homolycorine, obliquine, pancracine, sanguinine, tazzetine, vittatine and crinine were kindly obtained from Professor Antonio Evidente (Institute of Biomolecular Chemistry, National Research Council, Pozzuoli, NA, Italy). Standards of 3′-*O*-methylnorbelladine, 4′-*O*-methylnorbelladine,

3′,4′-*O*-dimethylnorbelladine, and norbelladine were synthesized as described in (Girard *et al.*, 2022). Standards of 3,4-dihydroxybenzaldehyde (97%), 4-hydroxybenzaldehyde (99%), isovanillic acid (99%), isovanillin (98%) and trans-cinnamic acid (98%) were purchased from Acros Organics (Massachusetts, USA). Standards of 3,4-dihydroxybenzoic acid (97%), levodopa (98%), L-tyrosine (99%), and *p*-coumaric acid (98%) were purchased from Alfa Aesar (Massachusetts, USA). Standards of caffeic acid (98%), dopamine (98%), ferulic acid (99%), lycorine (98%), papaverine (98%), tyramine (99%), and vanillin (99%) were procured from Millipore Sigma (Massachusetts, USA). Standards of galanthamine (98%) and narciclasine (98%) were purchased from Tocris Bioscience (Bristol, United Kingdom). Standards of norgalanthamine, lycoramine (97%), coclaurine (95%), isoferulic acid (98%), and phenylalanine (98%) were obtained from Toronto Research Chemicals (Ontario, Canada), US Biological, Musechem (New Jersey, USA), TCI America (Oregon, USA), and MP Biomedicals (California, USA) respectively. Analytical LC-MS grade methanol was purchased from Fisher Scientific (New Hampshire, USA)

2.3.3. Identification of NMT transcripts

In the assembled transcriptome of *Leucojum aestivum*, one complete transcript was annotated as CNMT-like NMT(Tousignant *et al.*, 2022).

The exact transcript was blasted against the laboratory's in-house transcriptome database containing publicly available Amaryllidoideae transcriptomes, already assembled or assembled using Trinity 2.14.0 with default parameters(Lamichhane *et al.*, 2025), to identify the candidates from *L. radiata* and *Hippeastrum* cv. hybridum using blast+ 2.130. Primers for restriction cloning and qRT-PCR were prepared using those sequences (Supplementary Table A1), and for the qRT-PCR, a universal primer pair was used (Supplementary Table A2).

2.3.4. Quantitative real-time expression of *NMT*

Total RNA was extracted from three different organs (leaves, roots, and bulbs) of the three selected species (*L*. aestivum, *L*. *radiata*, and *H*. *papilio*) using the GeneJET Plant RNA Purification Kit (Thermo Scientific™) and from the stress-treated shoot cultures of *H. papilio* using TRIzol reagent (Invitrogen), according to the manufacturer's instructions, using 100 mg of flash-frozen homogenized tissues. A NanoPhotometer (Implen) and 1.5% (w/v) agarose gel electrophoresis were used to confirm the amount and quality of RNA isolated from various tissues. cDNA was synthesized from 1 µg of the freshly extracted RNA using SuperScript™ IV VILO™ Master Mix (Invitrogen™) according to the product manual. After that, RT-qPCR was carried out using 1 µL of cDNA and 0.25 mM of gene-specific primers (Supplementary Table A2) in Luna Universal qPCR Master Mix (New England Biolabs) to assess

the expression of two genes: *histone 3*, as an endogenous reference gene, and *NMT*, which codes for *N*-methyltransferase. The $2^{-\Delta Ct}$ method was used to calculate the gene's relative expression. The results obtained were analyzed and visualized using GraphPad Prism 10 software.

2.3.5. Extraction, LC-MS detection, and quantification of Amaryllidaceae alkaloids

One hundred milligrams of the homogenized fresh tissues and 20 milligrams of lyophilized shoot cultures of *H. papilio* were utilized to extract metabolites. One milliliter of 90% methanol was added to extract the crude metabolites, left in the sonication bath for one hour and then in a water bath at 60°C for two hours. After that, 0.2 µm PTFE syringe filters were used to filter the extracts. The SpeedVac Vacuum Concentrator (Thermo Fisher) evaporated the solvents completely. After being weighed and reconstituted in the mobile phase (methanol and milli-Q water (90:10), both containing formic acid 0.1% v/v) as 1000 $mg.L^{-1}$ of crude plant metabolite extract, with 1 $mg.L^{-1}$ papaverine as an internal standard, the dry crude extract was again filtered through 0.2 µm PTFE syringe filters.

A high-performance liquid chromatography (HPLC) coupled with a tandem mass spectrometer (MS/MS) (Agilent, QC, Canada) equipped with an Agilent Jet Stream ionization source, a Kinetex EVO C18 column

(150 × 4.6 mm, 5 µm, 100 Å; Phenomenex, Torrance, USA), a binary pump, an autosampler set at 4°C and a column compartment were used for the analysis. Five microliters of each sample were injected into the column set at 30°C. A gradient made of (A) formic acid 0.1% v/v in Milli-Q water and (B) formic acid 0.1% v/v in methanol, with a flow rate of 0.4 mL/min, was used to achieve chromatographic separation. The HPLC elution program started with 10% solvent B; 0–10 min, isocratic conditions with 10% solvent B; 10–20 min, linear gradient to reach 100% B; 20–25 min, isocratic conditions with 100% B; 25–26 min, linear gradient to return to initial conditions of 10% B. The total run time was 30 min per sample to allow the reconditioning of the column before the next injection. The parameters used for the MS/MS source to perform the analyses were set as follows: gas flow rate 10 L/min, gas temperature 300°C, nebulizer 45 psi, sheath gas flow 11 L/min, sheath gas temperature 300°C, capillary voltage 4000 V in ESI^+ and 3500 V in ESI^- and nozzle voltage 500 V. Agilent MassHunter Data Acquisition (version 1.2) software was used to control the HPLC-MS/MS, MassHunter Qualitative Analysis (version 10.0) and MassHunter Quantitative QQQ Analysis (version 10.0) software were used for data processing. Multiple reaction monitoring (MRM) transitions and instrument parameters used for targeted compound identification during HPLC-MS/MS analysis are included in supplementary tables 1.A3 and 1.A4. A standard calibration curve was prepared as follows: a working

stock solution containing galanthamine at 100 $mg.mL^{-1}$ in LC-MS grade methanol. This stock solution was further diluted to prepare calibration solutions with the following concentrations in triplicate: 0, 1.25, 2.5, 5, 50, 1000, 2000, 5000, and 10000 $ng.mL^{-1}$, to which the internal standard papaverine was added at a final concentration of 1000 $ng.mL^{-1}$ each. These standard solutions were injected into the HPLC-MS/MS system to generate calibration curve regression. Supplementary Figure 1.A1 shows the calibration curve obtained by plotting the area ratio (*i.e., the* peak area of galanthamine divided by the peak area of the papaverine) as a function of galanthamine's concentration, which allowed galanthamine quantification in the various tissues of *L*. aestivum, *L*. *radiata*, and *H*. *papilio*. The results obtained were analyzed and visualized using GraphPad Prism 10 software.

2.3.6. Isolation, cloning, and heterologous protein production

The open reading frames of CNMT-like NMTs from the three different Amaryllidoidae species (*L*. aestivum, *L*. *radiata*, and *H*. *papilio*) were amplified using the leaf cDNA using Terra™ PCR mix (Takara Bio) in 50 µl with 0.3 µM of gene-specific primers having EcoRI and HindIII restriction sites (Supplementary Table A2) according to the user manual. A typical PCR cycle consisted of 98°C for 2 min, followed by 98 °C for 10 s, 60 °C for 15 s, 68 °C for 1.5 min for 40 cycles, followed by 5 min hold at 68 °C and then an infinite hold at 4 °C. After digestion, the

amplified cDNA region was cleaned using high-fidelity EcoRI and HindIII restriction enzymes (New England Biolabs) with the Geneaid GenepHlow Gel/PCR kit. The digested PCR products were cloned into pMAL-c2X vectors using T4 DNA ligase (New England Biolabs) in frame with maltose-binding protein (MBP). Heat shock was used to transform the recombinant plasmids into chemically competent *E. coli* DH5α cells, and colonies were chosen on LB agar plates supplemented with ampicillin (100 $mg.mL^{-1}$, Thermo Fisher Scientific). The presence of the targeted gene was verified by colony PCR, and the identity of the gene was confirmed by sequencing (three clones per transformation) using Sanger sequencing at the Genome Quebec sequencing facility.

2.3.7. NMT sequence analysis and phylogenetics

The NMT clones from this study and their corresponding sequences are available in Supplementary Table 1.A5. Protein molecular weights and pI predictions were made using the Expasy tool (Supplementary Table 1.A6) (https://www.expasy.org/resources/compute-pi-mw/). The candidate NMTs studied here were aligned to the amino acid sequences of the characterized NMTs in the BIA alkaloid pathway (obtained from NCBI, https://www.ncbi.nlm.nih.gov, Table 2.1) using the Clustal Omega algorithm integrated with Unipro UGene version 46.0 (Okonechnikov *et al.*, 2012). Phylogenetic analysis was done using the aligned sequences by PhyML maximum likelihood method with LG substitution model with

1000 bootstraps employed in Unipro UGene version 46.0 (Okonechnikov *et al.*, 2012).

Table 2.1. List of *N*-methyltransferases used for alignment and phylogenetic tree in this study. Sequences were obtained from NCBI (https://www.ncbi.nlm.nih.gov).

Species	Name	Accession number
Aristolochia fimbriata	*Af*CNMT	ADP76529.1
Coptis japonica	*Cj*CNMT	BAB71802.1
Ephedra sinica	EsNMT	AWJ64115.1
Eschscholzia californica	*Ec*TNMT	ACO90222.1
Liriodendron chinense	*Lc*CNMT1	Lchi24863
Nelumbo nucifera	*Nn*CNMT	WEE66564.1
Papaver somniferum	*Ps*CNMT	Q7XB08.1
Papaver somniferum	*Ps*RNMT	AOR51552.1
Papaver somniferum	*Ps*TNMT	AAY79177.1
Thalitricum flavum subsp. glaucum	*Tf*CNMT	Q5C9L6.1
Thalitricum flavum	*Tf*PavNMT	ACO90251.1
Stephania intermedia	*Si*CNMT1	QFU85193.1
Stephania intermedia	*Si*CNMT2	QFU85194.1
Sinopodophylum hexandrum	*Sh*CNMT	AJD20224.1

2.3.8. *In silico* analysis of NMT

Folding prediction of coclaurine-like *N*-methyltransferase candidates and mutants from *L. aestivum*, *H. papilio,* and *L. radiata* was performed using AlphaFold Server Beta powered by AlphaFold3 (Abramson *et al.*, 2024). Receptor preparation and docking were performed using the MOE2022.09 software with the AMBER10: EHT force field (Chemical

Computing Group) performed the reactor preparation and docking. Predicted enzymes were superimposed with reference crystal structures of *Cj*NMT in MOE (6GKY (Bennett *et al.*, 2018a)). Methyl donor *S*-adenosylmethionine (SAM) was included in the active sites at coordinates of orthologous crystal structures (see Supplementary Figure 1.A2). The docking site was predicted based on residues in interaction with ligands of orthologous crystal structure and included SAM. Ligands (norgalanthamine, tyramine) isomeric smiles codes retrieved from PubChem were submitted to the ZINC20 database to obtain 3D charged data files (Irwin *et al.*, 2020). Protomers predicted at pH=8.5 were included as possible ligands.

Triangle Matcher was selected as a placement method for 200 poses generated by flexible docking with tethered induced fit refinement. Ten docking poses for each ligand were compared with crystalized protein-ligand complexes. The pose with the best docking score coherent with the catalyzed reaction was selected. PLIP was used to detect the interactions between ligands and receptor residues (Adasme *et al.*, 2021). Visualization, superimposition, and figure preparation were performed using Pymol 3.0.0 (Schrödinger).

2.3.9. *NMT* site-directed mutagenesis and cloning

Ten *LaLrHp*NMT1 mutant constructs were generated by Gibson assembly using the NEBuilder® HiFi DNA Assembly Bundle for Large

Fragments (New England Biolabs, Canada). Fragments for the assemblies were amplified by PCR with PrimeSTAR GXL DNA Polymerase (Takara Bio, Japan) according to the manufacturer's protocol, using the plasmid pMAL-c2X_*LaLrHp*NMT1 as the template and the primers listed in Table 1.A2 in Supplementary Data. *E. coli* DH5α cells were transformed, and mutagenesis was confirmed, as described in section 2.6. Heterologous protein production and enzymatic assays. Purified recombinant plasmids were transformed into chemically competent *E. coli* Rosetta (DE3) pLysS (Novagen) by heat shock for heterologous enzyme production. Colony PCR was conducted to screen positive transformants, and then protein expression and purification were done. Seed cultures were prepared for protein production with 12.5 mL of LB medium supplemented with 100 $\mu g.mL^{-1}$ ampicillin and 35 $\mu g.mL^{-1}$ chloramphenicol using single colonies incubated overnight at 37°C with orbital shaking at 200 rpm. The following day 250 mL of LB media in 1 L flasks (containing 100 $\mu g.mL^{-1}$ of ampicillin and 35 $\mu g.mL^{-1}$ of chloramphenicol) were inoculated with the seed cultures and incubated in the same conditions for a few hours until reaching the OD of the cultures to A_{600} = 0.6; after cooling on ice, IPTG was added to the cultures at a final concentration of 1 mM to induce the generation of recombinant protein, they had been cultivated at 18°C with orbital shaking at 200 rpm for 16 hours. Cells were extracted by centrifugation at 5000 g for 10 min at 4˚C. After that, the cell pellets were stored at -

80˚C until protein purification. Enzyme purification was initiated by re-suspending the cells in 25 mL of protein extraction buffer (30 mM Tris–HCl, pH 8, 150 mM NaCl, 1 mM EDTA, 10% (v/v) glycerol). They were then incubated for 30 minutes on ice and sonicated for 8 minutes (15 s on, 30 s off). The crude lysate was centrifuged at 16,000 g for 15 minutes at 4 ˚C to eliminate cellular debris. One milliliter of amylose resin beads (New England Biolabs) was added to the cleared supernatant and then incubated at 4 ˚C while constantly shaken. The mixture was run through a gravity column at 4 ˚C after an hour, and the remaining beads were then rinsed three times using the same buffer without NaCl. Elution buffer, the same as lysis buffer without NaCl but containing 25 mM of freshly made maltose, was used to elute the purified enzymes. Using bovine serum albumin as the standard, the Bradford reagent was used to measure the concentration of purified MBP-tagged protein utilizing the manufacturer's procedure (Thermo Fisher Scientific). Protein purity was evaluated using a 10% (w/v) SDS-PAGE gel. Freshly purified enzymes were utilized for enzymatic tests.

After that, the recombinant NMTs' enzymatic activity for the synthesis of galanthamine was evaluated. A 50 µL mixture of 50 mM Tris-HCl (pH 8.5), 500 µM SAM as the methyl donor, 250 µM norgalanthamine as the substrate, and 50 µg of pure protein was used to conduct the reaction. Purified MBP-tag protein from the empty vector was used as the negative control. After 16 hours of incubation at 37°C, the mixtures were

terminated by adding 50 µL of methanol. Following 15 minutes of centrifugation at 10,000 rpm at 4˚C, adding papaverine at 20 $mg.L^{-1}$ as internal standard and performing a sample dilution of 20-fold in the mobile phase (methanol and milli-Q water (90:10), both containing formic acid 0.1% v/v), LC-MS/MS analysis was carried out.

Instrumentation and chromatographic conditions for enzyme assays done with norgalanthamine as substrate were conducted as described in subsection 2.5, except that the only compounds monitored by the LC-MS/MS during those enzymatic assays were norgalanthamine, galanthamine, and papaverine.

2.3.10. Optimization of enzymatic conditions

Since *LaLrHp*NMT1 was present in all three species and had the maximum activity for galanthamine synthesis, it was used to determine optimal parameters, kinetics, and substrate specificity. Tests were conducted for 16 hours under the same circumstances as the initial enzymatic tests in 50 mM Tris-HCl, pH 8.0, and between 10 and 70°C to identify the ideal temperature. Next, assays were conducted in 50 mM sodium phosphate buffer (pH 6.0–7.0), Tris-HCl (pH 7.0–9.0), and glycine/NaOH buffer (pH 9.0–10.0) at 42°C for 16 hours to identify the ideal pH.

2.3.11. Substrate specificity assay

Next, substrate specificity was determined by incubating 250 µM of possible substrates for 16 hours at 42°C in 50 mM Tris-HCl, pH 8.5, to determine the substrate specificity. The chemical structure of these substrates is presented in supplementary figure 1.A3. Purified protein denatured by boiling for ten minutes was used in adverse control reactions. After 16 hours of incubation at 37°C, the mixtures were terminated by adding 50 µL of methanol. Following 15 minutes of centrifugation at 10,000 rpm at 4°C, adding papaverine at 20 $mg.L^{-1}$ as internal standard and performing a sample dilution of 20-fold in the mobile phase (methanol and milli-Q water (90:10), both containing formic acid 0.1% v/v), LC-MS/MS analysis was carried out. The same LC-MS/MS methodology described in subsection 2.5 was applied to analyze samples from substrate specificity assays, except that they were analyzed in Single Ion Monitoring (SIM) mode instead of MRM. Each substrate was monitored by the mass-to-charge (m/z) ratio corresponding to their molecular weight ionized in positive electrospray ionization (ESI^+) (*i.e.* $[M+H]^+$).

In contrast, the corresponding expected product was monitored with an added mass of +14 m/z, +28 m/z, and/or +42 m/z (*i.e.* $[M+H+14]^+$, $[M+H+28]^+$ and/or $[M+H+42]^+$) to determine if one, two or three N-methylation reaction(s) occurred on the substrate during assays.

Analyses were done using authentic standards to obtain the retention time of each substrate and by comparing Extracted Ion Chromatograms (EIC) from assays to the ones of corresponding negative controls. New signals detected at the expected retention time and m/z of the product(s) or a more abundant signal compared to negative controls were considered positive results for those experiments. Each assay, along with negative controls, was performed in triplicate. Supplementary Table A3 presents the instrumental parameters used for analyzing substrate specificity tests by LC-MS/MS. The substrate conversion percentage was calculated based on the decrease in substrate levels in the enzymatic assay compared to the negative control relative to the formation of the added mass of +14 m/z, +28 m/z, and/or +42 m/z.

2.3.12. *In vivo* enzymatic assay and subcellular localization *in planta*

The *LaLrHp*NMT1 gene from *Leucojum aestivum* was amplified from cDNA using Takara high-fidelity DNA polymerase in a 25 µL reaction volume. The PCR mixture consisted of 12.5 µL of enzyme, 1.5 µL of each primer (10 mM), 1 µL of template cDNA, and 8.5 µL of distilled water. Amplification was carried out with an initial denaturation at 98°C for 30 seconds, followed by 30 cycles of denaturation at 98°C for 10 seconds, annealing at 72°C for 30 seconds, and extension at 72°C for 1.3 minutes, concluding with a final extension at 72°C for 5 minutes. The AttB-flanked

PCR products were purified using the Gel/PCR DNA Fragment Purification Kit (Geneaid) and subjected to a Gateway BP recombination reaction with the pDONR221 vector (Thermo Fisher Scientific). The resulting entry clone was transformed into *Escherichia coli* DH5α, and positive clones were selected on LB agar containing 50 $\mu g.mL^{-1}$ kanamycin. Sequence identity was verified by sequencing, and the clones were further used in LR recombination reactions with pK7WG2 for *in vivo* assay, and either the pB7FWG2 (*C*-terminal GFP) or pB7WGF2 (*N*-terminal GFP) destination vectors for localization experiment. Positive *E. coli* DH5α transformants were selected on LB agar containing 50 $\mu g.mL^{-1}$ spectinomycin.

The *LaLrHp*NMT1 constructs in pK7WG2, pB7FWG2, or pB7WGF2 were then introduced into *Agrobacterium tumefaciens* strain GV3101 via electroporation, and positive colonies were selected on LB agar plates containing rifampicin, spectinomycin, and gentamicin (50 $\mu g.mL^{-1}$ each) at 28°C. Single colonies were cultured in LB media supplemented with the appropriate antibiotics, harvested, and washed twice with induction buffer (10 mM $MgCl_2$, 10 mM MES, pH 5.6, 200 µM acetosyringone). The cultures were adjusted to an OD_{600} of 0.6 and incubated in induction buffer for 2 hours at room temperature. These *A. tumefaciens* cultures harboring the gene of interest were infiltrated into 4-week-old *Nicotiana benthamiana* leaves. In the *in vivo* assay, norgalanthamine (100 µM) was infiltrated 48 hours later, and plants were further incubated for 24

hours. Leaves were harvested, and metabolite analysis was performed by LC-MS/MS as in (Lamichhane *et al.*, 2025) . For co-localization analysis, pB7FWG2 or pB7WGF2 constructs were co-infiltrated with RFP (nucleo-cytosolic marker) and mCherry (ER marker with a signal peptide). Forty-eight hours post-infiltration, abaxial epidermal cells were imaged using a Leica TCS SP8 confocal laser scanning microscope with a 40x oil immersion objective. GFP fluorescence was excited at 488 nm with emission detected between 500 and 525 nm, chlorophyll autofluorescence was excited at 552 nm with emissions detected between 620 and 670 nm, and mCherry fluorescence was excited at 587 nm with emission detected at 619 nm. Image processing was performed using the Leica LasX software.

2.4. Results

2.4.1. Candidate coclaurine-like NMT mining, expression analysis, and galanthamine levels in tissues of three species of Amaryllidaceae.

The coclaurine-like NMT candidate was identified by searching annotated transcripts in the transcriptome of *L. aestivum* (Tousignant *et al.*, 2022). A single, complete mRNA sequence (1,065 bp) encoding a 355 amino acid protein was detected and selected as the *CNMT-like NMT* candidate for this study. This sequence served as a query to BLAST against our Amaryllidoideae transcriptome database

(Lamichhane *et al.*, 2025), identifying one ortholog in both *L. radiata* and *Hippeastrum* cv. hybridum transcriptomes. We designed a universal RT-qPCR primer pair for gene expression analysis targeting conserved regions across all three *CNMT-like NMT* sequences. In contrast, species-specific primers were developed for cloning into expression vectors (Supplementary Table 1.A2).

CNMT-like NMT expression levels varied among tissues (leaf, bulb, and root) of the three species, with the highest expression observed in leaves of *H. papilio* at 2.65 ± 0.87, over twice that of the other species (Fig. 2.2A). In contrast, *L. aestivum* roots exhibited the lowest *NMT* expression level, recorded at 0.03 ± 0.03, while *L. radiata* showed moderate expression across all sampled organs (Fig. 2.2A). Galanthamine accumulation patterns did not mirror exactly these expression trends (Fib. 2.2B). Bulbs of *H. papilio* contained especially high galanthamine concentrations, reaching 1.62 ± 0.07 mg per gram of fresh tissue. In contrast, galanthamine levels were relatively moderate in *L. aestivum* tissues and lowest in *L. radiata,* where it was only detected in bulbs and not in the leaves and roots (Fig. 2.2B).

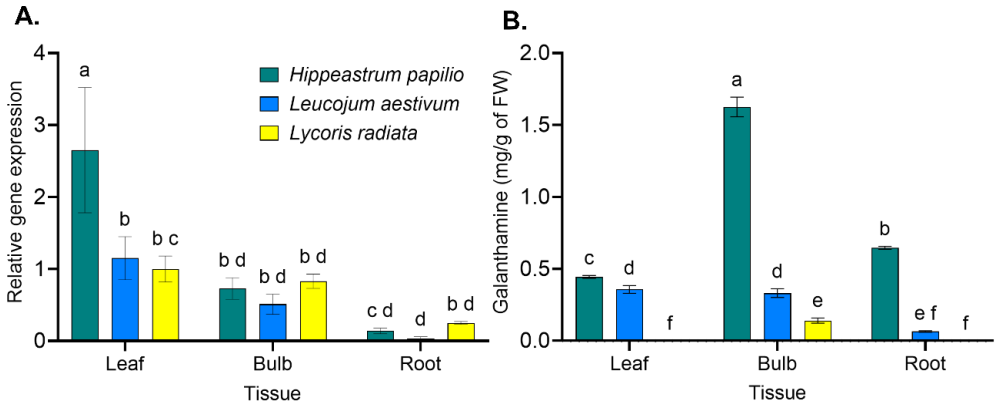

Fig. 2.2. Comparison of relative expression of NMT with galanthamine content of three Amaryllidaceae in different tissues in the vegetative stage. **A.** Relative NMT expression ($2^{-(\Delta\Delta Ct)}$) was measured by qRT-PCR normalized by the housekeeping gene Am_Histone3. **B.** Galanthamine content was measured by LC-MS/MS using authentic standard and a standard curve. All the values are shown as means ± standard deviation of three independent biological replicates. Plants were grown under the same conditions for 12 months before the experiment. Statistical significance was calculated with a two-way ANOVA followed by Tukey's multiple comparisons. Lowercase letters indicate significant differences between treatments ($p < 0.05$).

2.4.2. Amaryllidaceae NMT candidates cluster together with coclaurine NMTs

After verifying NMT transcripts' expression in galanthamine-producing plants, full-length transcripts were cloned and analyzed. In *L. aestivum*, three isoforms were identified: *LaNMT1* identical to the reference mRNA sequence, *LaNMT2* with two nucleotide differences; and *LaNMT3,* which contained 19 substitutions (Supplementary Table 1.A5). In *L. radiata*, two isoforms were detected: *LrNMT1,* which displayed 42 nucleotide substitutions compared to the reference *NMT* sequence*,* and four silent nucleotide differences relative to *LaNMT1*, and *LrNMT2*, which exhibited 38 substitutions compared to the reference sequence. *H. papilio* presented two unique sequences: *HpNMT1*, identical to the reference

sequence, and *HpNMT2*, which contained 13 nucleotide substitutions (Supplementary Table 1.A5). *LaNMT1, LrNMT1*, and *HpNMT1* encoded an identical amino acid sequence, which we designated *LaLrHpNMT1.* Thus, five unique isoforms from three species were included in this study. All sequences were 1068 bp long and translated into a protein of 355 amino acids. *LaLrHp*NMT1, *La*NMT2, *La*NMT3, *Lr*NMT2, and *Hp*NMT2 displayed theoretical molecular weights of 41.3, 41.2, 41.3, 41.3, and 41.3 kDa and isoelectric points of 6.09, 6.09, 6.56, 6.76, and 8.48, respectively (Supplementary Table 1.A6). The predicted isoelectric points are similar for all the enzymes except *Hp*NMT2.

Phylogenetic analysis showed that the five Amaryllidaceae NMT isoforms form a distinct clade with *Nn*CNMT (*Nelumbo nucifera*) and *Si*CNMT1 (*Stephania intermedia*), suggesting evolutionary conservation (Fig. 2.3A). This clade was closely related to phenylalkylamide *Es*NMT from *Ephedra sinica*, forming a distinct subgroup. *Si*CNMT2 from *S. intermedia* was positioned adjacent to this cluster, suggesting possible functional and structural similarities among these enzymes. In contrast, a separate clade included CNMTs from *Thalictrum flavum* subsp. *glaucum*, *Liriodendron chinense*, *Sinopodophyllum hexandrum*, *Aristolochia fimbriata*, and *Coptis japonica*. A more distant phylogenetic relationship was observed between the candidates and reticuline NMT (RNMT) or tetrahydroxyprotoberberine NMT (TNMT), consistent with previous studies (Liscombe *et al.*, 2010).

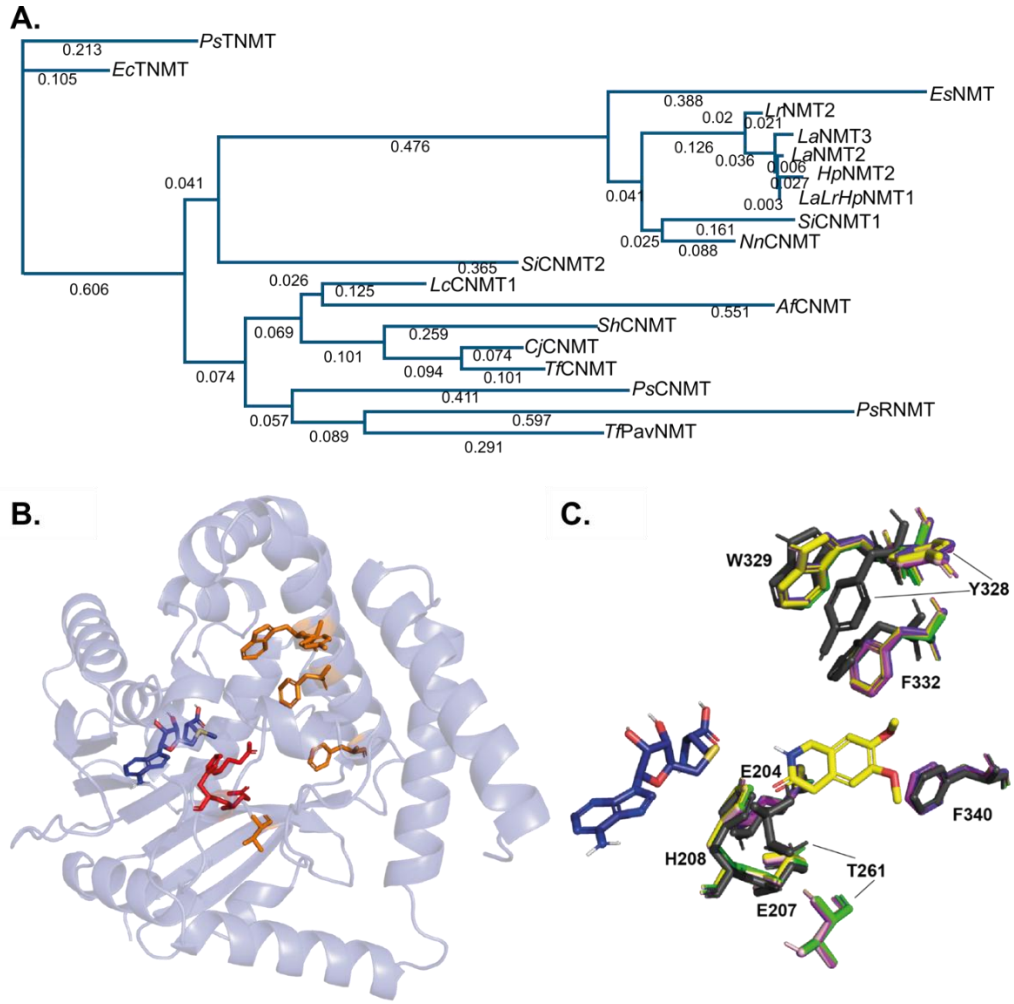

Fig. 2.3. *In silico* analysis of coclaurine-like NMT candidates from *Leucojum aestivum*, *Hippeastrum papilio*, and *Lycoris radiata*. **A.** The evolutionary relationships of the NMTs in this work and other identified plant NMTs from the BIA alkaloid pathway are compared using a phylogenetic tree. The aligned sequences were used for the phylogenetic analysis using the PhyML maximum likelihood technique with the LG substitution model and 1000 bootstraps used in Unipro UGene version 46.0. The National Centre for Biotechnology Information (NCBI) search engine (http://www.ncbi.nlm.nih.gov/protein/) was used to get the amino acid sequences of the plant BIA NMT. The methodology includes the accession numbers. **B.** AlphaFold3 predicted the folding of *LaLrHp*NMT1 in cartoon representation, with putative catalytic residues (Glu204, Glu207, and His208) as red sticks and other conserved active site residues as orange sticks. SAM is shown as purple sticks. **C.** Superimposed conserved active site residues of Amaryllidaceae CNMT-like enzyme candidates with *Cj*NMT pocket (dark grey sticks) containing SAM (dark purple sticks) and heliamine (yellow sticks). *La*NMT2 is shown in yellow, *La*NMT3 light pink, *Lr*NMT2 bright pink, *LaLrHp*NMT1 violet, and *Hp*NMT2 green. Residues are numbered according to the *Cj*NMT structure.

At the amino-acid level, the five Amaryllidaceae NMT isoforms exhibited high similarity (91- 99%), supporting a close evolutionary relationship

and a potential functional conservation. These isoforms shared 40-80% similarity with known NMTs involved in BIA biosynthesis (Supplementary Table 1.A7), aligning with previously observed evolutionary patterns in BIA pathways (Cheng *et al.*, 2022b; Morris and Facchini, 2019; Morris *et al.*, 2018). Additionally, the isoform sequences exhibited approximately 62% similarity with phenylalkylamide *Es*NMT, indicating possible evolutionary divergence. *Cj*CNMT and *Si*CNMT showed 75% to 82% similarity with the Amaryllidaceae NMT isoforms, coinciding with the phylogenetic analysis (Fig. 2.3A, Supplementary Table 1.A7).

2.4.3. Conserved catalytic residues and active site conformation

The predicted structures of the CNMT-like enzyme candidates were compared to the *Cj*NMT crystal structure (Fig. 2.3B). The Amaryllidaceae NMT isoforms exhibited high structural similarity, with root mean square deviation (RMSD) values ranging from 0.105-0.146 Å and were closely aligned with the *Cj*CNMT folding pattern (RMSD = 0.515 Å) (Fig. 2.3B). This overall structure followed the class I methyltransferase α/β Rossmann fold and a catalytic pocket composed mainly of α-helices (Fig. 2.3B). Superimposition with *Cj*CNMT showed a high degree of structural conservation, except for the *N*-terminal α-helices, which were predicted with lower confidence by AlphaFold3 (Fig. 2.3B).

The Amaryllidaceae NMT isoforms shared conserved regions with other NMT enzymes involved in BIA biosynthesis (Fig. 2.3B and 2.3C,

Supplementary Fig. 1.A2 and 1.A4). All five isoform sequences exhibited typical SAM-dependent methyltransferase domain, which is critical for catalytic activity and is characteristic of BIA-pathway NMTs (Morris and Facchini, 2019). They shared catalytic residues Glu207 and His208 with RNMTs and TNMTs (Morris *et al.*, 2020), and Glu204 with CNMTs, replacing Gly204 in RNMTs and Ala204 in pavine NMTs (PavNMTs) (Morris *et al.*, 2020). Glu204, Glu207, and His208, as well as active site residues Trp329, Phe332, and Phe340 shared a similar orientation across all isoforms, remaining close to the SAM methyl group and the substrate in CNMTs (Fig. 2.3C, Supplementary Figure 1.A2), where they are implicated in stabilizing ligand interactions via H-bonding or salt-bridge formation (Bennett *et al.*, 2018b). Glu204 and His208 act as a catalytic dyad, while Glu207 plays a key role in PavNMT catalysis. During N-methylation of coclaurine by *Cj*CNMT, the conserved residue Glu204 forms a hydrogen bond with the nitrogen of the substrate, stabilizing the transition state and facilitating proton transfer.. Site-directed mutagenesis showed that His208 functions as a general base, deprotonating the substrate's ammonium ion to enable a nucleophilic attack on the methyl group of SAM (Bennett *et al.*, 2018b).

Several other key catalytic residues were conserved across the studied NMTs and known CNMT enzymes, including Thr261, Phe340 (Phe337 in Amaryllidaceae), Tyr328 (Tyr325 in Amaryllidaceae), Trp329 (Trp326 in Amaryllidaceae), and Phe332 (Phe329 in Amaryllidaceae) (Bennett *et*

al., 2018b). Thr261, Tyr325 (or Ser325 in *HpNMT2*), and Phe329, were arranged differently from the reference CNMT crystal structure (Fig. 2.3C). In CNMTs, Tyr328, Trp329, and Phe332 are particularly important for substrate binding and orientation relative to SAM, as demonstrated by the loss of activity following their mutation, although the effect is less pronounced for Tyr328 (Bennett *et al.*, 2018b). Interestingly, a serine residue is observed in *HpNMT2 at this position*, suggesting a potential functional variation in this isoform (Supplementary Fig. 1.A2 and 1.A4).

2.4.4. CNMT-like Amaryllidaceae NMTs catalyze *N*-methylation of norgalanthamine to produce galanthamine

To investigate if Amaryllidaceae NMT isoforms were involved in galanthamine formation (Fig. 2.4A), we assessed whether norgalanthamine could fit within the putative enzyme active site pocket in a position conducive to *N*-methylation. We performed flexible docking simulations using *LaLrHp*NMT1 as the receptor. *In silico* predictions revealed that Glu204 consistently forms a hydrogen bond with the substrate's nitrogen atom (with a score of -7.9 kCal.mol^{-1}), positioning it optimally for methyl transfer (Fig. 2.4B, Supplementary Table 1.A8). However, interactions with Tyr325, Phe329, and Phe337 were not predicted. Instead, an alternative H-bond with Tyr288 (with the nitrogen of norgalanthamine) and hydrophobic interactions with Phe234 and Phe257, which stabilized its rings, were observed. These results suggest

a conserved mechanism of action for this CNMT-like enzyme, supporting norgalanthamine as a viable substrate. Furthermore, the involvement of alternative residues hints at a possible substrate promiscuity, allowing the enzyme to accommodate various structurally related alkaloid substrates.

To validate this prediction, we evaluated the *in vitro* catalytic activity of the five heterologously produced Amaryllidaceae NMT isoforms for their ability to catalyze galanthamine synthesis from norgalanthamine, as determined by LC-MS/MS analysis (Fig. 2.4C). All tested NMT isoforms exhibited detectable activity above background levels (compared to the negative control, Fig. 2.4C). Specifically, *LaLrHp*NMT1 (79.93-fold compared to control) and *Hp*NMT2 (69.38-fold) produced significantly higher amounts of galanthamine compared to the other three enzymes ($p < 0.0001$, One-way ANOVA). In contrast, *La*NMT3 exhibited the lowest activity (11.7-fold, $p = 0.9998$) (Fig. 2.4C). Despite a 99% similarity between *La*NMT2 and *LaLrHp*NMT1 (differing by only three amino acid differences: Pro68Leu, Asn151Tyr, and Leu234Phe), the activity of *La*NMT2 was significantly lower (30.32-fold, $p = 0.0004$, one-way ANOVA), suggesting that these specific residues play a crucial role in enzymatic efficiency (Fig. 2.3, Supplementary Table 1.A7, Fig. 2.4C).

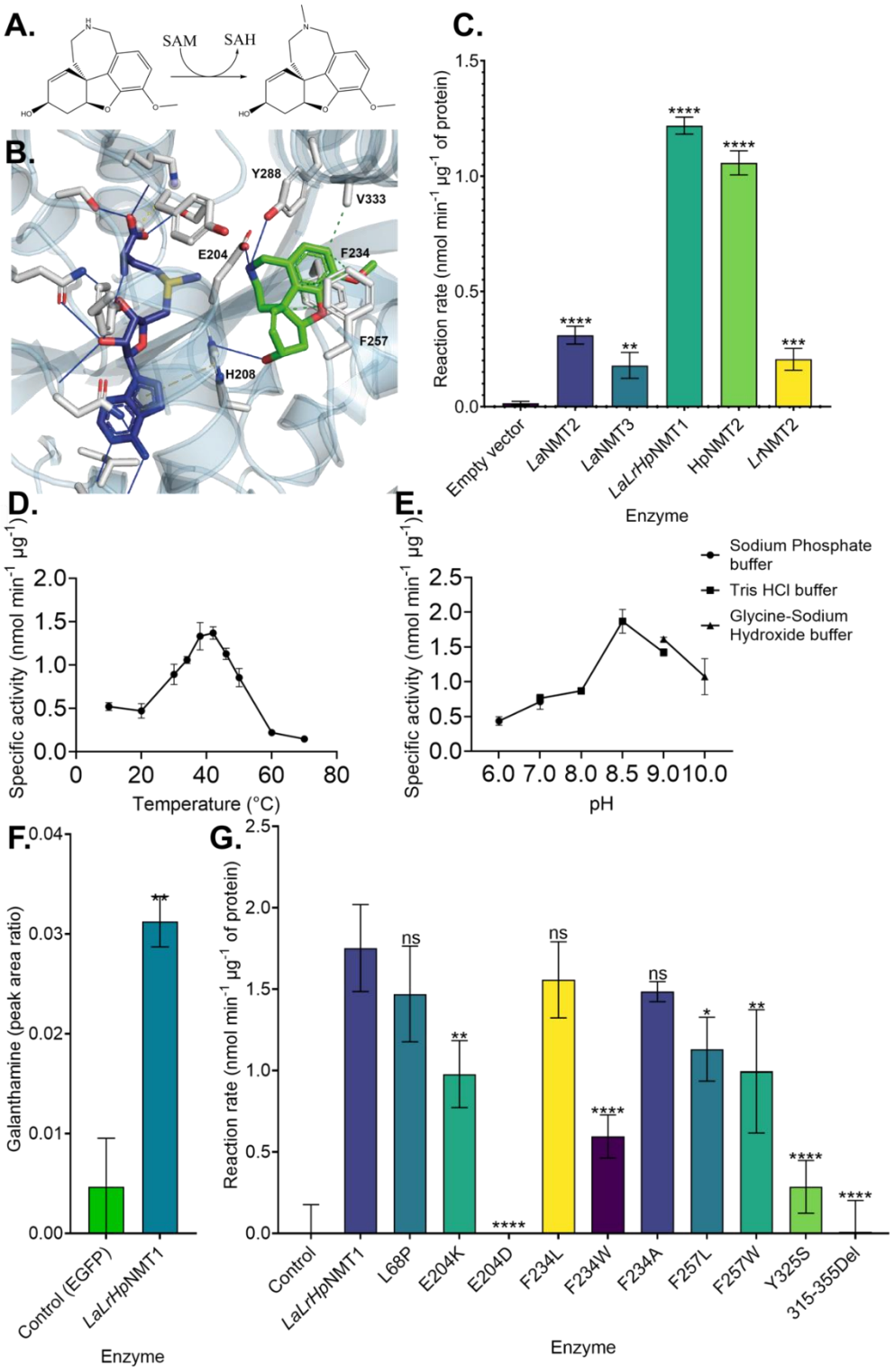

Fig. 2.4. Amaryllidaceae coclaurine-like N-methyltransferases catalyze N-methylation of norgalanthamine. **A.** Schematic conversion of norgalanthamine to galanthamine. **B.** *LaHpLr*NMT1 active site residue (grey) in interaction with docked norgalanthamine (green) and SAM (dark purple). H-bonds are shown as blue lines, p-stacking interaction as yellow dashed lines, and hydrophobic interactions as green dashed lines. **C.**

Comparison of the activity of the five heterologously produced Amaryllidaceae NMT isoforms for the catalysis of norgalanthamine to galanthamine. Control: the empty vector was used here as the negative control. **D.** Production rate of galanthamine for *LaLrHp*NMT1. under different pH. **E.** Production rate of galanthamine for *LaLrHp*NMT1 under different temperatures. **F.** Relative quantification of galanthamine *in planta*. The area ratio was obtained by dividing the peak area of galanthamine by the internal standard papaverine. *N. benthamiana* infiltrated with *Agrobacterium* harboring EGFP, which was used as a negative control. Three biological replicates were included, and galanthamine was detected in two out of three samples. The bar *LaLrHp*NMT1 represents the mean of the two positive samples with standard deviation. **G**. Comparison of the activity of the mutants of *LaLrHp*NMT1 for the production of galanthamine. Data are shown as means ± SD of three biological repeats with background subtracted. *p* values presented as Dunnett's multiple comparisons test of one-way ANOVA. **** = $p < 0.0001$, *** = $p < 0.001$, ** = $p < 0.01$.

Notably, *Hp*NMT2 exhibited similar catalytic efficiency to *LaLrHp*NMT1, despite containing a serine at position 325 instead of a tyrosine, indicating functional tolerance for this substitution with the enzyme active site. The optimal enzymatic parameters were evaluated for *LaLrHp*NMT1, the most active isoform, by assessing its activity across a pH range from 6.0 to 10.0 and a temperature range of 10 to 70˚C. The enzyme exhibited peak activity *in vitro* at pH 8.5 and 42°C (Fig. 2.4D and 2.4E). To substantiate the enzyme's functionality, we conducted *in vivo* assays by expressing *LaLrHp*NMT1 in *Nicotiana benthamiana* leaves, infiltrating norgalanthamine as substrate (Fig. 2.4F). A significant level of galanthamine ($p < 0.05$) was observed in *N. benthamiana* leaves in two out of three plants. These results showed that *LaLrHp*NMT1 catalyzes norgalanthamine *N*-methylation *in vitro* and *in vivo*.

2.4.5. Mutational analysis reveals essential residues for *LaLrHp*NMT1 activity

Docking analysis suggested that norgalanthamine interacted with several key active site residues. Among them, Glu204, Phe234, and Phe257 were selected as mutation site candidates to enhance the catalytic efficiency of *LaLrHp*NMT1 for *N*-methylation of norgalanthamine. These residues were mutated into amino acids with similar (Phe234Leu/Ala/Trp, Phe257Leu/Ala/Trp, Glu204Asp) or distinct physicochemical properties (Glu204Lys/Gln). Docking simulations were performed to evaluate the potential effects of these mutations on substrate binding. Most mutations did not result in a noticeable change in the binding energy of norgalanthamine within the enzyme pocket, except for two mutations, *i.e.,* Phe257Ala and Glu204Gln, which exhibited a binding energy difference of >1 kcal/mol and an increased distance between SAM and the substrate (Supplementary Table 1.A9). Consequently, these two mutants were excluded as candidates for enhancing enzyme activity. Interaction with catalytic residue His208 was conserved for all mutants except Phe257Ala and Phe257Leu. Similarly, interactions with Glu204 were conserved in Phe mutants, except for Phe257Ala. Mutations of Glu204 led to a conserved interaction with the ligand for Lys204 or Asp204, but not Gln204. The latter resulted in norgalanthamine forming new H-bonds with His80 and Tyr98. Glu204Asp lost hydrophobic bonding with Val333, whereas in Glu204Lys, norgalanthamine lost interactions with Phe234 but not Phe329. In Glu204Gln, a new bond with Phe337 was predicted.

Hydrophobic interaction with Phe329 was observed in all Phe257 mutants and Phe234Leu, while new interaction with Phe337 was predicted for Phe234Ala. Structurally, Phe337 is positioned near Phe234, whereas Phe329 is adjacent to Phe257 in the enzyme active site. Interestingly, the Phe234Trp mutation was predicted to disrupt interactions between the substrate and the active site Phe residues, suggesting that mutations at this position could alter enzyme activity.

To assess the functional impact of these mutations, enzyme activity was evaluated based on the ability of *LaLrHp*NMT1 variants to yield galanthamine (Fig. 2.4G). In addition to the active site mutations tested by docking; two more substitutions were introduced to explore their potential impact on enzyme function. Tyr325Ser was selected because *Hp*NMT2 naturally possesses Ser325, whereas all four other homologs contain Tyr325. Similarly, Leu68 is conserved in *LaLrHp*NMT1 and *Hp*NMT2, while the other three isoforms carry a Pro at this position. A truncated version of the enzyme was generated by removing residues 315–355 to evaluate the importance of the C-terminal region in catalysis. None of the mutations resulted in an increase in norgalanthamine N-methylation. The Glu204Asp mutant and the truncated enzyme variant (315–355Δ) exhibited a complete loss of activity ($p < 0.0001$). Phe234Trp ($p < 0.0001$) and Tyr325Ser ($p < 0.0001$) mutants resulted in a significant reduction in galanthamine production. Glu204Lys ($p = 0.0022$), Phe257Leu ($p = 0.0159$), and Phe257Trp ($p = 0.0027$) retained

lower but detectable levels of activity. Leu68Pro, Phe234Leu, and Phe234Ala did not result in a significant modulation of galanthamine production. These mutational analyses highlight how conserved residues such as Glu204 and Phe234 form the catalytic framework for substrate binding and orientation, while peripheral residues like Phe329 provide structural flexibility that supports the observed substrate promiscuity..

2.4.6. *LaLrHp*NMT1 is promiscuous

To investigate the substrate promiscuity of the CNMT-like enzyme *LaLrHp*NMT1, we tested its ability to convert 18 different substrates possessing free hydrogen on the nitrogen (Supplementary Figure 1.A3), making them potential candidates for *N*-methylation. Methylation activity was confirmed by detecting both a decrease in substrate concentration and the appearance of a new signal in ESI^+ mode with a mass-to-charge ratio (m/z) corresponding to the molecular weight of the expected methylated product ($[M+H+14]^+$). The tested substrates included aromatic amino acids (phenylalanine, tryptophan and tyrosine), amines (tryptamine, tyramine, *N*-methyltyramine, hordenine), AAs (norgalanthamine, norbelladine, 3′-*O*-methylnorbelladine, 3′,4′-*O*-dimethylnorbelladine, 4′-*O*-dimethylnorbelladine) and *N*-demethylated plant alkaloids (huperzine, heliamine, coclaurine, *N*-demethylricinie) (Supplementary Figure 1.A3).

*LaLrHp*NMT1 demonstrated *N*-methylation activity on eight substrates: heliamine (42.23%), huperzine A (28.76%), norgalanthamine (25.11%), tryptamine (25.03%), tyramine (24.09% converted), 3′,4′-*O*-dimethylnorbelladine (15.84%), 3′-*O*-methylnorbelladine (8.64%), *N*-desmethylivabradine (2.49%) (Fig. 2.5). Among them, heliamine, a basic tetrahydroisoquinoline structure, was most efficiently converted substrate, consistent with its known role as a preferred substrate of CNMTs (Bennett *et al.*, 2018b). While *LaLrHp*NMT1 did not methylate aromatic amino acids, it accepted their decarboxylated amines, tryptamine and tyramine, at levels comparable to norgalanthamine (~25%). Interestingly, despite clustering phylogenetically with CNMT enzymes (Fig. 2.3A), *LaLrHp*NMT1 did not accept coclaurine as a substrate. It catalyzed the *N*-methylation of 3′-*O*-methylnorbelladine and 3′,4′-*O*-dimethylnorbelladine but not of norbelladine or 4′-*O*-methylnorbelladine (Fig. 2.5), suggesting that methylation at 3′-*O* position may be required for *in vitro* enzyme activity.

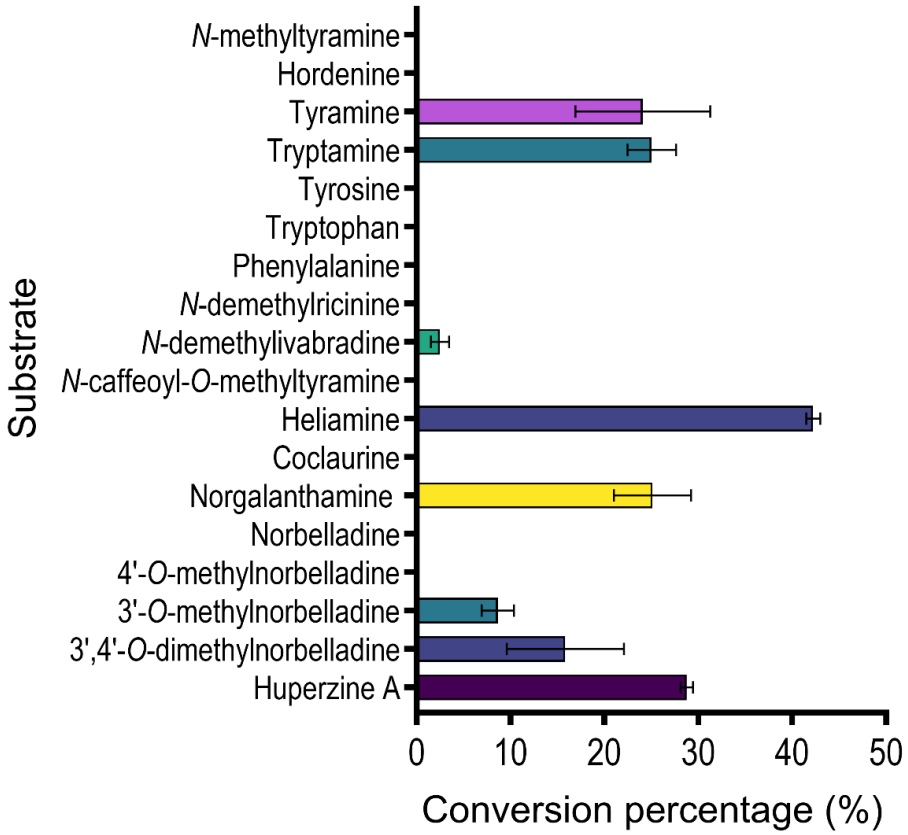

Fig. 2.5. Substrate specificity of *LaLrHp*NMT1 tested with multiple demethylated substrates. *N*-methylation catalysis was considered significant when both a decrease in substrate amount and detection of a signal with m/z corresponding to the molecular weight of the expected product ionized in ESI^+ with an added mass of +14 m/z ($[M+H+14]^+$) were considered. The conversion percentage was calculated as the decrease in substrate compared to the negative control, i.e., heat-deactivated enzyme. Values are presented as mean ± SD with three independent replicates.

2.4.7. *LaLrHp*NMT1 localizes in the cell cytoplasm, and ER

Key enzymes involved in the AA biosynthetic pathway in *L. aestivum*—*La*NBS, *La*NR, and *La*N4′OMT—are localized in the cytosol, while *La*CYP96T is associated with the endoplasmic reticulum (ER) (Lamichhane *et al.*, 2025; Majhi *et al.*, 2023). To determine the

subcellular localization of *LaLrHp*NMT1, we expressed both N- and C-terminal enhanced green fluorescent protein (eGFP)-tagged constructs and assessed their distribution in plant cells (Fig. 2.6). The integrity of the fusion proteins was confirmed via western blot (Supplementary Figure 1.A5). Fluorescence microscopy revealed similar localization between the two constructs (Fig. 6). Both the N- and C-terminally tagged *LaLrHp*NMT1 constructs displayed strong fluorescence signals in the cytosol as well as the ER (Fig. 6), indicating a dual site localization pattern.

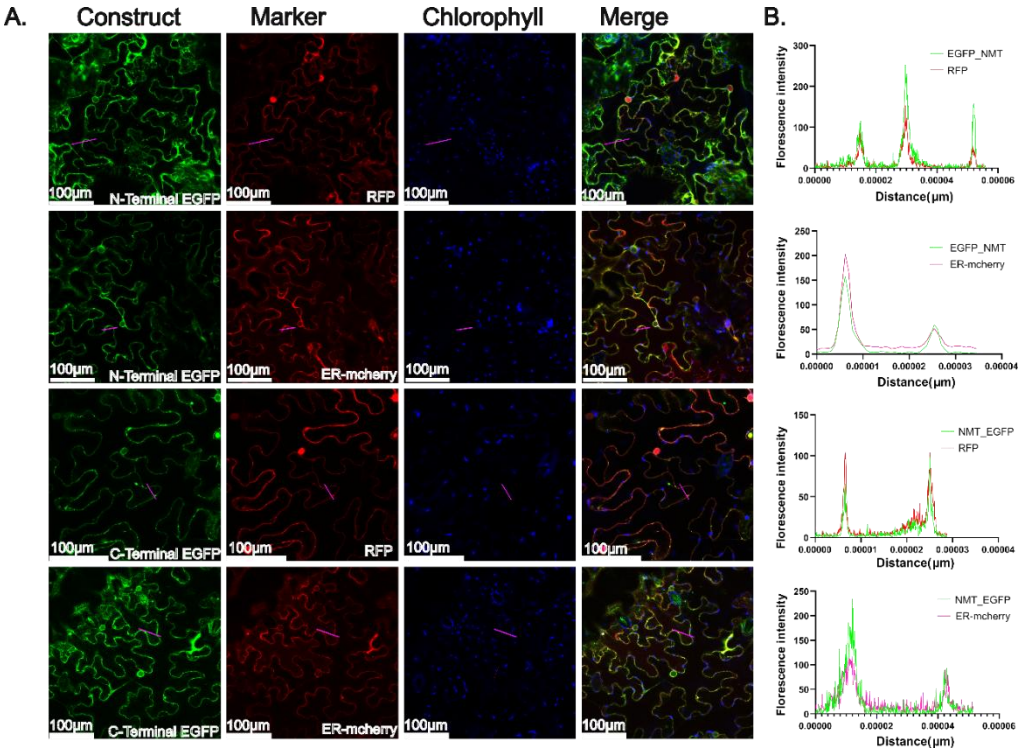

Fig. 2.6. *LaLrHp*NMT1 localizes in the cytoplasm and endoplasmic reticulum. **A.** Subcellular localization of eGFP-tagged NMT. N- and C-terminal GFP fusion *LaLrHp*NMT1 was co-expressed with red fluorescent protein (RFP) or ER-mCherry constructs in the epidermal cell of *Nicotiana benthamiana* leaves, and images were taken after 48 h with confocal microscopy. Panels 1 and 3 display *LaLrHp*NMT1-eGFP with RFP, whereas Panels 2 and 4 show *LaLrHp*NMT1-eGFP with ER-mCherry. For all panels, chlorophyll and merge images, along with **B.** fluorescent intensity during co-localization, are shown in the graph. The scale bar represents 100 µm.

2.4.8. Up-regulation of *NMT* expression under different environmental stresses

The current supply of galanthamine primarily depends on plant extraction (Berkov *et al.*, 2022). *In vitro,* shoot culture has been extensively studied as a more sustainable and cost-effective means of producing AAs (Berkov *et al.*, 2022; Koirala *et al.*, 2022; Ptak *et al.*, 2016; Ptak *et al.*, 2020), and it is well established that environmental stresses can act as potent inducers of alkaloid biosynthesis (Ali *et al.*, 2019; Koirala *et al.*, 2023). In this study, we examined the effects of different environmental stressors on *H. papilio* shoot cultures by evaluating relative gene expression levels of NMT and alkaloid production at 6, 24, and 48 h post-treatment (Fig. 2.7, Supplementary Figure 1.A8-15). Chemical stress inducers included methyl jasmonate (MeJA), the bacterial toxin coronatine, $CdCl_2$, saline (NaCl), and sodium nitroprusside (SNP). Physical stressors included cold (4°C), heat (35°C), and drought (PEG6000).

Intriguingly, *NMT* expression responded to all tested stress conditions, with a 1.2- to 6.4-fold increase in expression compared to controls (Fig. 2.7). Heat stress had the most pronounced and sustained effect, with a mean relative gene expression of 6.464 ± 1.179. Other stressors, such as coronatine, $CdCl_2$, saline, cold, and drought, triggered a sharp increase in *NMT* levels within the first 6-24 hours, followed by a gradual

decline, though expression remained significantly elevated compared to untreated controls. For example, MeJA treatment resulted in a 1.345 ± 0.12 increase in relative *NMT* expression after 6 hours, which rose to 3.132 ± 0.403 at 24 hours before decreasing to 2.048 ± 0.271 at 48 hours (Fig. 2.7).

Concomitant targeted metabolite analysis revealed that galanthamine accumulation varied under different stress conditions (Supplementary Fig. 1.A8-A16), especially after adding MeJA, coronatine, heat, and $CdCl_2$. There was no positive correlation between levels of galanthamine and *NMT* gene expression (Pearson r = -0.02368, p = 0.9048). Nonetheless, there was a positive correlation with narwedine (Pearson r = 0.3823, p = 0.0447), 11-hydroxyvittatine (Pearson r = 0.5326, p = 0.0035) and crinine/vittatine (Pearson r =0.5256, p = 0.0041) (Supplementary Table 1.A9). These correlations further support the involvement of NMT in the AA biosynthetic pathway.

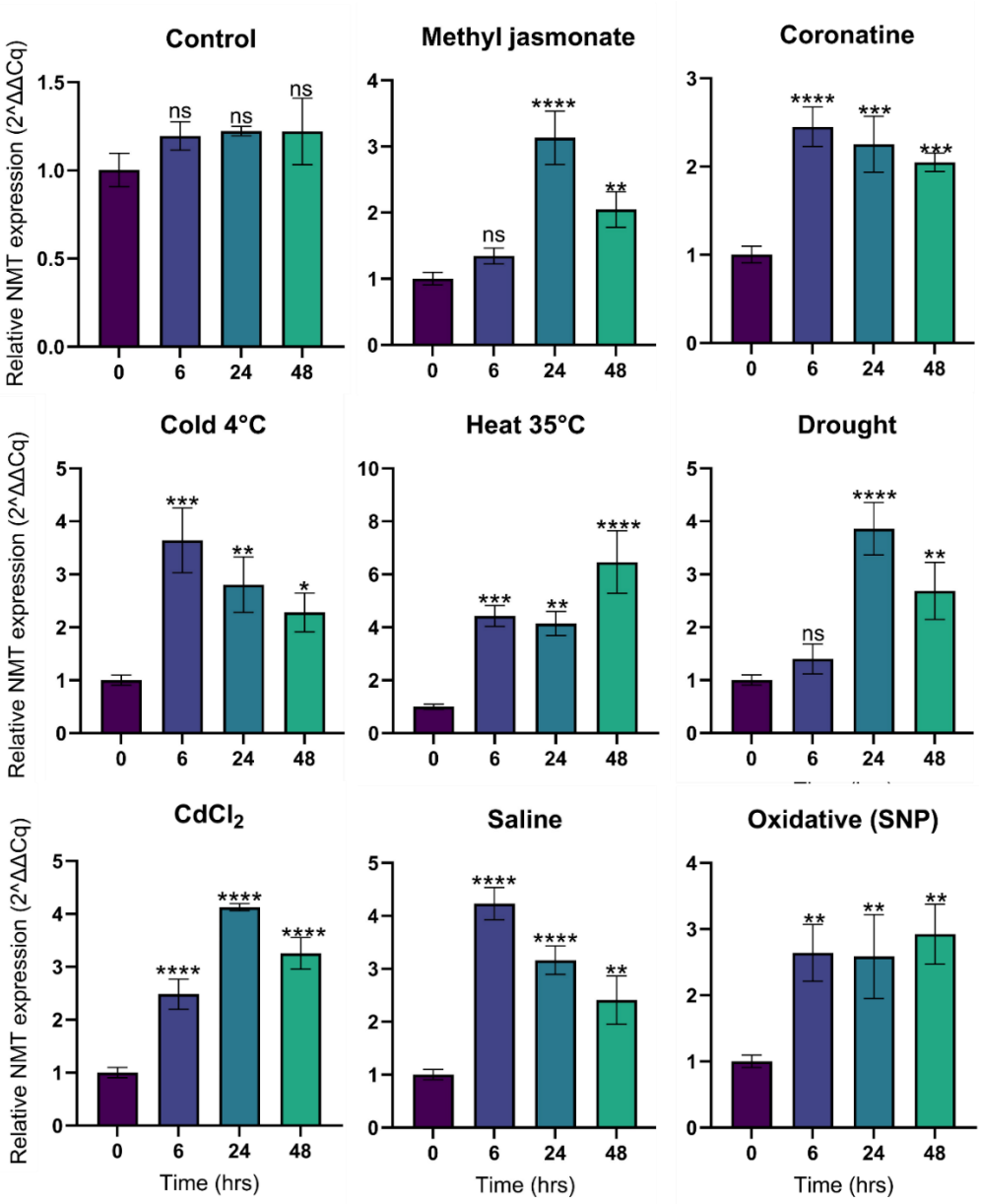

Fig. 2.7. Relative expression patterns of *NMT* following stress treatments of *H. papilio* shoot cultures. Shoots liquid cultures were treated with different stresses: methyl jasmonate, coronatine, cold (4°C), heat (35°C), drought (20% PEG6000), $CdCl_2$, saline (NaCl), and sodium nitroprusside (SNP) for oxidative stress, for 48 hours. RT-qPCR measured relative *NMT* expression with samples collected at 6-, 24-, and 48-hour intervals and normalized to the housekeeping gene *Am_Histone3*. The *NMT* expression of the control at 0 hrs was taken as the relative expression 1.00 ($2^{-(\Delta\Delta Ct)}$); the values are shown as means ± standard deviation of three independent biological replicates. All the *in vitro* shoots were derived from a single *H. papilio* bulb and grown for 6 months before the experiment. Dunnett's multiple comparisons test of one-way ANOVA was used to assess statistical significance. **** = $p < 0.0001$, *** = $p < 0.001$, ** = $p < 0.01$, * = $p < 0.1$, ns = p values are not significant.

2.5. Discussion

The present study focused on the functional characterization of CNMT-like NMT in Amaryllidaceae. First, to investigate a potential link between *CNMT-like NMT* expression and galanthamine biosynthesis, we measured transcript expression and alkaloid levels in different tissues of three Amaryllidoideae species. *H. papilio* displayed the highest quantities of galanthamine across all tissues (Fig. 2.2B), aligning with previous studies highlighting this species as a rich source (Berkov *et al.*, 2022). Although this species displayed the highest levels of *NMT* expression as well, the two factors, *i.e.,* galanthamine and transcript levels, were not correlated regarding their repartition across tissues. *NMT* was expressed across tissues of *L. radiata*, but galanthamine was undetectable in the leaves and roots (Fig. 2.2), suggesting that its accumulation may be highly species- and tissue-specific.

A recent study proposed that young leaves are the preferential site of AA biosynthesis in Amaryllidaceae, a result consistent with the higher expression of our candidates in the three here-studied species(Mehta *et al.*, 2024). However, other studies comparing gene expression of other key enzymes implicated in the early AA pathway, such as NBS, NR, and OMT in *L. aestivum* and *L. radiata,* have indicated that the biosynthetic origin of AA is not clear, and transcripts levels do not necessarily correlate with enrichment in AA. For example, relative gene expression

of *NBS* is higher in roots, while *NR* and *OMT* transcript levels are enriched in bulbs of *L. aestivum* and *L. radiata* at the flowering stage, and galanthamine accumulates more in the bulbs (Karimzadegan *et al.*, 2024; Li *et al.*, 2019; Majhi *et al.*, 2023). During the vegetative stage of *N. papyraceus, OMT* and *NR* expression were higher in bulbs, and *NBS* was enriched in roots that contained more AAs (Koirala *et al.*, 2024). These differences imply that AAs' biosynthetic pathways and accumulation sites may vary significantly by environment, species, tissue type, and growth stage. The blooming season may also impact gene expression, suggesting that AA biosynthesis is complex and not restricted to a uniform tissue-specific pattern across different species. These findings indicate that galanthamine accumulation is not solely determined by the transcript expression of AA biosynthetic enzymes, such as *NMT*, and that additional factors, such as enzyme activity, substrate availability, transport mechanisms, or regulatory pathways, may influence its distribution across tissues.

Among the identified isoforms, *LaNMT1, LrNMT1*, and *HpNMT1* encoded an identical protein sequence, suggesting strong conservation across species. The theoretical molecular weights of all five isoforms identified in this study were consistent with previously characterized CNMT-like NMTs, such as *Si*CNMT1 and *Si*CNMT2 from *Stephania intermedia* and *Nn*CNMT from *Nelumbo nucifera* (Chen *et al.*, 2024; Zhao *et al.*, 2020), indicating a conserved structural profile. However, the

predicted isoelectric points were generally similar, except *HpNMT2*, which displayed a notably higher pI, potentially reflecting differences in biochemical properties or stability.

The phylogenetic clustering patterns of CNMTs from *N. nucifera* and *S. intermedia* with target Amaryllidaceae NMTs, along with their proximity to the phenylalkylamide NMT from *E. sinica* (Fig. 2.3), suggests a conserved evolutionary trajectory likely linked to structural requirements for methylation in isoquinoline-based molecules (Chen *et al.*, 2024; Morris *et al.*, 2018; Rønsted *et al.*, 2012; Zhao *et al.*, 2020). Amaryllidaceae NMTs may have evolved from a common ancestral NMT, which later diverged to facilitate specialized alkaloid biosynthetic pathways, including AA and BIA. In contrast, the divergence of CNMTs from *T. flavum*, *L. chinense*, *S. hexandrum*, *A. fimbriata*, and *C. japonica* into a separate clade may indicate functional specialization or lineage-specific adaptations within their plant families (Cheng *et al.*, 2022b). This phylogenetic distance aligns with the hypothesis that evolutionary pressures have driven substrate specificity and catalytic function diversification, particularly in pathways involving coclaurine or similar intermediates in alkaloid biosynthesis. The clustering of phenylalkylamide *Es*NMT within the same group suggests a shared methylation mechanism among species and potentially reflects convergent evolution in the biosynthesis of phenylalkylamide and isoquinoline (AA) alkaloids despite taxonomic divergence (Morris *et al.*,

2018). The phylogenetic analysis points to an earlier evolutionary split between gymnosperm and angiosperm NMTs, reinforcing the idea that selective pressures across diverse plant lineages have driven the structural convergence of NMTs, optimizing their function in alkaloid biosynthesis.

The conservation of catalytic motifs across the Amaryllidaceae NMTs and BIA-pathway NMTs supports a shared evolutionary origin and suggests functional conservation in alkaloid biosynthesis. Glu204 and His208 as a catalytic dyad in CNMTs and their implication in substrate stabilization and methyl transfer indicate that similar enzymatic mechanisms may be at play in the studied candidates. The serine substitution at position 325 in *Hp*NMT2 could reflect a substrate specificity or enzyme activity divergence, possibly linked to species-specific adaptations in alkaloid metabolism. Overall, the sequence and structure analysis highlight the conservation of catalytic domains coclaurine-like NMTs from AA and BIA biosynthesis (Lee *et al.*, 2024; Morris and Facchini, 2019). The structural folding analysis of the Amaryllidaceae NMT isoforms indicates that they could accommodate isoquinoline alkaloids as potential substrates for *N*-methylation, supporting the functional link between these enzyme families.

The *in vitro* assays confirmed that all five heterologously produced Amaryllidaceae NMT isoforms catalyze the *N*-methylation of

norgalanthamine to galanthamine (Fig. 2.4), supporting their functional role in AA biosynthesis. *LaLrHp*NMT1 and *Hp*NMT2 were the most potent, yielding 4-5-fold more galanthamine than other isoforms. The most active isoform, *LaLrHp*NMT1, exhibited peak activity *in vitro* at pH 8.5 and 42°C (Fig. 2.4). Its expression in *Nicotiana bethamiana* leaves confirmed its activity *in vivo*. CNMTs from BIA-producing plants, such as *N. nucifera* and *S*. *intermedia*, have been reported to function optimally with a basic pH range (7.5 to 9) and at temperatures between 35 and 45°C *in vitro* (Chen *et al.*, 2024; Zhao *et al.*, 2020). Optimal activity conditions of NMTs may differ due to evolutionary adaptation to different biochemical environments and substrate specificities. These findings confirm that the putative NMT isoform identified in *H. papilio*, *L. aestivum,* and *L. radiata* catalyzes the *N*-methylation of norgalanthamine, a key step in galanthamine biosynthesis.

The variability in catalytic efficiency across the tested enzymes suggests that specific amino acid substitutions significantly influence enzymatic activity. Several mutations targeting Leu68, Glu204, Phe234, Phe257, and Tyr325 were introduced to understand the role of specific polymorphic residues or to confirm their role in the active site. In the active site, Phe234Trp mutation resulted in a loss of activity and hydrophobic interaction with the 234th residue and Phe257. By contrast, Phe234Leu conserved enzyme activity and interaction with Phe329 and the 234th mutated residue. Phe257Trp exhibited reduced activity despite

conserving norgalanthamine interaction with Phe234 and gaining Phe329 hydrophobic bond. A previous study showed that Phe257Ala mutation in *Nn*CNMT increased the production of nuciferine more than two-fold (Chen *et al.*, 2024). This particular mutation was not performed here as the docking simulation predicted >1 kCal/mol difference and an increased distance between SAM and norgalanthamine. This suggests that Phe234 and Phe257 are not essential for catalysis but could contribute to substrate orientation. The larger size of tryptophan might explain why it did not fully substitute for Phe at this position.

Despite the similar nucleophilic nature of Glu and Asp, Glu204Asp resulted in a complete loss in activity. The slight difference in pKa could lead to a subtle difference in enzyme activity at the pH used for the enzyme reaction (Herrington and Kellogg, 2021). The loss could also be caused by the difference in the size of the two amino acids. Surprisingly, replacement with Lys (Glu204Lys), despite introducing an opposite charge at pH 8.5 (protonated Lys versus deprotonated Glu), resulted only in a modest reduction of activity. This suggests that while Lys cannot replicate the exact electrostatic environment of Glu, its side chain length and capacity to form alternative hydrogen bonds (as predicted *in silico* with Phe329) partially compensate for the catalytic function. Previous studies on CNMTs showed that flipping the amino acids from Glu204Gly and Gly204Glu resulted in a loss of catalysis of the canonical substrate (Morris *et al.*, 2020).

Two additional residues were mutated, Leu68Pro and Tyr325Ser. Further from the ligand, Tyr325 was shown to be important for the reaction catalyzed by other CNMTs (corresponding to Tyr328)(Bennett *et al.*, 2018b). Interestingly, *Hp*NMT2, which showed high galanthamine synthesis catalysis, contained instead for Ser325. Similarly, while *LaLrHp*NMT1 and *Hp*NMT2 displayed Leu at the 68th position, other isoforms, with less activity, encoded for a proline. Thus, we tested if the corresponding mutations would alter *LaLrHp*NMT1 activity. While Leu68Pro had no significant impact, Tyr325Ser resulted in a drastic decrease in *LaLrHp*NMT1 enzyme activity. This finding is consistent with a previous study (Bennett *et al.*, 2018b), suggesting that mutating Ty325 impacts substrate positioning or active site conformation. However, the results also indicate that the required residue at this position is context-dependent, as *Hp*NMT2 with Ser325 had high activity. Overall, the results strengthen the evidence that Glu204, Phe234, Phe257, and Tyr325 play a key role in norgalanthamine *N*-methylation in the enzyme active site. While the role of His208 is well known (Bennett *et al.*, 2018b), other key ligand interacting residues, such as Tyr288 and Val333, remain to be characterized.

Subcellular localization of NMTs varies across different biosynthetic pathways. For instance, the NMT involved in monoterpenoid indole alkaloid biosynthesis, which catalyzes the final step of vinblastine production, is chloroplastic (Dethier and De Luca, 1993). In contrast,

CNMT and TNMT from *P. somniferum* (opium poppy) localized in the cytosol (Facchini and St-Pierre, 2005; Hagel and Facchini, 2012). The dual cytosolic and ER localization of *LaLrHp*NMT1 (Fig. 2.6) suggests potential involvement in intracellular transport mechanisms or interactions with ER-associated proteins. This is consistent with the dynamic interplay between cytoplasmic and ER functions in cellular signaling pathways (Liu and Li, 2019). Based on these results, *LaLrHp*NMT1 likely catalyzes the final step of galanthamine synthesis at the cytosol-ER interface in Amaryllidaceae cells, where other pathway enzymes are produced and localized (Fig. 2.8).

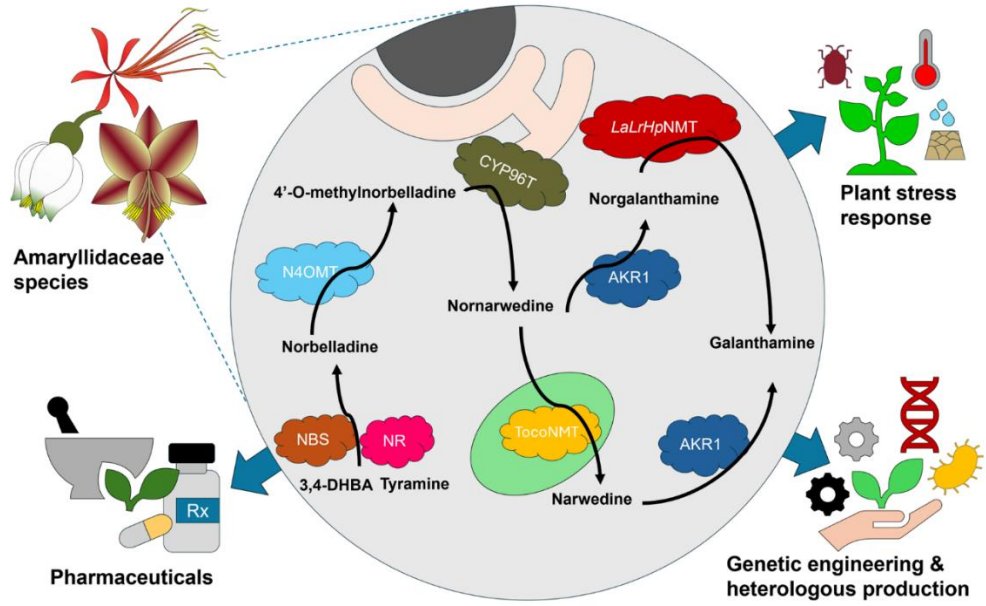

Fig. 2.8. Schematic representation of galanthamine biosynthesis and translational potential in Amaryllidaceae species. This integrative model highlights the enzymatic steps, subcellular localization, and biotechnological implications of galanthamine biosynthesis. **Top left**: Representative Amaryllidaceae species (*Leucojum aestivum*, *Lycoris radiata*, *Hippeastrum papilio*) used in this study which naturally produce galanthamine. **Center**: A magnified schematic of a plant cell illustrating the subcellular distribution of biosynthetic enzymes. Cytosolic enzymes are shown freely in the cytoplasm; *LaLrHp*NMT and other biosynthetic enzymes (NBS, NR, N4OMT, AKR1) catalyze sequential reactions. CYP96T, a cytochrome P450 enzyme, is localized on the cytosolic face of the endoplasmic reticulum (ER) membrane, while a putative chloroplast-localized TocoNMT is also depicted, suggesting possible plastidial

involvement. Black arrows indicate the direction of metabolic flow toward galanthamine. **Outer panels**: Blue arrows point to downstream implications: regulation by plant stress responses, potential for genetic/metabolic engineering & heterologous production, and pharmaceutical relevance (e.g. for treating Alzheimer's disease).

CNMTs are a well-known group of enzymes in the BIA pathway, which are characterized by several phylogenetically distinct plant families [39, 49, 58]. In almost all of them, the primary substrates are *(S)*- or *(R)*-coclaurine, while there are other BIA substrates [58]. The observed substrate promiscuity of *LaLrHp*NMT1 (Fig. 5) aligns with several reports on CNMTs from various plant species (Morris and Facchini, 2019). For example, CNMTs from *E. sinica* catalyze *N*-methylation across structurally diverse compounds, including phenylalkylamines, tryptamine alkaloids, tetrahydroisoquinoline alkaloids, β-carboline, and BIAs (Morris *et al.*, 2018). Similarly, CNMT2 from *Stephania intermedia* exhibits broad specificity, catalyzing the *N*-methylation of norcoclaurine, *N*-methylnorcoclaurine, *N*,*N*-dimethylnorcoclaurine, and magnocurarine (Zhao *et al.*, 2020). The CNMT from *L. chinense* catalyzes methylation of coclaurine, *N*-methylcoclaurine, norarmepavine and armepavine (Cheng *et al.*, 2022b; Zhao *et al.*, 2020). Conversely, some CNMTs, such as those from *N. nucifera*, display higher substrate specificity, only methylating nuciferine among ten tested isoquinoline, BIA, and aporphine alkaloids (Chen *et al.*, 2024). Here, we report a few novel reactions catalyzed by CNMT-like NMTs, which are involved in a different alkaloid biosynthetic pathway than BIA. The ability of *LaLrHp*NMT1 to methylate pathway precursors such as tyramine and

3′-*O*-methylnorbelladine suggests a potential role in additional biochemical steps of AA biosynthesis, maybe towards belladine-type AAs (Fig. 2.1). This broad specificity may reflect an adaptive advantage, allowing plants to fine-tune alkaloid biosynthesis by expanding the range of intermediates available for downstream modification.

Studies in other plant species have shown that *NMT* expression responds dynamically to environmental challenges, consistent with our findings in *H. papilio* shoot cultures under various stress conditions (Fig. 2.7). For example, salinity, drought, and wounding stressors have been reported to up-regulate expression of *NMT* involved in caffeine biosynthesis, potentially helping the plant defense mechanisms and the regulation of key metabolites for stress resilience (Zhou *et al.*, 2020b). Similarly, MeJA, a key mediator of plants' responses to biotic and abiotic stresses, has been shown to up-regulate *NBS* in *L. longituba* while down-regulating *CYP96T1* (Jan *et al.*, 2021; Li *et al.*, 2021). Other Amaryllidaceae-related enzymes, such as *O*-methyltransferases, also exhibit stress-responsive expression patterns (Koirala *et al.*, 2023; Li *et al.*, 2021; Sun *et al.*, 2018). In *Lycoris aurea* roots, cold (4˚C), SNP, MeJA, PEG, and NaCl treatments up-regulated *norbelladine 4'-OMT* expression, whereas abscisic acid down-regulated it. The observed up-regulation of *OMT* (Li *et al.*, 2021; Sun *et al.*, 2018) and *NMT* (present study) under stress conditions suggests a broader role for methyltransferases in modulating biosynthetic pathways in response to

environmental cues, potentially aiding plant protection. The targeted alkaloid analysis also supports this idea. Although the correlation between galanthamine and relative *NMT* expression was not evident, some treatments like MeJA and coronatine increased galanthamine production compared to the controls. Another *N*-methylated AA, i.e., narwedine, strongly correlated with the *NMT* expression. This could be due to the function of each metabolite in response to specific stress conditions. For example, some studies suggest that galanthamine has an antibacterial activity, and coronatine is a bacterial toxin (Ločárek *et al.*, 2015). Our findings indicate that interactions between multiple stress-responsive signaling pathways may fine-tune alkaloid production in the Amaryllidoideae subfamily. Given that specialized metabolites, such as alkaloids, often serve protective functions under stress, our results suggest that NMT may play a role in the plant's adaptive response to high temperatures and other environmental challenges.

Another recently characterized NMT from *Narcissus* cv. Tête-à-Tête, a tocopherol methyltransferase-like named TocoNMT, catalyzed the conversion of nornarwedine to narwedine (Fig. 1), another intermediate in galanthamine biosynthesis but did not *N*-methylate norgalanthamine (Mehta *et al.*, 2024). The proposition of an alternate path towards *N*-methylation is consistent with previous studies indicating that multiple distinct enzymatic routes contribute to galanthamine production(Eichhorn *et al.*, 1998). Tissue-specific expression patterns

suggest that different pathways might be optimized for distinct plant organs, such as bulbs for storage or leaves for defense. Metabolic flexibility and redundancy allow plants to maintain alkaloid production even if environmental changes or genetic mutations disrupt one pathway. Evolutionary convergence from ancestral enzyme families could have led to the recruitment of different enzymatic routes, while enzyme promiscuity may have facilitated pathway divergence. Additionally, compartmentalizing biosynthetic steps across different organelles and regulating intermediate pools ensure metabolic efficiency. Given galanthamine's potential role in plant defense, having multiple biosynthetic routes may also enhance adaptability to varying biotic pressures, such as herbivore predation or microbial attack. These factors collectively contribute to the evolutionary advantage of maintaining distinct but converging pathways for galanthamine biosynthesis (Fig. 2.8).

2.6. Conclusion

In this study, we identified, isolated, and characterized a set of CNMT-like NMTs from three key Amaryllidaceae species. We demonstrate their critical role in the catalysis of norgalanthamine *N*-methylation, indicating a new and alternative route for galanthamine biosynthesis. These enzymes, particularly *LaLrHp*NMT1, exhibit high structural and functional conservation with known NMTs from BIA pathways and

display notable substrate promiscuity. Flexible docking and *in vitro* assays confirmed that *LaLrHp*NMT1 catalyzes the *N*-methylation of norgalanthamine—a pivotal step in galanthamine production—and that subtle amino acid variations can significantly affect catalytic efficiency. Moreover, subcellular localization studies placed *LaLrHp*NMT1 at the cytosol-ER interface, suggesting a coordinated role with other biosynthetic enzymes in these cellular compartments. Our investigation into the stress-responsive expression of NMTs further indicates that environmental cues, such as heat, salinity, and chemical elicitors like MeJA, modulate the expression of these enzymes. This dynamic regulation likely contributes to the adaptive capacity of plants by fine-tuning alkaloid biosynthesis in response to fluctuating environmental conditions. Such plasticity underpins the evolutionary advantage of maintaining multiple enzymatic pathways for galanthamine synthesis and opens avenues for metabolic engineering aimed at sustainable galanthamine production. Collectively, our results deepen the understanding of the molecular and biochemical underpinnings of alkaloid biosynthesis in Amaryllidaceae and highlight the potential of leveraging these insights to enhance the production of valuable specialized metabolites for pharmaceutical applications. Future research focusing on the regulatory networks and protein-protein interactions at the cytosol-ER interface may further elucidate the integration of these pathways and inform strategies for biotechnological intervention.

2.7. Acknowledgments

The authors thank lab mates Dr. Karen Cristine Goncalves dos Santos, Dr. Manoj Koirala, Dr. Narimane Fradj, and Dr. Bharat Bhusan Majhi for their valuable input and contributions. We also thank Mélodie B. Plourde, Dr. Snehi Gazal, and Prof. Hugo Germain (Université du Québec à Trois-Rivières, QC, Canada) for the sub-cellular localization vectors for assisting with the confocal microscopy. Warm thanks to Xiwei Chen (China) for providing *Lycoris radiata* bulbs and Prof. Antonio Evidente (Institute of Biomolecular Chemistry, National Research Council, Via Campi Flegrei, Pozzuoli, NA, Italy) for providing some alkaloid standards. While preparing this work, the authors used ChatGPT version 4.0, a free AI language model, and Grammarly to correct grammatical errors and enhance readability. After using these tools, the authors reviewed and edited the content as needed and took full responsibility for the publication's content. This research was funded by Canada Research Chair on plant specialized metabolism Award No CRC-2018-00137 to I.D-P. Thanks are extended to the Canadian taxpayers and the Canadian government for supporting the Canada Research Chairs Program. Additional support from the the Natural Sciences and Engineering Research Council of Canada (NSERC) award number RGPIN/3218-2021 to IDP. This work was also supported by the NSERC award number EQPEQ 472990-2015 (Research tools and instruments) for the acquisition of the rt-qPCR and the Canada Foundation for

Innovation program John R. Evans Leaders Fund for the acquisition of the LC-qqq-MS.

CHAPTER III

This chapter contains a study that presents the spatial arrangement of Amaryllidaceae alkaloids and their biosynthetic intermediates of a high galanthamine-producing Amaryllidaceae species, *Hippeastrum papilio*, using matrix-assisted laser desorption ionization- mass spectrometry imaging (MALDI-MSI). The chapter was written in an article format to submit to Journal of Experimental Botany; however, the content unavoidably overlaps with that of other chapters.

Contribution: Nuwan Sameera Liyanage: Conceptualization, Methodology, Experiments, Analysis, Writing- Original draft, Writing- Reviewing and Editing; Natacha Merindol: Multivariate analysis, supervision, Writing- Reviewing and Editing; Sajjad Sobhanverdi: qRT-PCR Experiments, Writing- Reviewing and Editing; Kenneth Munk Pedersen: LC-MS and analysis; Christian Janfelt: Conceptualization, Methodology, Resources, supervision, funding acquisition, Writing- Original draft, Writing- Reviewing and Editing Isabel Desgagné-Penix: Resources, supervision, funding acquisition, Writing- Original draft, Writing- Reviewing and Editing.

3. Dissecting specialized metabolism in space: A MALDI-MSI atlas of Amaryllidaceae alkaloids in *Hippeastrum papilio* (Ravenna) Van Scheepen.

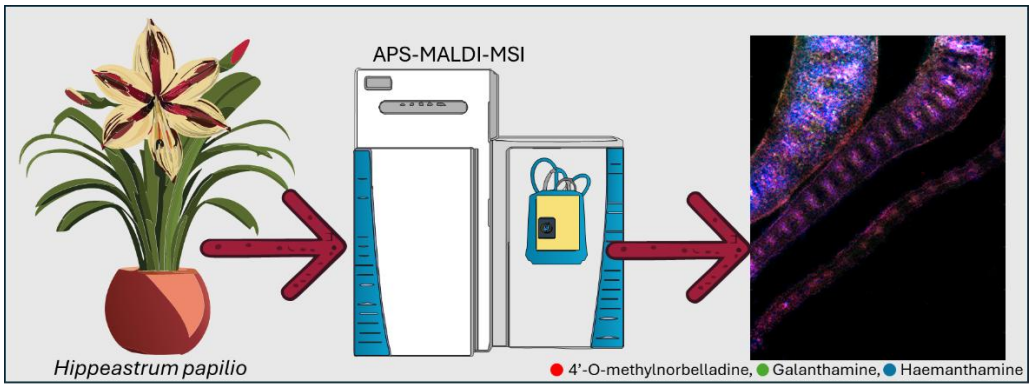

Nuwan Sameera Liyanage[1], Natacha Mérindol[1],Sajjad Sobhanverdi[1], Kenneth Munk Pedersen[2], Christian Janfelt[2], Isabel Desgagné-Penix[1,3] *

[1]Department of Chemistry, Biochemistry and Physics, Université du Québec à Trois-Rivières, Trois-Rivières, QC, Canada.

[2]Toxicology and drug metabolism group, Department of Pharmacy, University of Copenhagen, Universitetsparken 2,

DK-2100 Copenhagen, Denmark

[3]Plant Biology Research Group, Université du Québec à Trois-Rivières Trois-Rivières, Québec, Canada.

Keywords: Amaryllidaceae alkaloids; Spatial metabolomics; Galanthamine; Haemanthamine; Metabolite transport; Epidermis; Mass spectrometry imaging; Metabolite localization; Vascular tissues

3.1. Abstract

Amaryllidoideae produce specific specialized metabolites known as Amaryllidaceae alkaloids (AAs), extensively studied for their significant pharmacological potential. AAs' spatial distribution and biosynthesis within plant tissues remain poorly understood. This study investigates organ- and tissue-specific localization in *Hippeastrum papilio*, from precursors to galanthamine and haemanthamine, using matrix-assisted laser desorption/ionization mass spectrometry imaging. Consistent accumulation of AAs was observed in epidermal and vascular tissues, with leaves exhibiting a uniform distribution across all ages and positions. Bulbs exhibited higher concentrations in the outer-scales and basal-plates, while roots displayed compartmentalized patterns, with galanthamine being uniquely abundant in the vascular bundles. Haemanthamine and galanthamine were detected in high quantities in the leaves' and bulbs' mucilage, while precursors were scarce. Multivariate analyses revealed that precursors clustered separately from end-products and were specifically enriched in the middle-scales and apical leaves of the bulbs. Nonetheless, biosynthetic intermediates were observed in all tissues, indicating widespread AA biosynthesis across all organs. Transcript analysis confirmed that multiple biosynthetic genes are differentially expressed across leaves, bulbs, and roots, consistent with the widespread and multi-organ biosynthesis of Amaryllidaceae alkaloids revealed by MSI.These findings suggest a coordinated

metabolic network in *H*. *papilio*, which challenges existing hypotheses on organ-specific AA biosynthesis and hints at the transport of end-products. This study refines current models of alkaloid biosynthesis and underscore the value of *H. papilio* as a promising resource for sustainable production of therapeutic AAs.

3.2. Introduction

The Amaryllidaceae (*s.s.*) comprises diverse flowering plants commonly known as amaryllis or daffodils, with notable ecological, ornamental, and pharmacological significance (Berkov *et al.*, 2020). Belonging to the order Asparagales, this family includes approximately 75 genera with around 900 species, primarily characterized by their bulbous growth forms, linear leaves, and showy, often fragrant flowers (Meerow and Snijman, 1998; Meerow *et al.*, 2020). They exhibit a cosmopolitan distribution, with species native to various temperate, tropical, and subtropical regions across the globe. Most Amaryllidaceae are concentrated in South America and southern Africa, serving as biodiversity hotspots for the family (Meerow, 2023; Rønsted *et al.*, 2012). Other notable areas of diversity include the Mediterranean basin, Southeast Asia, and parts of Australia (Meerow, 2023). These plants are typically adapted to environments ranging from arid and semi-arid conditions to more mesic habitats, including grasslands and forest understories (Meerow and Snijman, 1998). Their ability to thrive across diverse ecological niches has contributed to their widespread cultivation

and naturalization beyond their native ranges (Meerow and Snijman, 1998). Species such as *Amaryllis belladonna*, *Leucojum aestivum* (snowdrops), *Lycoris radiata* (spider lilies), *Nerine*, *Narcissus* hybrids (daffodils), and *Hippeastrum* hybrids are widely grown as ornamental plants in gardens, parks, and indoor settings.

Beyond their ornamental appeal, the Amaryllidaceae family holds significant medicinal value. For centuries, traditional medicine systems in various cultures have employed these plants to treat ailments ranging from skin disorders and wounds to more complex conditions such as epilepsy and inflammation (Jin and Yao, 2019; Nair and van Staden, 2013). Ethnopharmacological practices often rely on bulbs and leaves (Desgagné-Penix, 2021; Jayawardena *et al.*, 2024; Nair and van Staden, 2013; Nair and van Staden, 2020, 2023), which contain a rich array of specialized metabolites, mainly isoquinoline-derived alkaloids with a wide range of pharmacological activities, drawing considerable attention from the scientific community (Berkov *et al.*, 2020; Ka *et al.*, 2020). More than 700 distinct Amaryllidaceae alkaloids (AAs) have been identified, with notable representatives, including galanthamine, lycorine, and haemanthamine (Jayawardena *et al.*, 2024). Galanthamine, isolated initially from *Galanthus* species, has become a therapeutic agent for Alzheimer's disease symptoms due to its acetylcholinesterase inhibitory activity (Heinrich and Teoh, 2004; Loy and Schneider, 2006). Lycorine has demonstrated potent antiviral, antitumor, and anti-inflammatory

effects, while haemanthamine is known for its cytotoxic properties, making it a promising candidate for cancer research (Cahlíková *et al.*, 2021; Jayawardena *et al.*, 2024; Zhang *et al.*, 2024). The current supply of these compounds is limited, primarily sourced from the extraction of only a few Amaryllidaceae species, such as *L. aestivum* and *Narcissus pseudonarcissus, Lycoris radiata, and Ungernia victoris* (Berkov *et al.*, 2022; de Andrade *et al.*, 2011) highlighting the need to identify more highly productive species and understand their biosynthetic pathways.

Some *Hippeastrum* species have been reported to produce high amounts of galanthamine and haemanthamine, as well as several other AAs (Figure 1), holding promise for sustainable and efficient extraction relative to other plant sources (de Andrade *et al.*, 2011; Guo *et al.*, 2016; Haist *et al.*, 2024b; Tallini *et al.*, 2021). This diverse genus comprises over 100 bulbous perennial species native to South America's tropical and subtropical regions (García *et al.*, 2019). *Hippeastrum papilio*, commonly known as the Butterfly Amaryllis, stands out for its unique floral morphology and the significance of its natural habitats (Govaerts). Originating from the Atlantic forests of southern Brazil, *H. papilio* naturally grows on tall trees as an epiphyte, unlike most of the geophytic Amaryllidaceae species (Campos-Rocha *et al.*, 2023). It is valued in horticulture for its distinctive green and burgundy flowers, often used in breeding programs to develop hybrids with enhanced ornamental traits (de Andrade *et al.*, 2011; Fellers, 1998).

Unravelling the precise tissue and organ distribution of specific alkaloids in this species is required to provide the critical knowledge to optimize the species' industrial and pharmaceutical applications. Various techniques can be employed for the *in situ* detection of metabolites in plants, including autofluorescence, staining, labelling, and, more recently, mass spectrometry imaging (MSI) (Donaldson, 2020; Qin *et al.*, 2018). Recent research has begun to explore alkaloid distribution at both histochemical and organ-specific levels of *H. papilio*, shedding light on their biosynthetic pathway using Dragendorff's reagent (Haist *et al.*, 2024b). Haist et al. demonstrated that alkaloids are present in all plant tissues, with higher concentrations accumulating in bulbs (inner part followed by outer scales) and roots compared to leaves. Alkaloids were enriched in phloem sap of leaves, bulbs, roots, leaf parenchyma, and vascular bundles. However, Dragendorff's staining lacks the resolution to identify individual alkaloid components and is associated with a false positivity of non-nitrogenous oxygenated compounds (Habib, 1980).

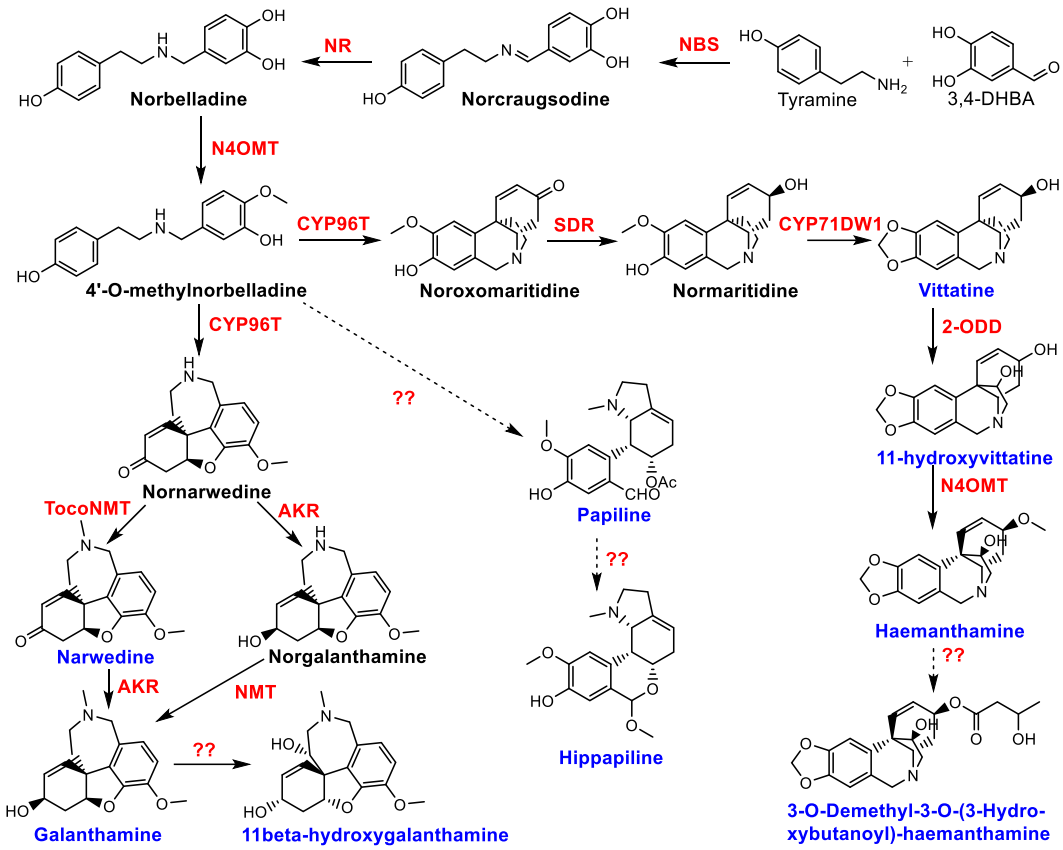

Figure 3.1. Biosynthetic pathway representing Amaryllidaceae alkaloids from *Hippeastrum papilio* starting from the initial precursors, tyramine and 3,4-dihydroxybenzaldehyde (3,4-DHBA). The bold letters (black and blue) represent the compounds examined in this study, and the blue letters indicate the alkaloids previously recorded in *H. papilio*. Single arrows represent a single enzymatic reaction, whereas the dotted arrows signify multiple enzymatic steps. Red letters indicate the characterized enzymatic reactions of the pathway. NBS: Norbelladine synthase, NR: Norcraugsodine/noroxomaritidine reductase, N4OMT: Norbelladine 4'-O-methyltransferase, CYP96T: Cytochrome P450 96T, TocoNMT: Tocopherol N-methyltransferase, AKR: Aldoketoreductase, SDR: Short chain dehydrogenase/reductase, NMT: N-methyltransferase, 2-ODD: 2-oxoglutarate-dependent dioxygenase (Haist *et al.*, 2024b; Lamichhane *et al.*, 2025; Liyanage *et al.*, 2025b; Mehta *et al.*, 2024).

MSI combines the spatial resolution of imaging with the molecular specificity of MS (Bjarnholt *et al.*, 2014). This technology works by ionizing molecules from the surface of a sample and analyzing their mass-to-charge ratios to create molecular maps that represent the spatial localization of specific compounds (Bjarnholt *et al.*, 2014; Buchberger *et al.*, 2017; Granborg *et al.*, 2022). MSI can detect a wide range of molecules simultaneously, making it a highly efficient tool for comprehensive analysis. The technique has been employed to unravel biosynthetic pathways, allowing researchers to trace the origin, transformation, and final deposition sites of plant metabolites (Horn and Chapman, 2024; Spengler, 2015).

Matrix-assisted laser desorption/ionization (MALDI)-MSI uses a laser to desorb and ionize analytes with an applied chemical matrix, whereas desorption electrospray ionization (DESI)-MSI employs a stream of charged droplets to sample analytes directly from the surface, making it ideal for analyzing delicate plant tissues (Bjarnholt *et al.*, 2014; Horn and Chapman, 2024). Monoterpenoid indole alkaloid imaging of *Rauvolfia tetraphylla* by MALDI and DESI-MSI provided detailed information on the localization of reserpine and its precursors, such as their compartmentalization in the xylem in stem tissues (Lorensen *et al.*, 2023). In *Daphniphyllum macropodum,* MALDI-MSI revealed that the distribution of alkaloids within tissues is complex, likely involving intercellular transport (Eljounaidi *et al.*, 2024). Alkaloids were localized

in specific regions of the petiole and stem tissues, with larger C30-carbon skeleton subtypes preferentially associated with vascular tissue (phloem), and smaller C22 subtypes more frequently localized to the epidermis and enriched in immature leaves. In Amaryllidaceae, DESI-MSI showed that the leaf bases of *Narcissus* cv. Tête à Tête preferentially accumulated vittatine synthesized from radiolabelled 4'-*O*-methylnorbelladine, whereas mid-leaf accumulated non-radiolabeled lycorine (Mehta *et al.*, 2024). In *Narcissus tazetta*, MALDI-MSI revealed that galanthamine was mainly concentrated in future leaves (inner bulb), while lycorine and tazettine did not exhibit a discernible distribution pattern within the bulb. No significant differences in distribution were observed among the three alkaloids in the leaf cross-sections (Nakagawa *et al.*, 2024). These studies emphasize the diversity of alkaloid repartition among species, organs, tissues, and structural types, underscoring the need for further research on high-galanthamine-producing species.

By focusing on the tissue-specific localization of alkaloids in *H*. *papilio*, this study aims to enhance our understanding of its phytochemistry and potential as a high-value bioresource. We used MALDI-MS to provide a detailed analysis of the tissue distribution of AAs and their biosynthetic partners in *H*. *papilio*. A combination of principal component analysis (PCA), *t*-distributed stochastic neighbor embedding (*t*-SNE), Spearman correlation, and hierarchical clustering analyses was employed to isolate

the structure- and tissue-specific distribution patterns of *H. papilio* alkaloids, aiming to elucidate their biosynthetic compartmentalization. RT-qPCR was then applied to different organ sections to validate the proposed biosynthetic model. This study addresses two critical questions regarding the spatial distribution of AAs in *H. papilio*: a. In which tissues and organs do galanthamine and intermediates predominantly accumulate in high-galanthamine-producing *H. papilio*? and b. Do other key AAs, such as haemanthamine, exhibit similar spatial arrangements within the plant tissues? Understanding these distribution patterns will provide insights into the tissue-specific biosynthesis and accumulation of these pharmacologically significant alkaloids, potentially revealing their ecological roles and the regulation of their biosynthesis.

3.3. Materials and methods

3.3.1. Plant material

Mature bulbs (Four bulbs in flowering level maturity) of *H. papilio* were purchased from Fluwel V.O.F., Belkmerweg 20A, 1754 GB Burgerbrug, The Netherlands (https://www.fluwel.com/en-gb/products/amaryllis-papillio). The plants were grown in garden soil mixed with perlite to enhance aeration around the roots, using plastic pots placed next to a windowsill for six months, with watering as needed. Once the plants had fully entered their vegetative stage, they were uprooted, and the soil was carefully removed and thoroughly washed with tap water before being

patted dry. The plants were then sectioned systematically. For the leaves, outer, middle, and inner leaves were sampled, and from each leaf, leaf tip, leaf mid, and the leaf base were separated. From the bulbs, a few 2-3 outer scales, middle scales, and inner scales, along with the basal plate sectioned for the analysis. Roots were separated into three sections: root base, middle, and tip. To minimize ice crystal formation because of the high-water content of the plant, immediately after sectioning, samples were dipped in 5 mM sucrose in phosphate-buffered saline for 30 minutes. Following this, they were washed three times with distilled water to remove excess sucrose from around the tissues. After drying them quickly with tissues, the sections were frozen on a metal sheet over dry ice.

3.3.2 Sample preparation for MALDI-MSI

Samples were cryo-sectioned using techniques adapted from those developed by Kawamoto and employed for sample embedding by Montini et al (Kawamoto, 2003; Kawamoto and Kawamoto, 2021; Montini *et al.*, 2020). Briefly, an n-heptane and dry ice slurry was prepared in a Dewar jar. A 2.5 × 2.0 cm mold (SECTION-LAB Co. Ltd.) was filled with a 3% (w/v) carboxymethyl cellulose aqueous gel and partially submerged in the n-heptane dry ice slurry. The samples were inserted into the embedding medium as the edges began to freeze, after which the mold was carefully immersed in n-heptane until the gel solidified completely. Once frozen, the block was removed from the mold and stored at -80 °C

before cryo-sectioning. In this case it was nine leaf cross sections per block, seven cross sections from the bulb tissues per block and six cross sections of roots per block were taken in the main experiments. A Leica CM3050S cryo-microtome (Leica Microsystems, Wetzlar, Germany) was utilized to create cryo-sections of embedded plant samples at a temperature of -20 °C. The sample was appropriately trimmed using the cryo-microtome before sectioning. Then the sample was covered with cryo-film (SECTION-LAB Co. Ltd., Hiroshima, Japan) to generate slices of the plant tissue measuring 10–20 µm. After sectioning, double-sided carbon tape (Electron Microscopy Sciences, Hatfield, PA, USA) was used to attach the opposite side of the cryofilms to glass slides. The films were then stored at -80 °C until the MALDI imaging analysis.

Cryo-sectioned samples were placed in a vacuum desiccator for ten minutes for desiccation. An Olympus BH-2 microscope with reflected light was then used to capture optical images of the plant samples. Next, an iMatrixSpray was used to apply a solution of 2,5-dihydroxybenzoic acid (DHB) (30 mg/mL in 90% MeOH) as the MALDI matrix (Stoeckli ***et al.***, 2014). The sprayer settings were established at a height of 80 mm, with a line distance of 1 mm, a speed of 90 mm/s, a density of 3 µL/cm², and a total of 15 cycles over a 40 x 40 mm area. Following this, MALDI-MSI data were obtained after the evaluation of crystal formation using compound light microscopy.

3.3.3. MALDI-MS analysis

A Thermo QExactive Orbitrap mass spectrometer (Thermo Scientific, Bremen, Germany), equipped with an AP-SMALDI5 ion source (TransMIT GmbH, Giessen, Germany), was utilized for MALDI mass spectrometry imaging (MSI). The instrument operated within a scan range of *m/z* 100–600, achieving a mass resolving power of 140,000 at *m/z* 200, and data were collected in positive ion mode (Minimum N=2 per organ). The matrix peak of DHB (*m/z* 273.03937) was used as a lock mass for internal mass calibration, ensuring a mass accuracy of ±1 ppm. The pixel size is specified for the individual images in the figure captions. Available Amaryllidaceae alkaloid standards were tested in the MALDI-MS prior to the analysis to observe the detection of the compounds (Supplementary Fig. 2.A1a-2.A1g).

3.3.4 Data processing and image generation

The "RAW + UDP to IMZML" program (version 1.6R170; TransMIT, Bremen, Germany) was used to convert the raw data files into imzML files (Schramm *et al.*, 2012). Mass images were then generated using MSiReader v1.02 (Bokhart *et al.*, 2017), with a mass tolerance of 1 ppm. The color scale was adjusted to enhance the visibility of the compounds of interest. Table 3.1 provides the masses of the studied compounds in their protonated and deprotonated forms. We included only the AAs that have been previously reported in *H. papilio* and their biosynthetic intermediates, as mentioned in Fig. 3.1 (de Andrade *et al.*, 2011; Guo *et*

al., 2016; Haist *et al.*, 2024b). Di-hexose ([$C_{12}H_{22}O_{11}$ + K]+, *m/z* 381.07937) was used as a tissue marker to outline the contours. The MS images are representative of both studies and were produced using n = 2 biological replicates. All the data generated in this study was uploaded to the Metaspace metabolite annotation data platform for mass spectrometry imaging data (https://metaspace2020.org/), and annotated with KEGG-V1, ChEBI-2018-01, HMDB-v4, and NPA-2019-08 databases (Palmer *et al.*, 2017).

Table 3.1. Exact masses of the compounds, their ionized form, and imaged in the MSI analysis.

Alkaloid	**Molecular formula**	**Monoisotopic mass (Da)**	**[M+H]+**	**[M+K]+**	**Isomers**
Norcraugsodine	$C_{15}H_{15}NO_3$	257.10518	258.11245	296.06833	n.a.
Norbelladine	$C_{15}H_{17}NO_3$	259.12083	260.12810	298.08398	n.a.
4'-O-Methylnorbelladine	$C_{16}H_{19}NO_3$	273.13648	274.14375	312.09963	Norgalanthamine, Normaritidine
Nornarwedine	$C_{16}H_{17}NO_3$	271.12083	272.12810	310.08398	Noroxomaritidine, Vittatine
Narwedine	$C_{17}H_{19}NO_3$	285.13648	286.14375	324.09963	n.a.
Norgalanthamine	$C_{16}H_{19}NO_3$	273.13648	274.14375	312.09963	4'-O-methylnorbelladine,

					Normaritidine
Galanthamine	$C_{17}H_{21}NO_3$	287.15213	288.15940	326.11528	n.a.
11β-Hydroxygalanthamine	$C_{17}H_{21}NO_4$	303.14704	304.15431	342.11019	n.a.
Noroxomaritidine	$C_{16}H_{17}NO_3$	271.12083	272.12810	310.08398	Nornarwedine, Vittatine
Normaritidine	$C_{16}H_{19}NO_3$	273.13648	274.14375	312.09963	4'-O-methylnorbelladine, Norgalanthamine
Vittatine	$C_{16}H_{17}NO_3$	271.12083	272.12810	310.08398	Nornarwedine, Noroxomaritidine
11-Hydroxyvittatine	$C_{16}H_{17}NO_4$	287.11574	288.12301	326.07889	n.a.
Haemanthamine	$C_{17}H_{19}NO_4$	301.13139	302.13866	340.09454	n.a.
3-O-Demethyl-3-O-(3-hydroxybutanoyl)-haemanthamine	$C_{20}H_{23}NO_6$	373.15251	374.15978	412.11566	n.a.
Papiline	$C_{19}H_{23}NO_5$	345.15760	346.16487	384.12075	n.a.
Hippapiline	$C_{18}H_{23}NO_4$	317.16269	318.16996	356.12584	n.a.
Di-hexose (Sucrose)	$C_{12}H_{22}O_{11}$	342.11616	343.12344	381.07932	n.a.

n.a.: not applicable

3.3.5. Mucilage analysis

While sampling the tissues of *H*. *papilio* leaves and bulbs, the secreted mucilage was collected from the three positions of the leaves (leaf tip, mid, and base) and the bulb into the Eppendorf tubes, and kept on ice. To precipitate proteins, a 1:1 ratio of methanol was added to the collected mucilage (50 µL mucilage + 50 µL methanol), then vortexed and centrifuged at 10,000 rpm for 15 minutes. 10 µL supernatant was diluted in 90 µL deionized water with papaverine 1 ppm as internal standard before analysis by LC-MS.

3.3.6. LC-MS analysis.

A high-performance liquid chromatography (HPLC) system (Agilent 1100, USA) combined with a tandem quadrupole mass spectrometer (Waters Micromass Quattro Micro, USA), equipped with an electrospray ionization (ESI) source, was utilized for the alkaloid analysis. Chromatographic separation was performed using a Phenomenex Kinetex biphenyl column (75 × 2.1 mm, 2.6 µm, 100 Å pore size) maintained at a constant temperature of 30°C. A volume of five microliters from each sample was injected onto the column, which maintained a flow rate of 0.3 mL/min. The mobile phase consisted of solvent A (Milli-Q water with 0.1% formic acid) and solvent B (methanol with 0.1% formic acid). The elution gradient was as follows: from 0 to 5 minutes, isocratic at 10% B; from 5 to 7 minutes, a linear increase to 25% B; from 7 to 10 minutes, a ramp to 98% B; from 10 to 15 minutes, held

at 98% B; from 15 to 16 minutes, a return to 10% B; and reconditioning from 16 to 25 minutes.

The mass spectrometer was operated under the following source conditions: a cone voltage of 30 V, a source temperature of 120°C, a desolvation temperature of 300°C, and a desolvation gas flow rate of 500 L/h. Analysis was conducted in multiple reaction monitoring (MRM) mode, with three ion transitions monitored for each compound to ensure specificity and sensitivity. Detailed information on all transitions and compound-specific parameters can be found in Supplementary Table A1. Relative quantitative analysis was conducted using calibration curves generated from standard solutions of the target alkaloids, which were processed with internal standards (compound/papaverine ratio). Data acquisition and processing were managed using MassLynx software (Waters, version details if applicable). The results were visualized and statistically analyzed using GraphPad Prism v10.

3.3.7. Dimension reduction and multivariate clustering analyses

Organ-level normalized abundance data and binary fine-tissue × organ-zone localization profiles were compiled into structured matrices for multivariate analysis. Principal component analysis (PCA) was first applied to the organ-level abundance matrix, after z-score standardization, to capture global variance in metabolite distribution patterns. A hybrid matrix was then constructed by integrating the binary fine-tissue localization data with normalized organ-level abundance

values. This matrix was likewise z-score standardized and subjected to PCA to assess spatial localization and tissue-level accumulation trends jointly. t-Distributed Stochastic Neighbor Embedding (t-SNE) was performed on the hybrid matrix using the following parameters: perplexity = 5, learning rate = 200, number of iterations = 3000, and random seed = 42. This allowed for the visualization of metabolite relationships in a two-dimensional space while preserving the local neighborhood structure from the high-dimensional input. Pairwise Spearman's rank correlation coefficients were calculated based on the hybrid matrix, and a hierarchical clustering heatmap was generated to validate metabolite groupings according to spatial and quantitative similarity. The PCA and t-SNE axes are unitless and optimized, respectively, for variance explanation and neighborhood preservation. Assistance from generative AI tools (ChatGPT, OpenAI GPT-4, 2024 release) was used in the development of the initial Python scripts used. All code was critically reviewed, iteratively adjusted, and executed locally on laboratory computers by the authors. The final analyses and figure generation were performed entirely offline, using these customized scripts in interaction with the AI to improve reproducibility, visualization clarity, and parameter selection.

Statistical differences in individual feature distributions between precursor metabolites and other alkaloid groups were assessed using a two-tailed Mann–Whitney *U* test. Hierarchical clustering was applied to

the z-score standardized hybrid matrix using Ward's linkage and Euclidean distance. Although the original matrix includes binary tissue localization features, standardization produced a continuous distribution of feature values, allowing the application of Ward's method (Chavent *et al.*, 2012; Kaufman and Rousseeuw, 2009). This approach yielded a dendrogram structure that was consistent with known biosynthetic relationships among alkaloids.

3.3.8. Total RNA Extraction and qRT-PCR

Total RNA was extracted using a modified cetyltrimethylammonium bromide (CTAB) protocol based on Meisel *et al.* (2005). Approximately 200 mg of finely ground tissue (using liquid nitrogen) was homogenized in 2 mL of CTAB lysis buffer supplemented with 10% (v/v) β-mercaptoethanol and 50 µL of spermidine trihydrochloride. The homogenate was incubated at 65 °C for 10 minutes in a water bath to ensure efficient cell lysis. Phase separation was then carried out by adding 1 mL of chloroform:isoamyl alcohol (24:1, v/v), followed by vigorous vortexing for 30 seconds and centrifugation at 13,000 rpm for 15 minutes. This step was repeated once to remove proteins. The resulting aqueous phase was transferred to a new tube and mixed with an equal volume of 10 M lithium chloride, followed by overnight incubation at -20 °C to precipitate RNA. The RNA was pelleted by centrifugation at 15,000 rpm for 45 minutes, washed with 80% cold ethanol, and air-dried at room temperature. The dried pellet was

resuspended in 50 µL of RNase-free water and treated with the TURBO DNA-free™ Kit (Invitrogen) to remove genomic DNA contamination. After inactivating DNase, final RNA purification was performed using the Monarch® RNA Cleanup Kit according to the manufacturer's instructions. The relative expression levels of genes involved in AA biosynthesis, including *TYDC1*, *TYDC2*, *NBS*, *NR*, *OMT*, *CYP96T1*, and *NMT* (Supplementary Table 2.A2) were quantified using the One Step Luna® Universal qRT-PCR Kit (New England Biolabs). *Actin* was used as the internal reference gene for normalization, as the *histone3* candidate was not stably expressed. Each qRT-PCR reaction was performed with gene-specific primers and 100 ng of total RNA in a final reaction volume of 10 µl. Amplification and detection were carried out on the CFX Connect™ Real-Time PCR Detection System (Bio-Rad). The $2^{-\Delta Ct}$ method was used to calculate the relative expression of each transcript relative to actin in each tissue.

3.4. Results

The spatial distribution of AAs in-key plant structures, such as the roots, leaves, and bulbs, was analyzed using MALDI-MSI. Images of di-hexose were included in each MSI experiment, outlining the morphology and contours of the analyzed tissues and serving as internal references for spatial orientation. Compound detection was based on accurate mass measurements and comparison to authenticated standards.

3.4.1. Amaryllidaceae alkaloids in *H. papilio* leaf tissues

For the MALDI-MSI analysis of *H. papilio* leaf tissues, cross sections were prepared from three distinct regions: the innermost, middle, and outermost leaf (Figure 3.2a). Each leaf was further sectioned into three anatomical sections, i.e., the leaf base, mid-leaf, and leaf tip, resulting in a total of nine leaf cross sections per plant. These sections were embedded together in a 3% (w/v) carboxymethyl cellulose gel as a single block and scanned collectively to generate a comprehensive image, allowing for the comparison of signal intensities across the individual samples in the image. The leaves of *H. papilio* exhibited typical monocotyledonous anatomical features.

The MALDI-MSI focuses on the spatial distribution twelve alkaloids spanning the AA biosynthetic pathway (Figure 3.1), including early precursors such as norcraugsodine (*m/z* 258.1125) and norbelladine (*m/z* 260.1281) (Figure 2a; top panels), major products like galanthamine (*m/z* 288.1594) and haemanthamine (*m/z* 302.1386), and several derivatives such as 11β-hydroxygalanthamine (*m/z* 304.1543) and 3-O-demethyl-3-O-(3-hydroxybutanoyl)-haemanthamine (*m/z* 374.1597) (Figure 2a, 2b; Supplementary Table A1). Imaging was performed at a pixel size of 40 µm, with select tissues imaged at higher resolutions of 10 µm and 5 µm for finer structural detail (Supplementary Fig. 2.A2 and in Metaspace https://metaspace2020.org/).

The spatial distribution patterns of each alkaloid were remarkably consistent across different leaf ages (outermost to innermost leaves) and positions (base, mid, and tip). Most targeted alkaloids were detected across multiple leaf regions and developmental stages, though some were absent from specific zones, such as the midsection of the outermost leaves (Figure 3.2a, 3.2b; Supplementary Table 2.A1). Although MALDI-MSI is inherently semi-quantitative and ion intensities do not directly reflect absolute compound abundance due to potential variability in ionization efficiency, we carefully interpreted relative abundance patterns within this dataset. Notably, the alkaloids analyzed here share highly similar core structures, functional groups, and molecular weights, which likely result in comparable ionization behaviors under the applied matrix and instrumental conditions. Therefore, while we recognize that differences in ionization efficiencies may still influence signal strength, the structural similarity of the compounds provides a reasonable basis for cautious comparison of ion intensities across alkaloids in this study. This approach allowed us to gain insight into the relative distribution and accumulation trends of major versus minor alkaloids across tissues.

Among the detected signals, galanthamine and haemanthamine exhibited the highest ion intensities, which is consistent with their known accumulation as major AAs in *H. papilio*. Intermediate compounds such as norcraugsodine, norbelladine, and 4′-O-methylnorbelladine (including

isomers norgalanthamine and normaritidine), as well as minor alkaloids like hippapiline and 3-O-demethyl-3-O-(3-hydroxybutanoyl)-haemanthamine, were detected at comparatively lower ion intensities. While intensities do not translate linearly into compound abundances, they suggest that the biosynthetic intermediates and minor alkaloids are present throughout the leaf tissues at substantially lower concentrations compared to major alkaloids. Norcraugsodine, norbelladine, 4'-O-methylnorbelladine/norgalanthamine/normaritidine, nornarwedine/vittatine/ noroxomaritidine, 11-hydroxyvittatine, haemanthamine, and 3-O-demethyl-3-O-(3-hydroxybutanoyl)-haemanthamine were not detected in the midsection of the outermost leaves (Figure 3.2). Almost all metabolites were detected in epidermal tissues, vascular bundles, and mesophylls (parenchyma), with higher abundances observed in the epidermal and vascular regions, particularly in the lower epidermal areas of the leaf bases. In contrast, AAs were absent in the aerenchyma, which consists primarily of air spaces within the leaf tissues. Norbelladine and 3-O-Demethyl-3-O-(3-hydroxybutanoyl)-haemanthamine were not detected in the outer epidermis layer, which may correspond to the cuticle, although this was not confirmed histologically.

4'-O-Methylnorbelladine/norgalanthamine/normaritidine, papilline-type, and galanthamine-type consistently accumulated in vascular bundles of most cross sections. 3-O-Demethyl-3-O-(3-hydroxybutanoyl)-

haemanthamine was not detected in most epidermal tissues. Overall, galanthamine displayed the broadest and most uniform distribution across both tissues and leaf regions, highlighting its dominance among the alkaloids detected in *H. papilio* leaf tissues.

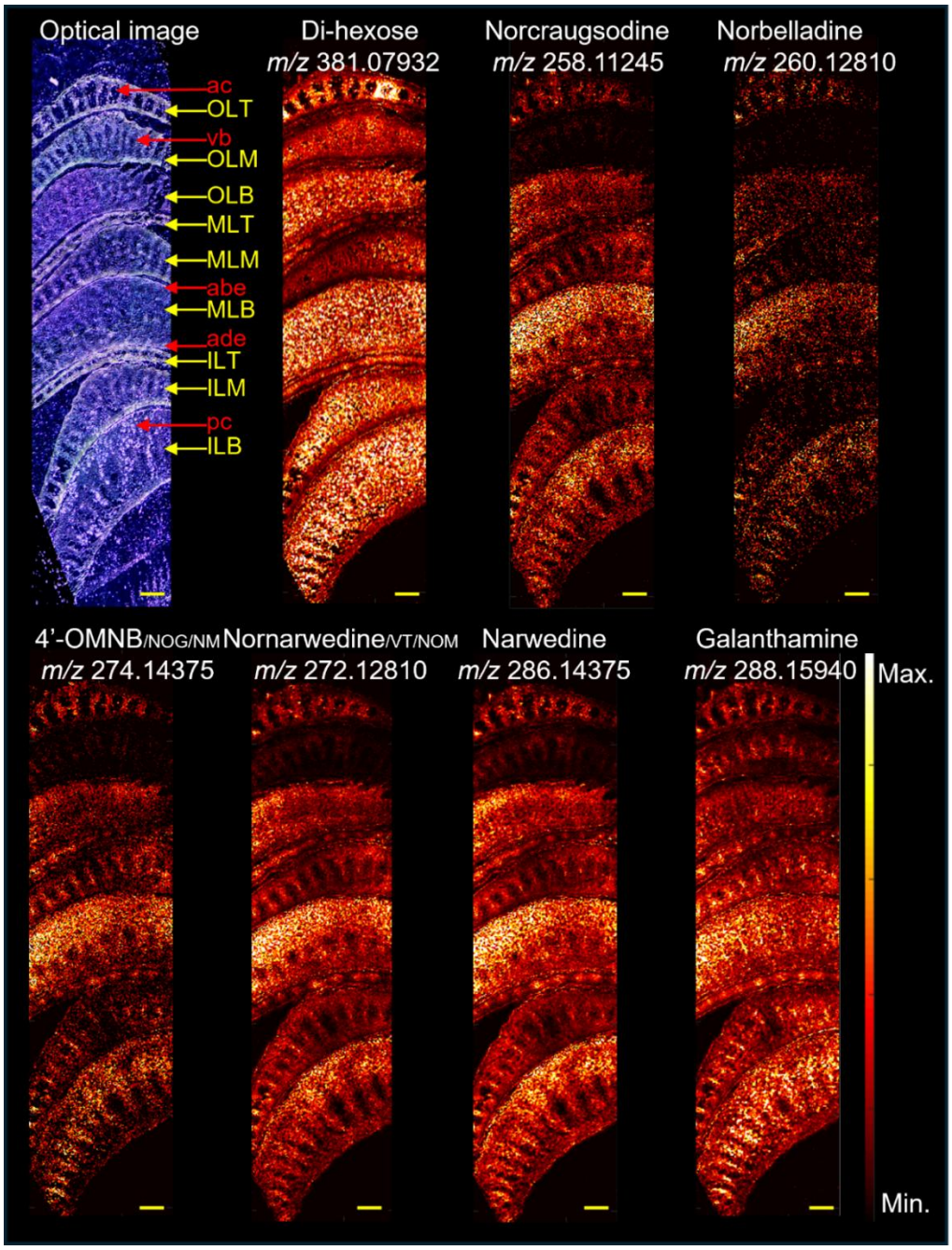

Figure 3.2a. MALDI-MSI of *Hippeastrum papilio* leaf cross sections. From top to bottom, yellow arrows indicate the position of the leaf sections: outermost leaf (OLT = tip, OLM = mid, OLB = base), middle leaf (MLT = tip, MLM = mid, MLB = base), and innermost leaf (ILT = tip, ILM = mid, ILB = base). Red arrows indicate tissue types: ac = aerenchyma, vb = vascular bundles, abe = abaxial (lower) epidermis, ade = adaxial (upper) epidermis, and pc = parenchyma. Compound abbreviations: 4′OMNB = 4′-O-methylnorbelladine, NOG = norgalanthamine, NM = normaritidine, VT = vittatine, and NOM = noroxomaritidine. Pixel size: 40 µm. Scale bars: 1 mm.

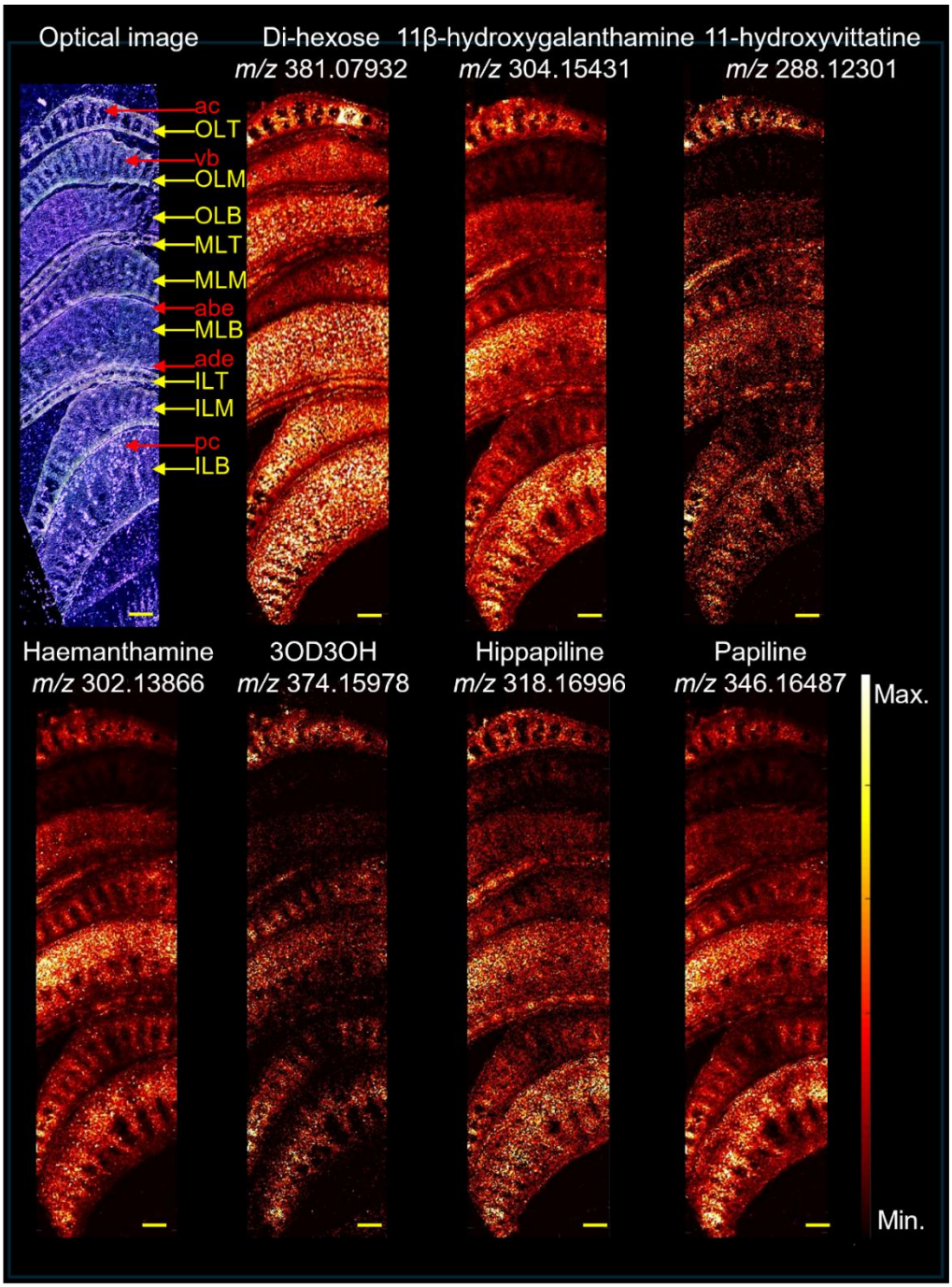

Figure 3.2b. MALDI-MSI of *Hippeastrum papilio* leaf cross sections. From top to bottom, yellow arrows indicate the position of the leaf sections: outermost leaf (OLT = tip, OLM = mid, OLB = base), middle leaf (MLT = tip, MLM = mid, MLB = base), and innermost leaf (ILT = tip, ILM = mid, ILB = base). Red arrows indicate tissue types: ac = aerenchyma, vb = vascular bundles, abe = abaxial (lower) epidermis, ade = adaxial (upper) epidermis, and pc = parenchyma. Compound abbreviation: 3OD3OH = 3-O-demethyl-3-O-(3-hydroxybutanoyl)-haemanthamine. The pixel size is 40 µm—scale bars: 1 mm.

3.4.2. Amaryllidaceae alkaloids in *H. papilio* bulb tissues

To investigate alkaloid localization in bulb tissues of *H. papilio*, MALDI-MSI was performed on two outer scales, two middle scales, two apex leaves (leaf primordia), and a portion of the basal plate, all embedded together in a single imaging block. All twelve alkaloids previously identified in leaf tissues were detected, confirming their presence in the bulb (Figure 3.3a and 3.3b, Supplementary Table 2.A1), but with markedly different distribution patterns. Variations in spatial localization were observed both between tissue layers and among different anatomical regions within the bulb. At the tissue level, alkaloids were predominantly detected in vascular bundles, epidermal tissues, and parenchyma.

Alkaloid signals were primarily concentrated in the basal plate. Norcraugsodine, norbelladine, narwedine, and nornarwedine/vittatine/noroxomaritidine were consistently dispersed across both outer and inner bulb scales (Supplementary Table 2.A1). In contrast, 4'-O-methylnorbelladine/norgalanthamine/normaritidine, galanthamine, 11-hydroxyvittatine, haemanthamine, and hippapiline

were more abundant in the outer scales. Intermediates norcraugsodine, norbelladine, nornarwedine, narwedine, as well as haemanthamine, and papilline were detected in one of the apical leaves, while others were not. Norbelladine, 11β-hydroxygalanthamine, 11-hydroxyvittatine, haemanthamine, and 3-O-demethyl-3-O-(3-hydroxybutanoyl)-haemanthamine were not detected in the outer epidermis layer (possibly the cuticle) of bulb scales.

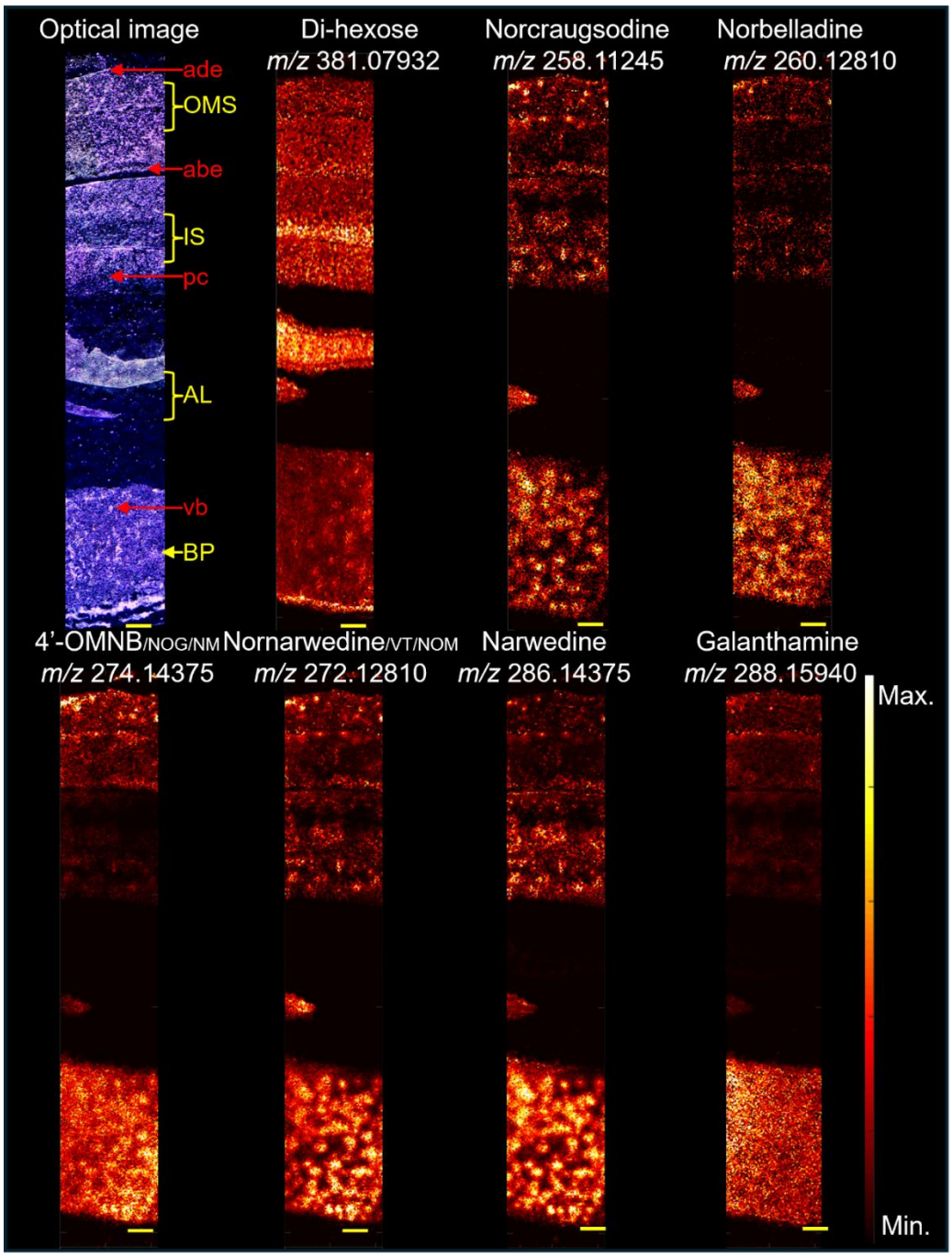

Figure 3.3a. MALDI-MSI of *Hippeastrum papilio* bulb cross sections. In each panel, from top to bottom, yellow arrows indicate the position of the tissue sections: OMS = outermost scales (two sections), IS = inner scales, AL = apical leaves (two sections), and BP = basal plate. Red arrows denote tissue types: ade = adaxial (outer) epidermis, abe = abaxial (inner) epidermis, pc = parenchyma cells, and vb = vascular bundles. Compound abbreviations: 4′OMNB = 4′-O-methylnorbelladine, NOG = norgalanthamine, NM = normaritidine, VT = vittatine, and NOM = noroxomaritidine. The pixel size is 30 µm. Scale bars: 1 mm.

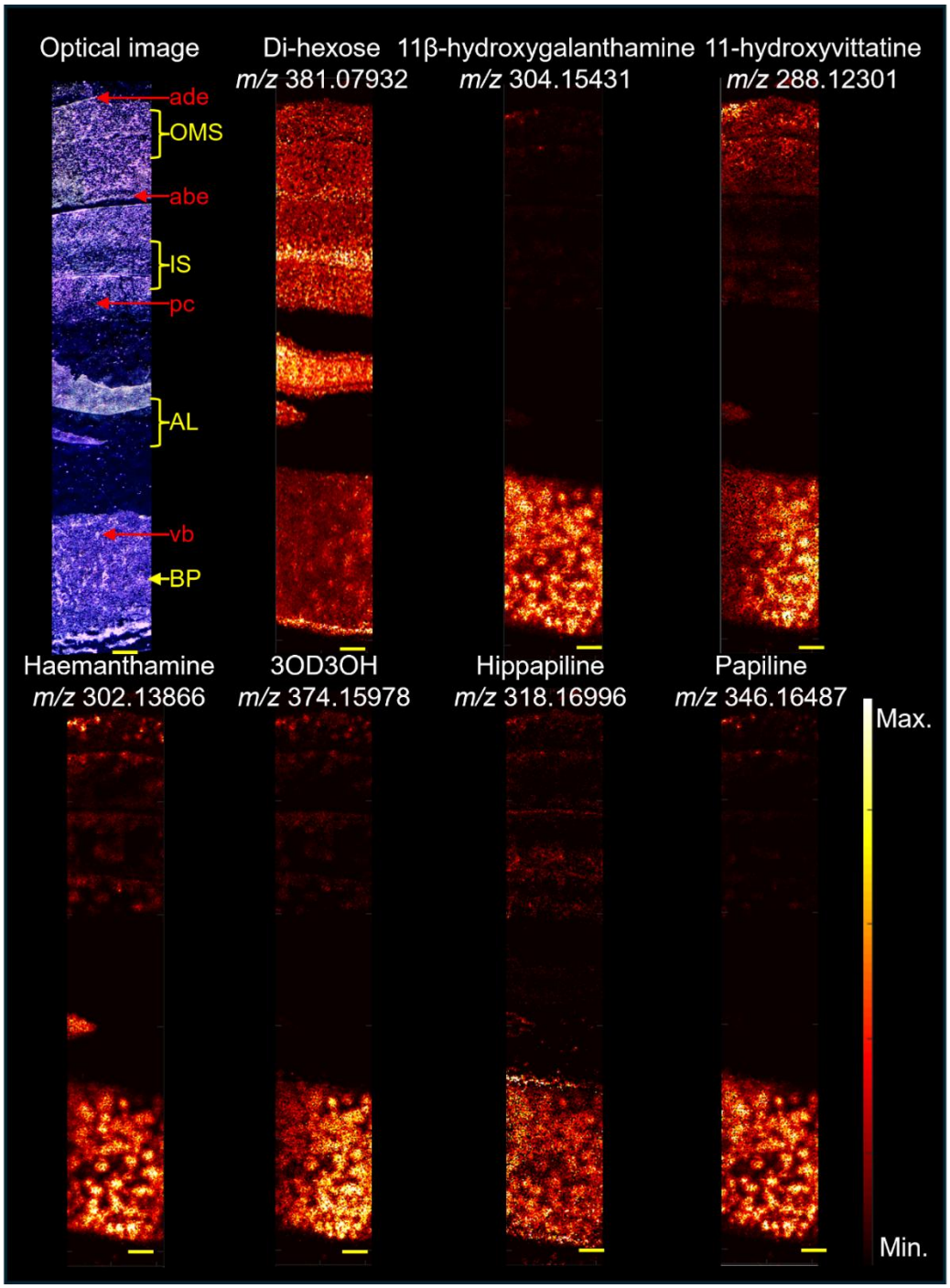

Figure 3.3b. MALDI-MSI of *Hippeastrum papilio* bulb cross sections. In each panel, from top to bottom, yellow arrows indicate the position of the tissue sections: OMS = outermost scales (two sections), IS = inner scales, AL = apical leaves (two sections), and BP = basal plate. Red arrows denote tissue types: ade = adaxial (outer) epidermis, abe = abaxial (inner) epidermis, pc = parenchyma cells, and vb = vascular bundles. Compound abbreviation: 3OD3OH = 3-O-demethyl-3-O-(3-hydroxybutanoyl)-haemanthamine. Pixel size: 30 µm. Scale bars: 1 mm.

Metabolites were more abundant in the basal plates' vascular bundles, except galanthamine, which was evenly distributed throughout the basal plate tissues. Regarding ion intensity, galanthamine, haemanthamine, 11β-hydroxygalanthamine, narwedine, and papiline were the most abundant alkaloids in *H*. *papilio* bulb tissues. These were followed by 4'-O-methylnorbelladine/norgalanthamine/normaritidine, nornarwedine/ noroxomaritidine/vittatine, and 11-hydroxyvittatine. Biosynthetic intermediates such as norcraugsodine and norbelladine, as well as minor alkaloids like hippapiline and 3-O-demethyl-3-O-(3-hydroxybutanoyl)-haemanthamine, were detected at relatively lower ion intensities. These findings suggest that while biosynthetic intermediates and minor alkaloids are present throughout the bulb tissues, their concentrations are lower compared to the major alkaloids. Overall, the distribution patterns of alkaloids in bulb tissues differed markedly from those observed in leaf tissues.

In addition to internal organ analysis, we collected mucilage from the leaf and bulb of *H*. *papilio* and measured the concentrations of alkaloids and precursors (Figure 3.4). Only alkaloids for which standards were available were included. Interestingly, intermediate compounds, such as norbelladine, 4'-O-methylnorbelladine, and norgalanthamine, were poorly detected in this waxy substance, except for a significant detection of 4'-O-methylnorbelladine in the mucilage coming from the bulb (119.713±3.235 relative concentration as internal standard responsive

ratio). However, galanthamine (733.26-1952.634 relative concentration as internal standard responsive ratio) and haemanthamine (417.205-1036.464 relative concentration as internal standard responsive ratio) were detected in high amounts in the mucilage of the two organs. Interestingly 4'-O-methylnorbelladine (8.11 times higher than leaf base, $p = 0.0113$), 11'-hydroxyvittatine (14.64 times than leaf base, $p < 0.0001$), galanthamine (1.57 times than leaf base, $p < 0.0001$) and haemanthamine (1.51 times than leaf base, $p < 0.0001$) were significantly higher in the mucilage extracted from the bulb compared to leaf cross-sections (Figure 4). These findings confirm that end-products accumulate in both leaves and bulbs and are present in higher amounts compared to precursors.

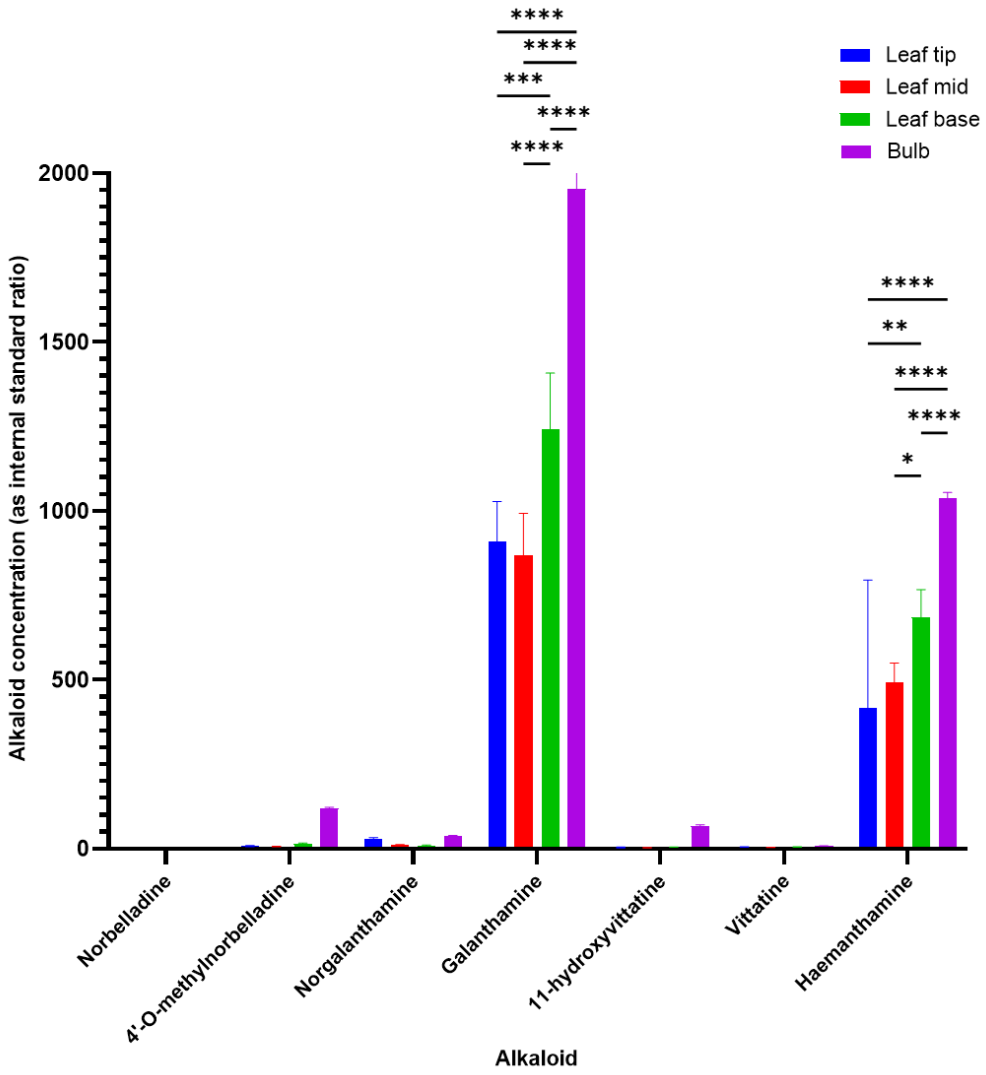

Figure 3.4. Alkaloid comparison of the mucilage of *Hippeastrum papilio*. Alkaloid contents were measured by LC-MS/MS and normalized using the papaverine internal standard. All the values are shown as means ± standard deviation of three independent biological replicates. *P*-values presented as Dunnett's multiple comparisons test of one-way ANOVA. **** = $p < 0.0001$, *** = $p < 0.001$, ** = $p < 0.01$, * = $p < 0.1$. Non-significant interactions are not presented in the graph.

3.4.3. Amaryllidaceae alkaloids in *H. papilio* root tissues

To analyze the AA arrangement in the root tissues of *H*. *papilio*, single images containing two root sections from the beginning of the root, two from the middle, and two from the root tip were included to study the distribution of each AA. The MALDI-MSI analysis of alkaloids in *H*. *papilio* revealed distinct distribution patterns across root tissues compared to bulbs and leaves (Figure 3.5a, 3.5b; Supplementary Fig. 2.A3, Supplementary Table 2.A1).

The spatial distribution of these alkaloids varied significantly across different regions, tissue types, and position along the root. At the tissue level, distinct distribution patterns emerged. Almost all tested metabolites were detected in the exodermis, cortex, and vascular bundle regions, with varying intensities (Figure 3.5a and 3.5b). For instance, norcraugsodine, norbelladine, nornarwedine/vittatine/noroxomaritidine, and haemanthamine were abundant in the exodermis and the cortex region adjacent to the exodermis (Supplementary Table A1). In contrast, 4'-*O*-methylnorbelladine/norgalanthamine/normaritidine showed higher abundance in the exodermis and cortex regions closer to the vascular bundle. Galanthamine was predominantly localized in the exodermis and vascular bundles. Hippapiline and 3-O-demethyl-3-O-(3-hydroxybutanoyl)-haemanthamine were more concentrated in the cortex, while papiline and 11β-hydroxygalanthamine were more abundant in the exodermis and cortex. Additionally, alkaloid concentrations were generally higher at the base of the roots and

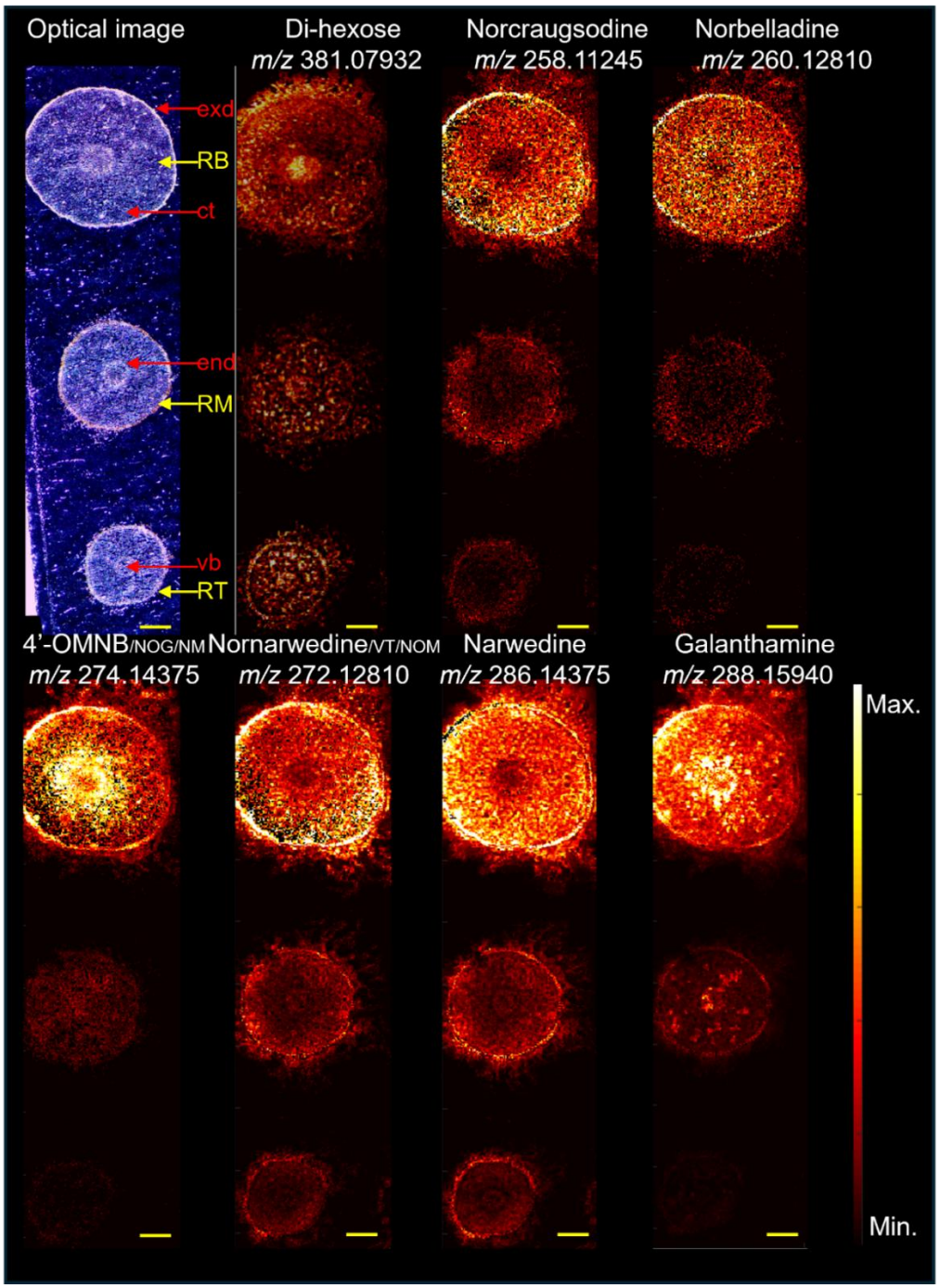

Figure 3.5a. MALDI-MSI of *Hippeastrum papilio* root cross sections. In each panel, from top to bottom, yellow arrows indicate the position of the tissue sections: RB = root base, RM = root middle, and RT = root tip. Red arrows indicate tissue types: exd = exodermis, ct = cortex, end = endodermis, and vb = vascular bundles. Compound abbreviations: 4′OMNB = 4′-O-methylnorbelladine, NOG = norgalanthamine, NM = normaritidine, VT = vittatine, and NOM = noroxomaritidine. Pixel size: 40 µm. Scale bars: 1 mm.

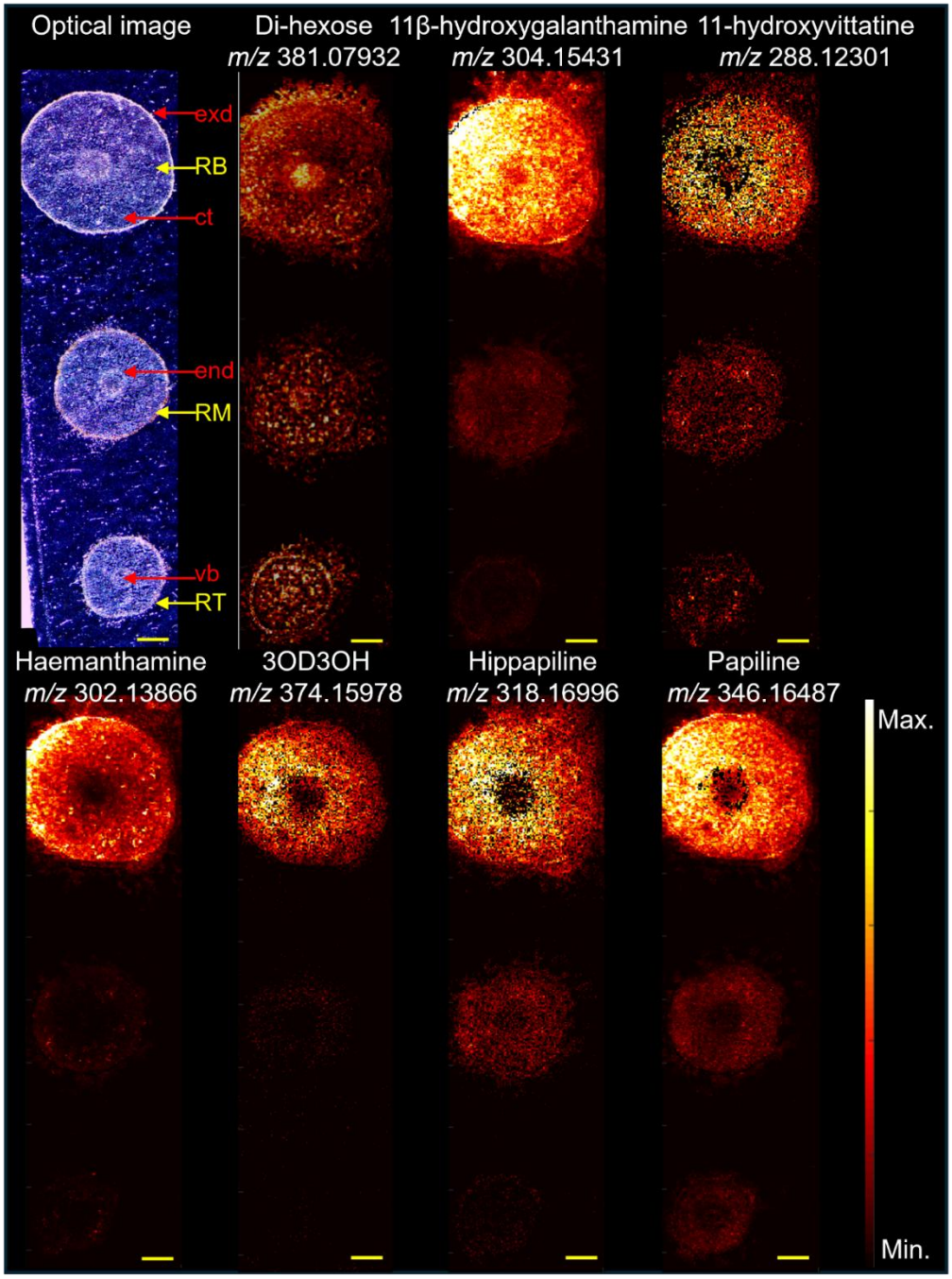

Figure 3.5b. MALDI-MS images a cross sections of *Hippeastrum papilio* root tissues. In each panel, from top to bottom, yellow arrows indicate the position of the tissue sections: RB = root base, RM = root middle, and RT = root tip. Red arrows indicate tissue types: exd = exodermis, ct = cortex, end = endodermis, and vb = vascular bundles. Compound abbreviation: 3OD3OH = 3-O-demethyl-3-O-(3-hydroxybutanoyl)-haemanthamine. The pixel size is 40 µm. Scale bars: 1 mm.

decreased toward the root tips. These findings suggest that the distribution of AAs in root tissues was more compartmentalized

compared to leaves and bulbs. In summary, roots of *H. papilio* accumulate a narrower spectrum of AAs compared to bulbs and leaves. The spatial distribution is predominantly restricted to the cortex and endodermis of the root base, with narwedine and papiline dominating the chemical landscape. The absence of early intermediates suggests that the root may play a more limited or specialized role in alkaloid metabolism.

3.4.4. Spatial distribution and accumulation clustering of alkaloids in *Hippeastrum papilio*

Hierarchical clustering revealed three primary groups that corresponded broadly to organ type, i.e., leaves, bulbs, and roots, highlighting tissue-specific accumulation profiles. Leaf and bulb samples formed two distinct but closely related clusters, reflecting their shared accumulation of major alkaloids such as galanthamine, haemanthamine, and 11β-hydroxygalanthamine, while still maintaining organ-specific differences. In contrast, root samples formed a separate and more distinct cluster, characterized by a narrower alkaloid profile and generally lower overall signal intensity (Supplementary Table 2.A1).

To better understand patterns of localization, spatial distribution of alkaloids, and potential tissue-specific functions in *H. papilio*, we performed a series of multivariate analyses. A hybrid matrix was constructed that combined fine-tissue localization (presence/absence)

with detection frequency across organ cross-sections. This enabled dimensionality reduction and spatial clustering of alkaloid distribution patterns. A PCA using only normalized detection frequencies across leaf, bulb, and root cross-sectional zones (tip, mid, and base) (Supplementary Figure 2.A4) first identified metabolites based on their organ-level distribution patterns. Precursor and intermediate compounds, including norcraugsodine, norbelladine, nornarwedine, and narwedine, clustered together, reflecting similar organ cross-section-level distribution. Haemanthamine was positioned close to these precursors. Most other alkaloids appeared more dispersed, indicating greater variability in their spatial profiles (Supplementary Figure 2.A4). 4′-O-methylnorbelladine (co-detected with norgalanthamine and normaritidine) clustered in proximity to galanthamine and 11β-hydroxygalanthamine, suggesting overlapping organ-level accumulation. Conversely, 3-O-demethyl-3-O-(3-hydroxybutanoyl)-haemanthamine was positioned further from the other metabolites, reflecting a more divergent detection profile and possible tissue-specific specialization. A second PCA was performed using a hybrid matrix built from Supplementary Table 2.A1 that combined fine-tissue × organ-zone presence/absence data with organ-level detection frequency values (Figure 3.6A). This integrated analysis confirmed the clear separation between precursor/intermediate metabolites (norcraugsodine, narwedine, norbelladine, nornarwedine) and more specialized derivatives, including papiline-type and

galanthamine-type alkaloids. 3-O-demethyl-3-O-(3-hydroxybutanoyl)-haemanthamine remained isolated from other compounds, consistent with a distinct tissue localization profile, while 4'-O-methylnorbelladine/norgalanthamine/normaritidine position stayed close to galanthamine. Differences in tissue-level distributions, particularly in the apical bulb leaf and the tip and mid sections of the root, contributed significantly to the separation between precursor metabolites and galanthamine-type compounds (Mann–Whitney *U* test, $p < 0.05$).

To verify local similarities among metabolites based on their tissue-level distribution, *t*-SNE was applied to the hybrid dataset (Supplementary Figure 2.A4B). The nonlinear dimensionality reduction confirmed the distinct clustering of intermediate compounds (e.g., norbelladine, norcraugsodine, narwedine) from galanthamine-type and papiline-type alkaloids. These clusters further emphasized differences between compounds detected in the apical leaves of the bulb versus those enriched in the leaf tips and root tissues, reinforcing the notion of tissue-specific specialization along the biosynthetic pathway. A pairwise Spearman correlation analysis was performed on the hybrid matrix to assess similarities in metabolite distribution patterns quantitatively (Supplementary Figure 2.A4C). Positive correlations ($\rho > 0.76$) were observed among intermediate compounds, consistent with their tight clustering in both PCA and *t*-SNE projections. Notably, narwedine and nornarwedine exhibited the highest correlation ($\rho = 0.89$), while

galanthamine and 11β-hydroxygalanthamine also showed substantial similarity in their spatial profiles (ρ = 0.85). Interestingly, across all multivariate analyses, haemanthamine consistently clustered more closely with intermediate precursors. To further explore alkaloid relationships based on tissue localization patterns, we applied hierarchical clustering using Ward's method to the hybrid matrix (Figure 6B). This analysis grouped the twelve alkaloids into four main clusters. To assess the reliability of the hierarchical clustering structure, we computed the cophenetic correlation coefficient between the original distance matrix and the dendrogram derived from Ward's method. The resulting coefficient r = 0.77 indicates concordance between the dendrogram topology and the underlying data structure, supporting the robustness of the observed alkaloid groupings. The first cluster included the majority of precursor and intermediate compounds, i.e., norcraugsodine, norbelladine, nornarwedine (vittatine/noroxomaritidine), and narwedine, as well as haemanthamine. These compounds were predominantly detected in the apical bulb leaf and the mid-section of the root, and showed limited presence in vascular zones. The second cluster comprised 4'-O-methylnorbelladine/norgalanthamine/normaritidine, galanthamine, 11ß-hydroxygalanthamine, and the papiline-type alkaloids (papiline and hippapiline), which were more frequently detected in vascular bundles, leaf base, and root tip tissues, including the endodermis and epidermis. A third cluster contained only

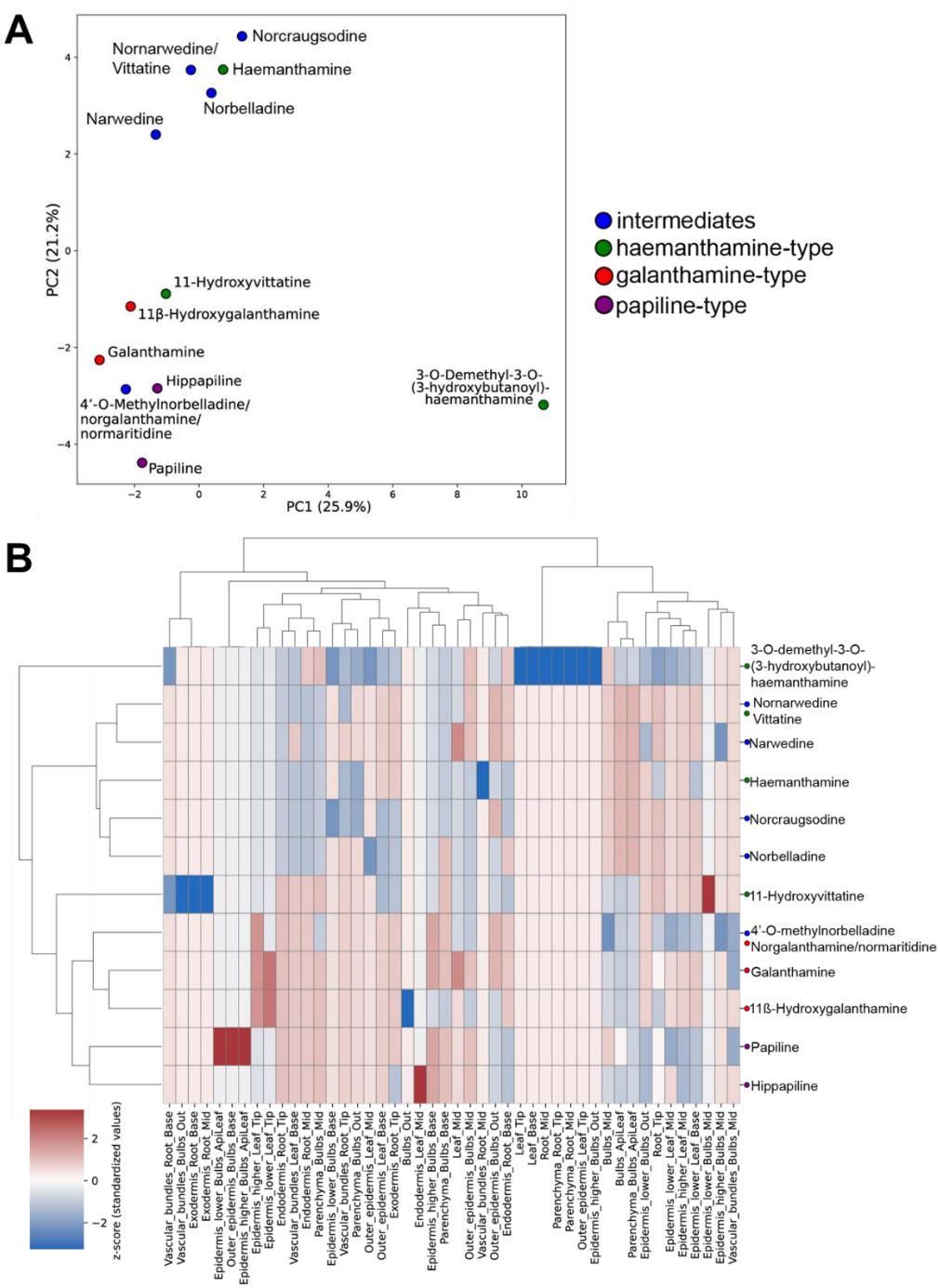
A
Norcraugsodine
Nornarwedine/
Vittatine
Haemanthamine
Norbelladine
Narwedine
11-Hydroxyvittatine
11β-Hydroxygalanthamine
Galanthamine
Hippapiline
4'-O-Methylnorbelladine/
norgalanthamine/
normaritidine
Papiline
3-O-Demethyl-3-O-
(3-hydroxybutanoyl)-
haemanthamine
PC1 (25.9%)
PC2 (21.2%)
intermediates
haemanthamine-type
galanthamine-type
papiline-type
B
3-O-demethyl-3-O-
(3-hydroxybutanoyl)-
haemanthamine
Nornarwedine
Vittatine
Narwedine
Haemanthamine
Norcraugsodine
Norbelladine
11-Hydroxyvittatine
4'-O-methylnorbelladine
Norgalanthamine/normaritidine
Galanthamine
11ß-Hydroxygalanthamine
Papiline
Hippapiline
z-score (standardized values)

Figure 3.6. Integrated analysis of alkaloid distribution in *Hippeastrum papilio* tissues. **A.** Principal component analysis of Supplementary Table A1, integrating organ-level detection frequency and fine-tissue × organ-zone localization data. The matrix was standardized before dimensionality reduction. Metabolites are color-coded by chemical group. **B.** Hierarchical clustering of alkaloids based on their spatial distribution across organs and fine tissue zones. The hybrid matrix integrates organ-level detection frequencies and binary fine-tissue × organ-zone localization data, which are standardized using a z-score transformation. Clustering was performed using Ward's linkage and Euclidean distance, and the resulting heatmap displays the relative spatial profiles of each alkaloid (rows) across all anatomical features (columns). Row colors denote chemical classes: blue = precursor/intermediate compounds, red = galanthamine-type, green = crinine-type, purple = papiline-type. The dendrogram reflects groupings based on overall similarity in tissue-level detection, with a cophenetic correlation coefficient r =0.77, indicating a match between clustering topology and original data structure

11-hydroxyvittatine, characterized by detection in both cortex and vascular regions of the root and bulb, suggesting a partially overlapping but distinct localization. The fourth cluster grouped 3-O-demethyl-3-O-(3-hydroxybutanoyl)-haemanthamine, which showed a unique pattern with detection restricted to bulb parenchyma and mid-root cortex but absent from most other tissue zones. These groupings were also consistent with the spatial separation patterns observed in the PCA and t-SNE analyses.

3.4.5. Biosynthetic gene candidates' expression across organ sections.

To test whether biosynthesis at the transcription levels matches the spatial partitions inferred from MSI, i.e., whether early *vs* late-step genes expression segregates across organs and whether young apical leaf

tissue constitutes a biosynthetic hotspot, we quantified transcripts for seven AA pathway candidates across root, bulb, and leaf sections, normalizing to *Actin* and analyzing by the $2^{-\Delta Ct}$ method. We profiled candidates of two entry-point decarboxylases (*TYDC1*/*2*)(Hu *et al.*, 2021), the first committed condensation enzyme (*NBS*) and the putative reductase (*NR*) (Lamichhane *et al.*, 2025), the *O*-methyltransferase acting on norbelladine or precursors (*OMT*), the phenol-coupling P450 (*CYP96T1*) (Kilgore *et al.*, 2016a), and an *N*-methyltransferase (*NMT*) implicated in downstream tailoring of norgalanthamine to galanthamine (Liyanage *et al.*). Sections assayed were root tip (Ro_Ti), root base (Ro_Ba), basal plate (Ba_Pl), bulb outer middle scale (Bu_OMS), bulb apical leaf (Bu_ApLe), leaf base (Le_Ba), and leaf tip (Le_Ti) to understand the contrast of the same organ related to the position (Figure 7A). Both *TYDC1* and *TYDC2* peaked at the leaf base (relative expression of *TYDC1* = 0.135 ± 0.062, *TYDC2* = 0.140 ± 0.074), and were lowest at the leaf tip, yielding large dynamic ranges (*TYDC1* ≈ 121-fold; *TYDC2* ≈ 15-fold). *NBS* was strongly enriched at the root base (1.122 ± 0.338), minimal at the leaf tip (0.0023 ± 0.001; ~500-fold range). *NR* transcripts were overall low, with a slight maximum at basal plate (0.0047 ± 0.001) > root base (0.0031 ± 0.002) and near-baseline in bulb apical leaves (0.000045 ± 0.000043) and the leaf tip (0.000068 ± 0.000012). *OMT* showed a striking expression in bulb apical leaves (1.279 ± 0.553), followed by leaf base (0.545 ± 0.089) and bulb outer

middle scales (0.393 ± 0.26). Leaf tip was near-zero (0.00043 ± 001), giving the most extensive dynamic range (~3,006-fold). Phenol-coupling P450 (*CYP96T1*) mirrored *OMT* with a bulb apical leaves maximum (0.243 ± 0.076) and elevated expression at root base (0.222 ± 0.092) and leaf base (0.172 ± 0.039); while the leaf tip contained lowest amounts (0.0029 ± 0.001; ~83-fold range). NMT was broadly expressed but highest at the root base (0.616 ± 0.145) > bulb outer middle scales (0.155 ± 0.007) ≈ leaf base (0.108 ± 0.02) ≈ basal plate (0.089 ± 0.048) ≈ bulb apical leaves (0.087 ± 0.023); root tip was lowest (0.060 ± 0.006; ~10-fold range).

There was a significant positive correlation of expression between *CYP96T1* and *NBS* (r = 0.810, $p = 0.0074$), *OMT* (r = 0.801, $p = 0.0084$), and *TYDC1* (r = 0.644, $p = 0.0424$); a possible correlation with *TYDC2* (r = 0.603, $p = 0.0567$) and *NMT* (r = 0.533, $p = 0.087$); although not significant (Figure 7B). *CYP96T1* expression was not correlated with *NR* (r = 0.084, $p = 0.422$) and. The strongest correlation observed was between *NBS* and NMT (r = 0.907, $p = 0.0009$), consistent with their shared root-base enrichment. The transcript maps support a division of steps across organs: early/branch-setting and coupling steps (*TYDC*s, *OMT*, *CYP96T1*) are enriched in young apical leaf and leaf base, whereas early condensation and late *N*-methylation capacity (*NBS*, *NMT*) are prominent in basal/root tissues. This distribution is consistent with the MSI-derived separation between zones enriched in

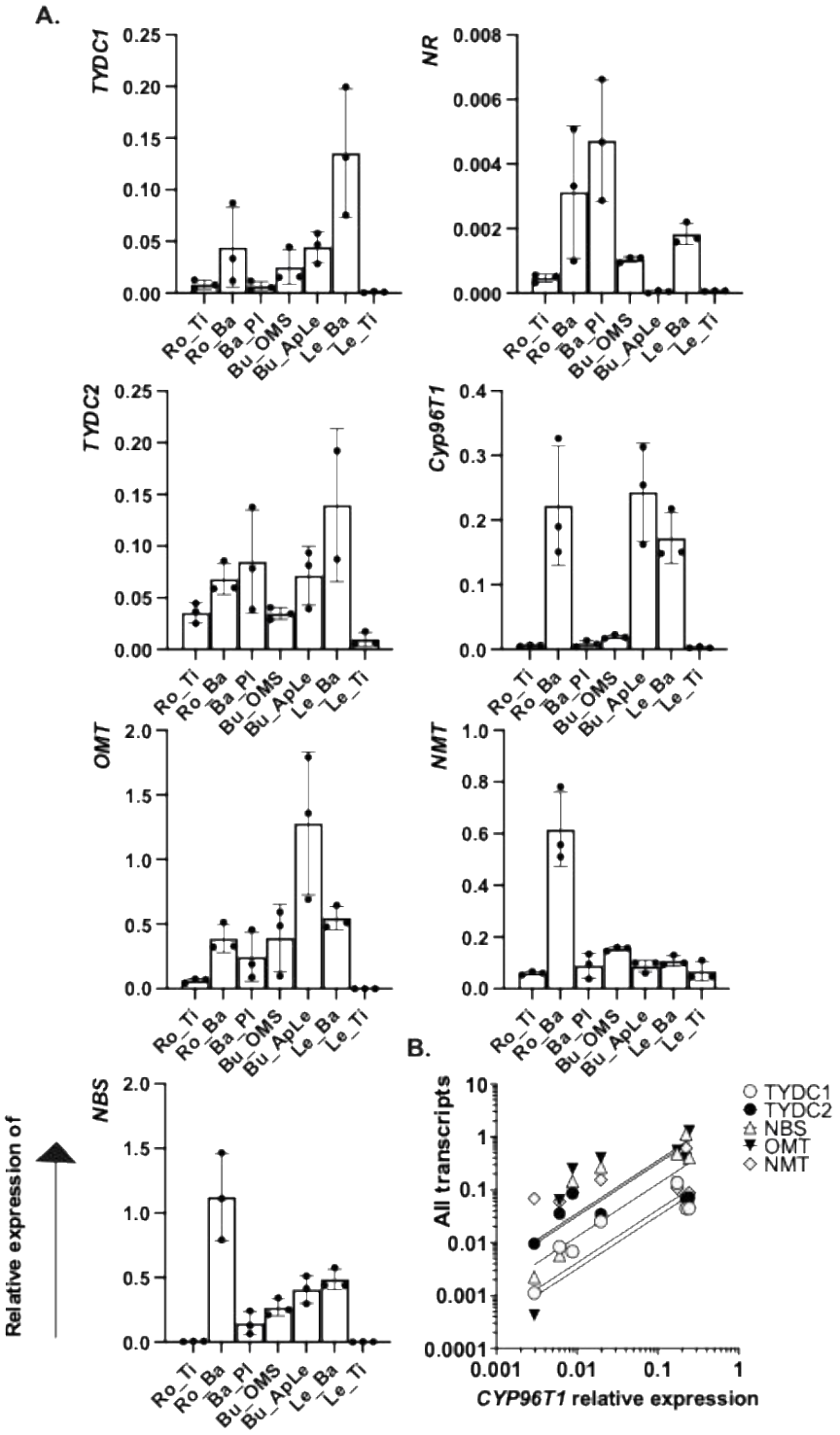

Figure 3.7. Amaryllidaceae alkaloid biosynthetic gene candidates' expression levels across organ sections. A. relative expression of transcripts, tyrosine decarboxylase1 (*TYDC1*), tyrosine decarboxylase2 (*TYDC2*), *O*-methyltransferase (*OMT*), norbelladine synthase (*NBS*), norcraugsodine reductase (*NR*), cytochrome p45096T1 (*CYP96T1*), *N*-methyltransferase (*NMT)* were normalized on the level of actin expression. Ro_Ti=

root tip, Ro_Ba = Root base, Ba_Pl = Basal plate, Bu_OMS = Bulb outer middle scale, Bu_ApLe = Bulb apical leaf, Le_Ba = leaf base, Le_Ti= Leaf tip. B. Association between levels of expression of CYP96T1 and other transcripts (Pearson correlation). NR expression is not displayed because not significantly associated.

precursors/intermediates versus those concentrating downstream alkaloids and specialized cell layers, and it highlights the apical bulb leaf as a transcriptional hotspot for key mid-pathway steps (Figure 3.7; MSI multivariate summary in Figure 3.6)

3.4.6. Additional compound annotations with Metaspace

In addition to using the comprehensive literature review on alkaloids reported in *H*. *papilio* as database, we utilized the MSI metabolite annotation platform Metaspace (Palmer *et al.*, 2017) to analyze the data obtained from our non-targeted MSI experiments. Even if the identification in Metaspace is based solely on accurate mass analysis (leaving the possibility open for the presence of several isomeric compounds instead of or in addition to the tentatively identified compound), it revealed the putative presence of multiple classes of compounds (Supplementary Table A3), such as colchicine derivatives (deacetylcolchicine, N-acetoacetyl-deacetylcolchicine, trimethylcolchicinic acid/ N-deacetylcolchiceine, demecolchine/androcymbine/isoandrocymbine) (Supplementary Fig. A5E-H), flavonoids (kaempferol-3-O-rutinoside/ kaempferol 3-O-rhamnoside-7-O-glucoside, luteolin/kaempferol, quercetin 3-O-glucoside, quercetin/8-hydroxykaempferol/6-hydroxykaempferol/8-hydroxyluteolin. 4'-methoxyflavanone), amides (N-*p*-trans-

coumaroyltyramine, N-trans-caffeoyltyramine), lignans (1-acetoxypinoresinol, deoxypodophyllotoxin), pigments (pheophorbide a, adonixanthin/ dinoxanthin/ didinoxanthin, echinenone, 4-ketomyxol), and fungicide (flumetover) (Supplementary Fig. A6, Supplementary Table A3)

Metaspace annotations also indicated the potential presence of AAs previously documented in other species of the Amaryllidaceae family but not yet reported in *H. papilio*. These findings are summarized in Figure 8, the accompanying Supplementary Table 2.A2, and Supplementary Fig. 2.A5, which provide detailed insights into the newly identified AAs and their potential biological and ecological significance. These included phenanthridine-type alkaloids such as crinasiadine and trisphaeridine, β-carboline alkaloids like trichotamine, and a variety of AA, including assoanine, oxoassoanine, albomaculine, ungeremine, hippeastrine, crinan/gamma-lycorane, O-methyllycorenine, belladine, amaryllisine/lycorenine, and papyramine. Additionally, metabolites associated with the alkaloid degradation pathway, such as galanthamine beta-D-glucuronide and O-demethyl-galanthamine beta-D-glucuronide, were identified. These findings highlight the chemical diversity of *H. papilio.*

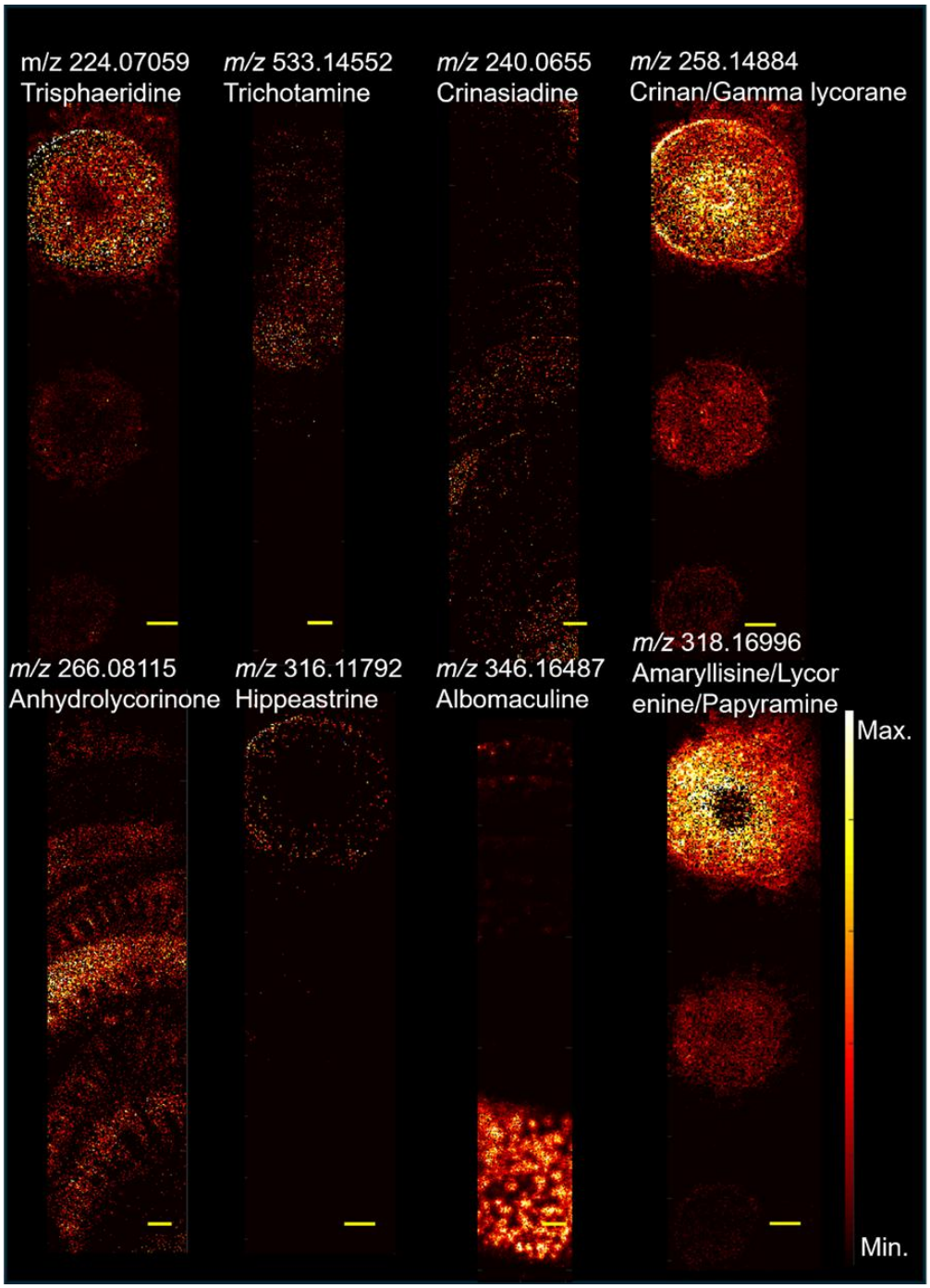

Figure 3.8. MALDI-MSI of multiple METASPACE-annotated compounds in cross sections of *Hippeastrum papilio* tissues. Panels A, D, F, and H show root sections (pixel size: 40 µm); panels B and G show bulb sections (pixel size: 30 µm); and panels C and E show leaf sections (pixel size: 40 µm). Scale bars: 1 mm.

3.5. Discussion

In this study, MALDI-MSI and LC-MS were used to gain insight into alkaloid biosynthesis in high levels of galanthamine-producing *H. papilio,* by analyzing the spatial distribution in different organs. One of the primary strengths of MSI is its label-free nature, which enables the direct analysis of a wide range of molecules simultaneously in various samples (Spengler, 2015). This feature preserves sample integrity and reduces preparation time (Dong *et al.*, 2016). It has revolutionized numerous scientific fields by enabling the visualization of the spatial distribution of molecules (Buchberger *et al.*, 2017). Unlike traditional MS, which provides bulk molecular information, MSI retains the spatial context of analytes, making it invaluable for understanding complex biological systems (Buchberger *et al.*, 2017; Qin *et al.*, 2018). Over the years, MSI has become an indispensable tool across various disciplines, from medicine and drug development to agriculture (Buchberger *et al.*, 2017; Granborg *et al.*, 2022), enabling researchers to map the spatial distribution of metabolites directly on plant tissues (Bjarnholt *et al.*, 2014). MALDI-MSI results are inherently qualitative for this type of plant tissue analysis. While the imaging data reveals the spatial distribution of compounds, it does not provide quantitative information. Variations in ionization efficiencies among different compounds also limit the direct comparison of their concentrations. In *H. papilio*, we first focused on the repartition of well-known alkaloids end products (such as galanthamine,

haemanthamine) and intermediates (such as norbelladine, norcraugsodine) in cross-sections of three organs (leaves, bulbs and roots). The presence of these specific alkaloids in each cross-section was deeper analyzed based on detection in specific tissues (e.g. parenchyma, epidermis). One limitation of the current analysis was the presence of isomers (same m/z) for 4'-O-methylnorbelladine (norgalanthamine, normaritidine) and nornarwedine (vittatine/ noroxomaritidine), which introduced signal overlap in these cases (Table 3.1).

3.5.1. Leaf tissues

Previous studies have suggested that AAs are biosynthesized in young leaf tissues (Mehta *et al.*, 2024). Consistently, all AAs were detected in the innermost part of the leaf. In contrast, intermediates like norcraugsosine, norbelladine, 4'-O-methylnorbelladine (norgalanthamine, or normaritidine), nornarwedine (vittatine/noroxomaritidine) were detected in some but not all outermost sections of the leaf. Yet, the detection of these intermediates in the base and tip leaf sections suggests that alkaloid biosynthesis could be a spatially widespread process, not confined to specific regions. Their detection at low ion intensities could indicate transient accumulation in the tissues, consistent with their role of precursors for the synthesis of more complex alkaloids (Li *et al.*, 2024). The distribution of galanthamine, papiline, and hippapiline across different leaf ages and

positions suggests that these compounds may play a generalized role in leaf physiology and serve analogous functions, such as protecting photosynthetic tissues, maintaining leaf structural integrity, and defending against pathogens and herbivores, rather than being specific to certain developmental stages or regions. This observation is consistent with the findings of Nakagawa et al. (2024), who reported no significant differences in the distribution patterns of galanthamine, lycorine, and tazettine in *N*. *tazetta* leaf tissues (Nakagawa *et al.*, 2024). While our study did not achieve subcellular resolution, the ultra-sensitivity of the MALDI-MSI instrumentation allowed the detection of alkaloids in specific tissues. Mehta et al. (2024) observed that alkaloids in *Narcissus* cv. Tête-à-Tête were localized near vascular tissues of leaves, a finding that resonates with the results of this study (Mehta *et al.*, 2024). The abundance of alkaloids in epidermal and vascular tissues, particularly in the lower epidermal regions of the leaf bases, underscores the potential role of these compounds in defence mechanisms (Tissier *et al.*, 2014). Epidermal tissues are the first living cells of a plant body that separate the plant from the environment, hence the presence of alkaloids in these regions may deter herbivory and microbial infections (Dietz and Hartung, 1996). Similarly, the localization of alkaloids in vascular bundles suggests their involvement in systemic defence and possibly their transport (Hagel *et al.*, 2012). The absence of alkaloids in the aerenchyma supports the idea that these compounds are

strategically localized in tissues with higher metabolic activity and defence requirements. This finding aligns with the histochemical localization study by Haist et al. (2024), which detected alkaloids in the cuticle, vascular bundles, intracellular spaces, nucleus, and vacuoles of *H. papilio* leaf tissues (Haist *et al.*, 2024b).

3.5.2. Bulb tissues

Compared to leaves, there was greater variation in AA repartition across the bulbs' cross-sections. AA accumulated intensely in the basal plates, followed by the outermost bulb scales and the middle bulb scales. Intriguingly, while most intermediates were detected in apical leaves, end-products AAs, except haemanthamine, were not. The differential distribution suggests that they may serve distinct functional roles depending on their localization. For instance, compared to middle scales and apical leaves, the higher abundance of galanthamine in the outer bulb scales and basal plates, which are more exposed to the external environment, implies a potential defensive role against herbivores or pathogens. Our results differ from those of Haist et al., which showed a high accumulation of all AAs, including galanthamine, in the inner bulb sections of *H. papilio* using a less sensitive method (Haist *et al.*, 2024b). Our results cannot be directly compared either with those of Mehta et al., who excluded apical leaves from their analysis (Mehta *et al.*, 2024). Most Amaryllidaceae species undergo hibernation periods during unfavourable conditions, such as winter or drought, where the bulbs are

the only organs that remain. Therefore, bulbs should accumulate a high amount of defense-responsive molecules to protect the plant. Our mucilage analysis also supports this idea that the AAs in the mucilage of bulbs are higher than in leaves. Nevertheless, the accumulation profile of galanthamine does not align with the findings by Nakagawa et al. (2024), who reported higher galanthamine levels in the apex leaves of *N*. *tazetta* bulbs (Nakagawa *et al.*, 2024). Their study did not examine the basal plates. Compared to the subterranean bulbs of *N*. *tazetta, H*. *papilio* is an epiphyte, and its bulb is more exposed, which may necessitate different defense strategies. The higher concentrations of AAs in epidermal and vascular tissues further support their involvement in defense mechanisms. Consistent with our analysis of the bulb, histochemical staining studies in *H*. *papilio* indicated that AAs were primarily localized in intercellular spaces, vacuoles, and nuclei, rather than in outer cell layers, such as the cuticle (Haist *et al.*, 2024b). The abundance of alkaloids in the basal plates, particularly around vascular regions, suggests a potential role in nutrient transport or storage. While most alkaloids were more specific to the vascular bundles, galanthamine was present in both the parenchymal and vascular bundles of the basal plates. This reinforces the particular physiological function of this metabolite, while its ubiquity is consistent with its high abundance in the species.

3.5.3. Root tissues

A unique distribution pattern of alkaloids was observed in *H*. *papilio* root tissues, exhibiting more complex and compartmentalized features compared to leaves and bulbs. One of the most intriguing observations was a specific intense accumulation of galanthamine, and to a lesser extent, of 4'O-methylnorbelladine/norgalanthamine/normaritidine and 11β-hydroxygalanthamine in the vascular regions of the roots. This contrasts with leaves and bulbs, where vascular areas showed a high abundance of most alkaloids. Previous studies, such as those on *N*. *tazzetta*, *N.* cv. Tête-à-Tête, did not investigate root tissues, preventing the possibility of comparison (Mehta *et al.*, 2024; Nakagawa *et al.*, 2024). Histochemical staining of *H*. *papilio* roots has previously indicated that alkaloids are present in all three main regions—exodermis, cortex, and vascular cylinder, with higher intensity in the vascular area (Haist *et al.*, 2024b). However, these findings represent the cumulative presence of all AAs, making it difficult to compare with the specific distribution patterns of individual alkaloids observed in this study. As epidermal and exodermal tissues are exposed to the environment, the chemical defense mechanism might be highly active in that area. For example, it has been shown that defense-responsive genes are expressed in epidermal cells of wheat in response to pathogen attacks (Altpeter *et al.*, 2005). The compartmentalized distribution of AAs in root tissues suggests a highly regulated biosynthetic pathway, which may be tailored

to the specific physiological and ecological roles of these compounds in *H*. *papilio*.

. 3.5.4 Differences in the precursors' distribution in *H. papilio*

Multivariate analysis in MSI studies often relies on quantitative ion intensities. Instead, we applied a hybrid matrix integrating binary fine localization patterns and the normalized frequency of organ-level detection. This structured approach aimed to enhance the biological interpretation of spatial metabolite compartmentalization. PCA, t-SNE, Spearman, and hierarchical clustering all revealed a clear spatial separation between precursor alkaloids (e.g., norbelladine, norcraugsodine, narwedine, nornarwedine/vittatine/noroxomaritidine) and downstream galanthamine-type and papiline-type compounds, with haemanthamine clustering with precursors. This observation suggests that early and late stages of the Amaryllidaceae alkaloid biosynthetic pathway may occur in spatially distinct tissues in *H. papilio*, consistent with the notion of tissue-specific partitioning of specialized metabolism. The clustering of precursors and intermediates was significantly associated with their enrichment in the apical bulb leaf, likely corresponding to the youngest and most biosynthetically active tissue. These results are partially consistent with Mehta et al's hypothesis that biosynthesis is more active in young tissues of leaves, even though they did not investigate young apical leaves (Mehta *et al.*, 2024). However, these compounds were also frequently detected in the epidermis of the

bulb mid-section and in the leaf base and mid-section, indicating that early biosynthetic steps may occur across both internal and peripheral tissues. This broader spatial distribution is in line with Haist et al, who reported high alkaloid concentrations in inner bulb tissues, but also observed signal in more superficial tissues, depending on compound type.

The consistent association of haemanthamine with precursors across PCA, t-SNE, and hierarchical clustering further suggests that this compound may be synthesized closer to the precursor zone than previously assumed. In contrast, galanthamine, 11β-hydroxygalanthamine, and papiline-type alkaloids clustered with features such as the root endodermis, leaf tip vascular bundles, and epidermal zones of distal organs, together with the detection of high levels of end-products in bulb and leaves mucilage, this suggests that late-stage tailoring may occur in more specialized cell layers, vascular-associated cells, distinct from the tissues synthesizing early intermediates. These spatial relationships reveal a likely progression from early, distributed biosynthesis toward more compartmentalized localization of end-products. Alternatively, active transport mechanisms could mediate the relocalization of galanthamine from its site of synthesis to specialized storage compartments, potentially minimizing self-toxicity or optimizing resource allocation within the plant. These patterns should be interpreted as exploratory correlations rather than definitive

biosynthetic maps, given the qualitative or semi-quantitative nature of the MSI analysis and the sampling that was performed during the vegetative stage. Nonetheless, the consistent separation between precursor and galanthamine-type compounds across unsupervised clustering, PCA, and t-SNE, along with their reproducible association with distinct tissue features, offers a strong foundation for future work that combines enzyme localization, gene expression, and transport assays to test these hypotheses experimentally.

While multivariate analyses have been increasingly adopted in metabolomics datasets, their application to MSI spatial profiles in plants remains limited, particularly for specialized metabolites. The integration of PCA, t-SNE, and hierarchical clustering with MSI datasets allowed the identification of structured tissue-level patterns that would not have been evident through descriptive visualization alone. Recent advances in plant MSI analysis increasingly highlighted the importance of such approaches for uncovering hidden biological organization (Boughton *et al.*, 2016; Dong *et al.*, 2016; Heyman and Dubery, 2016; Li *et al.*, 2024), and our study extends these concepts to the investigation of specialized metabolite biosynthesis and transport in Amaryllidaceae.

Overall, the qRT-PCR profiles reinforce our MSI-based interpretation of spatially organized alkaloid biosynthesis. While variability was observed with regards to the distribution of *TYDC1*/*2* expression among root, stem,

or leaf tissues using organ-level sampling methods in *Leucojum aestivum* and *Lycoris radiata* (Hu *et al.*, 2021; Karimzadegan *et al.*, 2024), here, we show that they were enriched in leaf bases. *NBS*, strongly expressed at the root base, mirrors findings in *Narcissus papyraceus* and *Leucojum aestivum* and supports roots as sites where scaffold condensation and terminal tailoring converge (Majhi *et al.*, 2023). In contrast, *OMT* and *CYP96T1* peaked in apical bulb leaves, consistent with proposals that young tissues are hotspots for phenol-coupling and diversification (Mehta *et al.*, 2024). *NR* expression remained uniformly low, in agreement with previous studies showing poor correlation between *NR* transcript levels and alkaloid abundance (Majhi *et al.*, 2023). Together, these patterns could suggest a spatial division of biosynthetic steps: precursor supply in leaf bases, scaffold formation and late tailoring in basal/root zones, and coupling/diversification in apical leaves. This tissue-level separation echoes models from other alkaloid systems such as *Papaver somniferum*, *Catharanthus roseus* and underscores the coordinated, multi-organ nature of Amaryllidaceae alkaloid biosynthesis (Watkins and Facchini, 2022).

In a nutshell, the distribution patterns of AAs observed in the three organs of *H. papilio*—leaves, bulbs, and roots—provide valuable insights into the potential biosynthetic pathway arrangement of galanthamine (Figure 9). The data suggest that the early steps of AA biosynthesis are

enriched in apical leaves, and the biosynthesis of galanthamine likely occurs in distinct tissue-specific compartments, with varying degrees of metabolic exchange between these regions. In the leaves and bulbs, the pathway appears to be localized primarily in the epidermal tissues and vascular areas, while precursors were comparatively enriched in the apical leaves. The presence of key intermediates in both tissues indicates that the biosynthetic reactions may occur in either compartment, with potential exchange of metabolites between the epidermis and vascular areas. This suggests a dynamic interplay between these regions, where specific steps of the pathway could be restricted to either the epidermis or the vascular tissues, followed by the transport of intermediates to the other compartment for subsequent reactions. In contrast, the roots exhibit a more compartmentalized biosynthetic profile. The limited exchange of intermediates observed in the roots, compared to the leaves and bulbs, implies that the reactions may be more spatially restricted. This compartmentalization could reflect a specialized metabolic strategy in the roots, potentially optimizing the utilization of resources or minimizing the exposure of toxic intermediates to other tissues.

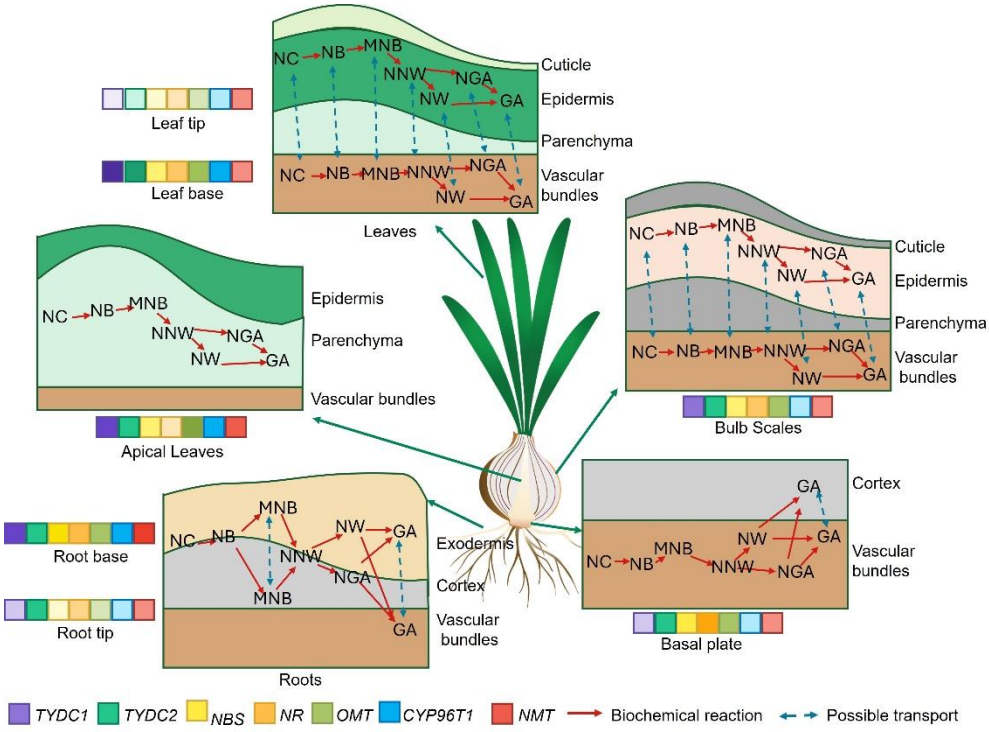

Figure 3.9. The proposed biosynthetic organization of galanthamine in *Hippeastrum papilio* is illustrated, with red arrows denoting biochemical steps and blue arrows indicating potential alkaloid transportation. NC = norcraugsodine, NB = norbelladine, MNB = 4'-O-methylnorbelladine, NNW = nornarwedine, NW = narwedine, NGA = norgalanthamine, GA = galanthamine. The intensity of the colors of each box representing the genes show the comparative relative expression of the relevant gene in corresponding organ .

It was shown that the change in withanolides in the aeroponically grown medicinal plant *Withania somnifera,* where withanolides usually accumulate in roots, starts to accumulate in the leaves when they grow aeroponically (Xu *et al.*, 2011). Thus, differences in growth conditions complicate the comparison of the biosynthesis of AA of *H*. *papilio* with geophytic species like *N*. *tazetta* or *Narcissus* cv. Tête-à-Tête (Mehta *et al.*, 2024). Based on our observations, the biosynthesis of AA in *H. papilio* does not exhibit an organ-specific pattern. This idea is supported by detection of biosynthetic gene expression in all the organs, although

the level of expression varies. For example, *norbelladine synthase* and *norcraugsodine/noroxomaritidine reductase* and *4'-O-methyltransferase* involved in the formation of precursors and intermediates are detected in all organs of *Leucojum aestivum* and *Narcissus papyraceus* (Koirala *et al.*, 2024; Majhi *et al.*, 2023). Similarly, the transcripts of *N*-methyltransferase, which can be involved in the formation of galanthamine, 3'-*O*,*N*-dimethylnorbelladine, 3,4'-*O*,*N*-trimethylnordelladine were present in all the studied organs of *L*. *aestivum*, *Lycoris radiata*, and *H*. *papilio* (Liyanage *et al.*). Some steps may be tissue-specific; however, further investigation, including multi-omics or single-cell-level analysis, is needed to determine the exact information that elucidates the pathway.

3.5.5. New metabolites uncovered in *H. papilio*

By leveraging multiple databases integrated with Metaspace, we identified several previously unreported AAs in *H*. *papilio*, expanding the known phytochemical profile of this species. Notably, our findings also provide evidence for compounds associated with colchicine biosynthesis, a pathway previously documented only in *Lycoris radiata* (Yan *et al.*, 2018). The detection of multiple intermediates in this pathway supports the possibility of shared or convergent biosynthetic routes within the Amaryllidaceae family. Additionally, we observed diverse alkaloid groups beyond the typical Amaryllidaceae-type structures, underscoring the metabolic complexity of this plant family (Berkov *et al.*,

2020; Jin and Yao, 2019). Beyond targeted alkaloid profiling, this non-targeted approach proves valuable for broader metabolomic investigations. The simultaneous detection of flavonoids, lignans, pigments, and other specialized metabolites highlights the potential of MALDI-MS in studying metabolic correlations, plant-environment interactions, and biosynthetic networks. Such comprehensive analyses could pave the way for future research on the ecological and physiological roles of diverse metabolite classes in plants.

In summary, this study employed MALDI-MSI to investigate the spatial distribution of AAs in *H. papilio* leaf, bulb, and root tissues. Galanthamine accumulated particularly in epidermal and vascular regions. Leaves showed consistent alkaloid distribution across ages and positions, while bulbs exhibited variations between outer and inner scales. Roots displayed compartmentalized alkaloid distribution, with higher concentrations at the proximal end. Biosynthetic intermediates and minor alkaloids were present but at lower intensities, and specifically concentrated in the bulb apical leaves. The findings highlight tissue-specific alkaloid distribution patterns, suggesting specialized biochemical pathways in different plant regions.

These findings contribute to a deeper understanding of the ecological and physiological significance of alkaloids in *H. papilio* and highlight the importance of tissue-specific metabolic profiling in plant research. Future studies could explore the subcellular localization of these alkaloids and

their biosynthetic pathways to further elucidate their functional roles and regulatory mechanisms in *H. papilio*. Additionally, comparative studies across different plant species with varying ecological niches could provide broader insights into the adaptive significance of alkaloid distribution patterns.

3.6. Conclusion

To the best of our knowledge, this is the first comprehensive study of the spatial metabolic arrangement of alkaloids in an Amaryllidaceae species. Our analysis revealed that galanthamine-type and papiline-type AAs exhibited a consistent spatial arrangement in the organs of *H. papilio, whic*h differed from that of intermediates and haemanthamine. The abundance of AAs in epidermal and vascular tissues highlights their potential role in defense mechanisms, while the presence of biosynthetic intermediates suggests widespread alkaloid biosynthesis. In leaves, the spatial distribution of metabolites appears interdependent: areas with early intermediates consistently show downstream metabolites, and conversely, regions with lower detection of precursors demonstrate reduced detection of AAs. In bulbs, while intermediates and end-products were detected in older scales and basal plates, intermediates were more specific to the apical leaves. In the basal plates, most localized in vascular bundles, while galanthamine was also abundant in the parenchyma. In roots, AAs were less prevalent in the vascular bundles than in the cortex, with galanthamine and its derivative being a

notable exception. This unique accumulation pattern of galanthamine potentially indicates distinct transport or storage mechanisms compared to other alkaloids. These findings provide crucial insights into the tissue-specific biosynthesis and localization of AAs, emphasizing the coordinated nature of their production and storage across various plant organs. This knowledge advances our understanding of the metabolic architecture of *H*. *papilio* and sets the stage for exploring its potential biotechnological applications.

3.7. Acknowledgements

The authors thank Dr. Marcus Daniel Brandbjerg Bohn Lorensen (University of Copenhagen) and Rohith Grandhi (Université du Québec à Trois-Rivières) for their valuable input and contributions. We also thank Prof. Antonio Evidente (Universitario Monte Sant'Angelo, Naples, Italy) for providing some alkaloid standards. During the preparation of this work, the authors used ChatGPT version 4.0, a free AI language model, in order to correct grammatical errors and enhance readability. After using this tool, the authors reviewed and edited the content as needed and take full responsibility for the content of the publication.

3.8. Funding Statement

This research was funded by Canada Research Chair on plant specialized metabolism Award No CRC-2018-00137 to I.D-P. Thanks are extended to the Canadian taxpayers and to the Canadian

government for supporting the Canada Research Chairs Program. Additional support from the Natural Sciences and Engineering Research Council of Canada (NSERC) award number RGPIN/3218-2021 to IDP. Funding from the Carlsberg Foundation and Independent Research Fund Denmark | Medical Sciences (grant no. DFF – 4002-00391) for MALDI-MSI instrumentation is gratefully acknowledged.

3.9. Data availability

Raw data in the form of imzML files of the presented data has been uploaded to the Metaspace platform (https://metaspace2020.org/project/Hippeastrum_paplio_MALDI) and annotated against multiple publicly available databases. Access to the reviewers by https://metaspace2020.org/api_auth/review?prj=0247bb56-4f1e-11ef-86c3-fbc99e2b8fbc&token=_Xv46BbxCZf8

Supplementary data to this article can be found in Appendix II.

CHAPTER IV

4. Conclusion

The research presented in this thesis explores the biosynthesis of Amaryllidaceae alkaloids (AAs), with a particular focus on galanthamine, a compound of significant pharmaceutical importance due to its use in treating the symptoms of Alzheimer's disease. The study integrates findings from two key research papers: one investigating the role of *N*-methyltransferases (NMTs) in galanthamine biosynthesis and the other employing mass spectrometry imaging (MSI) to map the spatial distribution of alkaloids in tissues of *Hippeastrum papilio*, a high galanthamine-producing species. Together, these studies provide a comprehensive understanding of the enzymatic mechanisms and spatial dynamics underlying AA biosynthesis, offering insights into metabolic engineering strategies for enhanced alkaloid production. The limited supply of galanthamine, primarily sourced from plant extraction, underscores the need for biotechnological solutions to meet pharmaceutical demands (Koirala *et al.*, 2022). By elucidating the biosynthetic pathways and regulatory mechanisms of AAs, this research contributes to the development of sustainable production methods, such as heterologous expression in microbial systems or optimized plant cultures (Koirala *et al.*, 2023; Lamichhane *et al.*, 2025). The integration of enzymatic characterization and spatial metabolomics represents a

novel approach to unraveling the complexities of plant specialized metabolism(Liyanage *et al.*, 2025a).

4.1. Coclaurine *N*-methyltransferase like NMTs: Integration of biosynthesis of Amaryllidaceae Alkaloids

The biosynthesis of galanthamine, a pharmacologically valuable Amaryllidaceae alkaloid, involves complex enzymatic reactions that culminate in structural diversification (Mehta *et al.*, 2024). This study elucidates a crucial enzymatic step in galanthamine biosynthesis by identifying and characterizing coclaurine *N*-methyltransferase (CNMT)-like enzymes from three galanthamine-producing species: *Leucojum aestivum*, *Lycoris radiata*, and *Hippeastrum papilio* (Liyanage *et al.*). The identification of *LaLrHp*NMT1, a highly conserved and catalytically efficient isoform, marks a pivotal advance in resolving the enzymatic conversion of norgalanthamine to galanthamine — a transformation not previously ascribed to known tocopherol *N*-methyltransferases (TocoNMT) (Liyanage *et al.*; Mehta *et al.*, 2024). Yet it is hard to compare the activity of both NMTs as the previous study was not focused on characterization of TocoNMT (Mehta *et al.*, 2024). These CNMT-like enzymes integrate into the broader AA biosynthetic framework, which begins with condensation of tyramine and 3,4-dihydroxybenzaldehyde by NBS, followed by multiple modifications including hydroxylation, methylation, and oxidative phenol coupling (Jayawardena *et al.*, 2024; Lamichhane *et al.*, 2025). The identified *LaLrHp*NMT1 complements this

pathway by catalyzing a final methylation step critical for galanthamine formation. Its activity bridges a gap left by TocoNMTs, which methylate narwedine but not norgalanthamine, thus validating isotope-labelling studies that proposed multiple methylation routes (Jayawardena *et al.*, 2024; Liyanage *et al.*, 2025a).

Moreover, this research indicates that *LaLrHp*NMT1 exhibits significant substrate promiscuity, accepting substrates like tyramine and tryptamine in addition to norgalanthamine. This flexibility mirrors the behavior of BIA-pathway NMTs and suggests the Amaryllidaceae pathway may harbor latent metabolic plasticity. The presence of multiple NMT isoforms with subtle sequence divergence further implies species-specific regulatory layers or specialized roles in shaping alkaloid diversity. The biosynthetic localization of *LaLrHp*NMT1 at the cytosol-endoplasmic reticulum interface aligns with the spatial compartmentalization observed for other AA biosynthetic enzymes, such as cytochrome P450s. This spatial arrangement may facilitate substrate channelling or protein-protein interactions, promoting metabolic flux toward galanthamine biosynthesis (Qin *et al.*, 2025). Altogether, the integration of *LaLrHpNMT*1 into the AA biosynthetic map not only clarifies an unresolved step but also broadens our understanding of methyltransferase involvement in alkaloid diversification. By capturing both functional specificity and catalytic plasticity, this enzyme exemplifies the sophisticated enzymatic architecture underlying the

metabolic networks in Amaryllidaceae plants (Lashley *et al.*, 2022; Sweetlove and Fernie, 2018).

4.1.1. Biological, Evolutionary, and Ecological Significance

From an evolutionary standpoint, the conservation of CNMT-like NMTs across three distinct Amaryllidaceae species underscores their fundamental biological role (Ribeiro *et al.*, 2023). The presence of orthologous sequences with highly similar catalytic domains suggests selective pressure to maintain galanthamine biosynthesis or related methylation processes across divergent lineages. Interestingly, these enzymes cluster phylogenetically with CNMTs from *Nelumbo nucifera* and *Stephania intermedia*, suggesting an ancient origin and potential functional convergence within isoquinoline alkaloid-producing lineages (Chen *et al.*, 2024; Zhao *et al.*, 2020). Moreover, the relationship to the NMTs from non-angiosperm plants like *Ephedra sinica* indicates the evolutionary origin of the gene (Morris *et al.*, 2018). The conserved Rossmann fold and signature catalytic triad (Glu204, Glu207, His208) indicate these enzymes retained essential features for SAM-dependent methylation over evolutionary timescales (Morris *et al.*, 2020). Yet, the emergence of isoforms with amino acid substitutions (e.g., *Hp*NMT2 with Ser at Tyr325 position) implies ongoing neofunctionalization or subfunctionalization. This could serve as a mechanism for expanding substrate scope, as observed in the enzymatic promiscuity of *LaLrHp*NMT1.

The cytosolic–ER interface localization of *LaLrHp*NMT1 resembles patterns observed in other alkaloid pathways, where ER-anchored CYP450s interact with soluble O-/N-methyltransferases to form transient enzyme complexes. For example, in *Catharanthus roseus*, CYP450s and OMTs involved in monoterpenoid indole alkaloid biosynthesis have been shown to co-localize to facilitate efficient substrate channeling (Guirimand *et al.*, 2011; Miettinen *et al.*, 2014). Likewise, the dhurrin pathway in Sorghum provides a canonical model of a plant metabolic metabolon at the ER membrane (Laursen *et al.*, 2016). The evidence that *LaLrHp*NMT1 operates at the cytosolic–ER interface suggests that Amaryllidaceae alkaloid biosynthesis may rely on similar metabolon-like assemblies to optimize flux toward galanthamine. Ecologically, alkaloids in Amaryllidaceae serve diverse roles, ranging from deterring herbivores to providing microbial defense (Berkov *et al.*, 2020). Environmental modulation of *NMT* expression, especially under heat and abiotic stress, suggests its involvement in stress-induced alkaloid biosynthesis (Sun *et al.*, 2018). This is consistent with broader observations that specialized metabolites serve adaptive roles under challenging environmental conditions. In *H. papilio*, the upregulation of *NMT* expression in response to stressors like methyl jasmonate (MeJA), salinity, and heavy metals further supports the hypothesis that galanthamine and related alkaloids act as inducible defense compounds (Jan *et al.*, 2021). Tissue-specific analysis revealed an interesting disconnect between transcript levels

and alkaloid accumulation. While *NMT* was most highly expressed in leaves, galanthamine content was maximal in bulbs. This discrepancy could reflect post-transcriptional regulation, transport of biosynthetic intermediates, or differences in storage versus synthesis sites—hallmarks of metabolically compartmentalized defense strategies (Heinig *et al.*, 2013). Thus, these NMTs are not merely catalytic actors in a pharmaceutical pathway but also evolutionarily refined tools shaped by ecological pressures. Their functional flexibility and stress-responsive regulation suggest that galanthamine biosynthesis is closely intertwined with the plant's adaptive biology, thereby helping to ensure survival while providing humans with access to neuroprotective compounds (Yin *et al.*, 2025).

4.1.2. Metabolic Redundancy and Enzyme Promiscuity in Galanthamine Biosynthesis

The observation that multiple enzymatic routes may converge on galanthamine biosynthesis highlights an important aspect of Amaryllidaceae alkaloid metabolism: metabolic redundancy and enzyme promiscuity. In this study, *LaLrHp*NMT1 was shown to catalyze the methylation of norgalanthamine to galanthamine—a step previously associated with tocopherol N-methyltransferases (TocoNMTs), which instead preferentially act on narwedine (Mehta *et al.*, 2024). The coexistence of both methylation routes suggests a layered biosynthetic

architecture where alternate substrates can be utilized depending on cellular context, developmental stage, or environmental cues (Weng *et al.*, 2012). This metabolic branching likely reflects a strategy to enhance biosynthetic resilience. By maintaining more than one route to galanthamine, the plant ensures consistent production of this pharmacologically and ecologically important compound even under variable conditions (Weng *et al.*, 2012). For instance, *LaLrHp*NMT-dependent routes require prior reduction of nornarwedine to norgalanthamine, which could be energetically or spatially constrained(Lange *et al.*, 2000). In contrast, *LaLrHp*NMT1's ability to act directly on norgalanthamine provides a streamlined alternative, particularly in tissues or developmental stages where reduction enzymes are limited. Or else it could be solely dependent on the sub-cellular arrangement of the pathway where TocoNMT is supposed to be in the chloroplast or other organelles and *LaLrHp*NMT1 is in the cytosol-ER surface (Wink, 2008).

Furthermore, the demonstrated substrate promiscuity of *LaLrHp*NMT1—accepting not only norgalanthamine but also simple amines like tyramine and tryptamine—indicates evolutionary adaptation for flexible catalytic function (Wink, 2013). Such promiscuity is frequently observed in the specialized metabolism of plants; it permits individual enzymes to play a role in various pathways or create unique metabolic arrangements, which facilitates chemical diversity arising from a constrained genetic

framework (Leong and Last, 2017). This flexibility is further supported by the presence of multiple NMT isoforms in the Amaryllidaceae transcriptome, some of which may show distinct substrate preferences or spatial expression patterns (Chezem and Clay, 2016). To summarize, the presence of parallel pathways and multifunctional enzymes contributes to the resilience and flexibility of the galanthamine biosynthetic network. It highlights the dynamic characteristics of specialized plant metabolism, where shared enzymatic roles are utilized to adjust production based on developmental and environmental influences (Ono and Murata, 2023). This insight expands our understanding of pathway evolution and highlights the importance of considering both enzyme specificity and network plasticity in the study of plant alkaloid biosynthesis.

4.1.3. Biotechnological Implications

The discovery and functional validation of NMTs open several avenues for biotechnological innovation. Galanthamine is commercially valuable as an acetylcholinesterase inhibitor used in Alzheimer's disease treatment, yet its extraction from natural sources remains inefficient and unsustainable (Berkov *et al.*, 2022). Engineering microbial or plant platforms for galanthamine production has long been constrained by incomplete knowledge of its biosynthetic pathway, particularly the final *N*-methylation step (Liyanage *et al.*, 2025a; Mehta *et al.*, 2024). By

confirming *LaLrHp*NMT1's ability to methylate norgalanthamine efficiently, this study identifies a robust biocatalyst for synthetic biology applications. Its catalytic efficiency and broad substrate acceptance make it an ideal candidate for heterologous expression in Heterologous chassis such as *Saccharomyces cerevisiae* or *Chlamydomonas reinhardii*, paving the way for full-pathway reconstruction (Bapat *et al.*, 2023).

Additionally, the dual localization of *LaLrHp*NMT1 to the cytosol and endoplasmic reticulum suggests that cellular compartmentalization strategies can be leveraged during metabolic engineering to enhance pathway efficiency (Heinig *et al.*, 2013). Co-localization of upstream enzymes (e.g., cytochrome P450s) with *LaLrHp*NMT1 could enable substrate channelling, reducing intermediate loss and boosting galanthamine yields (Li *et al.*, 2024). The enzyme's promiscuity also makes it suitable for the biosynthesis of novel alkaloid derivatives (Mai *et al.*, 2025). By feeding structurally diverse precursors into engineered systems expressing *LaLrHp*NMT1, it may be possible to generate methylated analogs with improved pharmacological profiles (Bradley *et al.*, 2023). Moreover, this work supports the utility of structure-guided protein engineering. Mutational analysis revealed critical roles of Glu204 and His208, providing targets for future modifications to enhance substrate specificity or catalytic efficiency (Chen *et al.*, 2024; Morris *et al.*, 2020). These findings lay the groundwork for directed evolution

experiments aimed at optimizing this enzyme for industrial-scale biosynthesis. In sum, *LaLrHp*NMT1 is not only a key to unlocking natural galanthamine production but also a versatile tool for synthetic pathway reconstruction and alkaloid diversification, with far-reaching implications in biotechnology, pharmaceuticals, and green chemistry (Bradley *et al.*, 2023).

4. 2. Mass spectrometry imaging of *Hippeastrum papilio*: Integration of Biosynthesis and Spatial Biology

This study presents an in-depth spatial analysis of AA biosynthesis in *Hippeastrum papilio*, utilizing mass spectrometry imaging (MSI) to track the accumulation and compartmentalization of key metabolites *in situ*. Employing high-resolution MALDI-MSI, we mapped the localization of twelve major alkaloids, including biosynthetic intermediates and pharmacologically important end-products, across leaf, bulb, and root tissues. This is one of the most comprehensive tissue-scale visualizations of alkaloid metabolism in the Amaryllidaceae family to date (Haist *et al.*, 2024b; Mehta *et al.*, 2024). Our results question previous hypothesis on AA biosynthesis, in the meantime reveal nuanced, organ-specific, and tissue-specific compartmentalization patterns that redefine our understanding of plant specialized metabolism (Mehta *et al.*, 2024). The galanthamine biosynthetic pathway begins with the condensation of tyramine and 3,4-DHBA to form norcraugsodine, which is subsequently reduced to norbelladine. Norbelladine undergoes methylation to produce

4'-*O*-methylnorbelladine (4'-*O*MNB), which is then channeled into multiple branches leading to galanthamine, haemanthamine, or other derivatives like papiline (Jayawardena *et al.*, 2024; Liyanage *et al.*, 2025a). While this linear progression is well-established at the biochemical level, the spatial context within which these steps occur has been largely speculative (Lamichhane *et al.*, 2025; Mehta *et al.*, 2024). Our MSI-based approach bridges this gap, providing direct visualization of metabolite localization across tissues.

4. 2.1. Leaf Tissues: Biosynthetic and Defensive Complexity

In the leaf, a clear developmental gradient in metabolite localization was observed. Leaf bases where the young developing cells situated exhibited high levels of early intermediates such as norbelladine and 4'-*O*-methylnorbelladine, particularly in the mesophyll and vascular bundles which goes along with previous hypothesis (Mehta *et al.*, 2024). Galanthamine, the major end-product, was widespread across all leaf zones, detected in parenchyma, vascular bundles, epidermis, and possibly, in the cuticle. The presence of galanthamine in both internal and surface tissues supports its dual function as a systemic defense compound and a potential signaling molecule (Matsuura and Fett-Neto, 2015). This outer-epidermis presence suggests extracellular export or secretion, likely serving as a deterrent against herbivory or microbial invasion (Berkov *et al.*, 2020; Matsuura and Fett-Neto, 2015). Haemanthamine, by contrast, was highly localized to the lower epidermis

and adjacent to vascular tissues in basal and middle leaf regions. Unlike galanthamine, it was not detected in the cuticle or upper leaf zones, suggesting a more localized biosynthesis or storage strategy. Papiline and hippapiline mirrored galanthamine's distribution but were less abundant and absent from surface layers. These findings suggest that the leaf serves as both a site of active biosynthesis and a functional barrier zone. Intermediates are largely synthesized in inner tissues, while final products like galanthamine are exported to the surface. The spatial divergence of AAs indicates possible tissue-specific enzyme localization, which may be regulated developmentally or in response to environmental stimuli.

4.2.2. Bulb Tissues: Storage, Regulation, and Remobilization

The bulb, a storage and regrowth organ, revealed a high concentration and diversity of alkaloids. MSI data showed that galanthamine was evenly distributed across parenchyma and vascular bundles in outer and middle scales, as well as in the basal plate. This supports the idea of systemic storage and potential remobilization during vegetative growth (Ali *et al.*, 2019; Haist *et al.*, 2024a). Haemanthamine and its derivatives were primarily found in vascular bundles and inner epidermis, with dense punctate accumulations suggesting storage vesicles or specialized cell clusters. The basal plate, in particular, was identified as a biosynthetic hotspot, with high levels of both intermediates and end-products. The presence of galanthamine in the external tissues of bulb scales,

suggests a limited role for external defense. However, its strong signal in internal tissues supports a model in which bulbs act as long-term storage organs, safeguarding high-value metabolites until needed for defense or regrowth (Haist *et al.*, 2024b).

4.2.3. Root Tissues: Compartmentalization and Defense Strategy

Roots exhibited a distinct pattern of metabolite localization characterized by strong compartmentalization. Early intermediates such as norcraugsodine and norbelladine were detected primarily in the exodermis and cortex, while galanthamine and 4'-*O*-methylnorbelladine were localized to vascular bundles and exodermis. End products Haemanthamine and papiline were restricted to cortical and exodermis tissues, with low signal in vascular zones. The spatial gradient observed along the root axis—from base to tip—further highlighted metabolic zonation. Alkaloid signals decreased progressively toward the root tip, which is inconsistent with the higher metabolic activity typically observed in the root tip (Bais *et al.*, 2001; Ghorbanzadeh *et al.*, 2023). This is the opposite observation compared to the leaves of Amaryllidaceae plants, where newly growing tissues located in the leaf bases are where we observe the highest signal of alkaloids (Mehta *et al.*, 2024). This zonation likely reflects a defense strategy wherein mature root tissues are chemically fortified, while growing tips prioritize elongation and resource acquisition. These results suggest that in roots, biosynthesis and storage are organized according to both tissue function and

developmental stage. The localization of early intermediates in the cortex and exodermis, paired with galanthamine in vascular bundles, implies a trans-tissue biosynthetic route where different steps occur in distinct cellular compartments.

4.2.4. Biosynthetic Modularity and Pathway Branching

The branching of the pathway at 4'-*O*MNB appears to be a crucial regulatory point. This intermediate was found in epidermal, exodermal tissues, parenchyma and cortex tissues, and vascular bundles across all organs, co-localizing with either galanthamine or haemanthamine depending on tissue context. In leaves and bulbs, galanthamine and 4'-OMNB shared distribution zones, whereas in roots, haemanthamine was more strongly correlated with 4'-*O*MNB. This suggests that enzyme expression for the conversion of 4'-*O*MNB into specific end-products is spatially regulated, potentially through cell-type-specific gene expression or subcellular compartmentalization. The detection of AAs specifically in vascular tissues and gradient through in epidermis or cortex supports the hypothesis of divergent cellular destinations for modified alkaloids (Uzaki *et al.*, 2024). Such localization is likely driven by distinct enzyme microenvironments or transport mechanisms operating at the tissue or cellular level (Li *et al.*, 2023a; Yu *et al.*, 2023).

Importantly, the presence of galanthamine and haemanthamine in both vascular tissues and secreted mucilage suggests that transport processes are central to their final accumulation sites. In other

specialized metabolic systems, transport and compartmentalization have been shown to be critical for shaping metabolite distributions. For example, in opium poppy, benzylisoquinoline alkaloids are synthesized in companion cells and transported into adjacent laticifers for storage (Beaudoin and Facchini, 2014; Ziegler and Facchini, 2008). Similarly, in *Nicotiana* spp., nicotine is produced in roots and subsequently translocated to the leaves through the xylem, where it accumulates as a defensive metabolite (Watkins and Facchini, 2022). These parallels suggest that Amaryllidaceae may employ analogous long-distance trafficking strategies, with alkaloids synthesized in multiple tissues but funneled into specialized compartments such as mucilage or vascular bundles for defense and ecological function.

This modularity further implies the existence of cellular “division of labor” in which biosynthetic steps are distributed across cell types, necessitating the transport of intermediates between compartments. Studies on the monoterpenoid indole alkaloid pathway in *Catharanthus roseus* showed that distinct intermediates are synthesized in epidermal cells but then transported to idioblasts and laticifers for downstream conversions (Guirimand *et al.*, 2011; Li *et al.*, 2023a). A similar scenario in *H. papilio* could explain the broader presence of 4′-OMNB across tissues, contrasted with the more restricted accumulation of end-products.

Taken together, the MSI evidence supports a model in which Amaryllidaceae alkaloid biosynthesis is both branched and spatially modular, with transport processes playing a critical role in connecting cellular microenvironments. Identifying the candidate transporters (e.g., ABC or MATE family members) and exploring their expression in relation to alkaloid hotspots will be an important future step (Wang *et al.*, 2021b). Such transport-based compartmentalization is not merely passive but shapes the metabolic flux toward different alkaloid classes and ultimately underpins the ecological functions of these compounds.

4.2.5. Evolutionary and Ecological Considerations

The spatial specialization observed in *H. papilio* may reflect evolutionary adaptation to varied environmental pressures. Galanthamine's cuticle/outer epidermal localization suggests an ecological role in surface defense, while the internal storage of haemanthamine and its derivatives implies a more regulated or conditional function, possibly inducible upon stress. The compartmentalization of biosynthetic steps across tissues supports the idea of metabolic economy, wherein energy-intensive synthesis is confined to protected, metabolically active zones (Bar-Peled and Kory, 2022). These spatial dynamics also have ecological implications (Watkins and Facchini, 2022). In leaves, the combination of wide galanthamine distribution and punctate haemanthamine accumulation could reflect a dual-layer defense system (Jan *et al.*, 2021; Malinowski *et al.*, 2024; Vaou *et al.*, 2021). In roots,

alkaloid presence in the exodermis and cortex may protect against soil pathogens, while vascular localization ensures systemic distribution (Malinowski *et al.*, 2024; Vaou *et al.*, 2021).

4.2.6. Biotechnological and Applied Implications

Understanding the tissue-specific localization of alkaloids can inform strategies for metabolic engineering (Li *et al.*, 2023a). For instance, targeting expression of galanthamine biosynthetic genes to leaf epidermis or bulb parenchyma may enhance yields in heterologous systems (Yamamoto *et al.*, 2016). Moreover, knowledge of spatial enzyme expression and metabolite accumulation could be leveraged to manipulate flux through the pathway, prioritizing desired compounds while suppressing undesired branches (Allen *et al.*, 2009). Mapping where these alkaloids are synthesized and stored also provides critical clues for pinpointing the underlying biosynthetic genes, facilitating their identification and characterization. The model established here also provides a framework for improving crop varieties. Selecting for cultivars with enhanced galanthamine accumulation in harvestable organs could increase yield and reduce extraction costs (Berkov *et al.*, 2022; Haist *et al.*, 2024a; Trujillo Chacón *et al.*, 2024). Similarly, identifying key transporters involved in alkaloid translocation might allow for redistribution of metabolites toward economically valuable tissues.

4.3. Conclusion

This thesis integrates enzymology and spatial metabolomics to provide a comprehensive understanding of galanthamine biosynthesis in Amaryllidaceae plants. By identifying and characterizing *LaLrHp*NMT1, a coclaurine N-methyltransferase-like enzyme, a critical methylation step in the galanthamine pathway was resolved, revealing its evolutionary conservation, catalytic efficiency, and substrate promiscuity. In parallel, mass spectrometry imaging offered unprecedented insights into the spatial distribution of alkaloids across leaves, bulbs, and roots, highlighting tissue-specific biosynthesis, compartmentalized storage, and ecological defense roles. Together, these findings establish a cohesive model where biochemical precision and spatial dynamics coordinate the production and regulation of pharmacologically important metabolites. Beyond advancing our knowledge of specialized plant metabolism, the work lays a foundation for metabolic engineering efforts aimed at heterologous galanthamine production, reduction of wild harvesting pressures, and creation of novel alkaloid analogs. The interdisciplinary approach exemplified here—linking molecular function with organ-level localization—offers a powerful template for decoding other complex plant pathways. Ultimately, this research not only contributes to sustainable drug development but also enriches our understanding of how plants balance metabolic complexity with ecological adaptation.

4.4. Future Directions

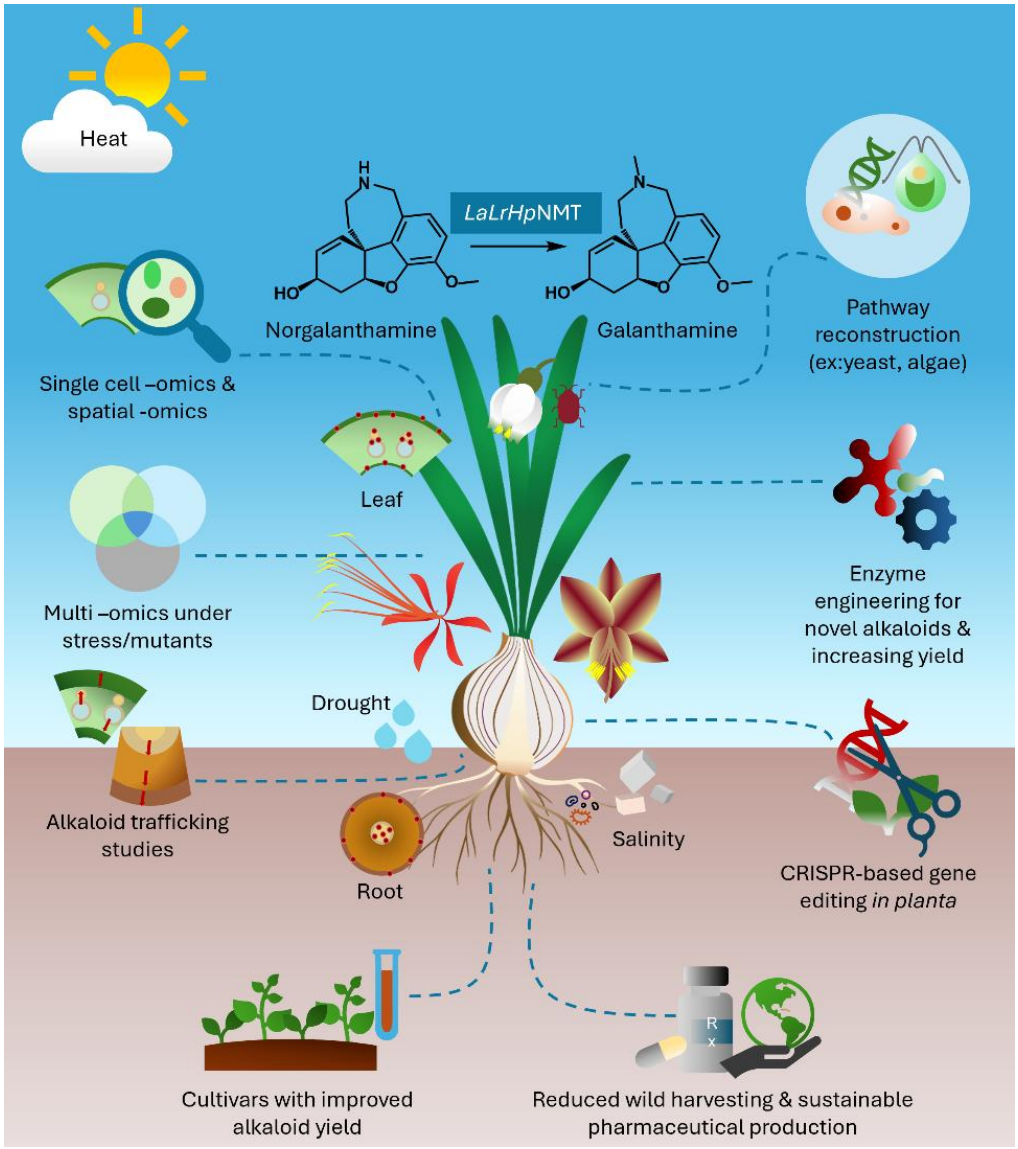

Figure 4.1. Summary of conclusions and future directions of the study.

Building upon the discoveries presented in this thesis, future research can significantly advance both the scientific understanding and biotechnological application of Amaryllidaceae alkaloid biosynthesis (Figure 4.1). A primary research priority remains the complete elucidation of the galanthamine biosynthetic pathway, including potential

alternate routes and branching mechanisms. Multi-omics strategies; encompassing transcriptomics, proteomics, and metabolomics; applied under stress conditions or in mutant backgrounds can reveal novel pathway enzymes and regulatory elements (Varadharajan *et al.*, 2025). High-resolution spatial transcriptomics and single-cell RNA sequencing will map biosynthetic gene expression at cellular resolution, while subcellular MSI and imaging mass spectrometry can uncover intracellular localization and trafficking of intermediates (Burlat *et al.*, 2023). Time-course isotope labeling will add dynamic information on precursor incorporation and intermediate turnover, thereby validating proposed pathway steps and quantifying flux through alternate routes (Dong *et al.*, 2024). Such kinetic insights would greatly strengthen the functional interpretation of spatial and omics datasets.

An equally pressing direction is the investigation of alkaloid transport and compartmentalization. The distribution patterns observed here strongly suggest the involvement of transporters and dynamic subcellular trafficking between cytosol, ER, and storage compartments such as mucilage. Identifying candidate ABC and MATE transporters, and testing their function using fluorescently tagged alkaloids and transporter proteins, could clarify how metabolites move across cells and tissues (Srinivasan and Smolke, 2021; Wang *et al.*, 2021b). Such insights would not only explain the decentralized alkaloid accumulation observed in *Hippeastrum papilio* but also inform strategies for redirecting metabolite

flow in engineered hosts.

The identification of *LaLrHp*NMT1 and several upstream enzymes (e.g., NBS, NR, CYP96T1) makes functional reconstruction of the galanthamine pathway in heterologous hosts now achievable. Yeast (*Saccharomyces cerevisiae*), moss (*Physcomitrella patens*), and microalgae (*Chlamydomonas reinhardtii*) represent promising platforms for scalable production. Expression optimization through codon usage, organelle targeting, and promoter tuning can enhance yields (Diaz-Garza *et al.*, 2024; Schmidt *et al.*, 2023). In parallel, protein–protein interaction studies could reveal whether Amaryllidaceae enzymes form metabolon-like assemblies, as observed in other alkaloid pathways, which may be recreated synthetically to improve flux (Laursen *et al.*, 2016; Zhang and Fernie, 2020).

The catalytic promiscuity of *LaLrHp*NMT1 provides an additional opportunity for combinatorial biosynthesis. Feeding non-canonical substrates or engineering active-site residues via directed evolution or computational modeling could yield novel galanthamine analogues with modified pharmacological properties (Bradley *et al.*, 2023). Such derivatives could be systematically evaluated for central nervous system (CNS) applications, broadening the therapeutic potential beyond galanthamine itself. Technological innovations will further drive progress. Advances in MSI toward true single-cell or subcellular resolution will uncover fine-grained heterogeneity of alkaloid biosynthesis, while

CRISPR-based editing of regulatory regions can be used to fine-tune pathway expression *in planta* (Burlat *et al.*, 2023). Comparative evolutionary studies across Amaryllidaceae and related lineages will help clarify how CNMT-like enzymes were co-opted into specialized metabolism, offering principles for discovering hidden alkaloid pathways in other taxa.

Applied outcomes include the breeding or engineering of cultivars with enhanced alkaloid accumulation in harvestable organs, manipulation of transporter expression to redirect metabolite flow, and integration of heterologous production into sustainable biomanufacturing pipelines (Mora-Vásquez *et al.*, 2022; Selma *et al.*, 2023). The societal impact of such innovations is considerable, offering a path toward reliable, sustainable galanthamine production and reducing dependence on wild plant harvesting (Fraser *et al.*, 2016; Howes *et al.*, 2020). Finally, the integrative framework developed here, combining enzymology, structural biology, and spatial metabolomics, can be extended to other valuable plant pathways. This not only accelerates discovery but also positions plant specialized metabolism at the center of future biotechnological and pharmaceutical innovation (Qin *et al.*, 2025). Collectively, these directions reflect the convergence of cutting-edge molecular tools, ecological insight, and translational goals, ensuring that future work will transform both our understanding and utilization of plant metabolic diversity.

REFERENCE

Abramson J, Adler Js, Dunger J, Evans R, Green T, Pritzel A, Ronneberger O, Willmore L, Ballard J, Bambrick J, Bodenstein SW, Evans DA, Hung C, O'Neill M, Reiman D, Tunyasuvunakool K, Wu Z, Žemgulytė A, Arvaniti E, Beattie C, Bertolli O, Bridgland AC, A., Congreve M, Cowen-Rivers Al, Cowie A, Figurnov M, Fuchs FB, Gladman H, Jain R, Khan YA, Low CMR, Perlin K, Potapenko A, Savy P, Singh S, Stecula A, Thillaisundaram A, Tong C, Yakneen S, Zhong ED, Zielinski M, Žídek A, Bapst V, Kohli P, Jaderberg M, Hassabis D, Jumper JM. 2024. Accurate structure prediction of biomolecular interactions with AlphaFold 3. Nature **630**, 493–500.

Adasme MF, Linnemann KL, Bolz SN, Kaiser F, Salentin S, Haupt VJ, Schroeder M. 2021. PLIP 2021: Expanding the scope of the protein–ligand interaction profiler to DNA and RNA. Nucleic Acids Research **49**, W530–W534.

Ali AH, Abdelrahman M, E, Magdi A. 2019. Alkaloid role in plant defense response to growth and stress. Bioactive molecules in plant defense: Signaling in growth and stress, 145–158.

Allen DK, Libourel IG, Shachar-Hill Y. 2009. Metabolic flux analysis in plants: coping with complexity. Plant, cell & environment **32**, 1241–1257.

Altpeter F, Varshney A, Abderhalden O, Douchkov D, Sautter C, Kumlehn J, Dudler R, Schweizer P. 2005. Stable expression of a defense-related gene in wheat epidermis under transcriptional control of a novel promoter confers pathogen resistance. Plant molecular biology **57**, 271–283.

APG. 2009. An update of the Angiosperm Phylogeny Group classification for the orders and families of flowering plants: APG III. Botanical Journal of the Linnean Society **161**, 105–121.

Bais HP, Loyola-Vargas VM, Flores HE, Vivanco JM. 2001. Root-specific metabolism: the biology and biochemistry of underground organs. *In Vitro* Cellular & Developmental Biology-Plant **37**, 730–741.

Bapat VA, Kavi Kishor PB, Penna S. 2023. Heterologous production of high value metabolites in plants and microbes. Vol. 14: Frontiers Media SA, 1223033.

Bar-Peled L, Kory N. 2022. Principles and functions of metabolic compartmentalization. Nature metabolism **4**, 1232–1244.

Barton D, Cohen T. 1957. Some biogenetic aspects of phenol oxidation. Festschrift Prof. Dr. Arthur Stoll. Birkhäuser, Basel.

Barton D, Kirby G. 1962. 153. Phenol oxidation and biosynthesis. Part V. The synthesis of galanthamine. Journal of the Chemical Society (Resumed), 806–817.

Barton D, Kirby G, Taylor J. 1962a. Origin Of Methylenedioxy-Groups In Nature.: Royal Soc Chemistry Thomas Graham House, Science Park, Milton Rd, Cambridge., 341–&.

Barton D, Kirby G, Taylor J, Thomas G. 1962b. Multiple labelling experiments in biosynthesis of Amaryllidaceae alkaloids. Proceedings of the Chemical Society, 179.

Barton D, Kirby G, Taylor J, Thomas G. 1963. 866. Phenol oxidation and biosynthesis. Part VI. The biogenesis of amaryllidaceae alkaloids. Journal of the Chemical Society (Resumed), 4545–4558.

Bastida J, Lavilla R, Viladomat F. 2006. Chapter 3 chemical and biological aspects of Narcissus. Alkaloids. The Alkaloids: Chemistry and Biology, 1st ed.; Cordell, AG, Ed, 87–179.

Battersby A, Fales H, Wildman W. 1961. Biosynthesis in the Amaryllidaceae. Tyrosine and norbelladine as precursors of haemanthamine. Journal of the American Chemical Society **83**, 4098–4099.

Beaudoin GA, Facchini PJ. 2014. Benzylisoquinoline alkaloid biosynthesis in opium poppy. Planta **240**, 19–32.

Bendaif H, Melhaoui A, Ramdani M, Elmsellem H, Douez C, El Ouadi Y. 2018. Antibacterial activity and virtual screening by molecular docking of lycorine from *Pancratium foetidum* Pom (Moroccan endemic Amaryllidaceae). Microbial Pathogenesis **115**, 138–145.

Bennett MR, Thompson ML, Shepherd SA, Dunstan MS, Herbert AJ, Smith DRM, Cronin VA, Menon BRK, Levy C, Micklefield J. 2018a. Structure and Biocatalytic Scope of Coclaurine N-Methyltransferase. Angew Chem Int Ed Engl **57**, 10600–10604.

Bennett MR, Thompson ML, Shepherd SA, Dunstan MS, Herbert AJ, Smith DRM, Cronin VA, Menon BRK, Levy C, Micklefield J. 2018b. Structure and Biocatalytic Scope of Coclaurine N-Methyltransferase. Angewandte Chemie International Edition **57**, 10600–10604.

Berkov S, Georgieva L, Sidjimova B, Bastida J. 2022. Evaluation of *Hippeastrum papilio* (Ravenna) Van Scheepen potencial as a new industrial source of galanthamine. Industrial Crops and Products **178**, 114619.

Berkov S, Martínez-Francés V, Bastida J, Codina C, Ríos S. 2014. Evolution of alkaloid biosynthesis in the genus *Narcissus*. Phytochemistry **99**, 95–106.

Berkov S, Osorio E, Viladomat F, Bastida J. 2020. Chemodiversity, chemotaxonomy and chemoecology of Amaryllidaceae alkaloids. The Alkaloids: Chemistry and Biology **83**, 113–185.

Berkov S, Sidjimova B, Evstatieva L, Popov S. 2004. Intraspecific variability in the alkaloid metabolism of *Galanthus elwesii*. Phytochemistry **65**, 579–586.

Bi Y-R, Yung K-H, Wong Y-S. 1998. Physiological effects of narciclasine from the mucilage of *Narcissus tazetta* L. bulbs. Plant science **135**, 103–108.

Bjarnholt N, Li B, D'Alvise J, Janfelt C. 2014. Mass spectrometry imaging of plant metabolites–principles and possibilities. Natural product reports **31**, 818–837.

Bogdanova Y, Pandova B, Yanev S, Stanilova M. 2009. Biosynthesis of lycorine by in vitro cultures of *Pancratium maritimum* L.(Amaryllidaceae). Biotechnology & Biotechnological Equipment **23**, 919–922.

Bokhart MT, Nazari M, Garrard KP, Muddiman DC. 2017. MSiReader v1. 0: evolving open-source mass spectrometry imaging software for targeted and untargeted analyses. Journal of The American Society for Mass Spectrometry **29**, 8–16.

Boughton BA, Thinagaran D, Sarabia D, Bacic A, Roessner U. 2016. Mass spectrometry imaging for plant biology: a review. Phytochem Rev **15**, 445–488.

Bradley SA, Lehka BJ, Hansson FG, Adhikari KB, Rago D, Rubaszka P, Haidar AK, Chen L, Hansen LG, Gudich O. 2023. Biosynthesis of natural and halogenated plant monoterpene indole alkaloids in yeast. Nature chemical biology **19**, 1551–1560.

Buchberger AR, DeLaney K, Johnson J, Li L. 2017. Mass spectrometry imaging: a review of emerging advancements and future insights. Analytical chemistry **90**, 240.

Burlat V, Papon N, Courdavault V. 2023. Medicinal plants enter the single-cell multi-omics era. Trends in Plant Science **28**, 1205–1207.

Cahlíková L, Kawano I, Řezáčová M, Blunden G, Hulcová D, Havelek R. 2021. The Amaryllidaceae alkaloids haemanthamine, haemanthidine and their semisynthetic derivatives as potential drugs. Phytochemistry Reviews **20**, 303–323.

Campos-Rocha A, Meerow AW, Peixoto M, Koch I, Messias PA, Dutilh JHA. 2023. To print in red ink. Plant Ecology and Evolution **156**, 239–256.

Caspi R, Billington R, Keseler IM, Kothari A, Krummenacker M, Midford PE, Ong WK, Paley S, Subhraveti P, Karp PD. 2020. The MetaCyc database of metabolic pathways and enzymes-a 2019 update. Nucleic Acids Research **48**, D445–D453.

Centeno-Betanzos LY, Reyes-Chilpa R, Pigni NB, Jankowski CK, Torras-Claveria L, Bastida J. 2021. Plants of the 'Libellus de Medicinalibus Indorum Herbis' from Mexico, 1552. Zephyranthes fosteri (Amaryllidaceae) Alkaloids. Chemistry & Biodiversity **18**, e2000834.

Chaichompoo W, Rojsitthisak P, Pabuprapap W, Siriwattanasathien Y, Yotmanee P, Suksamrarn A. 2023. Alkaloids with cholinesterase inhibitory activities from the bulbs of *Crinum*× *amabile* Donn ex Ker Gawl. Phytochemistry **205**, 113473.

Chaichompoo W, Rojsitthisak P, Pabuprapap W, Siriwattanasathien Y, Yotmanee P, Suksamrarn A. 2024. Amaryllidaceae alkaloids from the bulbs of *Crinum latifolium* L. and their cholinesterase inhibitory activities. Phytochemistry **217**, 113929.

Chang L, Chen J, Xiao Y, Xia Y. 2011. *De novo* characterization of *Lycoris sprengeri* transcriptome using Illumina GA II. African Journal of Biotechnology **10**, 12147–12155.

Chavent M, Kuentz-Simonet V, Liquet B, Saracco J. 2012. ClustOfVar: An R Package for the Clustering of Variables. Journal of Statistical Software **50**, 1 – 16.

Chen M-X, Huo J-M, Hu J, Xu Z-P, Zhang X. 2018. Amaryllidaceae alkaloids from *Crinum latifolium* with cytotoxic, antimicrobial, antioxidant, and anti-inflammatory activities. Fitoterapia **130**, 48–53.

Chen S, Wang Z, Dong G, Zhao H, Zhu Y, Liu Y, Yuan L, Jiang J, Liu X, Liu A. 2024. Characterization and Molecular Engineering of a N-Methyltransferase from Edible *Nelumbo nucifera* Leaves Involved in Nuciferine Biosynthesis. Journal of Agricultural and Food Chemistry.

Cheng G, Shu X, Wang Z, Wang N, Zhang F. 2023. Establishing a virus-induced gene silencing system in Lycoris chinensis. Plants **12**, 2458.

Cheng RY, Xie DF, Zhang XY, Fu X, He XJ, Zhou SD. 2022a. Comparative Plastome Analysis of Three Amaryllidaceae Subfamilies:

Insights into Variation of Genome Characteristics, Phylogeny, and Adaptive Evolution. Biomed Research International **2022**, 3909596.

Cheng S, Melkonian M, Smith SA, Brockington S. 2018. 10KP: a phylodiverse genome sequencing plan. Gigascience **7**.

Cheng W, Yao Y, Wang Q, Chang X, Shi Z, Fang X, Chen F, Chen S, Zhang Y, Zhang F. 2022b. Characterization of benzylisoquinoline alkaloid methyltransferases in *Liriodendron chinense* provides insights into the phylogenic basis of angiosperm alkaloid diversity. The Plant Journal **112**, 535–548.

Chezem WR, Clay NK. 2016. Regulation of plant secondary metabolism and associated specialized cell development by MYBs and bHLHs. Phytochemistry **131**, 26–43.

Colque R, Viladomat F, Bastida J, Codina C. 2002. Micropropagation of the rare *Eucrosia stricklandii* (Amaryllidaceae) by twin-scaling and shake liquid culture. The Journal of Horticultural Science and Biotechnology **77**, 739–743.

Cooper L, Elser J, Laporte M-A, Arnaud E, Jaiswal P. 2024. Planteome 2024 Update: Reference ontologies and knowledgebase for plant biology. Nucleic Acids Research **52**, D1548–D1555.

Cui X. 2019. Mucilage Secretion from Plants: Friends or Foes? Molecular Plant **12**, 16–17.

Databases CNG. 2017. 10KP: 10,000 Plant Genomes Project. Vol. 2023. Dapeng, China: China National Genebank Databases.

de Andrade JP, Berkov S, Viladomat F, Codina C, Zuanazzi JAS, Bastida J. 2011. Alkaloids from *Hippeastrum papilio*. Molecules **16**, 7097–7104.

de Vries S, Fürst-Jansen JM, Irisarri I, Dhabalia Ashok A, Ischebeck T, Feussner K, Abreu IN, Petersen M, Feussner I, de Vries J. 2021. The evolution of the phenylpropanoid pathway entailed pronounced radiations and divergences of enzyme families. The Plant Journal **107**, 975–1002.

Dennehy Z, Bilsborrow J, Culham A, David J, Konyves K. 2021. The complete plastome of the South African species, *Amaryllis belladonna* L. (Amaryllidaceae). Mitochondrial DNA B Resour **6**, 3393–3395.

Desgagné-Penix I. 2021. Biosynthesis of alkaloids in Amaryllidaceae plants: A review. Phytochemistry Reviews **20**, 409–431.

Dethier M, De Luca V. 1993. Partial purification of an N-methyltransferase involved in vindoline biosynthesis in *Catharanthus roseus*. Phytochemistry **32**, 673–678.

Diaz-Garza AM, Lavoie-Marchand F, Merindol N, Diamond A, Desgagné-Penix I. 2024. What is true for plants may not be true for Phaeodactylum tricornutum: The case of *Vanilla planifolia* vanillin synthase (Vp VAN) targeted to four subcellular compartments of the diatom. bioRxiv, 2024.2010. 2023.619700.

Dietz K-J, Hartung W. 1996. The leaf epidermis: its ecophysiological significance. *Progress in Botany/Fortschritte der Botanik: Structural Botany Physiology Genetics Taxonomy Geobotany/Struktur Physiologie Genetik Systematik Geobotanik*: Springer, 32–53.

Ding Y, Qu D, Zhang K-M, Cang X-X, Kou Z-N, Xiao W, Zhu J-B. 2017. Phytochemical and biological investigations of Amaryllidaceae alkaloids: a review. Journal of Asian Natural Products Research **19**, 53–100.

Donaldson L. 2020. Autofluorescence in plants. Molecules **25**, 2393.

Dong NQ, Lin HX. 2021. Contribution of phenylpropanoid metabolism to plant development and plant–environment interactions. Journal of integrative plant biology **63**, 180–209.

Dong Y, Li B, Malitsky S, Rogachev I, Aharoni A, Kaftan F, Svatoš A, Franceschi P. 2016. Sample preparation for mass spectrometry imaging of plant tissues: a review. Frontiers in Plant Science **7**, 60.

Eichhorn J, Takada T, Kita Y, Zenk MH. 1998. Biosynthesis of the Amaryllidaceae alkaloid galanthamine. Phytochemistry **49**, 1037–1047.

El-Naggar AH, El-Nasharty AB. 2009. Effect of Growing Media and Mineral Fertilization on Growth, Flowering, Bulbs Productivity and Chemical Constituents of *Hippeastrum vittatum*, Herb. Environ. Sci.

Elgorashi E, Zschocke S, Van Staden J, Eloff J. 2003. The anti-inflammatory and antibacterial activities of Amaryllidaceae alkaloids. South African Journal of Botany **69**, 448–449.

Eljounaidi K, Radzikowska BA, Whitehead CB, Taylor DJ, Conde S, Davis W, Dowle AA, Langer S, James S, Unsworth WP. 2024. Variation of terpene alkaloids in *Daphniphyllum macropodum* across plants and tissues. New Phytologist.

Erb M, Kliebenstein DJ. 2020. Plant secondary metabolites as defenses, regulators, and primary metabolites: the blurred functional trichotomy. Plant Physiology **184**, 39–52.

Facchini PJ, St-Pierre B. 2005. Synthesis and trafficking of alkaloid biosynthetic enzymes. Current Opinion in Plant Biology **8**, 657–666.

Feinstein AI. 1967. The incorporation of carbon-14-labeled beta-phenylethylamine derivatives and tritium-labeled vittatine into amaryllidaceae alkaloids, Iowa State University.

Fellers JD. 1998. Progeny of *Hippeastrum papilio*. Herbertia **53**, 129–144.

Fennell CW, Elgorashi EE, van Staden J. 2003. Alkaloid Production in *Crinum moorei* Cultures. Journal of Natural Products **66**, 1524–1526.

Ferdausi A, Chang X, Jones M. 2021. Transcriptomic analysis for differential expression of genes involved in secondary metabolite production in *Narcissus pseudonarcissus* field derived bulb and *in vitro* callus. Industrial crop and products **168**.

Field B, Fiston-Lavier A-S, Kemen A, Geisler K, Quesneville H, Osbourn AE. 2011. Formation of plant metabolic gene clusters within dynamic chromosomal regions. PNAS **108**, 16121.

Finkers R, van Kaauwen M, Ament K, Burger-Meijer K, Egging R, Huits H, Kodde L, Kroon L, Shigyo M, Sato S, Vosman B, van

Workum W, Scholten O. 2021. Insights from the first genome assembly of Onion (*Allium cepa*). G3 Genes|Genomes|Genetics **11**.

Fraser MD, Davies JR, Chang X. 2016. New gold in them thar hills: Testing a novel supply route for plant-derived galanthamine. Journal of Alzheimer's Disease **55**, 1321–1325.

Frey M, Chomet P, Glawischnig E, Stettner C, Grün S, Winklmair A, Eisenreich W, Bacher A, Meeley RB, Briggs SP, Simcox K, Gierl A. 1997. Analysis of a chemical plant defense mechanism in grasses. Science **277**, 699.

Fuganti C, Mazza M. 1971. Relative stereochemistry of protonation and hydroxylation in the biosynthesis of lycorenine and haemanthidine from protocatechualdehyde. Journal of the Chemical Society D: Chemical Communications, 1196–1197.

García N, Meerow AW, Arroyo-Leuenberger S, Oliveira RS, Dutilh JH, Soltis PS, Judd WS. 2019. Generic classification of Amaryllidaceae tribe Hippeastreae. Taxon **68**, 481–498.

Georgiev V, Ivanov I, Pavlov A. 2020. Recent Progress in Amaryllidaceae Biotechnology. Molecules **25**, 4670.

Gerrard A. 1877. The proximate principles of the *Narcissus pseudonarcissus*. The pharmaceutical journal and transactions **8**, 214.

Ghorbanzadeh Z, Hamid R, Jacob F, Zeinalabedini M, Salekdeh GH, Ghaffari MR. 2023. Comparative metabolomics of root-tips reveals distinct metabolic pathways conferring drought tolerance in contrasting genotypes of rice. BMC genomics **24**, 152.

Ghosal S, Saini KS, Razdan S. 1985. *Crinum* alkaloids: their chemistry and biology. Phytochemistry **24**, 2141–2156.

Girard M-P, Karimzadegan V, Héneault M, Cloutier F, Bérubé G, Berthoux L, Mérindol N, Desgagné-Penix I. 2022. Chemical Synthesis and Biological Activities of Amaryllidaceae Alkaloid Norbelladine Derivatives and Precursors. Molecules **27**, 5621.

Goossens J, Mertens J, Goossens A. 2017. Role and functioning of bHLH transcription factors in jasmonate signalling. Journal of Experimental Botany **68**, 1333–1347.

Govaerts R. Subgenera: H. subg. *Hippeastrum*–H. subg. *Tocantinia*.

Granborg JR, Handler AM, Janfelt C. 2022. Mass spectrometry imaging in drug distribution and drug metabolism studies–Principles, applications and perspectives. TrAC Trends in Analytical Chemistry **146**, 116482.

Guo Y, de Andrade JP, Pigni NB, Torras-Claveria L, Tallini LR, de S. Borges W, Viladomat F, Nair JJ, Zuanazzi JA, Bastida J. 2016. New alkaloids from *Hippeastrum papilio* (Ravenna) van Scheepen. Helvetica Chimica Acta **99**, 143–147.

Habib A-AM. 1980. False-positive alkaloid reactions. Journal of pharmaceutical sciences **69**, 37–43.

Hagel JM, Facchini PJ. 2012. Subcellular localization of sanguinarine biosynthetic enzymes in cultured opium poppy cells. *In Vitro* Cellular & Developmental Biology - Plant **48**, 233–240.

Hagel JM, Onoyovwi A, Yeung EC, Facchini PJ. 2012. Role of phloem metabolites in plant defense. Phloem: Molecular Cell Biology, Systemic Communication, Biotic Interactions, 249–270.

Haist G, Sidjimova B, Denev R, Bastida J, Berkov S. 2024a. Dynamics of Growth and Galanthamine Biosynthesis in *Hippeastrum papilio* (Ravena) Van Sheepen Hydroponic Culture. Agronomy **14**, 2115.

Haist G, Sidjimova B, Yankova-Tsvetkova E, Nikolova M, Denev R, Semerdjieva I, Bastida J, Berkov S. 2024b. Metabolite profiling and histochemical localization of alkaloids in *Hippeastrum papilio* (Ravena) van Scheepen. Journal of Plant Physiology, 154223.

Hawkins C, Ginzburg D, Zhao K, Dwyer W, Xue B, Xu A, Rice S, Cole B, Paley S, Karp P. 2021. Plant Metabolic Network 15: A resource of genome-wide metabolism databases for 126 plants and algae. Journal of integrative plant biology **63**, 1888–1905.

He M, Qu C, Gao O, Hu X, Hong X. 2015. Biological and pharmacological activities of amaryllidaceae alkaloids. RSC Advances **5**, 16562–16574.

Heinig U, Gutensohn M, Dudareva N, Aharoni A. 2013. The challenges of cellular compartmentalization in plant metabolic engineering. Current opinion in biotechnology **24**, 239–246.

Heinrich M, Teoh HL. 2004. Galanthamine from snowdrop—the development of a modern drug against Alzheimer's disease from local Caucasian knowledge. Journal of ethnopharmacology **92**, 147–162.

Herrington NB, Kellogg GE. 2021. 3D interaction homology: Computational titration of aspartic acid, glutamic acid and histidine can create pH-tunable hydropathic environment maps. Frontiers in Molecular Biosciences **8**, 773385.

Heyman HM, Dubery IA. 2016. The potential of mass spectrometry imaging in plant metabolomics: a review. Phytochemistry Reviews **15**, 297–316.

Hnin S, Nakashima Y, Kodama T, Morita H. 2023. Crystal Structure Analysis Of Norbelladine 4'-O-Methyltransferase From Lycoris Longituba. *4th International Conference on Natural Product Discovery and Development in the Genomic Era*: SIMB.

Hori TA, Hayashi A, Sasanuma T, Kurita S. 2006. Genetic variations in the chloroplast genome and phylogenetic clustering of Lycoris species. Genes & Genetic Systems **81**, 243–253.

Horn PJ, Chapman KD. 2024. Imaging plant metabolism in situ. Journal of Experimental Botany **75**, 1654–1670.

Hotchandani T, de Villers J, Desgagne-Penix I. 2019. Developmental regulation of the expression of amaryllidaceae alkaloid biosynthetic genes in *Narcissus papyraceus*. Genes (Basel) **10**.

Hotchandani T, Desgagne-Penix I. 2017. Heterocyclic Amaryllidaceae Alkaloids: Biosynthesis and Pharmacological Applications. Current Topics in Medicinal Chemistry **17**, 418–427.

Howes MJR, Quave CL, Collemare J, Tatsis EC, Twilley D, Lulekal E, Farlow A, Li L, Cazar ME, Leaman DJ. 2020. Molecules from nature: Reconciling biodiversity conservation and global healthcare imperatives for sustainable use of medicinal plants and fungi. Plants, People, Planet **2**, 463–481.

Hruz T, Laule O, Szabo G, Wessendorp F, Bleuler S, Oertle L, Widmayer P, Gruissem W, Zimmermann P. 2008. Genevestigator v3: a reference expression database for the meta-analysis of transcriptomes. Advances in bioinformatics **2008**.

Hu J, Li W, Liu Z, Zhang G, Luo Y. 2021. Molecular cloning and functional characterization of tyrosine decarboxylases from galanthamine-producing Lycoris radiata. Acta Physiologiae Plantarum **43**, 84.

Hüttel W, Müller M. 2021. Regio-and stereoselective intermolecular phenol coupling enzymes in secondary metabolite biosynthesis. Natural product reports **38**, 1011–1043.

Irwin JJ, Tang KG, Young J, Dandarchuluun C, Wong BR, Khurelbaatar M, Moroz YS, Mayfield J, Sayle RA. 2020. ZINC20-A Free Ultralarge-Scale Chemical Database for Ligand Discovery. J Chem Inf Model **60**, 6065–6073.

Jan R, Asaf S, Numan M, L., Kim K. 2021. Plant secondary metabolite biosynthesis and transcriptional regulation in response to biotic and abiotic stress conditions. Agronomy **11**, 968.

Jayawardena TU, Merindol N, Liyanage NS, Desgagné-Penix I. 2024. Unveiling Amaryllidaceae alkaloids: from biosynthesis to antiviral potential–a review. Natural product reports.

Jayaweera D. 1981. Medicinal plants (Indigenous and exotic) used in Ceylon: part I. NSC: Colombo; 232p.

Jiang X, Chen H, Wei X, Cai J. 2021. Proteomic analysis provides an insight into the molecular mechanism of development and flowering in *Lycoris radiata*. Acta Physiologiae Plantarum **43**.

Jin J, Tian F, Yang D-C, Meng Y-Q, Kong L, Luo J, Gao G. 2016. PlantTFDB 4.0: toward a central hub for transcription factors and regulatory interactions in plants. Nucleic Acids Research, gkw982.

Jin SW, Park JY, Kang SJ, Park HS, Shim H, Lee TJ, Kang JH, Sung SH, Yang TJ. 2018. The complete chloroplast genome sequence of Magic Lily (*Lycoris squamigera*). Mitochondrial DNA B Resour **3**, 1210–1211.

Jin Z. 2009. Amaryllidaceae and Sceletium alkaloids. Natural product reports **26**, 363–381.

Jin Z. 2013. Amaryllidaceae and Sceletium alkaloids. Natural product reports **30**, 849.

Jin Z, Yao G. 2019. Amaryllidaceae and Sceletium alkaloids. Natural product reports **36**, 1462–1488.

Jones K, Smith JB. 1967. Chromosome evolution in the genus *Crinum*. Caryologia **20**, 163–179.

Ka S, Merindol N, Koirala M, Desgagne-Penix I. 2020. Biosynthesis and biological activities of newly discovered Amaryllidaceae alkaloids. Molecules **25**, 4901.

Ka S, Merindol N, Sow AA, Singh A, Landelouci K, Plourde MB, Pépin G, Masi M, Di Lecce R, Evidente A. 2021. Amaryllidaceae alkaloid cherylline inhibits the replication of dengue and Zika viruses. Antimicrobial Agents and Chemotherapy, AAC. 00398–00321.

Karimzadegan V, Koirala M, Sobhanverdi S, Merindol N, Majhi BB, Gélinas S, Timokhin VI, Ralph J, Dastmalchi M, Desgagné-Penix I. 2024. Characterization of cinnamate 4-hydroxylase (CYP73A) and p-coumaroyl 3′-hydroxylase (CYP98A) from *Leucojum aestivum*, a source of Amaryllidaceae alkaloids. Plant Physiology and Biochemistry **210**, 108612.

Kaufman L, Rousseeuw PJ. 2009. *Finding groups in data: an introduction to cluster analysis*: John Wiley & Sons.

Kawamoto T. 2003. Use of a new adhesive film for the preparation of multi-purpose fresh-frozen sections from hard tissues, whole-animals, insects and plants. Archives of histology and cytology **66**, 123–143.

Kawamoto T, Kawamoto K. 2021. Preparation of thin frozen sections from nonfixed and undecalcified hard tissues using Kawamoto's film method (2020). Skeletal development and repair: Methods and protocols, 259–281.

Kekwick R. 2002. Latex and laticifers. In eLS. John Wiley & Sons, Chichester, UK, www. els. net, doi/0.1038/npg. els.

Kianfe B, Kühlborn J, Tchuenguem R, Tchegnitegni B, Ponou B, Groß J, Teponno R, Dzoyem J, Opatz T, Tapondjou L. 2020. Antimicrobial secondary metabolites from the medicinal plant *Crinum glaucum* A. Chev.(Amaryllidaceae). South African Journal of Botany **133**, 161–166.

Kilgore MB. 2015. The Identification of alkaloid pathway genes from Non-Model Plant Species in the Amaryllidaceae, Washington University in St. Louis.

Kilgore MB, Augustin MM, May GD, Crow JA, Kutchan TM. 2016a. CYP96T1 of *Narcissus* sp. aff. *pseudonarcissus* catalyzes formation of the Para-Para' C-C phenol couple in the Amaryllidaceae alkaloids. Frontiers in Plant Science **7**.

Kilgore MB, Augustin MM, Starks CM, O'Neil-Johnson M, May GD, Crow JA, Kutchan TM. 2014. Cloning and characterization of a norbelladine 4'-O-methyltransferase involved in the biosynthesis of the Alzheimer's drug galanthamine in *Narcissus* sp. *aff. pseudonarcissus*. PLoS One **9**, e103223.

Kilgore MB, Holland CK, Jez JM, Kutchan TM. 2016b. Identification of a noroxomaritidine reductase with Amaryllidaceae alkaloid biosynthesis related activities. Journal of Biological Chemistry **291**, 16740–16752.

Kilgore MB, Kutchan TM. 2016. The Amaryllidaceae alkaloids: biosynthesis and methods for enzyme discovery. Phytochemistry Reviews **15**, 317–337.

Kohelová E, Maříková J, Korábečný J, Hulcová D, Kučera T, Jun D, Chlebek J, Jenčo J, Šafratová M, Hrabinová M. 2021. Alkaloids of *Zephyranthes citrina* (Amaryllidaceae) and their implication to Alzheimer's disease: Isolation, structural elucidation and biological activity. Bioorganic chemistry **107**, 104567.

Koirala M, Cristine Goncalves dos Santos K, Gélinas S-E, Ricard S, Karimzadegan V, Lamichhane B, Sameera Liyanage N, Merindol N, Desgagné-Penix I. 2023. Auxin and light-mediated regulation of growth, morphogenesis, and alkaloid biosynthesis in *Crinum* x *powellii* 'Album' callus. Phytochemistry **216**, 113883.

Koirala M, Karimzadegan V, Liyanage NS, Mérindol N, Desgagné-Penix I. 2022. Biotechnological Approaches to Optimize the Production of Amaryllidaceae Alkaloids. Biomolecules **12**, 893.

Koirala M, Merindol N, Karimzadegan V, Gélinas S-E, Liyanage NS, Lamichhane B, Tobón MCG, Lagüe P, Desgagné-Penix I. 2024. Kinetic and in silico structural characterization of norbelladine O-methyltransferase of Amaryllidaceae alkaloids biosynthesis. Journal of Biological Chemistry **300**.

Konyves K, Bilsborrow J, Christodoulou MD, Culham A, David J. 2021. Comparative plastomics of Amaryllidaceae: inverted repeat expansion and the degradation of the ndh genes in Strumaria truncata Jacq. PeerJ **9**, e12400.

Lamesch P, Berardini TZ, Li D, Swarbreck D, Wilks C, Sasidharan R, Muller R, Dreher K, Alexander DL, Garcia-Hernandez M. 2012. The Arabidopsis Information Resource (TAIR): improved gene annotation and new tools. Nucleic Acids Research **40**, D1202–D1210.

Lamichhane B, Gélinas SE, Merindol N, Koirala M, Dos Santos KCG, Germain H, Desgagné-Penix I. 2025. Elucidating the enzyme network

driving Amaryllidaceae alkaloids biosynthesis in Leucojum aestivum. Plant Biotechnology Journal.

Lange BM, Rujan T, Martin W, Croteau R. 2000. Isoprenoid biosynthesis: the evolution of two ancient and distinct pathways across genomes. Proceedings of the National Academy of Sciences **97**, 13172–13177.

Lashley A, Miller R, Provenzano S, Jarecki S-A, Erba P, Salim V. 2022. Functional diversification and structural origins of plant natural product methyltransferases. Molecules **28**, 43.

Lau W, Fischbach MA, Osbourn A, Sattely ES. 2014. Key applications of plant metabolic engineering. PLoS biology **12**, e1001879.

Lee S, Park NI, Park Y, Park KC, Kim ES, Son YK, Choi BS, Kim NS, Choi IY. 2024. O- and N-Methyltransferases in benzylisoquinoline alkaloid producing plants. Genes Genomics **46**, 367–378.

Leitch IJ, Johnston E, Pellicer J, Hidalgo O, Bennett MD. 2019. Angiosperm DNA C-values database. Vol. 2024.

Lemos Cruz P, Carqueijeiro I, Koudounas K, Bomzan DP, Stander EA, Abdallah C, Kulagina N, Oudin A, Lanoue A, Giglioli-Guivarc'h N. 2023. Identification of a second 16-hydroxytabersonine-O-methyltransferase suggests an evolutionary relationship between alkaloid and flavonoid metabolisms in Catharanthus roseus. Protoplasma **260**, 607–624.

Leong BJ, Last RL. 2017. Promiscuity, impersonation and accommodation: evolution of plant specialized metabolism. Current Opinion in Structural Biology **47**, 105–112.

Li C, Wood JC, Vu AH, Hamilton JP, Lopez CER, Payne RME, Guerrero DAS, Gase K, Yamamoto K, Vaillancourt B, Caputi L, O'Connor SE, Buell CR. 2023a. Single-cell multi-omics in the medicinal plant *Catharanthus roseus*. Nature chemical biology **19**, 1041.

Li Q, Duncan S, Li Y, Huang S, Luo M. 2023b. Decoding plant specialized metabolism: new mechanistic insights. Trends in Plant Science.

Li Q, Xu J, Yang L, Zhou X, Cai Y, Zhang Y. 2020. Transcriptome analysis of different tissues reveals key genes associated with galanthamine biosynthesis in *Lycoris longituba*. Frontiers in Plant Science **11**, 519752.

Li Q, Xu J, Zheng Y, Zhang Y, Cai Y. 2021. Transcriptomic and metabolomic analyses reveals that exogenous methyl jasmonate regulates galanthamine biosynthesis in *Lycoris longituba* seedlings. Frontiers in Plant Science **12**, 713795.

Li W, Qiao C, Pang J, Zhang G, Luo Y. 2019. The versatile O-methyltransferase LrOMT catalyzes multiple O-methylation reactions in amaryllidaceae alkaloids biosynthesis. International journal of biological macromolecules **141**, 680–692.

Li W, Yang Y, Qiao C, Zhang G, Luo Y. 2018a. Functional characterization of phenylalanine ammonia-lyase-and cinnamate 4-hydroxylase-encoding genes from *Lycoris radiata*, a galanthamine-producing plant. International journal of biological macromolecules **117**, 1264–1279.

Li Y, Gao R, Zhang J, Wang Y, Kong P, Lu K, Adnan, Liu M, Ao F, Zhao C, Wang L, Gao X. 2022. The biochemical and molecular investigation of flower color and scent sheds lights on further genetic modification of ornamental traits in *Clivia miniata*. Hortic Res **9**, uhac114.

Li Y, Grotewold E, Dudareva N. 2024. Enough is enough: feedback control of specialized metabolism. Trends in Plant Science **29**, 514–523.

Li Y, Li J, Qian B, Cheng L, Xu S, Wang R. 2018b. De novo biosynthesis of p-coumaric acid in E. coli with a trans-cinnamic acid 4-hydroxylase from the Amaryllidaceae plant *Lycoris aurea*. Molecules **23**, 3185.

Liscombe DK, MacLeod BP, Loukanina N, Nandi OI, Facchini PJ. 2005. Evidence for the monophyletic evolution of benzylisoquinoline alkaloid biosynthesis in angiosperms. Phytochemistry **66**, 1374–1393.

Liscombe DK, Usera AR, O'Connor SE. 2010. Homolog of tocopherol C methyltransferases catalyzes N methylation in anticancer alkaloid biosynthesis. Proc Natl Acad Sci U S A **107**, 18793–18798.

Liu H, Wei J, Yang T, Mu W, Song B, Yang T, Fu Y, Wang X, Hu G, Li W, Zhou H, Chang Y, Chen X, Chen H, Cheng L, He X, Cai H, Cai X, Wang M, Li Y, Sahu SK, Yang J, Wang Y, Mu R, Liu J, Zhao J, Huang Z, Xu X, Liu X. 2019. Molecular digitization of a botanical garden: high-depth whole-genome sequencing of 689 vascular plant species from the Ruili Botanical Garden. Gigascience **8**.

Liu L, Li J. 2019. Communications between the endoplasmic reticulum and other organelles during abiotic stress response in plants. Frontiers in Plant Science **10**, 749.

Liu Z, Sun B, Li J, Xiang Y, Wang R, Jiang X, Zhu X, Xu S, Wang R. 2024. Functional characterization of CYP96T1-like cytochrome P450 from Lycoris aurea catalyzing para-para′ and para-ortho′ oxidative-coupling in Amaryllidaceae alkaloids biosynthesis. Frontiers in Plant Science **15**, 1438102.

Liyanage NS, Awwad F, Gonçalves dos Santos KC, Jayawardena TU, Mérindol N, Desgagné-Penix I. 2025a. Navigating Amaryllidaceae alkaloids: bridging gaps and charting biosynthetic territories. Journal of Experimental Botany **76**, 16–34.

Liyanage NS, Lamichhane B, Fantino E, Mérindol N, Gélinas S-E, Tobón MCG, Desgagné-Penix I. 2025b. Coclaurine N-methyltransferase-like enzymes drive the final biosynthetic reaction of the anti-Alzheimer's drug galanthamine in Amaryllidaceae. Plant Physiology and Biochemistry, 110067.

Ločárek M, Nováková J, Klouček P, Hošt'álková A, Kokoška L, Gábrlová L, Šafratová M, Opletal L, Cahlíková L. 2015. Antifungal and

antibacterial activity of extracts and alkaloids of selected Amaryllidaceae species. Natural product communications **10**, 1934578X1501000912.

Lorensen MDBB, Bjarnholt N, St-Pierre B, Heinicke S, Courdavault V, O'Connor S, Janfelt C. 2023. Spatial localization of monoterpenoid indole alkaloids in *Rauvolfia tetraphylla* by high resolution mass spectrometry imaging. Phytochemistry **209**, 113620.

Loy C, Schneider L. 2006. Galantamine for Alzheimer's disease and mild cognitive impairment. Cochrane database of systematic reviews.

Mai Z, Richardson MB, Mann SGA, Greene J, Paul AA, Perley JO, Deslongchamps G, Qu Y. 2025. Promiscuous and regiospecific *Vinca minor* hydroxylases for opioid akuammine biosynthesis and monoterpenoid indole alkaloid diversification. Plant Physiology and Biochemistry **223**, 109841.

Majhi BB, Gélinas S-E, Mérindol N, Ricard S, Desgagné-Penix I. 2023. Characterization of norbelladine synthase and noroxomaritidine/norcraugsodine reductase reveals a novel catalytic route for the biosynthesis of Amaryllidaceae alkaloids including the Alzheimer’s drug galanthamine. Frontiers in Plant Science **14**.

Malinowski R, Singh D, Kasprzewska A, Blicharz S, Basińska-Barczak A. 2024. Vascular tissue–boon or bane? How pathogens usurp long-distance transport in plants and the defence mechanisms deployed to counteract them. New Phytologist **243**, 2075–2092.

Mann JD, Fales HM, Mudd SH. 1963. Alkaloids and Plant Metabolism: VI. O-methylation in vitro of norbelladine, a precursor of amaryllidaceae alkaloids. Journal of Biological Chemistry **238**, 3820–3823.

Matsuba Y, Nguyen TTH, Wiegert K, Falara V, Gonzales-Vigil E, Leong B, Schäfer P, Kudrna D, Wing RA, Bolger AM, Usadel B, Tissier A, Fernie AR, Barry CS, Pichersky E. 2013. Evolution of a complex locus for terpene biosynthesis in *Solanum*. The plant cell **25**, 2036.

Matsuura HN, Fett-Neto AG. 2015. Plant alkaloids: main features, toxicity, and mechanisms of action. Plant toxins **2**, 1–15.

Meena S, Kanthaliya B, Joshi A, Khan F, Choudhary S, Arora J. 2022. In Vitro Production of Alkaloids. In: Belwal T, Georgiev MI, Al-Khayri JM, eds. *Nutraceuticals Production from Plant Cell Factory*. Singapore: Springer Nature, 143–168.

Meerow A. 2023. Classification and phylogeny of Amaryllidaceae, the modern synthesis and the road ahead: A review. Boletín de la Sociedad Argentina de Botánica **58**.

Meerow A, Snijman D. 1998. Amaryllidaceae. *Flowering Plants· Monocotyledons: Lilianae (except Orchidaceae)*: Springer, 83–110.

Meerow AW, Fay MF, Guy CL, Li QB, Zaman FQ, Chase MW. 1999. Systematics of Amaryllidaceae based on cladistic analysis of plastid sequence data. American Journal of Botany **86**, 1325–1345.

Meerow AW, Gardner EM, Nakamura K. 2020. Phylogenomics of the Andean tetraploid clade of the American Amaryllidaceae (subfamily Amaryllidoideae): unlocking a polyploid generic radiation abetted by continental geodynamics. Frontiers in Plant Science **11**, 582422.

Mehta N, Meng Y, Zare R, Kamenetsky-Goldstein R, Sattely E. 2024. A developmental gradient reveals biosynthetic pathways to eukaryotic toxins in monocot geophytes. Cell **187**, 5620–5637. e5610.

Meisel L, Fonseca B, Gonzalez S, Baeza-Yates R, Cambiazo V, Campos R, Gonzalez M, Orellana A, Retamales J, Silva H. 2005. A rapid and efficient method for purifying high quality total RNA from peaches (*Prunus persica*) for functional genomics analyses. Biol Res **38**, 83–88.

Merindol N, Belem Martins LL, Elfayres G, Custeau A, Berthoux L, Evidente A, Desgagne-Penix I. 2024. Amaryllidaceae Alkaloids Screen Unveils Potent Anticoronaviral Compounds and Associated Structural Determinants. ACS Pharmacol Transl Sci **7**, 3527–3539.

Méteignier L-V, Nützmann H-W, Papon N, Osbourn A, Courdavault V. 2023. Emerging mechanistic insights into the regulation of specialized metabolism in plants. Nature Plants **9**, 22–30.

Montini L, Crocoll C, Gleadow RM, Motawia MS, Janfelt C, Bjarnholt N. 2020. Matrix-assisted laser desorption/ionization-mass spectrometry imaging of metabolites during sorghum germination. Plant Physiology **183**, 925–942.

Mora-Vásquez S, Wells-Abascal GG, Espinosa-Leal C, Cardineau GA, García-Lara S. 2022. Application of metabolic engineering to enhance the content of alkaloids in medicinal plants. Metabolic Engineering Communications **14**, e00194.

Moriya Y, Shigemizu D, Hattori M, Tokimatsu T, Kotera M, Goto S, Kanehisa M. 2010. PathPred: an enzyme-catalyzed metabolic pathway prediction server. Nucleic Acids Research **38**, W138–W143.

Morris JS, Facchini PJ. 2019. Molecular origins of functional diversity in benzylisoquinoline alkaloid methyltransferases. Frontiers in Plant Science **10**, 1058.

Morris JS, Groves RA, Hagel JM, Facchini PJ. 2018. An N-methyltransferase from *Ephedra sinica* catalyzing the formation of ephedrine and pseudoephedrine enables microbial phenylalkylamine production. J Biol Chem **293**, 13364–13376.

Morris JS, Yu L, Facchini PJ. 2020. A single residue determines substrate preference in benzylisoquinoline alkaloid N-methyltransferases. Phytochemistry **170**, 112193.

Muro-Villanueva F, Nett RS. 2023. Emerging functions within the enzyme families of plant alkaloid biosynthesis. Phytochemistry Reviews.

Nair JJ, van Staden J. 2013. Pharmacological and toxicological insights to the South African Amaryllidaceae. Food and chemical toxicology **62**, 262–275.

Nair JJ, van Staden J. 2020. Insight to the antifungal properties of Amaryllidaceae constituents. Phytomedicine **73**, 152753.

Nair JJ, van Staden J. 2023. Antiviral alkaloid principles of the plant family Amaryllidaceae. Phytomedicine **108**, 154480.

Nakagawa K, Iida T, Kobayashi M, Shimma S. 2024. Combination of Probe Electrospray Ionization Mass Spectrometry and Mass Spectrometry Imaging to Analyze Plant Alkaloids in Narcissus tazetta. Mass Spectrometry **13**, A0163–A0163.

Nett RS, Dho Y, Low Y-Y, Sattely ES. 2021. A metabolic regulon reveals early and late acting enzymes in neuroactive Lycopodium alkaloid biosynthesis. Proceedings of the National Academy of Sciences **118**, e2102949118.

Nett RS, Lau W, Sattely ES. 2020. Discovery and engineering of colchicine alkaloid biosynthesis. Nature **584**, 148–153.

Nguyen T-D, Dang T-TT. 2021. Cytochrome P450 Enzymes as Key Drivers of Alkaloid Chemical Diversification in Plants. Frontiers in Plant Science **12**.

Okonechnikov K, Golosova O, Fursov M, team U. 2012. Unipro UGENE: a unified bioinformatics toolkit. Bioinformatics **28**, 1166–1167.

Olin JT, Schneider L. 2002. Galantamine for Alzheimer's disease. Cochrane database of systematic reviews.

One Thousand Plant Transcriptomes Initiative. 2019. One thousand plant transcriptomes and the phylogenomics of green plants. Nature **574**, 679–685.

Ono E, Murata J. 2023. Exploring the evolvability of plant specialized metabolism: uniqueness out of uniformity and uniqueness behind uniformity. Plant and Cell Physiology **64**, 1449–1465.

Orhan IE, Senol Deniz FS, Eren G, Sener B. 2021. Molecular approach to promising cholinesterase inhibitory effect of several amaryllidaceae alkaloids: Further re-investigation. South African Journal of Botany **136**, 175–181.

Otomo K, Kanno Y, Motegi A, Kenmoku H, Yamane H, Mitsuhashi W, Oikawa H, Toshima H, Itoh H, Matsuoka M, Sassa T, Toyomasu T.

2004. Diterpene cyclases responsible for the biosynthesis of phytoalexins, momilactones A, B, and oryzalexins A–F in rice. Bioscience, Biotechnology & Biochemistry **68**, 2006.

Palmer A, Phapale P, Chernyavsky I, Lavigne R, Fay D, Tarasov A, Kovalev V, Fuchser J, Nikolenko S, Pineau C. 2017. FDR-controlled metabolite annotation for high-resolution imaging mass spectrometry. Nature methods **14**, 57–60.

Park CH, Yeo HJ, Park YE, Baek S-A, Kim JK, Park SU. 2019. Transcriptome analysis and metabolic profiling of *Lycoris radiata*. Biology **8**, 63–63.

Peng W, Li Z, Wang S, Wang B. 2023. Unravelling the CC and CN coupling mechanism for the CYP96T1-catalyzed biosynthesis of Amaryllidaceae alkaloids. Molecular Catalysis **550**, 113609.

Ptak A, Morańska E, Saliba S, Zieliński A, Simlat M, Laurain-Mattar D. 2016. Elicitation of galanthamine and lycorine biosynthesis by *Leucojum aestivum* L. and *L. aestivum* 'Gravety Giant' plants cultured in bioreactor RITA®. Plant Cell, Tissue and Organ Culture (PCTOC) **128**, 335–345.

Ptak A, Morańska E, Saliba S, Zieliński A, Simlat M, Laurain-Mattar D. 2017. Elicitation of galanthamine and lycorine biosynthesis by *Leucojum aestivum* L. and *L. aestivum* 'Gravety Giant' plants cultured in bioreactor RITA®. Plant Cell, Tissue and Organ Culture (PCTOC) **128**, 335–345.

Ptak A, Morańska E, Skrzypek E, Warchoł M, Spina R, Laurain-Mattar D, Simlat M. 2020. Carbohydrates stimulated Amaryllidaceae alkaloids biosynthesis in *Leucojum aestivum* L. plants cultured in RITA® bioreactor. PeerJ **8**, e8688.

Ptak A, Morańska E, Warchoł M, Gurgul A, Skrzypek E, Dziurka M, Laurain-Mattar D, Spina R, Jaglarz A, Simlat M. 2022. Endophytic bacteria from in vitro culture of *Leucojum aestivum* L. a new source of

galanthamine and elicitor of alkaloid biosynthesis. Scientific Reports **12**, 13700.

Pulman J. 2014. A transcriptomics approach to understanding polymorphic and transcript level differences linked to isoquinoline alkaloid production in triploid varieties of *Narcissus pseudonarcissus*, University of Liverpool, 224.

Qin K, Liu F, Zhang C, Deng R, Fernie AR, Zhang Y. 2025. Systems and synthetic biology for plant natural product pathway elucidation. Cell Reports **44**, 115715.

Qin L, Zhang Y, Liu Y, He H, Han M, Li Y, Zeng M, Wang X. 2018. Recent advances in matrix-assisted laser desorption/ionisation mass spectrometry imaging (MALDI-MSI) for in situ analysis of endogenous molecules in plants. Phytochemical Analysis **29**, 351–364.

Qu Y, Safonova O, De Luca V. 2019. Completion of the canonical pathway for assembly of anticancer drugs vincristine/vinblastine in *Catharanthus roseus*. The Plant Journal **97**, 257–266.

Rapp JT, Bremer BJ, Romero PA. 2024. Self-driving laboratories to autonomously navigate the protein fitness landscape. Nature Chemical Engineering **1**, 97–107.

Reis A, Magne K, Massot S, Tallini LR, Scopel M, Bastida J, Ratet P, Zuanazzi JAS. 2019. Amaryllidaceae alkaloids: identification and partial characterization of montanine production in *Rhodophiala bifida* plant. Scientific Reports **9**, 8471.

Ren ZM, Zhang D, Jiao C, Li DQ, Wu Y, Wang XY, Gao C, Lin YF, Ruan YL, Xia YP. 2022. Comparative transcriptome and metabolome analyses identified the mode of sucrose degradation as a metabolic marker for early vegetative propagation in bulbs of *Lycoris*. Plant Journal **112**, 115–134.

Ribeiro AJ, Riziotis IG, Borkakoti N, Thornton JM. 2023. Enzyme function and evolution through the lens of bioinformatics. Biochemical Journal **480**, 1845–1863.

Rønsted N, Symonds MR, Birkholm T, Christensen SB, Meerow AW, Molander M, Mølgaard P, Petersen G, Rasmussen N, Van Staden J. 2012. Can phylogeny predict chemical diversity and potential medicinal activity of plants? A case study of Amaryllidaceae. BMC evolutionary biology **12**, 1–12.

Roy M, Liang L, Xiao X, Feng P, Ye M, Liu J. 2018. Lycorine: A prospective natural lead for anticancer drug discovery. Biomedicine & Pharmacotherapy **107**, 615–624.

Ru Q, Wang X, Liu T, Zheng H. 2013. Physiological and comparative proteomic analyses in response to nitrogen application in an Amaryllidaceae plant, *Lycoris aurea*. Acta Physiologiae Plantarum **35**, 271–282.

Santos-Gally R, De Castro A, Pérez-Barrales R, Arroyo J. 2015. Stylar polymorphism on the edge: unusual flower traits in Moroccan *Narcissus broussonetii* (Amaryllidaceae). Botanical Journal of the Linnean Society **177**, 644–656.

Santucci B, Picardo M. 1992. Occupational contact dermatitis to plants. Clinics in dermatology **10**, 157–165.

Schmidt M, Lee N, Zhan C, Roberts JB, Nava AA, Keiser LS, Vilchez AA, Chen Y, Petzold CJ, Haushalter RW. 2023. Maximizing heterologous expression of engineered type I polyketide synthases: Investigating codon optimization strategies. ACS Synthetic Biology **12**, 3366–3380.

Schramm T, Hester Z, Klinkert I, Both J-P, Heeren RM, Brunelle A, Laprévote O, Desbenoit N, Robbe M-F, Stoeckli M. 2012. imzML—a common data format for the flexible exchange and processing of mass spectrometry imaging data. Journal of proteomics **75**, 5106–5110.

science K. 2019. Plant DNA C-values Database. In: Gardens RB, ed, Vol. 2023: Kew science.

Selma S, Ntelkis N, Nguyen TH, Goossens A. 2023. Engineering the plant metabolic system by exploiting metabolic regulation. The Plant Journal **114**, 1149–1163.

Shi H, Wu X, Zhu Y, Jiang T, Wang Z, Li X, Liu J, Zhang Y, Chen F, Gao J. 2024. RefMetaPlant: a reference metabolome database for plants across five major phyla. Nucleic Acids Research **52**, D1614–D1628.

Shimura K, Okada A, Okada K, Jikumaru Y, Ko K-W, Toyomasu T, Sassa T, Hasegawa M, Kodama O, Shibuya N, Koga J, Nojiri H, Yamane H. 2007. Identification of a biosynthetic gene cluster in rice for momilactones. Journal of Biological Chemistry **282**, 34018.

Shitan N, Kato K, Shoji T. 2014. Alkaloid transporters in plants. Plant Biotechnology **31**, 453–463.

Singh A, Desgagné-Penix I. 2017. Transcriptome and metabolome profiling of *Narcissus pseudonarcissus* 'King Alfred' reveal components of Amaryllidaceae alkaloid metabolism. Scientific Reports **7**, 17356–17356.

Singh A, Massicotte M-A, Garand A, Tousignant L, Ouellette V, Bérubé G, Desgagné-Penix I. 2018. Cloning and characterization of norbelladine synthase catalyzing the first committed reaction in Amaryllidaceae alkaloid biosynthesis. BMC plant biology **18**, 1–12.

Sochacki D, Podwyszyńska M, Machlańska A, Dyki B. 2022. Nuclear DNA content, selected morphological and anatomical traits of *Narcissus* cultivars and breeding clones. Agronomy **12**.

Song J, Xu X, Chen Y, Chen G, Lai Z. 2019. Analyses of leaft transcriptome under heat stress in *Narcissus*. Chinese journal of tropical crops **40**, 1991–2000.

Špačková A, Vávra O, Raček T, Bazgier V, Sehnal D, Damborský J, Svobodová R, Bednář D, Berka K. 2024. ChannelsDB 2.0: a comprehensive database of protein tunnels and pores in AlphaFold era. Nucleic Acids Research **52**, D413–D418.

Spengler B. 2015. Mass spectrometry imaging of biomolecular information. Analytical chemistry **87**, 64–82.

Sreeraman S, Kannan MP, Singh Kushwah RB, Sundaram V, Veluchamy A, Thirunavukarasou A, Saravanan KM. 2023. Drug Design and Disease Diagnosis: The Potential of Deep Learning Models in Biology. Current Bioinformatics **18**, 208–220.

Srinivasan P, Smolke CD. 2021. Engineering cellular metabolite transport for biosynthesis of computationally predicted tropane alkaloid derivatives in yeast. Proceedings of the National Academy of Sciences **118**, e2104460118.

Stander EA, de Bernonville TD, Papon N, Courdavault V. 2022. Chromosome-scale genomes throw light on plant drug biosynthesis. Trends in Pharmacological Sciences.

Stoeckli M, Staab D, Wetzel M, Brechbuehl M. 2014. iMatrixSpray: a free and open source sample preparation device for mass spectrometric imaging. Chimia **68**, 146–146.

Su Y, Li HP, Zhang M, Ding XW, Xu JH, Chen Q, Zheng GW. 2022. Regioselectivity Inversion of an O-Methyltransferase via Semi-rational Mutagenesis Combined with Metal Ion Substitution. ChemCatChem **14**, e202200844.

Suhadolnik R, Fischer A, Zulalian J. 1962. The Biogenetic Origin of the CC Unit of Lycorine. Journal of the American Chemical Society **84**, 4348–4349.

Suhadolnik R, Fischer A, Zulalian J. 1963. Biogenesis of the Amaryllidaceae alkaloids. II. Studies with whole plants, floral primordia and cell free extracts. Biochemical and Biophysical Research Communications **11**, 208–212.

Sun B, Wang P, Wang R, Li Y, Xu S. 2018. Molecular Cloning and Characterization of a meta/para-O-Methyltransferase from Lycoris aurea. International journal of molecular sciences **19**, 1911.

Sun X, Zhu S, Li N, Cheng Y, Zhao J, Qiao X, Lu L, Liu S, Wang Y, Liu C, Li B, Guo W, Gao S, Yang Z, Li F, Zeng Z, Tang Q, Pan Y, Guan M, Zhao J, Lu X, Meng H, Han Z, Gao C, Jiang W, Zhao X, Tian S, Su J, Cheng Z, Liu T. 2020. A chromosome-level genome assembly of garlic (*Allium sativum*) provides insights into genome evolution and allicin biosynthesis. Molecular Plant **13**, 1339.

Sweetlove LJ, Fernie AR. 2018. The role of dynamic enzyme assemblies and substrate channelling in metabolic regulation. Nature communications **9**, 2136.

Takos AM, Rook F. 2013. Towards a Molecular Understanding of the Biosynthesis of Amaryllidaceae Alkaloids in Support of Their Expanding Medical Use. International journal of molecular sciences **14**, 11713–11741.

Tallini LR, Giordani RB, de Andrade JP, Bastida J, Zuanazzi JAS. 2021. Structural diversity and biological potential of alkaloids from the genus *Hippeastrum*, Amaryllidaceae: an update. Revista Brasileira de Farmacognosia **31**, 648–657.

Tang M, Li C, Zhang C, Cai Y, Zhang Y, Yang L, Chen M, Zhu F, Li Q, Li K. 2023. SWATH-MS-based proteomics reveals the regulatory metabolism of Amaryllidaceae alkaloids in three *Lycoris* species. International journal of molecular sciences **24**.

Tian Z, Hu X, Xu Y, Liu M, Liu H, Li D, Hu L, Wei G, Chen W. 2024. PMhub 1.0: a comprehensive plant metabolome database. Nucleic Acids Research **52**, D1579–D1587.

Tissier A, Ziegler J, Vogt T. 2014. Specialized plant metabolites: diversity and biosynthesis. Ecological biochemistry: environmental and interspecies interactions, 14–37.

Tousignant L, Diaz-Garza AM, Majhi BB, Gélinas S-E, Singh A, Desgagne-Penix I. 2022. Transcriptome analysis of *Leucojum aestivum* and identification of genes involved in norbelladine biosynthesis. Planta **255**, 30–30.

Trujillo Chacón LM, Leiva H, Rojas JM, Zapata Vahos IC, Castro D, Domínguez M, Osorio E. 2024. Histochemical Localization and Cytotoxic Potential of Alkaloids in *Phaedranassa lehmannii*. Plants **13**, 3251.

Trujillo Chacón LM, Leiva H, Zapata Vahos IC, Restrepo DC, Osorio E. 2023. Influence of plant growth regulators on in vitro biomass production and biosynthesis of cytotoxic Amaryllidaceae alkaloids in Caliphuria tenera Baker. Biocatalysis and Agricultural Biotechnology **50**, 102670.

Tsuda Y, Kashiwaba N, Kumar V. 1984. The alkaloidal constituents of Goda-manel (*Crinum zeylanicum* L.), a Sri Lankan folk medicine. Chemical and pharmaceutical bulletin **32**, 3023–3027.

Uzaki M, Mori T, Sato M, Wakazaki M, Takeda-Kamiya N, Yamamoto K, Murakami A, Guerrero DAS, Shichijo C, Ohnishi M. 2024. Integration of cell differentiation and initiation of monoterpenoid indole alkaloid metabolism in seed germination of *Catharanthus roseus*. New Phytologist **242**, 1156–1171.

Vaou N, Stavropoulou E, Voidarou C, Tsigalou C, Bezirtzoglou E. 2021. Towards advances in medicinal plant antimicrobial activity: A review study on challenges and future perspectives. Microorganisms **9**, 2041.

Varadharajan V, Rajendran R, Muthuramalingam P, Runthala A, Madhesh V, Swaminathan G, Murugan P, Srinivasan H, Park Y, Shin H. 2025. Multi-Omics Approaches Against Abiotic and Biotic Stress—A Review. Plants **14**, 865.

Vu GT, Cao HX, Reiss B, Schubert I. 2017. Deletion-bias in DNA double-strand break repair differentially contributes to plant genome shrinkage. New Phytologist **214**, 1712–1721.

Waese J, Provart NJ. 2017. The bio-analytic resource for plant biology. Plant Genomics Databases: Methods and Protocols, 119–148.

Wahkstrøm R, Laane MM. 2009. Chromosome analyses in African *Crinum* species (Amaryllidaceae). Hereditas **91**, 183–206.

Wang L, Zhang X-Q, Yin Z-Q, Wang Y, Ye W-C. 2009. Two new amaryllidaceae alkaloids from the bulbs of *Lycoris radiata*. Chemical and pharmaceutical bulletin **57**, 610–611.

Wang N, Shu X, Zhang F, Song G, Wang Z. 2024. Characterization of the Heat Shock Transcription Factor Family in *Lycoris radiata* and Its Potential Roles in Response to Abiotic Stresses. Plants **13**, 271.

Wang N, Shu X, Zhang F, Zhuang W, Wang T, Wang Z. 2021a. Comparative transcriptome analysis identifies key regulatory genes involved in anthocyanin metabolism during flower development in *Lycoris radiata*. Frontiers in Plant Science **12**.

Wang P, Yu S, Han X, Xu J, He Q, Xu S, Wang R. 2020. Identification, molecular characterization and expression of JAZ genes in Lycoris aurea. PLoS One **15**, e0230177.

Wang R, Han X, Xu S, Xia B, Jiang Y, Xue Y, Wang R. 2019. Cloning and characterization of a tyrosine decarboxylase involved in the biosynthesis of galanthamine in Lycoris aurea. PeerJ **7**, e6729.

Wang R, Liu Y, Xu S, Li J, Zhou J, Wang R. 2021b. An ATP-Binding Cassette Transporter, LaABCB11, Contributes to Alkaloid Transport in *Lycoris aurea*. International journal of molecular sciences **22**, 11458.

Wang R, Xu S, Jiang Y, Jiang J, Li X, Liang L, He J, Peng F, Xia B. 2013. *De novo* sequence assembly and characterization of *Lycoris aurea* transcriptome Using GS FLX titanium platform of 454 pyrosequencing. PLoS One **8**, e60449.

Wang R, Xu S, Wang N, Xia B, Jiang Y, Wang R. 2017. Transcriptome analysis of secondary metabolism pathway, transcription factors, and transporters in response to methyl jasmonate in *Lycoris aurea*. Frontiers in Plant Science **7**.

Wang XY, Wang PK, Huang MR, Zhou J, Han ZM. 2007. The localization of galanthamine in vegetative organ of *Lycoris aurea* Herb.

Fen zi xi bao Sheng wu xue bao= Journal of Molecular Cell Biology **40**, 339–345.

Wang Y, Chen D, He X, Shen J, Xiong M, Wang X, Zhou D, Wei Z. 2018. Revealing the complex genetic structure of cultivated amaryllis (*Hippeastrum hybridum*) using transcriptome-derived microsatellite markers. Scientific Reports **8**, 10645.

Wang Z, Song G, Zhang F, Shu X, Wang N. 2023. Functional Characterization of AP2/ERF Transcription Factors during Flower Development and Anthocyanin Biosynthesis Related Candidate Genes in Lycoris. International journal of molecular sciences **24**, 14464.

Watkins JL, Facchini PJ. 2022. Compartmentalization at the interface of primary and alkaloid metabolism. Current Opinion in Plant Biology **66**, 102186.

Weng J-K, Philippe RN, Noel JP. 2012. The rise of chemodiversity in plants. Science **336**, 1667–1670.

Wildman W. 1960. Alkaloids of the Amaryllidaceae. *The Alkaloids: Chemistry and Physiology*, Vol. 6: Elsevier, 289–413.

Wildman W, Battersby A, Breuer S. 1962. Biosynthesis in the Amaryllidaceae. Incorporation of 3-C14-Tyrosine and Phenylalanine in Nerine Bowdenii W. Wats. Journal of the American Chemical Society **84**, 4599–4600.

Wink M. 2008. Plant secondary metabolism: diversity, function and its evolution. Natural product communications **3**, 1934578X0800300801.

Wink M. 2013. Evolution of secondary metabolites in legumes (Fabaceae). South African Journal of Botany **89**, 164–175.

Winzer T, Gazda V, He Z, Kaminski F, Kern M, Larson TR, Li Y, Meade F, Teodor R, Vaistij FE, Walker C, Bowser TA, Graham IA. 2012. A *Papaver somniferum* 10-gene cluster for synthesis of the anticancer alkaloid noscapine. Science **336**, 1708.

Xiang X, Jiang X, Hu Z, Tang J, Quan M. 2022. Comparative transcriptome analysis of the key genes associated with the

accumulation of lycorine and galanthamine in *Lycoris aurea*. Bangladesh Journal of Botany **51**, 767–777.

Xu Y-m, Gao S, Bunting DP, Gunatilaka AL. 2011. Unusual withanolides from aeroponically grown *Withania somnifera*. Phytochemistry **72**, 518–522.

Yamada Y, Sato F. 2021. Transcription factors in alkaloid engineering. Biomolecules **11**, 1719.

Yamamoto K, Grzech D, Koudounas K, Stander EA, Caputi L, Mimura T, Courdavault V, O'Connor SE. 2021. Improved virus-induced gene silencing allows discovery of a serpentine synthase gene in Catharanthus roseus. Plant Physiology **187**, 846–857.

Yamamoto K, Takahashi K, Mizuno H, Anegawa A, Ishizaki K, Fukaki H, Ohnishi M, Yamazaki M, Masujima T, Mimura T. 2016. Cell-specific localization of alkaloids in *Catharanthus roseus* stem tissue measured with Imaging MS and Single-cell MS. Proceedings of the National Academy of Sciences **113**, 3891–3896.

Yan H, Xie N, Zhong C, Su A, Hui X, Zhang X, Jin Z, Li Z, Feng J, He J. 2018. Aphicidal activities of Amaryllidaceae alkaloids from bulbs of *Lycoris radiata* against *Aphis citricola*. Industrial Crops and Products **123**, 372–378.

Yang F, Li CH, Das D, Zheng YH, Song T, Wang LX, Chen MX, Li QZ, Zhang J. 2021a. Comprehensive transcriptome and metabolic profiling of petal color development in *Lycoris sprengeri*. Frontiers in Plant Science **12**, 747131.

Yang J, Ren Y, Zhang D, Chen X, Huang J, Xu Y, Aucapina CB, Zhang Y, Miao Y. 2021b. Transcriptome-based WGCNA analysis reveals regulated metabolite fluxes between floral color and scent in *Narcissus tazetta* flower. International journal Molecular Science **22**.

Yang J, Wu X, Aucapiña CB, Zhang D, Huang J, Hao Z, Zhang Y, Ren Y, Miao Y. 2023. NtMYB12 requires for competition between flavonol

and (pro)anthocyanin biosynthesis in *Narcissus tazetta* tepals. Molecular Horticulture **3**.

Yin Q, Zhu Z, Yang M. 2025. Biosynthesis of plant neuroactive alkaloids treating Alzheimer's disease. Frontiers in Pharmacology **16**, 1500955.

Yu X, Liu Z, Sun X. 2023. Single-cell and spatial multi-omics in the plant sciences: Technical advances, applications, and perspectives. Plant Communications **4**.

Yue Y, Liu J, Shi T, Chen M, Li Y, Du J, Jiang H, Yang X, Hu H, Wang L. 2019. Integrating transcriptomic and GC-MS metabolomic analysis to characterize color and aroma formation during tepal development in *Lycoris longituba*. Plants **8**, 53.

Zaragoza-Puchol D, Ortiz JE, Orden AA, Sanchez M, Palermo J, Tapia A, Bastida J, Feresin GE. 2021. Alkaloids Analysis of Habranthus cardenasianus (Amaryllidaceae), Anti-Cholinesterase Activity and Biomass Production by Propagation Strategies. Molecules **26**, 192.

Zhang CH, Shao XX, Wang XB, Shou LL, Liu YL, Xu ZG, Guo ZY. 2022a. Development of a general bioluminescent activity assay for peptide ligases. FEBS J **289**, 5241–5258.

Zhang F, Cheng G, Shu X, Wang N, Wang Z. 2022b. Transcriptome analysis of *Lycoris chinensis* bulbs reveals flowering in the age-mediated pathway. Biomolecules **12**.

Zhang F, Wang N, Cheng G, Shu X, Wang T, Zhuang W, Lu R, Wang Z. 2021. Comparative Chloroplast Genomes of Four Lycoris Species (Amaryllidaceae) Provides New Insight into Interspecific Relationship and Phylogeny. Biology (Basel) **10**.

Zhang Y-M, Li T, Xu C-C, Qian J-Y, Guo H, Zhang X, Zhan Z-J, Lu J-J. 2024. Uncover the anticancer potential of lycorine. Chinese Medicine **19**, 121.

Zhang Y, Fernie A. 2020. Metabolons, enzyme-enzyme assemblies that mediate substrate channeling, and their roles in plant metabolism. Plant Commun 2: 100081.

Zhao W, Shen C, Zhu J, Ou C, Liu M, Dai W, Liu X, Liu J. 2020. Identification and characterization of methyltransferases involved in benzylisoquinoline alkaloids biosynthesis from *Stephania intermedia*. Biotechnol Lett **42**, 461–469.

Zhou J, Liu Z, Wang S, Li J, Li Y, Chen W-K, Wang R. 2020a. Fungal endophytes promote the accumulation of Amaryllidaceae alkaloids in *Lycoris radiata*. Environmental Microbiology **22**, 1421–1434.

Zhou J, Stringlis IA, Wen J, Liu Y, Xu S, Wang R. 2023. Interplay between Amaryllidaceae alkaloids, the bacteriome and phytopathogens in *Lycoris radiata*. New Phytologist.

Zhou MZ, Yan CY, Zeng Z, Luo L, Zeng W, Huang YH. 2020b. N-Methyltransferases of Caffeine Biosynthetic Pathway in Plants. J Agric Food Chem **68**, 15359–15372.

Zhou P, Peng J, Zeng M, Wu L, Fan Y, Zeng L. 2021. Virus-induced gene silencing (VIGS) in Chinese narcissus and its use in functional analysis of NtMYB3. Horticultural Plant Journal **7**, 565–572.

Zhou Z, Wu M, Sun B, Li J, Li J, Liu Z, Gao M, Xue L, Xu S, Wang R. 2024. Identification of transcription factor genes responsive to MeJA and characterization of a LaMYC2 transcription factor positively regulates lycorine biosynthesis in *Lycoris aurea*. Journal of Plant Physiology, 154218.

Ziegler J, Facchini PJ. 2008. Alkaloid biosynthesis: metabolism and trafficking. Annu. Rev. Plant Biol. **59**, 735–769.

Zonneveld BJM, Grimshaw JM, Davis AP. 2003. The systematic value of nuclear DNA content in *Galanthus*. Plant systematics and evolution **241**, 89–102.

Zonneveld BJM, Leitch IJ, Bennett MD. 2005. First Nuclear DNA Amounts in more than 300 Angiosperms. Annals of botany **96**, 229–244.

APPENDIX I

Supplementary Data of Chapter II

Table 1.A1. Reference numbers of the RNA sequencing raw data.

Species name	NCBI Bioproject reference of raw data
Leucojum aestivum	PRJNA720900
Lycoris radiata	PRJNA529664
***Hippeastrum* cv. hybridum**	PRJNA608969

Table 1.A2. List of primers used in this study.

Primer name	Sequence	Purpose
***LaNMT*-F**	AAACCCGAATTCATGGGGAAATTGGTGGAGGTTCCGTA	Cloning
***LaNMT*-R**	AAACCCAAGCTTCTATTTCTTTTTGAAAAGAAAATGTGCAACCATCC	Cloning
***LrNMT*-F**	AAACCCGAATTCATGGGGAAATTGGTGGAGGTTCCGTA	Cloning
***LrNMT*-R**	AAACCCAAGCTTTTATTTCTTTTTGAAAAGATAATGTGCAACCATCC	Cloning
***H*pNMT-F**	AAACCCGAATTCATGGGGAAATTGGTTGAGGTCCCCTA	Cloning
HpNMT-R	AAACCCAAGCTTTTATTTCTTTTTGAAAAGATAATGTGCAACCATCC	Cloning
***LaNMT_del315-355*-F**	GCTATTAGACCAATCATGGAGTCAACCTATTAGAAGCTTGGCACTGGCCGTCGTTTTACA	Cloning
***pMAL_bb*-R**	TCTCTTCCGGGCGCTATCATGCCATACCGCGAAAGGTTTTGCACCATTCGATGGTGTCGG	Cloning
***pMAL_bb*-F**	CCGACACCATCGAATGGTGCAAAACCTTTCGCGGTATGGCATGATAGCGCCCGGAAGAGA	Cloning
***LaNMT_del315-355*-R**	TGTAAAACGACGGCCAGTGCCAAGCTTCTAATAGGTTGACTCCATGATTGGTCTAATAGC	Cloning
***LaNMT_F234L*-F**	GAAGCAGGATAGTCTCCTATTCGTTCATTACTTGTGCCACAAAGTATTTGC	Cloning
***LaNMT_F234L*-R**	GTCCTCAAAATGGTAAGCAAATACTTTGTGGCACAAGTAATGAACGAATAG	Cloning
***LaNMT_F234W*-R**	CATTTATGTCCTCAAAATGGTAAGCAAATACTTTGTGGCACCAGTAATGAACGAATAG	Cloning
***LaNMT_F234W*-F**	GGATGAAGCAGGATAGTCTCCTATTCGTTCATTACTGGTGCCACAAAGTATTTGCTTACC	Cloning
***LaNMT_F234A*-F**	GCAGGATAGTCTCCTATTCGTTCATTACGCGTGCCACAAAGTATTTGC	Cloning
***LaNMT_F234A*-R**	CATCTTCATTTATGTCCTCAAAATGGTAAGCAAATACTTTGTGGCACGCGTAATGAACG	Cloning
***LaNMT_F257L*-F**	GGACATAAATGAAGATGACTGGATTACAAGACATTTCTTGAGTGGAGGAACAATGCC	Cloning
***LaNMT_F257L*-R**	CCTGAAAATAGAGAAGCAGGTTTGCAGAAGGCATTGTTCCTCCACTCAAGAAATGTCTTG	Cloning
***LaNMT_F257W*-F**	GGACATAAATGAAGATGACTGGATTACAAGACATTTCTGGAGTGGAGGAACAATG	Cloning

***LaNMT_F257W*-R**	CCTGAAAATAGAGAAGCAGGTTTGCAGAAGGCATTGTTCCTCCACTCCAGAAATGTCTTG	Cloning
***LaNMT_E204K*-F**	GGAGGCATCATTTGACCGGGTTATATCTATCAAGATGTTCGAGCACATGAAG	Cloning
***LaNMT_E204K*-R**	GCTATCTTTTTCATAAGTGCTTTGTAGTTCTTCATGTGCTCGAACATCTTGATAGATATAAC	Cloning
***LaNMT_E204D*-F**	GTTTGAAATGGAGGCATCATTTGACCGGGTTATATCTATCGACATGTTCGAGCACATG	Cloning
***LaNMT_E204D*- R**	CTTTTTCATAAGTGCTTTGTAGTTCTTCATGTGCTCGAACATGTCGATAGATATAAC	Cloning
***LaNMT_L68P*-F**	CTCATTCAGTTCAAGCAGTCTCTTGAAGATATGCCTATAGCTGTGGAAAC	Cloning
***LaNMT_L68P*-R**	CTCGTAATGTTGGGTTTTTGCTTTATCAGTTTCCACAGCTATAGGCATATCTTCAAG	Cloning
***LaNMT_Y325S*- R**	CTCTGCAACTGCAATGAAGAATGTTCGCCAAGAAACAGTCCACTTGGTAGCCAAATCCTC	Cloning
***LaNMT_Y325S*- F**	GAGGATTTGGCTACCAAGTGGACTGTTTCTTGGCGAACATTCTTCATTGCAGTTGCAGAG	Cloning
MBP_5'SEQ	GGTCGTCAGACTGTCGATGAAGCC	Colony PCR
MBP_3'SEQ	CGCCAGGGTTTTCCCAGTCACGAC	Colony PCR
***NMT*-F**	GGAGGTTCCGTACAATGCGA	RT-qPCR
***NMT*-R**	CGTGTCAGCCTCCTGATGAC	RT-qPCR
***Histone3*-F**	ACAAGCCTTTGGAAGGGCAG	RT-qPCR
***Histone3*-R**	GGAGTGAAGAAGCCCCACC	RT-qPCR

Table 1.A3. Instrumental parameters used in Single Ion Monitoring (SIM) mode for substrate specificity assays on HPLC-MS/MS.

Substrate name	Substrate [M+H]+ (m/z)	Expected product $[M+H+14]^+$ (m/z)	Expected product $[M+H+28]^+$ (m/z)	Expected product $[M+H+42]^+$ (m/z)	Fragmentor (V)	Polarity (ESI +/-)
3'-*O*-methylnorbelladine	274	288			105	Positive
4'-*O*-methylnorbelladine	274	288			105	Positive
3',4'-*O*-dimethylnorbelladine	288	302			100	Positive
Coclaurine	286	300			115	Positive
Epinephrine	184	198			60	Positive
Heliamine	194	208			100	Positive

Hordenine	166	180			70	Positive
Huperzine A	243	257	271	285	100	Positive
Levodopa	198	212			78	Positive
Narciclasine	308	322			82	Positive
***N*-caffeoyl-*O*-methyltyramine**	314	328			110	Positive
***N*-demethyl Ivabradine**	456	470			100	Positive
***N*-demethylricine**	154	168			100	Positive
***N*-methyltyramine**	152	166			65	Positive
Noradrenaline	152	166			60	Positive
Norbelladine	260	274			86	Positive
Norephedrine	152	166			100	Positive
Norgalanthamine	274	288			115	Positive
Papaverine	340				165	Positive
Phenylalanine	166	180			74	Positive
Phenylephrine	168	182			100	Positive
Tryptamine	161	175			100	Positive
Tryptophane	205	219			100	Positive
Tyramine	138	152			81	Positive
Tyrosine	182	196			83	Positive

Table 1.A4. MRM transitions and instrumental parameters used for metabolite analysis and enzyme assays with norgalanthamine as substrate on HPLC-MS/MS.

Compound name	Retention time (min)	Precursor ion (m/z)	Product ion (m/z)	Fragmentor (V)	Collision energy (V)	Polarity (ESI +/-)
3,4-dihydroxybenzaldehyde	15.861	137	119	114	20	Negative
			108		26	
			92		26	
3,4-dihydroxybenzoic acid	12.232	153	**109**	45	13	Negative
			108		29	
			91		29	

			137		18	
3'-*O*-methylnorbelladine	16.893	274	121	105	15	Positive
			109		40	
			120		18	
4-hydroxybenzaldehyde	18.068	121	**92**	69	26	Negative
			65		30	
			137		18	
4'-*O*-methylnorbelladine	15.632	274	122	105	40	Positive
			94		40	
			284		22	
9-*O*-demethylhomolycorine	8.343	302	251	120	34	Positive
			94		30	
			226		26	
11-hydroxyvittatine	4.546	288	**196**	105	34	Positive
			153		40	
			151		10	
3',4'-*O*-dimethylnorbelladine	16.686	288	135	100	40	Positive
			107		40	
			163		5	
Caffeic acid	18.362	181	135	76	10	Positive
			117		21	
			243		18	
Cherylline	7.590	286	165	103	40	Positive
			137		18	
			269		14	
Coclaurine	16.057	286	175	115	20	Positive
			107		30	
			137		10	
Dopamine	3.291	154	119	78	18	Positive
			91		26	
			177		5	
Ferulic acid	19.591	195	145	81	20	Positive
			117		21	
			242		26	
Flexinine	8.425	288	149	110	34	Positive
			147		30	
			270		14	
Galanthamine	4.656	288	225	120	18	Positive
			213		22	
			214		34	
Gigancrinine	6.973	288	213	110	34	Positive
			170		34	
			257		20	
Gigantelline	15.626	300	194	135	20	Positive
			107		40	

			273		20	
Gigantellinine	13.750	316	192	135	20	Positive
			137		20	
			211		22	
Haemanthamine	12.206	302	**196**	105	34	Positive
			181		30	
			300		30	
Homolycorine	15.910	316	**298**	115	22	Positive
			94		26	
			177		5	
Isoferulic acid	19.764	195	145	81	20	Positive
			117		21	
			151		10	
Isovanillic acid	18.394	169	125	81	5	Positive
			93		9	
			125		10	
Isovanillin	18.595	153	**93**	86	13	Positive
			65		25	
			181		10	
Levodopa	3.887	198	**152**	78	10	Positive
			139		14	
			165		10	
L-Tyrosine	4.361	182	**136**	83	10	Positive
			123		14	
			233		20	
Lycoramine	4.844	290	215	99	20	Positive
			189		24	
			270		20	
Lycorine	3.995	288	177	92	20	Positive
			147		28	
			119		40	
			248		28	
Narciclasine	18.386	308	218	82	36	Positive
			202		40	
			138		5	
Norbelladine	7.198	260	123	86	20	Positive
			121		17	
			231		14	
Norgalanthamine	4.201	274	**213**	115	18	Positive
			198		40	
			329		26	
Obliquine	21.096	449	244	135	38	Positive
			121		40	
Pancracine	6.516	288	**270**	95	18	Positive
			185		34	

			165		40	
			324		40	
Papaverine	18.006	340	**202**	165	27	Positive
			171		40	
			147		5	
p-coumaric acid	19.451	165	119	76	17	Positive
			91		20	
			120		9	
Phenylalanine	6.221	166	103	74	29	Positive
			77		40	
			128		13	
Phenylalanine-d8	6.080	174	108	69	29	Positive
			81		40	
			217		14	
Sanguinine	3.523	274	**199**	85	22	Positive
			184		40	
			314		14	
Tazzetine	17.218	332	181	90	30	Positive
			153		40	
Trans-cinnamic acid	21.283	147	**103**	65	9	Negative
			77		20	
			121		5	
Tyramine	3.497	138	91	81	20	Positive
			77		20	
			125		10	
Vanillin	18.758	153	**93**	86	13	Positive
			65		25	
			226		26	
Vittatine and/or crinine	10.193	272	196	105	34	Positive
			136		26	

Table 1.A5. Full-length reference mRNA and protein sequences.

Name	Sequenced obtained in this study
LaNMT_ **Reference**	ATGGGGAAATTGGTGGAGGTTCCGTACAATGCGACGGTGAGCGTAATGTTAGCGTCCCTAGAGAGAAAT TTGCTGCCGGATTTAGTCATCAGGAGGCTGACACGTGTCCTCCTAGCCACCCGGCTCCGCCATGGCTAC CTCCCTTCTGCAGAGCTTCAACTCTCTAATCTCATTCAGTTCAAGCAGTCTCTTGAAGATATGCCTATAGC TGTGGAAACTGATAAAGCAAAAACCCAACATTACGAGTTACCCACCTCTTTTTTCGAACTGGTGTTGGGA AAGAATCTCAAGTACAGCTGCTGTTACTTCAACGGTACGTCGAACACATTGGAAGATGCTGAGAATGCAA TGCTGGAGCTGTATTGTGAGCGAGCACAAGTAAAAGATGGTCAATCAATACTTGATGTAGGATGTGGATG GGGTTCCCTTTCTTTGTACATTGCAAGGAAATACAAAGGTTGCAGCATTACTGGGATATGCAATTCTACAA CACAAAGAGCTTATATAGAGGAACAGTGCAGGGACCTTCAATTGTCAAATGTAAAGATTATTGTTGCAGAT ATCAGGGAGTTTGAAATGGAGGCATCATTTGACCGGGTTATATCTATCGAGATGTTCGAGCACATGAAGA ACTACAAAGCACTTATGAAAAAGATAGCAACATGGATGAAGCAGGATAGTCTCCTATTCGTTCATTACTTTT GCCACAAAGTATTTGCTTACCACTTTGAGGACATAAATGAAGATGACTGGATTACAAGACATTTCTTCAGT GGAGGAACAATGCCTTCTGCAAACCTGCTTCTCTATTTTCAGGATGATGTTGCTGTGGTCAACCACTGGC TTGTGAATGGGATGCATTATTCAAGGACAAGCGAAGAGTGGCTCAAAAGAATGGATCAGAATAGAGCTGC TATTAGACCAATCATGGAGTCAACCTATGGCGAGGATTTGGCTACC AAGTGGACTGTTTATTGGCGAACATTCTTCATTGCCGTTGCAGAGCTCTTTGGTTATAACAATGGAGAAGA ATGGATGGTTGCACATTTTCTTTTCAAAAAGAAATAG

LrNMT_Reference	ATGGGGAAATTGGTGGAGGTTCCGTACAATGCGACGGTGTGCGTAATGTTAGCGTCTCTAGAGAGAAA TTTGCTGCCAGATTTAGTCATCAGGAGGCTGACACGTGTTCTCCTAGCCAGCCGGCTCCGCCATGGCTA CCTCCCTTCTGCAGAGCTTCAGCTCTCTAATCTCATTCAGTTCAAGCAGTCTCTTGAAGATATGCCTATAG CTGTGGAAACTGACAAAGCAAAAATCCAACATTATGAGTTGCCCACCTCTTTTTTCGAACTGGTGTTGGG AAAGAATCTCAAGTACAGCTGCTGTTACTTCAACGTTAAGTCAAACACATTGGAAGATGCTGAGAATTCAA TGCTGGAGCTGTATTGTGAGCGAGCACAAGTAAAAGATGGCCAATCAATACTTGATGTAGGATGCGGATG GGGTTCCCTTTCTTTGTACATTGCAAGGAAATACAGAAGTTGCAGCATCACGGGGATATGCAATTCTACAA CACAAAGAGCTTACATCGAGGAACAGTGCAGGGGCCTTCAATTGTCAAATATAAAGATTATTGTTGCAGAT ATCAGCAAGTTTGAAATGGACGCATCATTTGACCGGGTTATATCTATCGAGATGTTTGAGCACATGAAGAA CTACAAAGCACTTCTGAAAAAGATATCCACATGGATGAAGCAGGATAGTCTCCTATTTGTTCATTACTTTTG CCACAAAGTATTTGCTTACCATTTTGAGGATATAAATGAAGATGACTGGATTACAAGATATTTCTTTAGTGG AGGAACAATGCCTTCTGCAAACTTACTTCTCTATTTTCAGGATGATGTTGCCGTGGTCGACCACTGGCTT GTGAATGGGATGCATTATTCAAGTACAAGTGAAGAGTGGCTCAAAAGAATGGATCAGAATAGAGCTGCTA TTAGACCAATCATGGAGTCAACCTATGGTAAGGATTCTGCTACCAAGTGGACTGTTTATTGGCGAACATTC TTCATTGCAGTTGCTGAGCTCTTCGGCTATAACAATGGAGAAGAATGGATGGTTGCACATTATCTTTTCAA AAAGAAATAA
HpNMT_Reference	ATGGGGAAATTGGTGGAGGTTCCGTACAATGCGACGGTGAGCGTAATGTTAGCGTCCCTAGAGAGAAAT TTGCTGCCGGATTTAGTCATCAGGAGGCTGACACGTGTCCTCCTAGCCACCCGGCTCCGCCATGGCTAC CTCCCTTCTGCAGAGCTTCAACTCTCTAATCTCATTCAGTTCAAGCAGTCTCTTGAAGATATGCTTATAGC TGTGGAAACTGATAAAGCAAAAACCCAACATTACGAGTTACCCACCTCTTTTTTCGAACTGGTGTTGGGA AAGAATCTCAAGTACAGCTGCTGTTACTTCAACGGTACGTCGAACACATTGGAAGATGCTGAGAATGCAA TGCTGGAGCTGTATTGTGAGCGAGCACAAGTAAAAGATGGTCAATCAATACTTGATGTAGGATGTGGATG GGGTTCCCTTTCTTTGTACATTGCAAGGAAATACAAAGGTTGCAGCATTACTGGGATATGCAATTCTACAA CACAAAGAGCTTATATAGAGGAACAGTGCAGGGACCTTCAATTGTCAAATGTAAAGATTATTGTTGCAGAT ATCAGGGAGTTTGAAATGGAGGCATCATTTGACCGGGTTATATCTATCGAGATGTTCGAGCACATGAAGA ACTACAAAGCACTTATGAAAAAGATAGCAACATGGATGAAGCAGGATAGTCTCCTATTCGTTCATTACTTTT GCCACAAAGTATTTGCTTACCATTTTGAGGACATAAATGAAGATGACTGGATTACAAGACATTTCTTCAGT GGAGGAACAATGCCTTCTGCAAACCTGCTTCTCTATTTTCAGGATGATGTTGCTGTGGTCAACCACTGGC TTGTGAATGGGATGCATTATTCAAGGACAAGCGAANAGTGGCTCAAAAGAATGGATCAGAACAGAGCTG CTATTAGACCAATCAGGGAGTCAACCTATGGTGAGGATTTGGCTACCAAGTGGACTGTTTCTTGGCGAAC ATNCTTCAATGCAGTTGCAAAGCTCTTTGGTTATAACAATGGAAAAAAATGGAAGGTTCCCCATTTTTTTTT CAAAAAGAAATAG
LaNMT2	ATGGGGAAATTGGTGGAGGTTCCGTACAATGCGACGGTGAGCGTAATGTTAGCGTCCCTAGAGAGAAAT TTGCTGCCGGATTTAGTCATCAGGAGGCTGACACGTGTCCTCCTAGCCACCCGGCTCCGCCATGGCTAC CTCCCTTCTGCAGAGCTTCAACTCTCTAATCTCATTCAGTTCAAGCAGTCTCTTGAAGATATGCCTATAGC TGTGGAAACTGATAAAGCAAAAACCCAACATTACGAGTTACCCACCTCTTTTTTCGAACTGGTGTTGGGA AAGAATCTCAAGTACAGCTGCTGTTACTTCAACGGTACGTCGAACACATTGGAAGATGCTGAGAATGCAA TGCTGGAGCTGTATTGTGAGCGAGCACAAGTAAAAGATGGTCAATCAATACTTGATGTAGGATGTGGATG GGGTTCCCTTTCTTTGTACATTGCAAGGAAAAACAAAGGTTGCAGCATTACTGGGATATGCAATTCTACAA CACAAAGAGCTTATATAGAGGAACAGTGCAGGGACCTTCAATTGTCAAATGTAAAGATTATTGTTGCAGAT ATCAGGGAGTTTGAAATGGAGGCATCATTTGACCGGGTTATATCTATCGAGATGTTCGAGCACATGAAGA ACTACAAAGCACTTATGAAAAAGATAGCAACATGGATGAAGCAGGATAGTCTCCTATTCGTTCATTACCTTT GCCACAAAGTATTTGCTTACCACTTTGAGGACATAAATGAAGATGACTGGATTACAAGACATTTCTTCAGT GGAGGAACAATGCCTTCTGCAAACCTGCTTCTCTATTTTCAGGATGATGTTGCTGTGGTCAACCACTGGC TTGTGAATGGGATGCATTATTCAAGGACAAGCGAAGAGTGGCTCAAAAGAATGGATCAGAATAGAGCTGC TATTAGACCAATCATGGAGTCAACCTATGGCGAGGATTTGGCTACCAAGTGGACTGTTTATTGGCGAACAT TCTTCATTGCCGTTGCAGAGCTCTTTGGTTATAACAATGGAGAAGAATGGATGGTTGCACATTTTCTTTTC AAAAAGAAATAG
LaNMT3	ATGGGGAAATTGGTGGAGGTTCCGTACAATGCGACGGTGAGCGTAATGTTAGCGTCTCTAGAGAGAAAT TTGCTACCGGATTTAGTCATCAGGAGACTGACACGTGTCCTCCTAGCCACCCGGTTCCGCCATGGCTAC ATCCCTTCTGCAGAACTTCAACTCTCTAATCTCATTCAGTTCAAGCAGTCTCTTGAAGATATGCCTATAGCT GTGGAAACTGATAAAGCAAAAACGCAACATTACGAGTTACCCACCTCTTTTTTCAAACTGGTGTTGGGAA AGAATCTCAAGTACAGCTGCTGTTACTTCAATGGTACGTCGAACACATTGGAAGATGCTGAGAATGCAAT GCTGGAGCTGTGTTGTGAGCGAGCACAAGTAAAAGATGGTCAATCAATACTTGATGTAGGATGTGGATG GGGTTCCCTTTCTTTGTACATTGCAAGGAAATACAAAGGTTGCAGCATTACTGGGATATGCAATTCTACAA CACAAAGAGCTTATATAGAGGAACAGTGCAGGGACCTTCGATTGTCAAATGTAAAGATTATTGTTGCAGAT ATCAGGGAGTTTGAAATGGAGGCATCGTTTGACCGGGTTATATCTATCGAGATGTTTGAGCACATGAAGA ACTACAAAGCACTTATGAAAAAGATAGCAACATGGATGAAGCAGGATAGTCTCCTATTCGTTCATTACTTTT GCCACAAAGTACTTTCTTACCACTTTGAGGACATAAATGAAGATGACTGGATTACAAGACATTTCTTCAGT GGAGGAACAATGCCTTCTGCAAACCTGCTTCTCTATTTTCAGGATGATGTTGCTGTGGTCAACCACTGGC TTGTGAATGGGATGCATTATTCAAGGACAAGCGAAGAGTGGCTCAAAAGAATGGATCAGAATAGAGCTGC TATTAGACCAATCATGGAGTCAACCTATGGTGAGGATTTGGCTACCAAGTGGACTGTTTATTGGCGAACAT TCTTCATTGCAGTTGCAGAGCTCTTCAGTTATAACAATGGAGAAGAATGGATGGTTGCACATTTTCTTTTC AAAAAGAAATAG
LaNMT1	ATGGGGAAATTGGTGGAGGTTCCGTACAATGCGACGGTGAGCGTAATGTTAGCGTCCCTAGAGAGAAA TTTGCTGCCGGATTTAGTCATCAGGAGGCTGACACGTGTCCTCCTAGCCACCCGGCTCCGCCATGGCT ACCTCCCTTCTGCAGAGCTTCAACTCTCTAATCTCATTCAGTTCAAGCAGTCTCTTGAAGATATGCTTAT AGCTGTGGAAACTGATAAAGCAAAAACCCAACATTACGAGTTACCCACCTCTTTTTTCGAACTGGTGTTG GGAAAGAATCTCAAGTACAGCTGCTGTTACTTCAACGGTACGTCGAACACATTGGAAGATGCTGAGAAT GCAATGCTGGAGCTGTATTGTGAGCGAGCACAAGTAAAAGATGGTCAATCAATACTTGATGTAGGATGT GGATGGGGTTCCCTTTCTTTGTACATTGCAAGGAAATACAAAGGTTGCAGCATTACTGGGATATGCAATT CTACAACACAAAGAGCTTATATAGAGGAACAGTGCAGGGACCTTCAATTGTCAAATGTAAAGATTATTGT TGCAGATATCAGGGAGTTTGAAATGGAGGCATCATTTGACCGGGTTATATCTATCGAGATGTTCGAGCA CATGAAGAACTACAAAGCACTTATGAAAAAGATAGCAACATGGATGAAGCAGGATAGTCTCCTATTCGTT CATTACTTTTGCCACAAAGTATTTGCTTACCATTTTGAGGACATAAATGAAGATGACTGGATTACAAGAC ATTTCTTCAGTGGAGGAACAATGCCTTCTGCAAACCTGCTTCTCTATTTTCAGGATGATGTTGCTGTGGT CAACCACTGGCTTGTGAATGGGATGCATTATTCAAGGACAAGCGAAGAGTGGCTCAAAAGAATGGATCA GAATAGAGCTGCTATTAGACCAATCATGGAGTCAACCTATGGTGAGGATTTGGCTACCAAGTGGACTGT TTATTGGCGAACATTCTTCATTGCAGTTGCAGAGCTCTTTGGTTATAACAATGGAGAAGAATGGATGGTT GCACATTTTCTTTTCAAAAAGAAATAG

LrNMT1	ATGGGGAAATTGGTGGAGGTTCCGTACAATGCGACGGTGAGCGTAATGTTAGCGTCCCTAGAGAGAAA TTTGCTGCCGGATTTAGTCATCAGGAGGCTGACACGTGTCCTCCTAGCCACCCGGCTCCGCCATGGCT ACCTCCCTTCTGCAGAGCTTCAACTCTCTAATCTCATTCAGTTCAAGCAGTCTCTTGAAGATATGCTTAT AGCTGTGGAAACTGATAAAGCAAAAACCCAACATTACGAGTTACCCACCTCTTTTTTCGAACTGGTGTTG GGAAAGAATCTCAAGTACAGCTGCTGTTACTTCAACGGTACGTCGAACACATTGGAAGATGCTGAGAAT GCAATGCTGGAGCTGTATTGTGAGCGAGCACAAGTAAAAGATGGTCAATCAATACTTGATGTAGGATGT GGATGGGGTTCCCTTTCTTTGTACATTGCAAGGAAATACAAAGGTTGCAGCATTACTGGGATATGCAATT CTACAACACAAAGAGCTTATATAGAGGAACAGTGCAGGGACCTTCAATTGTCAAATGTAAAGATTATTGT TGCAGATATCAGGGAGTTTGAAATGGAGGCATCATTTGACCGGGTTATATCTATCGAGATGTTCGAGCA CATGAAGAACTACAAAGCACTTATGAAAAAGATAGCAACATGGATGAAGCAGGATAGTCTCCTATTCGTT CATTACTTTTGCCACAAAGTATTTGCTTACCATTTTGAGGACATAAATGAAGATGACTGGATTACAAGAC ATTTCTTCAGTGGAGGAACAATGCCTTCTGCAAACCTGCTTCTCTATTTTCAGGATGATGTTGCTGTGGT CAACCACTGGCTTGTGAATGGGATGCATTATTCAAGGACAAGCGAAGAGTGGCTCAAAAGAATGGATCA GAATAGAGCTGCTATTAGACCAATCATGGAGTCAACCTATGGTGAGGATTTGGCTACCAAGTGGACTGT TTATTGGCGAACATTCTTCATTGCAGTTGCAGAGCTCTTTGGTTATAACAATGGAGAAGAATGGATGGTT GCACATTTTCTTTTCAAAAAGAAATAG
LrNMT2	ATGGGGAAATTGGTGGAGGTTCCGTACAATGCGACGGTGAGCGTAATGTTGGCATCTCTAGAGAGAAA TTTGCTGCCGGATTTAGTCATCAGGAGGCTGACACGTGTCCTCCTCGCCAGCCGACTCCGCCATGGCT ACCTCCCTTCTGCAGAGCTTCAACTCTCTAATCTCATTCAGTTCAAGCAGTCTCTTGAAGATATGCCTAT AGCTGTGGAAACTGATAAAGCAAAAATCCAACATTATGAGTTGCCCACCTCTTTTTTCAAACTGGTGTTG GGAAAGAATCTCAAGTACAGCTGCTGTTACTTCAAAGTTAAGTCGAATACATTGGAAGATGCTGAGAAT GCAATGCTGGAGCTGTATTGTGAGCGAGCACAAGTAAAAGATGGCCAATCAATACTTGATGTAGGATGT GGATGGGGTTCCCTTTCTTTGTACATTGCAAGGAAATACAAAAGTTGCAGCATCACGGGGATATGCAAT TCTACAACACAAAGAACTTATATAGAGGAACAGTGCAGGGAGCTTCAATTGTCAAATGTAAAGATTATTG TTGCAGATATTAGCAAGTTTGAAATGGAGGCATCATTTGACCGGGTTATATCTATTGAGATGTTTGAGCA CATGAAGAACTACAAAGCACTTCTGAAAAAGATATCCACCTGGATGAAGGAGGATAGTCTCCTATTCGTT CATTACTTTTGCCACAAAGTATTTGCTTACCATTTTGAGGACATAAATGAAGATGACTGGATTACAAGATA TTTCTTCAGTGGAGGAACAATGCCTTCTGCGAACCTACTTCTCTATTTTCAGGATGATGTTGCTGTGGTT AACCACTGGCTTGTGAATGGGATGCATTATTCAAGTACAAGTGAAGAGTGGCTCAAGAGAATGGATCAG AATACAGCTGCTATTAGACCAATCATGGAGTCAACCTATGGTAAGGATTTGGCTACCAAGTGGACTGTTT ATTGGCGAACATTCTTCATTGCGGTTGCAGAGCTCTTTGGTTATAACAATGGAGAAGAATGGATGGTTG CACATTATCTTTTCAAAAAGAAATAG
HpNMT1	ATGGGGAAATTGGTGGAGGTTCCGTACAATGCGACGGTGAGCGTAATGTTAGCGTCCCTAGAGAGAAA TTTGCTGCCGGATTTAGTCATCAGGAGGCTGACACGTGTCCTCCTAGCCACCCGGCTCCGCCATGGCT ACCTCCCTTCTGCAGAGCTTCAACTCTCTAATCTCATTCAGTTCAAGCAGTCTCTTGAAGATATGCTTAT AGCTGTGGAAACTGATAAAGCAAAAACCCAACATTACGAGTTACCCACCTCTTTTTTCGAACTGGTGTTG GGAAAGAATCTCAAGTACAGCTGCTGTTACTTCAACGGTACGTCGAACACATTGGAAGATGCTGAGAAT GCAATGCTGGAGCTGTATTGTGAGCGAGCACAAGTAAAAGATGGTCAATCAATACTTGATGTAGGATGT GGATGGGGTTCCCTTTCTTTGTACATTGCAAGGAAATACAAAGGTTGCAGCATTACTGGGATATGCAATT CTACAACACAAAGAGCTTATATAGAGGAACAGTGCAGGGACCTTCAATTGTCAAATGTAAAGATTATTGT TGCAGATATCAGGGAGTTTGAAATGGAGGCATCATTTGACCGGGTTATATCTATCGAGATGTTCGAGCA CATGAAGAACTACAAAGCACTTATGAAAAAGATAGCAACATGGATGAAGCAGGATAGTCTCCTATTCGTT CATTACTTTTGCCACAAAGTATTTGCTTACCATTTTGAGGACATAAATGAAGATGACTGGATTACAAGAC ATTTCTTCAGTGGAGGAACAATGCCTTCTGCAAACCTGCTTCTCTATTTTCAGGATGATGTTGCTGTGGT CAACCACTGGCTTGTGAATGGGATGCATTATTCAAGGACAAGCGAAGAGTGGCTCAAAAGAATGGATCA GAATAGAGCTGCTATTAGACCAATCATGGAGTCAACCTATGGTGAGGATTTGGCTACCAAGTGGACTGT TTATTGGCGAACATTCTTCATTGCAGTTGCAGAGCTCTTTGGTTATAACAATGGAGAAGAATGGATGGTT GCACATTTTCTTTTCAAAAAGAAATAG
HpNMT2	ATGGGGAAATTGGTGGAGGTTCCGTACAATGCGACGGTGAGCGTAATGTTAGCGTCCCTAGAGAGAAAT TTGCTGCCGGATTTAGTCATCAGGAGGCTGACACGTGTCCTCCTAGCCACCCGGCTCCGCCATGGCTAC CTCCCTTCTGCAGAGCTTCAACTCTCTAATCTCATTCAGTTCAAGCAGTCTCTTGAAGATATGCTTATAGC TGTGGAAACTGATAAAGCAAAAACCCAACATTACGAGTTACCCACCTCTTTTTTCGAACTGGTGTTGGGA AAGAATCTCAAGTACAGCTGCTGTTACTTCAACGGTACGTCGAACACATTGGAAGATGCTGAGAATGCAA TGCTGGAGCTGTATTGTGAGCGAGCACAAGTAAAAGATGGTCAATCAATACTTGATGTAGGATGTGGATG GGGTTCCCTTTCTTTGTACATTGCAAGGAAATACAAAGGTTGCAGCATTACTGGGATATGCAATTCTACAA CACAAAGAGCTTATATAGAGGAACAGTGCAGGGACCTTCAATTGTCAAATGTAAAGATTATTGTTGCAGAT ATCAGGGAGTTTGAAATGGAGGCATCATTTGACCGGGTTATATCTATCGAGATGTTCGAGCACATGAAGA ACTACAAAGCACTTATGAAAAAGATAGCAACATGGATGAAGCAGGATAGTCTCCTATTCGTTCATTACTTTT GCCACAAAGTATTTGCTTACCATTTTGAGGACATAAATGAAGATGACTGGATTACAAGACATTTCTTCAGT GGAGGAACAATGCCTTCTGCAAACCTGCTTCTCTATTTTCAGGATGATGTTGCTGTGGTCAACCACTGGC TTGTGAATGGGATGCATTATTCAAGGACAAGCGAAGAGTGGCTCAAAAGAATGGATCAGAACAGAGCTG CTATTAGACCAATCAGGGAGTCAACCTATGGTGAGGATTTGGCTACCAAGTGGACTGTTTCTTGGCGAAC ATTCTTCAATGCAGTTGCAAAGCTCTTTGGTTATAACAATGGAAAAAAATGGAAGGTTCCCCATTTTTTTTT CAAAAAGAAATAG
La NMT2	MGKLVEVPYNATVSVMLASLERNLLPDLVIRRLTRVLLATRLRHGYLPSAELQLSNLIQFKQSLEDMPIAVETD KAKTQHYELPTSFFELVLGKNLKYSCCYFNGTSNTLEDAENAMLELYCERAQVKDGQSILDVGCGWGSLSL YIARKNKGCSITGICNSTTQRAYIEEQCRDLQLSNVKIIVADIREFEMEASFDRVISIEMFEHMKNYKALMKKIA TWMKQDSLLFVHYLCHKVFAYHFEDINEDDWITRHFFSGGTMPSANLLLYFQDDVAVVNHWLVNGMHYSR TSEEWLKRMDQNRAAIRPIMESTYGEDLATKWTVYWRTFFIAVAELFGYNNGEEWMVAHFLFKKK
La NMT3	MGKLVEVPYNATVSVMLASLERNLLPDLVIRRLTRVLLATRFRHGYIPSAELQLSNLIQFKQSLEDMPIAVETD KAKTQHYELPTSFFKLVLGKNLKYSCCYFNGTSNTLEDAENAMLELCCERAQVKDGQSILDVGCGWGSLSL YIARKYKGCSITGICNSTTQRAYIEEQCRDLRLSNVKIIVADIREFEMEASFDRVISIEMFEHMKNYKALMKKIAT WMKQDSLLFVHYFCHKVLSYHFEDINEDDWITRHFFSGGTMPSANLLLYFQDDVAVVNHWLVNGMHYSRT SEEWLKRMDQNRAAIRPIMESTYGEDLATKWTVYWRTFFIAVAELFSYNNGEEWMVAHFLFKKK
LaLrHp	MGKLVEVPYNATVSVMLASLERNLLPDLVIRRLTRVLLATRLRHGYLPSAELQLSNLIQFKQSLEDMLIAVETD KAKTQHYELPTSFFELVLGKNLKYSCCYFNGTSNTLEDAENAMLELYCERAQVKDGQSILDVGCGWGSLSL YIARKYKGCSITGICNSTTQRAYIEEQCRDLQLSNVKIIVADIREFEMEASFDRVISIEMFEHMKNYKALMKKIA TWMKQDSLLFVHYFCHKVFAYHFEDINEDDWITRHFFSGGTMPSANLLLYFQDDVAVVNHWLVNGMHYSR TSEEWLKRMDQNRAAIRPIMESTYGEDLATKWTVYWRTFFIAVAELFGYNNGEEWMVAHFLFKKK

NMT1	
***Lr*NMT2**	MGKLVEVPYNATVSVMLASLERNLLPDLVIRRLTRVLLASRLRHGYLPSAELQLSNLIQFKQSLEDMPIAVETD KAKIQHYELPTSFFKLVLGKNLKYSCCYFKVKSNTLEDAENAMLELYCERAQVKDGQSILDVGCGWGSLSLY IARKYKSCSITGICNSTTQRTYIEEQCRELQLSNVKIIVADISKFEMEASFDRVISIEMFEHMKNYKALLKKISTW MKEDSLLFVHYFCHKVFAYHFEDINEDDWITRYFFSGGTMPSANLLLYFQDDVAVVNHWLVNGMHYSSTSE EWLKRMDQNTAAIRPIMESTYGKDLATKWTVYWRTFFIAVAELFGYNNGEEWMVAHYLFKKK
***Hp*NMT2**	MGKLVEVPYNATVSVMLASLERNLLPDLVIRRLTRVLLATRLRHGYLPSAELQLSNLIQFKQSLEDMLIAVETD KAKTQHYELPTSFFELVLGKNLKYSCCYFNGTSNTLEDAENAMLELYCERAQVKDGQSILDVGCGWGSLSL YIARKYKGCSITGICNSTTQRAYIEEQCRDLQLSNVKIIVADIREFEMEASFDRVISIEMFEHMKNYKALMKKIA TWMKQDSLLFVHYFCHKVFAYHFEDINEDDWITRHFFSGGTMPSANLLLYFQDDVAVVNHWLVNGMHYSR TSEEWLKRMDQNRAAIRPIRESTYGEDLATKWTVSWRTFFNAVAKLFGYNNGKKWKVPHFFFKKK
Y325S	ATGGGGAAATTGGTGGAGGTTCCGTACAATGCGACGGTGAGCGTAATGTTAGCGTCCCTAGAGAGAAA TTTGCTGCCGGATTTAGTCATCAGGAGGCTGACACGTGTCCTCCTAGCCACCCGGCTCCGCCATGGCT ACCTCCCTTCTGCAGAGCTTCAACTCTCTAATCTCATTCAGTTCAAGCAGTCTCTTGAAGATATGCTTAT AGCTGTGGAAACTGATAAAGCAAAAACCCAACATTACGAGTTACCCACCTCTTTTTTCGAACTGGTGTTG GGAAAGAATCTCAAGTACAGCTGCTGTTACTTCAACGGTACGTCGAACACATTGGAAGATGCTGAGAAT GCAATGCTGGAGCTGTATTGTGAGCGAGCACAAGTAAAAGATGGTCAATCAATACTTGATGTAGGATGT GGATGGGGTTCCCTTTCTTTGTACATTGCAAGGAAATACAAAGGTTGCAGCATTACTGGGATATGCAATT CTACAACACAAAGAGCTTATATAGAGGAACAGTGCAGGGACCTTCAATTGTCAAATGTAAAGATTATTGT TGCAGATATCAGGGAGTTTGAAATGGAGGCATCATTTGACCGGGTTATATCTATCGAGATGTTCGAGCA CATGAAGAACTACAAAGCACTTATGAAAAAGATAGCAACATGGATGAAGCAGGATAGTCTCCTATTCGTT CATTACTTTTGCCACAAAGTATTTGCTTACCATTTTGAGGACATAAATGAAGATGACTGGATTACAAGAC ATTTCTTCAGTGGAGGAACAATGCCTTCTGCAAACCTGCTTCTCTATTTTCAGGATGATGTTGCTGTGGT CAACCACTGGCTTGTGAATGGGATGCATTATTCAAGGACAAGCGAAGAGTGGCTCAAAAGAATGGATCA GAATAGAGCTGCTATTAGACCAATCATGGAGTCAACCTATGGTGAGGATTTGGCTACCAAGTGGACTGT TTCTTGGCGAACATTCTTCATTGCAGTTGCAGAGCTCTTTGGTTATAACAATGGAGAAGAATGGATGGTT GCACATTTTCTTTTCAAAAAGAAATAG
315-355Del	ATGGGGAAATTGGTGGAGGTTCCGTACAATGCGACGGTGAGCGTAATGTTAGCGTCCCTAGAGAGAAA TTTGCTGCCGGATTTAGTCATCAGGAGGCTGACACGTGTCCTCCTAGCCACCCGGCTCCGCCATGGCT ACCTCCCTTCTGCAGAGCTTCAACTCTCTAATCTCATTCAGTTCAAGCAGTCTCTTGAAGATATGCTTAT AGCTGTGGAAACTGATAAAGCAAAAACCCAACATTACGAGTTACCCACCTCTTTTTTCGAACTGGTGTTG GGAAAGAATCTCAAGTACAGCTGCTGTTACTTCAACGGTACGTCGAACACATTGGAAGATGCTGAGAAT GCAATGCTGGAGCTGTATTGTGAGCGAGCACAAGTAAAAGATGGTCAATCAATACTTGATGTAGGATGT GGATGGGGTTCCCTTTCTTTGTACATTGCAAGGAAATACAAAGGTTGCAGCATTACTGGGATATGCAATT CTACAACACAAAGAGCTTATATAGAGGAACAGTGCAGGGACCTTCAATTGTCAAATGTAAAGATTATTGT TGCAGATATCAGGGAGTTTGAAATGGAGGCATCATTTGACCGGGTTATATCTATCGAGATGTTCGAGCA CATGAAGAACTACAAAGCACTTATGAAAAAGATAGCAACATGGATGAAGCAGGATAGTCTCCTATTCGTT CATTACTTTTGCCACAAAGTATTTGCTTACCATTTTGAGGACATAAATGAAGATGACTGGATTACAAGAC ATTTCTTCAGTGGAGGAACAATGCCTTCTGCAAACCTGCTTCTCTATTTTCAGGATGATGTTGCTGTGGT CAACCACTGGCTTGTGAATGGGATGCATTATTCAAGGACAAGCGAAGAGTGGCTCAAAAGAATGGATCA GAATAGAGCTGCTATTAGACCAATCATGGAGTCAACCTATTAG
F234L	ATGGGGAAATTGGTGGAGGTTCCGTACAATGCGACGGTGAGCGTAATGTTAGCGTCCCTAGAGAGAAA TTTGCTGCCGGATTTAGTCATCAGGAGGCTGACACGTGTCCTCCTAGCCACCCGGCTCCGCCATGGCT ACCTCCCTTCTGCAGAGCTTCAACTCTCTAATCTCATTCAGTTCAAGCAGTCTCTTGAAGATATGCTTAT AGCTGTGGAAACTGATAAAGCAAAAACCCAACATTACGAGTTACCCACCTCTTTTTTCGAACTGGTGTTG GGAAAGAATCTCAAGTACAGCTGCTGTTACTTCAACGGTACGTCGAACACATTGGAAGATGCTGAGAAT GCAATGCTGGAGCTGTATTGTGAGCGAGCACAAGTAAAAGATGGTCAATCAATACTTGATGTAGGATGT GGATGGGGTTCCCTTTCTTTGTACATTGCAAGGAAATACAAAGGTTGCAGCATTACTGGGATATGCAATT CTACAACACAAAGAGCTTATATAGAGGAACAGTGCAGGGACCTTCAATTGTCAAATGTAAAGATTATTGT TGCAGATATCAGGGAGTTTGAAATGGAGGCATCATTTGACCGGGTTATATCTATCGAGATGTTCGAGCA CATGAAGAACTACAAAGCACTTATGAAAAAGATAGCAACATGGATGAAGCAGGATAGTCTCCTATTCGTT CATTACTTGTGCCACAAAGTATTTGCTTACCATTTTGAGGACATAAATGAAGATGACTGGATTACAAGAC ATTTCTTCAGTGGAGGAACAATGCCTTCTGCAAACCTGCTTCTCTATTTTCAGGATGATGTTGCTGTGGT CAACCACTGGCTTGTGAATGGGATGCATTATTCAAGGACAAGCGAAGAGTGGCTCAAAAGAATGGATCA GAATAGAGCTGCTATTAGACCAATCATGGAGTCAACCTATGGTGAGGATTTGGCTACCAAGTGGACTGT TTATTGGCGAACATTCTTCATTGCAGTTGCAGAGCTCTTTGGTTATAACAATGGAGAAGAATGGATGGTT GCACATTTTCTTTTCAAAAAGAAATAG
F234W	ATGGGGAAATTGGTGGAGGTTCCGTACAATGCGACGGTGAGCGTAATGTTAGCGTCCCTAGAGAGAAA TTTGCTGCCGGATTTAGTCATCAGGAGGCTGACACGTGTCCTCCTAGCCACCCGGCTCCGCCATGGCT ACCTCCCTTCTGCAGAGCTTCAACTCTCTAATCTCATTCAGTTCAAGCAGTCTCTTGAAGATATGCTTAT AGCTGTGGAAACTGATAAAGCAAAAACCCAACATTACGAGTTACCCACCTCTTTTTTCGAACTGGTGTTG GGAAAGAATCTCAAGTACAGCTGCTGTTACTTCAACGGTACGTCGAACACATTGGAAGATGCTGAGAAT GCAATGCTGGAGCTGTATTGTGAGCGAGCACAAGTAAAAGATGGTCAATCAATACTTGATGTAGGATGT GGATGGGGTTCCCTTTCTTTGTACATTGCAAGGAAATACAAAGGTTGCAGCATTACTGGGATATGCAATT CTACAACACAAAGAGCTTATATAGAGGAACAGTGCAGGGACCTTCAATTGTCAAATGTAAAGATTATTGT TGCAGATATCAGGGAGTTTGAAATGGAGGCATCATTTGACCGGGTTATATCTATCGAGATGTTCGAGCA CATGAAGAACTACAAAGCACTTATGAAAAAGATAGCAACATGGATGAAGCAGGATAGTCTCCTATTCGTT CATTACTGGTGCCACAAAGTATTTGCTTACCATTTTGAGGACATAAATGAAGATGACTGGATTACAAGAC ATTTCTTCAGTGGAGGAACAATGCCTTCTGCAAACCTGCTTCTCTATTTTCAGGATGATGTTGCTGTGGT CAACCACTGGCTTGTGAATGGGATGCATTATTCAAGGACAAGCGAAGAGTGGCTCAAAAGAATGGATCA GAATAGAGCTGCTATTAGACCAATCATGGAGTCAACCTATGGTGAGGATTTGGCTACCAAGTGGACTGT TTATTGGCGAACATTCTTCATTGCAGTTGCAGAGCTCTTTGGTTATAACAATGGAGAAGAATGGATGGTT GCACATTTTCTTTTCAAAAAGAAATAG

F234A	ATGGGGAAATTGGTGGAGGTTCCGTACAATGCGACGGTGAGCGTAATGTTAGCGTCCCTAGAGAGAAA TTTGCTGCCGGATTTAGTCATCAGGAGGCTGACACGTGTCCTCCTAGCCACCCGGCTCCGCCATGGCT ACCTCCCTTCTGCAGAGCTTCAACTCTCTAATCTCATTCAGTTCAAGCAGTCTCTTGAAGATATGCTTAT AGCTGTGGAAACTGATAAAGCAAAAACCCAACATTACGAGTTACCCACCTCTTTTTTCGAACTGGTGTTG GGAAAGAATCTCAAGTACAGCTGCTGTTACTTCAACGGTACGTCGAACACATTGGAAGATGCTGAGAAT GCAATGCTGGAGCTGTATTGTGAGCGAGCACAAGTAAAAGATGGTCAATCAATACTTGATGTAGGATGT GGATGGGGTTCCCTTTCTTTGTACATTGCAAGGAAATACAAAGGTTGCAGCATTACTGGGATATGCAATT CTACAACACAAAGAGCTTATATAGAGGAACAGTGCAGGGACCTTCAATTGTCAAATGTAAAGATTATTGT TGCAGATATCAGGGAGTTTGAAATGGAGGCATCATTTGACCGGGTTATATCTATCGAGATGTTCGAGCA CATGAAGAACTACAAAGCACTTATGAAAAAGATAGCAACATGGATGAAGCAGGATAGTCTCCTATTCGTT CATTACGCGTGCCACAAAGTATTTGCTTACCATTTTGAGGACATAAATGAAGATGACTGGATTACAAGAC ATTTCTTCAGTGGAGGAACAATGCCTTCTGCAAACCTGCTTCTCTATTTTCAGGATGATGTTGCTGTGGT CAACCACTGGCTTGTGAATGGGATGCATTATTCAAGGACAAGCGAAGAGTGGCTCAAAAGAATGGATCA GAATAGAGCTGCTATTAGACCAATCATGGAGTCAACCTATGGTGAGGATTTGGCTACCAAGTGGACTGT TTATTGGCGAACATTCTTCATTGCAGTTGCAGAGCTCTTTGGTTATAACAATGGAGAAGAATGGATGGTT GCACATTTTCTTTTCAAAAAGAAATAG
F257L	ATGGGGAAATTGGTGGAGGTTCCGTACAATGCGACGGTGAGCGTAATGTTAGCGTCCCTAGAGAGAAA TTTGCTGCCGGATTTAGTCATCAGGAGGCTGACACGTGTCCTCCTAGCCACCCGGCTCCGCCATGGCT ACCTCCCTTCTGCAGAGCTTCAACTCTCTAATCTCATTCAGTTCAAGCAGTCTCTTGAAGATATGCTTAT AGCTGTGGAAACTGATAAAGCAAAAACCCAACATTACGAGTTACCCACCTCTTTTTTCGAACTGGTGTTG GGAAAGAATCTCAAGTACAGCTGCTGTTACTTCAACGGTACGTCGAACACATTGGAAGATGCTGAGAAT GCAATGCTGGAGCTGTATTGTGAGCGAGCACAAGTAAAAGATGGTCAATCAATACTTGATGTAGGATGT GGATGGGGTTCCCTTTCTTTGTACATTGCAAGGAAATACAAAGGTTGCAGCATTACTGGGATATGCAATT CTACAACACAAAGAGCTTATATAGAGGAACAGTGCAGGGACCTTCAATTGTCAAATGTAAAGATTATTGT TGCAGATATCAGGGAGTTTGAAATGGAGGCATCATTTGACCGGGTTATATCTATCGAGATGTTCGAGCA CATGAAGAACTACAAAGCACTTATGAAAAAGATAGCAACATGGATGAAGCAGGATAGTCTCCTATTCGTT CATTACTTTTGCCACAAAGTATTTGCTTACCATTTTGAGGACATAAATGAAGATGACTGGATTACAAGAC ATTTCTTGAGTGGAGGAACAATGCCTTCTGCAAACCTGCTTCTCTATTTTCAGGATGATGTTGCTGTGGT CAACCACTGGCTTGTGAATGGGATGCATTATTCAAGGACAAGCGAAGAGTGGCTCAAAAGAATGGATCA GAATAGAGCTGCTATTAGACCAATCATGGAGTCAACCTATGGTGAGGATTTGGCTACCAAGTGGACTGT TTATTGGCGAACATTCTTCATTGCAGTTGCAGAGCTCTTTGGTTATAACAATGGAGAAGAATGGATGGTT GCACATTTTCTTTTCAAAAAGAAATAG
F257W	ATGGGGAAATTGGTGGAGGTTCCGTACAATGCGACGGTGAGCGTAATGTTAGCGTCCCTAGAGAGAAA TTTGCTGCCGGATTTAGTCATCAGGAGGCTGACACGTGTCCTCCTAGCCACCCGGCTCCGCCATGGCT ACCTCCCTTCTGCAGAGCTTCAACTCTCTAATCTCATTCAGTTCAAGCAGTCTCTTGAAGATATGCTTAT AGCTGTGGAAACTGATAAAGCAAAAACCCAACATTACGAGTTACCCACCTCTTTTTTCGAACTGGTGTTG GGAAAGAATCTCAAGTACAGCTGCTGTTACTTCAACGGTACGTCGAACACATTGGAAGATGCTGAGAAT GCAATGCTGGAGCTGTATTGTGAGCGAGCACAAGTAAAAGATGGTCAATCAATACTTGATGTAGGATGT GGATGGGGTTCCCTTTCTTTGTACATTGCAAGGAAATACAAAGGTTGCAGCATTACTGGGATATGCAATT CTACAACACAAAGAGCTTATATAGAGGAACAGTGCAGGGACCTTCAATTGTCAAATGTAAAGATTATTGT TGCAGATATCAGGGAGTTTGAAATGGAGGCATCATTTGACCGGGTTATATCTATCGAGATGTTCGAGCA CATGAAGAACTACAAAGCACTTATGAAAAAGATAGCAACATGGATGAAGCAGGATAGTCTCCTATTCGTT CATTACTTTTGCCACAAAGTATTTGCTTACCATTTTGAGGACATAAATGAAGATGACTGGATTACAAGAC ATTTCTGGAGTGGAGGAACAATGCCTTCTGCAAACCTGCTTCTCTATTTTCAGGATGATGTTGCTGTGGT CAACCACTGGCTTGTGAATGGGATGCATTATTCAAGGACAAGCGAAGAGTGGCTCAAAAGAATGGATCA GAATAGAGCTGCTATTAGACCAATCATGGAGTCAACCTATGGTGAGGATTTGGCTACCAAGTGGACTGT TTATTGGCGAACATTCTTCATTGCAGTTGCAGAGCTCTTTGGTTATAACAATGGAGAAGAATGGATGGTT GCACATTTTCTTTTCAAAAAGAAATAG
E204K	ATGGGGAAATTGGTGGAGGTTCCGTACAATGCGACGGTGAGCGTAATGTTAGCGTCCCTAGAGAGAAA TTTGCTGCCGGATTTAGTCATCAGGAGGCTGACACGTGTCCTCCTAGCCACCCGGCTCCGCCATGGCT ACCTCCCTTCTGCAGAGCTTCAACTCTCTAATCTCATTCAGTTCAAGCAGTCTCTTGAAGATATGCTTAT AGCTGTGGAAACTGATAAAGCAAAAACCCAACATTACGAGTTACCCACCTCTTTTTTCGAACTGGTGTTG GGAAAGAATCTCAAGTACAGCTGCTGTTACTTCAACGGTACGTCGAACACATTGGAAGATGCTGAGAAT GCAATGCTGGAGCTGTATTGTGAGCGAGCACAAGTAAAAGATGGTCAATCAATACTTGATGTAGGATGT GGATGGGGTTCCCTTTCTTTGTACATTGCAAGGAAATACAAAGGTTGCAGCATTACTGGGATATGCAATT CTACAACACAAAGAGCTTATATAGAGGAACAGTGCAGGGACCTTCAATTGTCAAATGTAAAGATTATTGT TGCAGATATCAGGGAGTTTGAAATGGAGGCATCATTTGACCGGGTTATATCTATCGAAGATGTTCGAGCA CATGAAGAACTACAAAGCACTTATGAAAAAGATAGCAACATGGATGAAGCAGGATAGTCTCCTATTCGTT CATTACTTTTGCCACAAAGTATTTGCTTACCATTTTGAGGACATAAATGAAGATGACTGGATTACAAGAC ATTTCTTCAGTGGAGGAACAATGCCTTCTGCAAACCTGCTTCTCTATTTTCAGGATGATGTTGCTGTGGT CAACCACTGGCTTGTGAATGGGATGCATTATTCAAGGACAAGCGAAGAGTGGCTCAAAAGAATGGATCA GAATAGAGCTGCTATTAGACCAATCATGGAGTCAACCTATGGTGAGGATTTGGCTACCAAGTGGACTGT TTATTGGCGAACATTCTTCATTGCAGTTGCAGAGCTCTTTGGTTATAACAATGGAGAAGAATGGATGGTT GCACATTTTCTTTTCAAAAAGAAATAG
E204D	ATGGGGAAATTGGTGGAGGTTCCGTACAATGCGACGGTGAGCGTAATGTTAGCGTCCCTAGAGAGAAA TTTGCTGCCGGATTTAGTCATCAGGAGGCTGACACGTGTCCTCCTAGCCACCCGGCTCCGCCATGGCT ACCTCCCTTCTGCAGAGCTTCAACTCTCTAATCTCATTCAGTTCAAGCAGTCTCTTGAAGATATGCTTAT AGCTGTGGAAACTGATAAAGCAAAAACCCAACATTACGAGTTACCCACCTCTTTTTTCGAACTGGTGTTG GGAAAGAATCTCAAGTACAGCTGCTGTTACTTCAACGGTACGTCGAACACATTGGAAGATGCTGAGAAT GCAATGCTGGAGCTGTATTGTGAGCGAGCACAAGTAAAAGATGGTCAATCAATACTTGATGTAGGATGT GGATGGGGTTCCCTTTCTTTGTACATTGCAAGGAAATACAAAGGTTGCAGCATTACTGGGATATGCAATT CTACAACACAAAGAGCTTATATAGAGGAACAGTGCAGGGACCTTCAATTGTCAAATGTAAAGATTATTGT TGCAGATATCAGGGAGTTTGAAATGGAGGCATCATTTGACCGGGTTATATCTATCGACATGTTCGAGCA CATGAAGAACTACAAAGCACTTATGAAAAAGATAGCAACATGGATGAAGCAGGATAGTCTCCTATTCGTT CATTACTTTTGCCACAAAGTATTTGCTTACCATTTTGAGGACATAAATGAAGATGACTGGATTACAAGAC ATTTCTTCAGTGGAGGAACAATGCCTTCTGCAAACCTGCTTCTCTATTTTCAGGATGATGTTGCTGTGGT CAACCACTGGCTTGTGAATGGGATGCATTATTCAAGGACAAGCGAAGAGTGGCTCAAAAGAATGGATCA GAATAGAGCTGCTATTAGACCAATCATGGAGTCAACCTATGGTGAGGATTTGGCTACCAAGTGGACTGT TTATTGGCGAACATTCTTCATTGCAGTTGCAGAGCTCTTTGGTTATAACAATGGAGAAGAATGGATGGTT GCACATTTTCTTTTCAAAAAGAAATAG

L68P	ATGGGGAAATTGGTGGAGGTTCCGTACAATGCGACGGTGAGCGTAATGTTAGCGTCCCTAGAGAGAAA TTTGCTGCCGGATTTAGTCATCAGGAGGCTGACACGTGTCCTCCTAGCCACCCGGCTCCGCCATGGCT ACCTCCCTTCTGCAGAGCTTCAACTCTCTAATCTCATTCAGTTCAAGCAGTCTCTTGAAGATATGCCTAT AGCTGTGGAAACTGATAAAGCAAAAACCCAACATTACGAGTTACCCACCTCTTTTTTCGAACTGGTGTTG GGAAAGAATCTCAAGTACAGCTGCTGTTACTTCAACGGTACGTCGAACACATTGGAAGATGCTGAGAAT GCAATGCTGGAGCTGTATTGTGAGCGAGCACAAGTAAAAGATGGTCAATCAATACTTGATGTAGGATGT GGATGGGGTTCCCTTTCTTTGTACATTGCAAGGAAATACAAAGGTTGCAGCATTACTGGGATATGCAATT CTACAACACAAAGAGCTTATATAGAGGAACAGTGCAGGGACCTTCAATTGTCAAATGTAAAGATTATTGT TGCAGATATCAGGGAGTTTGAAATGGAGGCATCATTTGACCGGGTTATATCTATCGAGATGTTCGAGCA CATGAAGAACTACAAAGCACTTATGAAAAAGATAGCAACATGGATGAAGCAGGATAGTCTCCTATTCGTT CATTACTTTTGCCACAAAGTATTTGCTTACCATTTTGAGGACATAAATGAAGATGACTGGATTACAAGAC ATTTCTTCAGTGGAGGAACAATGCCTTCTGCAAACCTGCTTCTCTATTTTCAGGATGATGTTGCTGTGGT CAACCACTGGCTTGTGAATGGGATGCATTATTCAAGGACAAGCGAAGAGTGGCTCAAAAGAATGGATCA GAATAGAGCTGCTATTAGACCAATCATGGAGTCAACCTATGGTGAGGATTTGGCTACCAAGTGGACTGT TTATTGGCGAACATTCTTCATTGCAGTTGCAGAGCTCTTTGGTTATAACAATGGAGAAGAATGGATGGTT GCACATTTTCTTTTCAAAAAGAAATAG

Table 1.A6. Theoretical isoelectric points and molecular weights of the proteins

NMT	PI	MW (KDa)
***La*Lr*Hp*NMT1**	6.09	41.316
***La*NMT2**	6.09	41.217
***La*NMT3**	6.56	41.313
***Lr*NMT2**	6.76	41.3
***Hp*NMT2**	8.48	41.267

Table 1.A7. Similarity matrix

	PsRNMT	TfPNMT	PbTNMT	EcTNMT	PsTNMT	CjCNMT	PsCNMT	TfCNMT	EsNorENMT	LcCNMT	NnCNMT	SiCNMT	LaLrHpNMT1
PsRNMT	100%	55%	42%	44%	43%	48%	49%	48%	41%	53%	43%	44%	41%
TfPNMT	56%	100%	48%	50%	48%	58%	55%	58%	47%	65%	46%	47%	47%
PbTNMT	43%	48%	100%	75%	98%	45%	48%	46%	42%	49%	46%	42%	44%
EcTNMT	45%	51%	77%	100%	77%	47%	47%	48%	45%	53%	46%	44%	45%
PsTNMT	43%	48%	98%	75%	100%	46%	48%	47%	41%	49%	46%	43%	44%
CjCNMT	49%	58%	45%	46%	46%	100%	61%	86%	48%	72%	54%	52%	49%
PsCNMT	51%	56%	49%	46%	49%	62%	100%	61%	48%	62%	52%	49%	48%
TfCNMT	49%	57%	46%	47%	47%	85%	60%	100%	48%	71%	52%	51%	49%
EsNorENMT	42%	46%	42%	43%	41%	48%	46%	49%	100%	49%	67%	66%	64%
LcCNMT	54%	65%	49%	52%	49%	72%	61%	72%	50%	100%	55%	53%	54%
NnCNMT	44%	46%	46%	45%	46%	54%	51%	53%	67%	55%	100%	80%	79%
SiCNMT	45%	48%	42%	44%	43%	52%	49%	52%	67%	54%	80%	100%	76%
LaLrHpNMT1	42%	47%	44%	44%	44%	50%	48%	50%	65%	54%	79%	76%	100%

Table 1.A8. *LaHpLr*NMT1 catalytic site residues interacting with docked substrates and SAM.

Active Site residues (n=184)	**Ligand**	**Score (kCal/mol)**	**Interactions**		
			Hydro-phobic	**H-bonds**	**Other**
Ala70, Val71, Glu72, Thr73, Ala76, Lys77, His80, Tyr81, Asn95, Leu96, Lys97, Tyr98, Ser99, Leu118, Tyr121, Asp135,	SAM	na	nd	Tyr98, Ser99, Gly137, Gly139, Ser142, Asn161 (n=3), Gln165, Asp187, Ile188, Ile203	p-stacking, His208 Salt bridge: Lys97
	Norgalanthamine	-7.9	Phe234, Phe257 (n=3), Val333	Glu204, His208, Tyr288	nd

Val136, Gly137, Cys138, Gly139, Trp140, Gly141, Ser142, Leu143, Ser144, Ile159, Cys160, Asn161, Gln165, Ala186, Asp187, Ile188, Arg189, Ile203, Glu204, Met205, Glu207, His208, Met209, Phe234, Phe243, Phe257, Met262, Tyr288, Ser292, Trp295, Phe329, Phe330, Val333, Leu336, Phe337

na: not applicable, nd: not detected. The score is in (kCal/mol).

Table 1.A9. *LaHpLr*NMT1 mutants interactions with docked norgalanthamine

Active Site residues (n=184)	Ligand	Score	Interactions		
			Hydrophobic	H-bonds	Other
Phe234Leu	Norgalanthamine	-8.0 (3.4 Å)	Glu207, Leu234, Phe329, Val333	Glu204, His208	n.d.
Phe234Ala		-7.7 (3.4 Å)	Phe257, Phe337	Glu204, His208	n.d.
Phe234Trp		-7.9 (3.7 Å)	Glu207, Leu234, Val333	Glu204, His208, Trp234	n.d.
Phe257Ala		-6.8 (3.7 Å)	Phe234, Phe329 (n=2), Val333, Phe337	Tyr288	n.d.
Phe257Leu		-7.8 (3.5 Å)	Phe234, Phe329, Val333	Glu204, Leu257, Gly260	n.d.
Phe257Trp		-7.8 (3.4 Å)	Phe234, Phe329, Val333	Glu204, His208	n.d.
Glu204Lys		-7.6 (3.3 Å)	Glu207, Phe257, Phe329, Val333	Tyr98, Lys204, His208	n.d.
Glu204Asp		-8.1 (3.4 Å)	Phe234, Phe257	Asp204, His208	n.d.
Glu204Gln		-6.5 (4.4 Å)	Phe234, Phe257, Tyr288(n=2), Val333, Phe337	His80, Tyr98, His208	n.d.

n.d. none detected. Score is expressed in (kCal/mol). The distance between the substrate and methyl donor was calculated between the nitrogen of norgalanthamine and the carbon of the methyl group of SAM. (3.6 Å for wildtype).

Table 1.A10. Correlation of relative *NMT* expression with alkaloid levels.

	***NMT* vs. Galanthamine**	***NMT* vs. Norgalanthamine**	***NMT* vs. Narwedine**	***NMT* vs. Sanguinine**	***NMT* vs. 4'-O-methylnorbelladine**	***NMT* vs. 11-Hydroxyvittatine**	***NMT* vs. Crinine/Vittatine**	***NMT* vs. Haemanthamine**
Pearson r	-0.02368	0.05856	0.3823	-0.03026	0.01152	0.5326	0.5256	-0.08527
95% confidence interval	-0.3933 to 0.3525	-0.3215 to 0.4224	0.01077 to 0.6611	-0.3988 to 0.3467	-0.3631 to 0.3830	0.1991 to 0.7556	0.1897 to 0.7514	-0.4442 to 0.2973
R squared	0.0005606	0.003429	0.1462	0.0009158	0.0001327	0.2837	0.2763	0.007270
***P* (two-tailed)**	0.9048	0.7672	0.0447	0.8785	0.9536	0.0035	0.0041	0.6662
P value summary	ns	ns	*	ns	ns	**	**	ns
Significant? (alpha = 0.05)	No	No	Yes	No	No	Yes	Yes	No
Number of XY Pairs	28	28	28	28	28	28	28	28

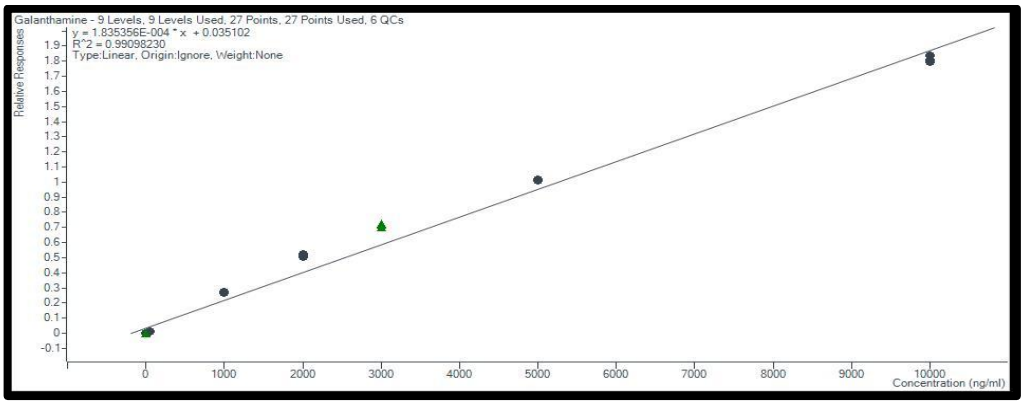

Figure 1.A1. Standard curve of galanthamine which represents the area ratio (*i.e.* peak area of galanthamine divided by the peak area of the papaverine) as a function of galanthamine's concentration. Each point of the curve was prepared in triplicate and was containing 1000 ng.mL^{-1} of internal standard papaverine.

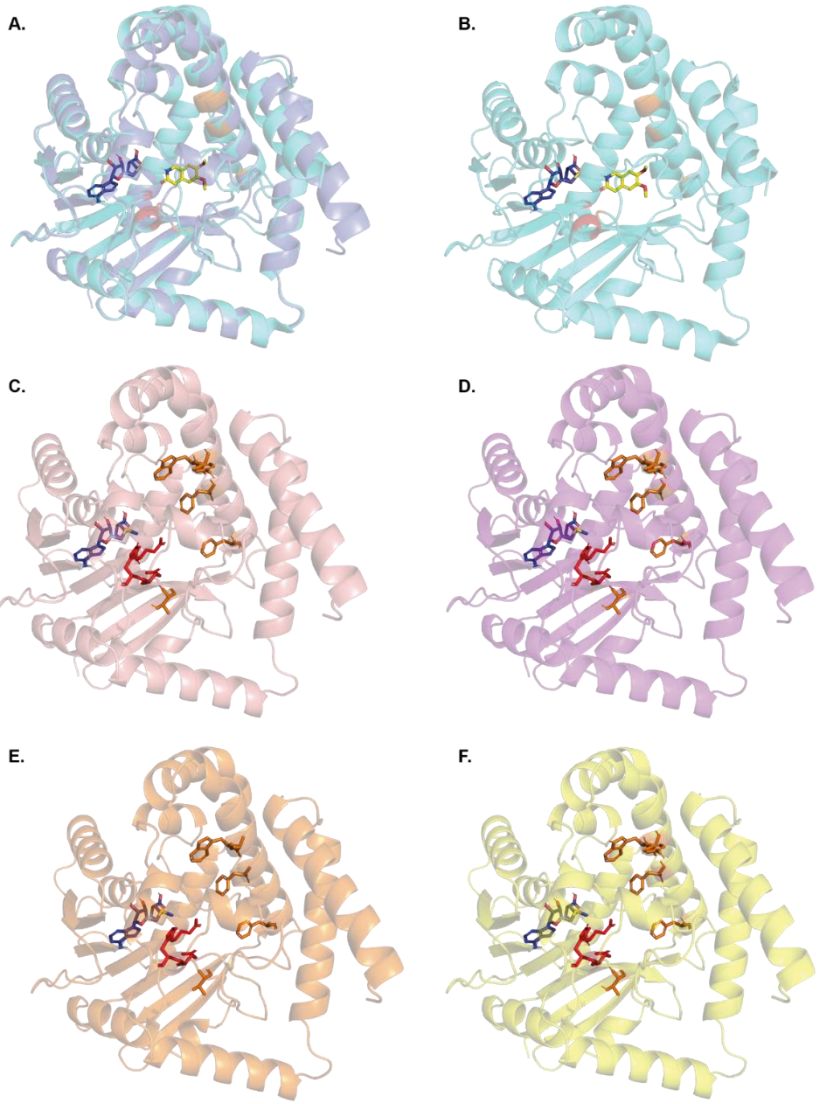

Figure 1.A2. A. Cartoon representation of *LaHpLr*NMT1 (purple) superimposed with *Cj*CNMT (turquoise) (RMSD=0.52 Å). **B.** Cartoon representation of cristalized structure *Cj*CNMT (turquoise) with SAH as dark purple sticks and heliamine as yellow sticks. **C.** *La*NMT3. **D.** *Lr*NMT2. **E.** *Hp*NMT2. **F.** *La*NMT2. SAH and SAM are represented as dark purple sticks and heliamine as yellow sticks. Catalytic residues position is indicated in red, other key active sites residues are shown as orange sticks. Amaryllidaceae NMT candidate structures were predicted with AlphaFold3.

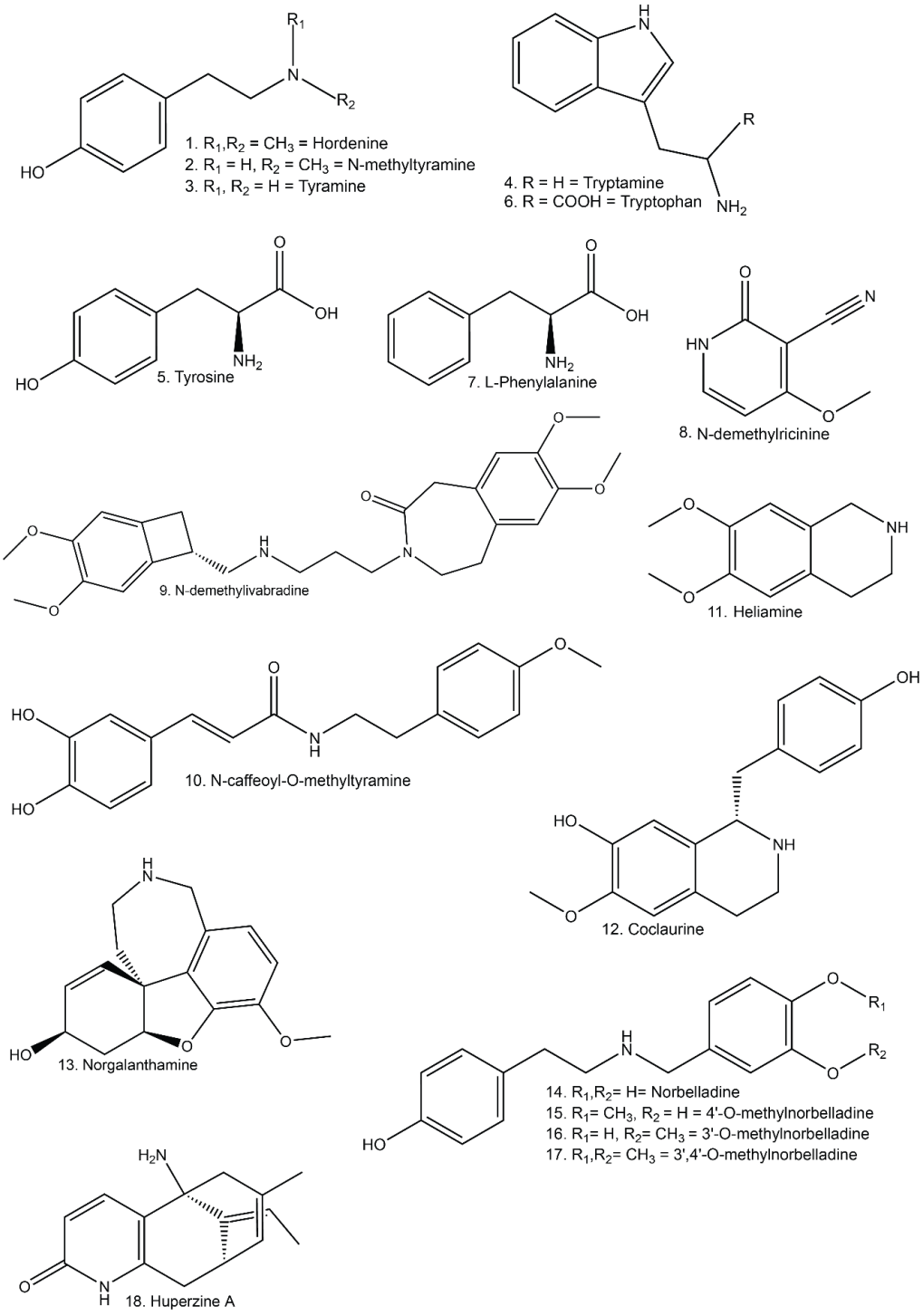

Figure 1.A3. Substrates used in the substrate specificity assay.

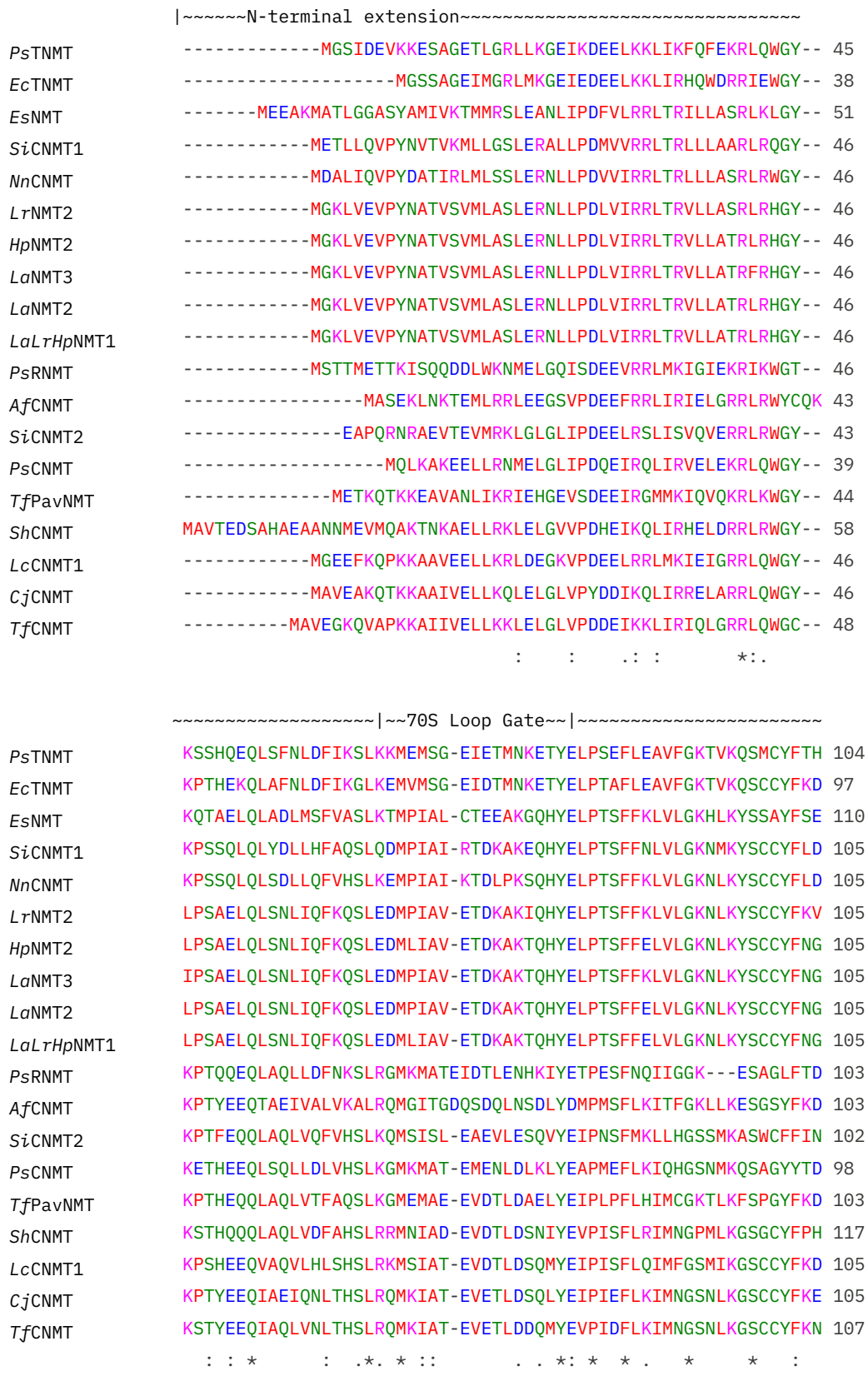
|~~~~~~N-terminal extension~~~~~~~~~~~~~~~~~~~~~~~~~~~~~~~~
PsTNMT ----------MGSIDEVKKESAGETLGRLLKGEIKDEELKKLIKFQFEKRLQWGY-- 45
EcTNMT ----------MGSSAGEIMGRLMKGEIEDEELKKLIRHQWDRRIEWGY-- 38
EsNMT -------MEEAKMATLGGASYAMIVKTMMRSLEANLIPDFVLRRLTRILLASRLKLGY-- 51
SiCNMT1 ----------METLLQVPYNVTVKMLLGSLERALLPDMVVRRLTRLLLAARLRQGY-- 46
NnCNMT ----------MDALIQVPYDATIRLMLSSLERNLLPDVVIRRLTRLLLASRLRWGY-- 46
LrNMT2 ----------MGKLVEVPYNATVSVMLASLERNLLPDLVIRRLTRVLLASRLRHGY-- 46
HpNMT2 ----------MGKLVEVPYNATVSVMLASLERNLLPDLVIRRLTRVLLATRLRHGY-- 46
LaNMT3 ----------MGKLVEVPYNATVSVMLASLERNLLPDLVIRRLTRVLLATRFRHGY-- 46
LaNMT2 ----------MGKLVEVPYNATVSVMLASLERNLLPDLVIRRLTRVLLATRLRHGY-- 46
LaLrHpNMT1 ----------MGKLVEVPYNATVSVMLASLERNLLPDLVIRRLTRVLLATRLRHGY-- 46
PsRNMT ----------MSTTMETTKISQQDDLWKNMELGQISDEEVRRLMKIGIEKRIKWGT-- 46
AfCNMT ----------MASEKLNKTEMLRRLEEGSVPDEEFRRLIRIELGRRLRWYCQK 43
SiCNMT2 ----------EAPQRNRAEVTEVMRKLGLGLIPDEELRSLISVQVERRLRWGY-- 43
PsCNMT ----------MQLKAKEELLRNMELGLIPDQEIRQLIRVELEKRLQWGY-- 39
TfPavNMT ----------METKQTKKEAVANLIKRIEHGEVSDEEIRGMMKIQVQKRLKWGY-- 44
ShCNMT MAVTEDSAHAEAANNMEVMQAKTNKAELLRKLELGVVPDHEIKQLIRHELDRRLRWGY-- 58
LcCNMT1 ----------MGEEFKQPKKAAVEELLKRLDEGKVPDEELRRLMKIEIGRRLQWGY-- 46
CjCNMT ----------MAVEAKQTKKAAIVELLKQLELGLVPYDDIKQLIRRELARRLQWGY-- 46
TfCNMT ----------MAVEGKQVAPKKAIIVELLKKLELGLVPDDEIKKLIRIQLGRRLQWGC-- 48
: : .: : *:.
~~~~~~~~~~~~~~~~~~~|~~70S Loop Gate~~|~~~~~~~~~~~~~~~~~~~~~~
PsTNMT KSSHQEQLSFNLDFIKSLKKMEMSG-EIETMNKETYELPSEFLEAVFGKTVKQSMCYFTH 104
EcTNMT KPTHEKQLAFNLDFIKGLKEMVMSG-EIDTMNKETYELPTAFLEAVFGKTVKQSCCYFKD 97
EsNMT KQTAELQLADLMSFVASLKTMPIAL-CTEEAKGQHYELPTSFFKLVLGKHLKYSSAYFSE 110
SiCNMT1 KPSSQLQLYDLLHFAQSLQDMPIAI-RTDKAKEQHYELPTSFFNLVLGKNMKYSCCYFLD 105
NnCNMT KPSSQLQLSDLLQFVHSLKEMPIAI-KTDLPKSQHYELPTSFFKLVLGKNLKYSCCYFLD 105
LrNMT2 LPSAELQLSNLIQFKQSLEDMPIAV-ETDKAKIQHYELPTSFFKLVLGKNLKYSCCYFKV 105
HpNMT2 LPSAELQLSNLIQFKQSLEDMLIAV-ETDKAKTQHYELPTSFFELVLGKNLKYSCCYFNG 105
LaNMT3 IPSAELQLSNLIQFKQSLEDMPIAV-ETDKAKTQHYELPTSFFKLVLGKNLKYSCCYFNG 105
LaNMT2 LPSAELQLSNLIQFKQSLEDMPIAV-ETDKAKTQHYELPTSFFELVLGKNLKYSCCYFNG 105
LaLrHpNMT1 LPSAELQLSNLIQFKQSLEDMLIAV-ETDKAKTQHYELPTSFFELVLGKNLKYSCCYFNG 105
PsRNMT KPTQQEQLAQLLDFNKSLRGMKMATEIDTLENHKIYETPESFNQIIGGK---ESAGLFTD 103
AfCNMT KPTYEEQTAEIVALVKALRQMGITGDQSDQLNSDLYDMPMSFLKITFGKLLKESGSYFKD 103
SiCNMT2 KPTFEQQLAQLVQFVHSLKQMSISL-EAEVLESQVYEIPNSFMKLLHGSSMKASWCFFIN 102
PsCNMT KETHEEQLSQLLDLVHSLKGMKMAT-EMENLDLKLYEAPMEFLKIQHGSNMKQSAGYYTD 98
TfPavNMT KPTHEQQLAQLVTFAQSLKGMEMAE-EVDTLDAELYEIPLPFLHIMCGKTLKFSPGYFKD 103
ShCNMT KSTHQQQLAQLVDFAHSLRRMNIAD-EVDTLDSNIYEVPISFLRIMNGPMLKGSGCYFPH 117
LcCNMT1 KPSHEEQVAQVLHLSHSLRKMSIAT-EVDTLDSQMYEIPISFLQIMFGSMIKGSCCYFKD 105
CjCNMT KPTYEEQIAEIQNLTHSLRQMKIAT-EVETLDSQLYEIPIEFLKIMNGSNLKGSCCYFKE 105
TfCNMT KSTYEEQIAQLVNLTHSLRQMKIAT-EVETLDDQMYEVPIDFLKIMNGSNLKGSCCYFKN 107
: : * : .*. * :: . . *: * * . * * :
~~~~~~~~~~~~~~~~~~~

```
              ~~~~SAM Binding~~~~~~~~~~~~~~~~~~~~~~~~~~~~~~~~~~~~~~~~~~~~~~~~~~~~~~~~
PsTNMT        E-SATIDEAEEAAHELYCERAQIKDGQTVLDIGCGQGGLVLYIAQKYKNCHVTGLTNSKA 163
EcTNMT        E-NSTIDEAEEAAHELYCERAQIKDGQTVLDIGCGQGGLVLYIAEKYKNCHVTGLTNSKA 156
EsNMT         H-TRTLDEAEEAMLALYCERAKIEDGQKILDIGCGWGSFSLYVAERYPKCEITGLCNSST 169
SiCNMT1       K-TSTLEDAENAMLELYCERAQLKDGHTVLDVGCGWGSLSLYIAQKYTNCRVTGICNSMT 164
NnCNMT        K-SSTLEDAEKAMLELYCERAQIKDGQSVLDVGCGWGSLSLYIAQKFSSCRITGICNSKT 164
LrNMT2        K-SNTLEDAENAMLELYCERAQVKDGQSILDVGCGWGSLSLYIARKYKSCSITGICNSTT 164
HpNMT2        T-SNTLEDAENAMLELYCERAQVKDGQSILDVGCGWGSLSLYIARKYKGCSITGICNSTT 164
LaNMT3        T-SNTLEDAENAMLELCCERAQVKDGQSILDVGCGWGSLSLYIARKYKGCSITGICNSTT 164
LaNMT2        T-SNTLEDAENAMLELYCERAQVKDGQSILDVGCGWGSLSLYIARKNKGCSITGICNSTT 164
LaLrHpNMT1    T-SNTLEDAENAMLELYCERAQVKDGQSILDVGCGWGSLSLYIARKYKGCSITGICNSTT 164
PsRNMT        ETTTTMEEANTKMMDLYCERAGLKDGHTILDLGCGAGLLVLHLAKKYKKSKITGITNTSS 163
AfCNMT        D-SMTLDEAEEAMLDLYCERAQLKDGQKILDLGCGQGAFTLHAAQKYKKSHVTAVTNSAT 162
SiCNMT2       D-STTLDEAEIAMLELYCDRSQIRDGDRVLDLGCGFGALATYIARKYPNCQVTGVTNSEF 161
PsCNMT        E-STTLDEAEIAMLDLYMERAQIKDGQSVLDLGCGLGAVALFGANKFKKCQFTGVTSSVE 157
TfPavNMT      E-STTLDESEVYMMDLYCERAQIKDGQSILDLGCGHGSLTLHVAQKYRGCKVTGITNSVS 162
ShCNMT        D-STTLAEAEIAMLDLYCERAQVRDGHTILDLGCGQGALTLHIAKKYTNCRVTAITNSVS 176
LcCNMT1       E-STTLDEAEIAMLDLYCERAQIKDGQSVLDLGCGQGALTLHVAQKYQKCHVTAITNSAS 164
CjCNMT        D-STTLDEAEIAMLDLYCERAQIQDGQSVLDLGCGQGALTLHVAQKYKNCRVTAVTNSVS 164
TfCNMT        D-STTLDEAEIAMLELYCERAQIKDGHSVLDLGCGQGALTLYVAQKYKNSRVTAVTNSVS 166
                . *: :::     *  :*: :.**. :**:*** * .  . *.:   . .*.: .:

              ~~~~~~~~~~~~~~~~~~~~~~~~~~~~~~~~~~~~~~~~~~~|~~~~~~~~~~~~~~~~~
PsTNMT        QVNYLLKQAEKLGLTNVDAILADVTQYESDKTYDRLLMIEAIEHMKNLQLFMKKLSTWMT 223
EcTNMT        QANYIEQQAEKLELTNVDVIFADVTKFDTDKTYDRILVVETIEHMKNIQLFMKKLSTWMT 216
EsNMT         QKAFIEQQCSERRLCNVTIYADDISTFDTESTYDRIISIEMFEHMKNYSTLLKKISKWMN 229
SiCNMT1       QKACIEEKCRELQVHNVEIIVADISTFEMEGTFDRIFSIEMFEHMKNYKELLKKISKWMT 224
NnCNMT        QKAYIEEQCRELKLQNVEIIVADISTFEMEASFDRILSIEMFEHMKNYKALLNKISKWMK 224
LrNMT2        QRTYIEEQCRELQLSNVKIIVADISKFEMEASFDRVISIEMFEHMKNYKALLKKISTWMK 224
HpNMT2        QRAYIEEQCRDLQLSNVKIIVADIREFEMEASFDRVISIEMFEHMKNYKALMKKIATWMK 224
LaNMT3        QRAYIEEQCRDLRLSNVKIIVADIREFEMEASFDRVISIEMFEHMKNYKALMKKIATWMK 224
LaNMT2        QRAYIEEQCRDLQLSNVKIIVADIREFEMEASFDRVISIEMFEHMKNYKALMKKIATWMK 224
LaLrHpNMT1    QRAYIEEQCRDLQLSNVKIIVADIREFEMEASFDRVISIEMFEHMKNYKALMKKIATWMK 224
PsRNMT        HKEYILKQCKNLNLSNVEIILADVTKVDIESTFDRVFVIGLIEHMKNFELFLRKISKWMK 223
AfCNMT        QKKYIEDQCQILELSNVEVLLEDITQLTMEATFDRIIVIGLLEHMKNYGLLLQNISQWMA 222
SiCNMT2       QKEFIEEQCKKDNLVNVEVILADVTTLEMDKEFDRVMAIGVIEHMKSYELLLKKISKWMK 221
PsCNMT        QKDYIEGKCKELKLTNVKVLLADITTYETEERFDRIFAVELIEHMKNYQLLLKKISEWMK 217
TfPavNMT      QKEFIMDQCKKLDLSNVEIILEDVTKFETEITYDRIFAVALIEHMKNYELFLKKVSTWIA 222
ShCNMT        QKHFIQDQCIKSNLTNVEVLLADITKHDTSHSFDRVFVIELLEHMKNYELLLKKISKWMS 236
LcCNMT1       QKDFIDEQSKKLKLSNVEVILADITKHKTEATFDRILVIELFEHMKNYELLLKKIAKWMK 224
CjCNMT        QKEYIEEESRRRNLLNVEVKLADITTHEMAETYDRILVIELFEHMKNYELLLRKISEWIS 224
TfCNMT        QKEFIEEESRKRNLSNVEVLLADITTHKMPDTYDRILVVELFEHMKNYELLLRKIKEWMA 226
              :   :  :.     : **      *:         :**:: :  :****.   ::.::  *:
```

```
                    ~~~~~~~~~~~~~~~~~~~BIA Binding~~~~~~~~~~~~~~~~~~~~~~~~~~~~~~~
PsTNMT              K-ESLLFVDHVCHKTFAHFFEAVDEDDWYSGFIFPPGCATILAANSLLYFQDDVSVVDHW 282
EcTNMT              E-DSLLFVDHISHKTFNHNFEALDEDDWYSGFIFPKGCVTILSSSTLLYFQDDVSALDHW 275
EsNMT               Q-ECLLFVHYFCHKTFAYHFEDVDEDDWMARYFFTGGT--MPASSLLLYFQDDVSVVDHW 286
SiCNMT1             Q-EGLLFVHYFCHKTFAYHFEDLSDDDWITRYFFTGGT--MPSANLLLYFQEDVSILNHW 281
NnCNMT              E-DSLLFVNYFCHKAFAYHFEDKNEDDWITRYFFTGGT--MPAANLLLYFQDDVSVVNHW 281
LrNMT2              E-DSLLFVHYFCHKVFAYHFEDINEDDWITRYFFSGGT--MPSANLLLYFQDDVAVVNHW 281
HpNMT2              Q-DSLLFVHYFCHKVFAYHFEDINEDDWITRHFFSGGT--MPSANLLLYFQDDVAVVNHW 281
LaNMT3              Q-DSLLFVHYFCHKVLSYHFEDINEDDWITRHFFSGGT--MPSANLLLYFQDDVAVVNHW 281
LaNMT2              Q-DSLLFVHYLCHKVFAYHFEDINEDDWITRHFFSGGT--MPSANLLLYFQDDVAVVNHW 281
LaLrHpNMT1          Q-DSLLFVHYFCHKVFAYHFEDINEDDWITRHFFSGGT--MPSANLLLYFQDDVAVVNHW 281
PsRNMT              D-DGLLLLEHLCHKSFSDHWEPLSEDDWYAKNFFPSGTLVIPSATCLLYFQEDVTVIDHW 282
AfCNMT              PADSLLFIDHVCHKSYFYQCEPLDEDDWFAEYFFPPGSFAMPSASFLLYFQDDVSIVDHW 282
SiCNMT2             Q-DGLLFVDHICHKAFAYHFEPIGEEDWIEEYIFPGGVMTIPSADLLLYFQDDISVVNHW 280
PsCNMT              D-DGLLFVEHVCHKTLAYHYEPVDAEDWYTNYIFPAGTLTLSSASMLLYFQDDVSVVNQW 276
TfPavNMT            Q-YGLLFVEHHCHKVFAYQYEPLDEDDWYTEYIFPSGTLVMSSSSILLYFQEDVSVVNHW 281
ShCNMT              Q-DGLLFIEHICHKTFAYHYDPLDEDDWFTDYVFPAGTMIIPSASFLLYFQDDVSVVNHW 295
LcCNMT1             Q-DGLLFIEHICHKTFAYHYEPLDEDDWYTEYIFPAGTMIIPSSSFLLYFQDDVSVVNHW 283
CjCNMT              K-DGLLFLEHICHKTFAYHYEPLDDDDWFTEYVFPAGTMIIPSASFFLYFQDDVSVVNHW 283
TfCNMT              K-DGLLFVEHICHKTFAYHYEPIDEDDWFTEYVFPAGTMIIPSASFFLYFQDDVSVVNHW 285
                        **::.: .**      :  . :**    .*  *   : ::  :****:*:: :::*

                    ~~~~~~~~~~~~~~~~~~~~~~~~~~~~~~~~~~~~~~~~~~~~~~~~~~~~~~~~~~~~~~
PsTNMT              VVNGMHMARSVDIWRKALDKNMEAAKEILLPGLGGSHETVNGVVTHIRTFCMGGYEQFSM 342
EcTNMT              VVNGMHMARSVEAWRKKLDETIEAAREILEPGLGSK-EAVNQVITHIRTFCIGGYEQFSY 334
EsNMT               LINGKHYAQTSEEWLKRMDHNLSSILPIFNETYGEN--AAKKWLAYWRTFFIAVAELFKY 344
SiCNMT1             LVNGKHYSQTSEEWLKRMDRNLASIKPIMESTYGKA--EAVKWTVYWRTFFIAVAELFGY 339
NnCNMT              LVNGNHYARTSEEWLKRMDQNMASIKPIMESTYGKD--SAVKWTAYWRTFFISVAELFGY 339
LrNMT2              LVNGMHYSSTSEEWLKRMDQNTAAIRPIMESTYGKD--LATKWTVYWRTFFIAVAELFGY 339
HpNMT2              LVNGMHYSRTSEXWLKRMDQNRAAIRPIRESTYGED--LATKWTVSWRTXFNAVAKLFGY 339
LaNMT3              LVNGMHYSRTSEEWLKRMDQNRAAIRPIMESTYGED--LATKWTVYWRTFFIAVAELFSY 339
LaNMT2              LVNGMHYSRTSEEWLKRMDQNRAAIRPIMESTYGED--LATKWTVYWRTFFIAVAELFGY 339
LaLrHpNMT1          LVNGMHYSRTSEEWLKRMDQNRAAIRPIMESTYGED--LATKWTVYWRTFFIAVAELFGY 339
PsRNMT              ILSGNNFARSNEVILKRIDGKIEEVKDIFMSFYGIGREEAVKLINWWRLLCITANELFKY 342
AfCNMT              ILSGKHFHRTAEEWVKQLDTNLEKGKEILESKYGSK-EAALKAFNHWRGLCIFSSEIFGY 341
SiCNMT2             AVNGKHYSRTNEEWLKRLDGNADAARAILEDSLGSK-EEAMKMLNYWRTFCFYGMELCKY 339
PsCNMT              TLSGKHYSRSHEEWLKNMDKNIVEFKEIMRSITKTE-KEAIKLLNFWRIFCMCGAELFGY 335
TfPavNMT            TLSGKHPSLGFKQWLKRLDDNIDEVKEIFESFYGSK-EKAMKFITYWRVFCIAHSQMYST 340
ShCNMT              TLSGKHFSRTNEEWLKRLDANVDTIKAIFEASLGSE-EAAVKLINYWKGFCFSGMEMFGS 354
LcCNMT1             TLSGKHYSRTNEEWLKRVDANVDAVREIMESFSGSK-EAAEKWIRYWRGFCMSGNELFGY 342
CjCNMT              TLSGKHFSRTNEEWLKRLDANLDVIKPMFETLMGNE-EEAVKLINYWRGFCLSGMEMFGY 342
TfCNMT              TLSGKHFSRTNEEWLKRLDANVELIKPMFVTITGQCRQEAMKLINYWRGFCLSGMEMFGY 345
                     :.* :     .   * :* .      :           .       :       :
```

```
                    ~~~~~~~~~~~~~~~~~~~~|
PsTNMT              NNGDEWMVAQLLFKKK-----       358
EcTNMT              NNGEEWMITQILFKKK-----       350
EsNMT               NDGEEWMVSHFLFKKK-----       360
SiCNMT1             NNGEEWMVAHFLFKKK-----       355
NnCNMT              NNGEEWMVALFLFKKKIN---       357
LrNMT2              NNGEEWMVAHYLFKKK-----       355
HpNMT2              NNGKKWKVPHFFFKKK-----       355
LaNMT3              NNGEEWMVAHFLFKKK-----       355
LaNMT2              NNGEEWMVAHFLFKKK-----       355
LaLrHpNMT1          NNGEEWMVAHFLFKKK-----       355
PsRNMT              NNGEEWLISQLLFKKKLMTCI       363
AfCNMT              NGGEEWMTSHLLFKKK-----       357
SiCNMT2             NNGEEWMSAHVLFKKK-----       355
PsCNMT              KNGEEWMLTHLLFKKK-----       351
TfPavNMT            NNGEEWMLSQVLFKKK-----       356
ShCNMT              NNGEEWMTSHLLLTRK-----       370
LcCNMT1             NNGEEWMASHILFKKP-----       358
CjCNMT              NNGEEWMASHVLFKKK-----       358
TfCNMT              NNGEEWMASHVLFKKK-----       361
                    :.*.:*     ::.:
```

Figure 1.A4. Amino acid alignment of NMTs in this study along with other known NMTs in BIA pathway, green highlights the amino acid 204 residue that is critical for the catalytic activity, and cyan highlights the catalytic dyad conserved in all BIA NMTs.

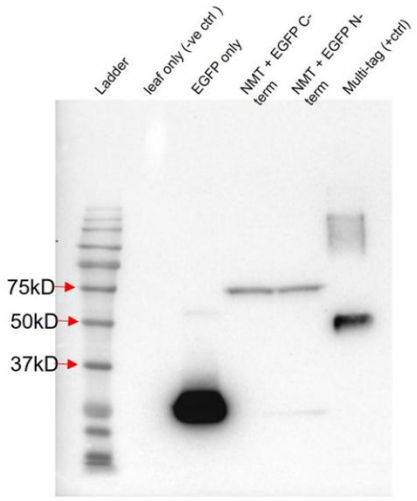

Figure 1.A5. Western blot analysis illustrating the expression of EGFP fusion proteins of *LaLrHp*NMT in *N. benthamiana*.

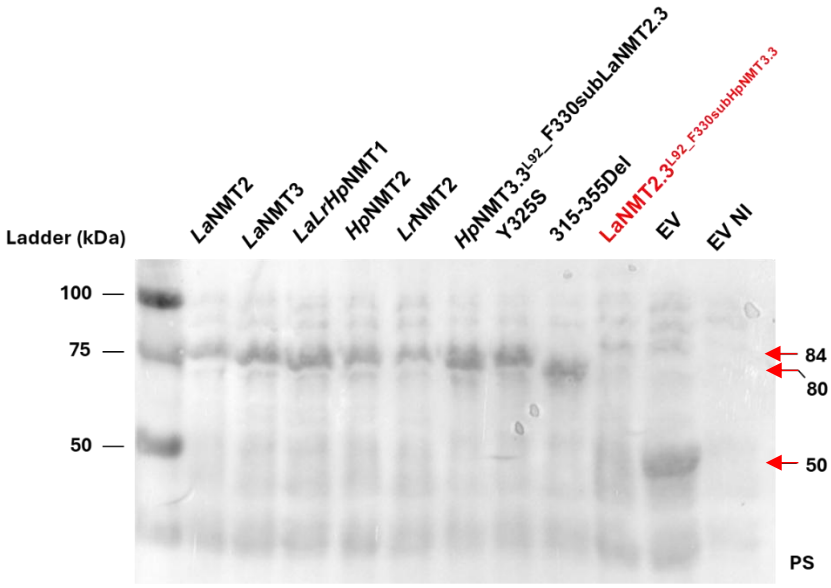

Figure 1.A6. SDS-page analysis illustrating the expression of MBP fusion proteins. EV- empty vector, EV NI- empty vector non-induced. Red arrows points the expected molecular weight.

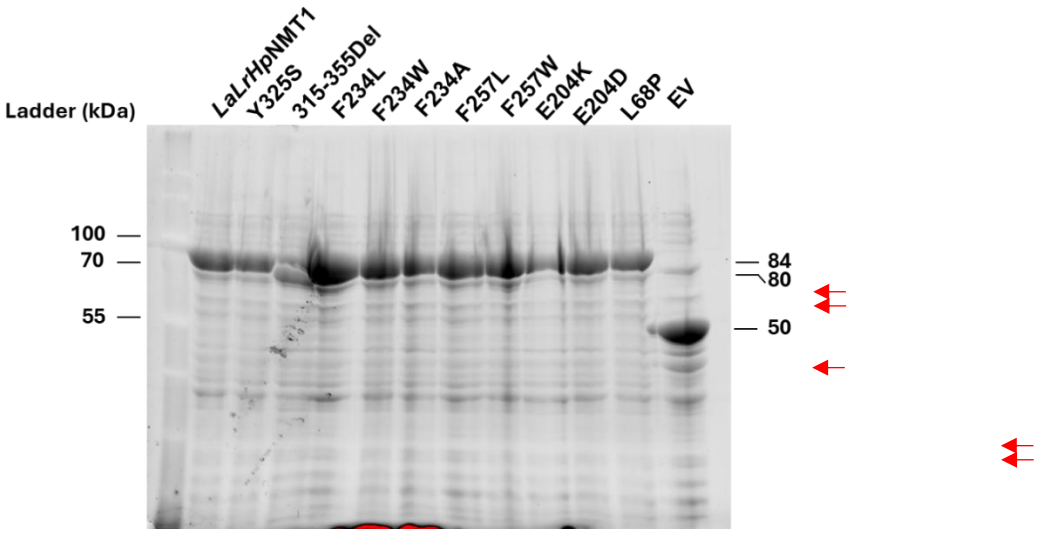

Figure 1.A7. SDS-page analysis illustrating the expression of MBP fusion mutant proteins following Comassie staining. EV- empty vector. Red arrows point towards the expected molecular weight.

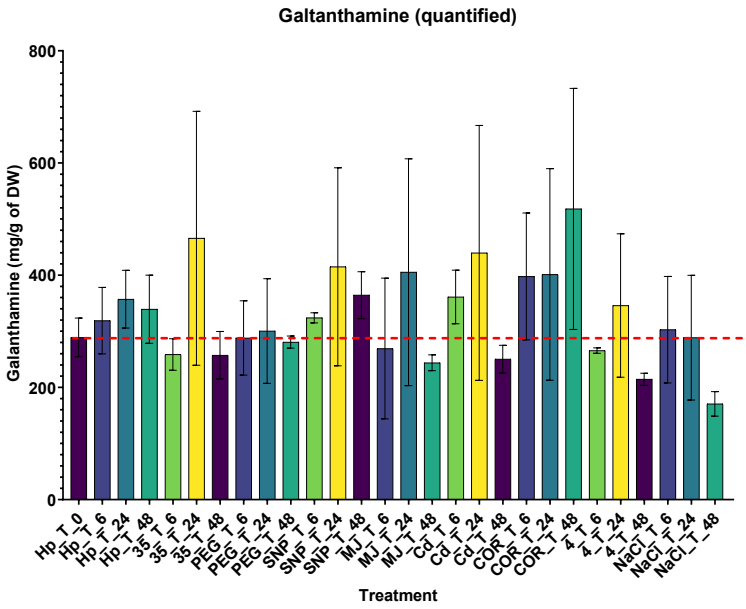

Figure 1.A8. Accumulation of galanthamine under different stress conditions in *H. papilio* shoots cultures at 0, 6, 24, and 48 hours post-treatment measured by LC-MS/MS. ISTD Resp. ratio: internal standard responsive ratio. DW: dry weight. *Hp*: *Hippeastrum papilio* (no treatment), 35:35˚C, PEG: PEG 40% for drought, SNP: sodium nitroprusside, MJ: Methyl jasmonate, Cd: $CdCl_2$ COR: Coronatine, 4: 4 ˚C. T: time (hours).

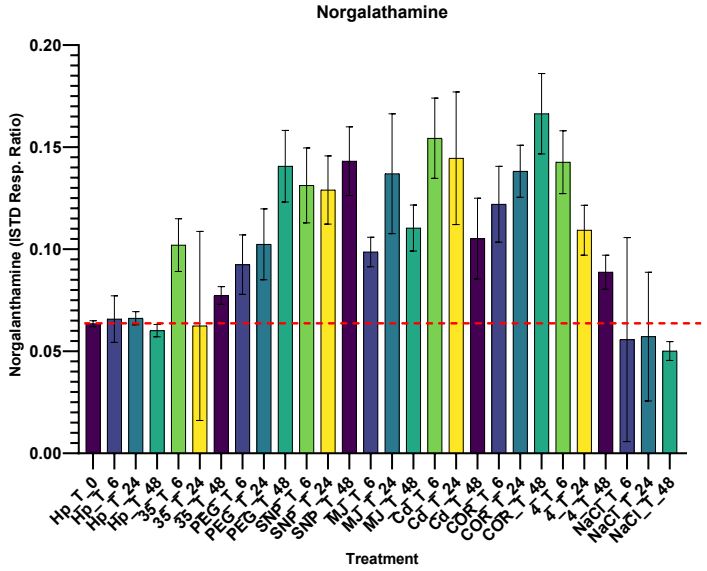

Figure 1.A9. Accumulation of norgalanthamine under different stress conditions in *H. papilio* shoots cultures at 0, 6, 24, and 48 hours post-treatment measured by LC-MS/MS. ISTD Resp. ratio: internal standard responsive ratio. DW: dry weight. *Hp*: *Hippeastrum papilio* (no treatment), 35:35˚C, PEG: PEG 40% for drought, SNP: sodium nitroprusside, MJ: Methyl jasmonate, Cd: $CdCl_2$ COR: Coronatine, 4: 4 ˚C. T: time (hours).

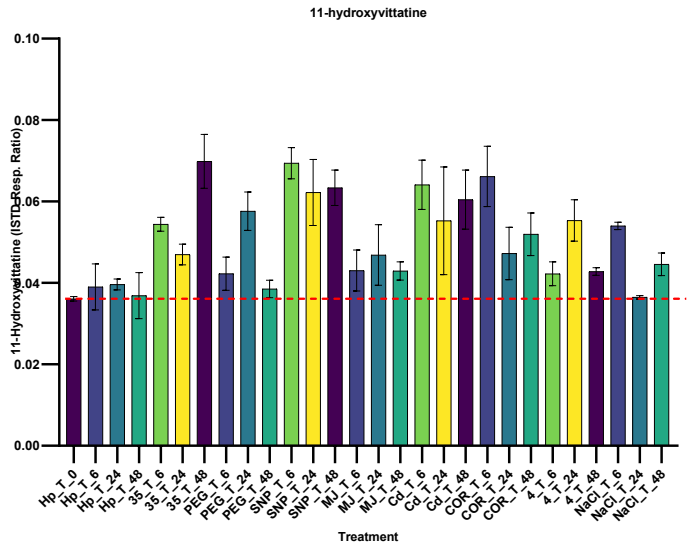

Figure 1.A10. Accumulation of 11-hydroxyvittatine under different stress conditions in *H. papilio* shoots cultures at 0, 6, 24, and 48 hours post-treatment measured by LC-MS/MS. ISTD Resp. ratio: internal standard responsive ratio. DW: dry weight. *Hp*: *Hippeastrum papilio* (no treatment), 35:35˚C, PEG: PEG 40% for drought, SNP: sodium nitroprusside, MJ: Methyl jasmonate, Cd: $CdCl_2$ COR: Coronatine, 4: 4 ˚C. T: time (hours).

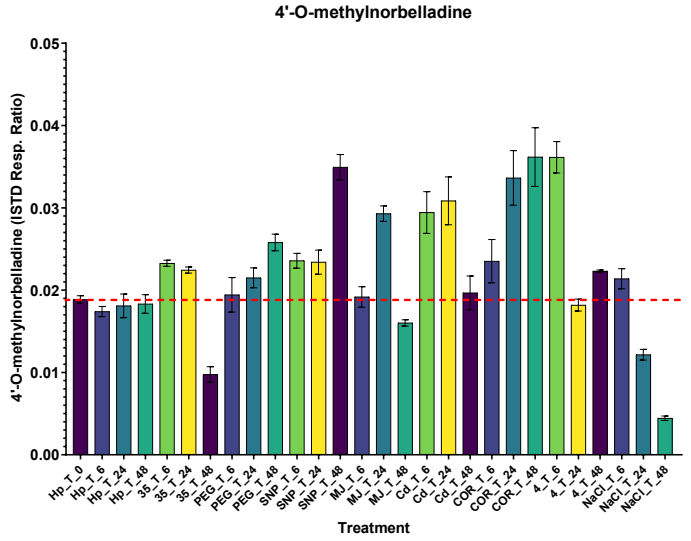

Figure 1.A11. Accumulation of 4'-O-methylnorbelladine under different stress conditions in *H. papilio* shoots cultures at 0, 6, 24, and 48 hours post-treatment measured by LC-MS/MS. ISTD Resp. ratio: internal standard responsive ratio. DW: dry weight. *Hp*: *Hippeastrum papilio* (no treatment), 35:35˚C, PEG: PEG 40% for drought, SNP: sodium nitroprusside, MJ: Methyl jasmonate, Cd: $CdCl_2$ COR: Coronatine, 4: 4 ˚C. T: time (hours).

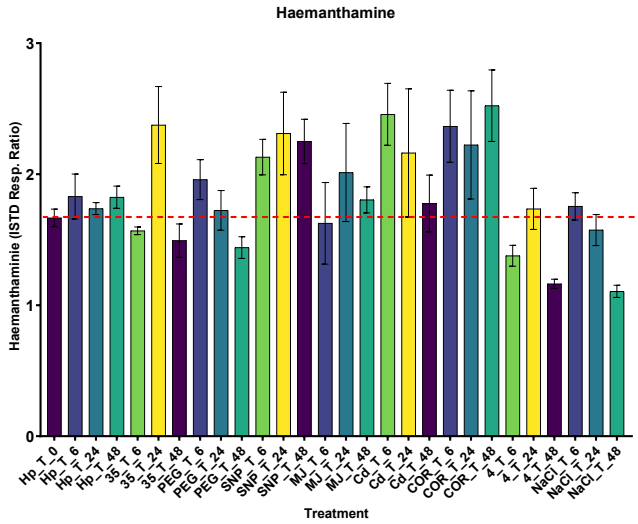

Figure 1.A12. Accumulation of haemanthamine under different stress conditions in *H. papilio* shoots cultures at 0, 6, 24, and 48 hours post-treatment measured by LC-MS/MS. ISTD Resp. ratio: internal standard responsive ratio. DW: dry weight. *Hp*: *Hippeastrum papilio* (no treatment), 35:35˚C, PEG: PEG 40% for drought, SNP: sodium nitroprusside, MJ: Methyl jasmonate, Cd: $CdCl_2$ COR: Coronatine, 4: 4 ˚C. T: time (hours).

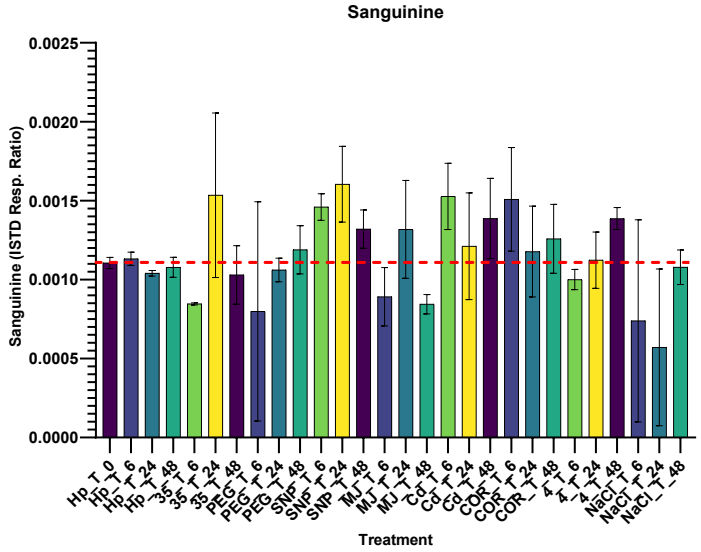

Figure 1.A13. Accumulation of Sanguinine under different stress conditions in *H. papilio* shoots cultures at 0, 6, 24, and 48 hours post-treatment measured by LC-MS/MS. ISTD Resp. ratio: internal standard responsive ratio. DW: dry weight. *Hp*: *Hippeastrum papilio* (no treatment), 35:35˚C, PEG: PEG 40% for drought, SNP: sodium nitroprusside, MJ: Methyl jasmonate, Cd: $CdCl_2$ COR: Coronatine, 4: 4 ˚C. T: time (hours).

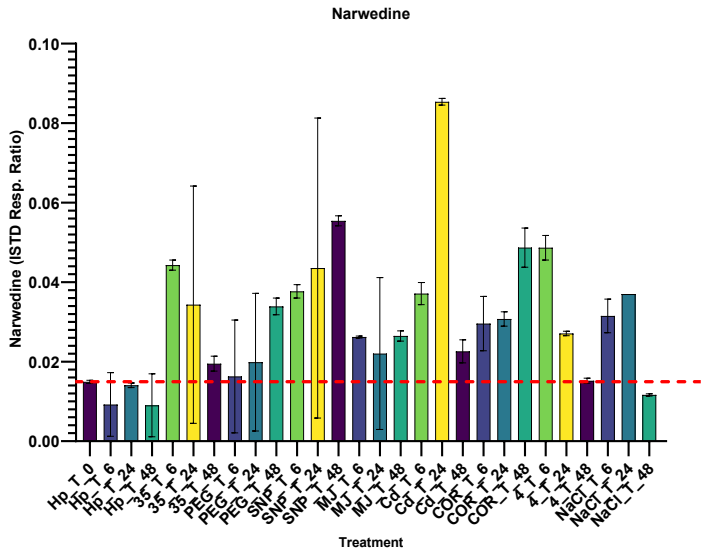

Figure 1.A14. Accumulation of narwedine under different stress conditions in *H. papilio* shoots cultures at 0, 6, 24, and 48 hours post-treatment measured by LC-MS/MS. ISTD Resp. ratio: internal standard responsive ratio. DW: dry weight. *Hp*: *Hippeastrum papilio* (no treatment), 35:35˚C, PEG: PEG 40% for drought, SNP: sodium nitroprusside, MJ: Methyl jasmonate, Cd: $CdCl_2$ COR: Coronatine, 4: 4 ˚C. T: time (hours).

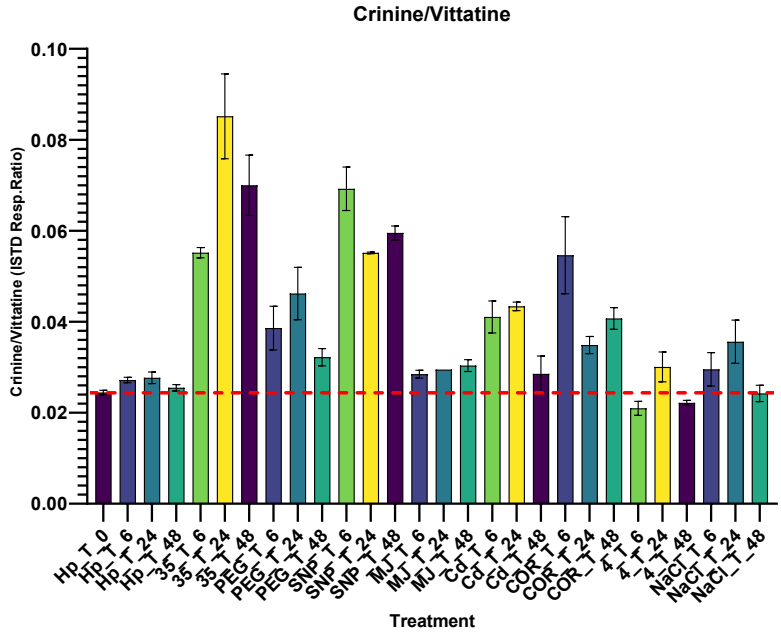

Figure 1.A15. Accumulation of crinine/vittatine under different stress conditions in *H. papilio* shoots cultures at 0, 6, 24, and 48 hours post-treatment measured by LC-MS/MS. ISTD Resp. ratio: internal standard responsive ratio. DW: dry weight. *Hp*: *Hippeastrum papilio* (no treatment), 35:35˚C, PEG: PEG 40% for drought, SNP: sodium nitroprusside, MJ: methyl jasmonate, Cd: $CdCl_2$ COR: coronatine, 4: 4 ˚C. T: time (hours).

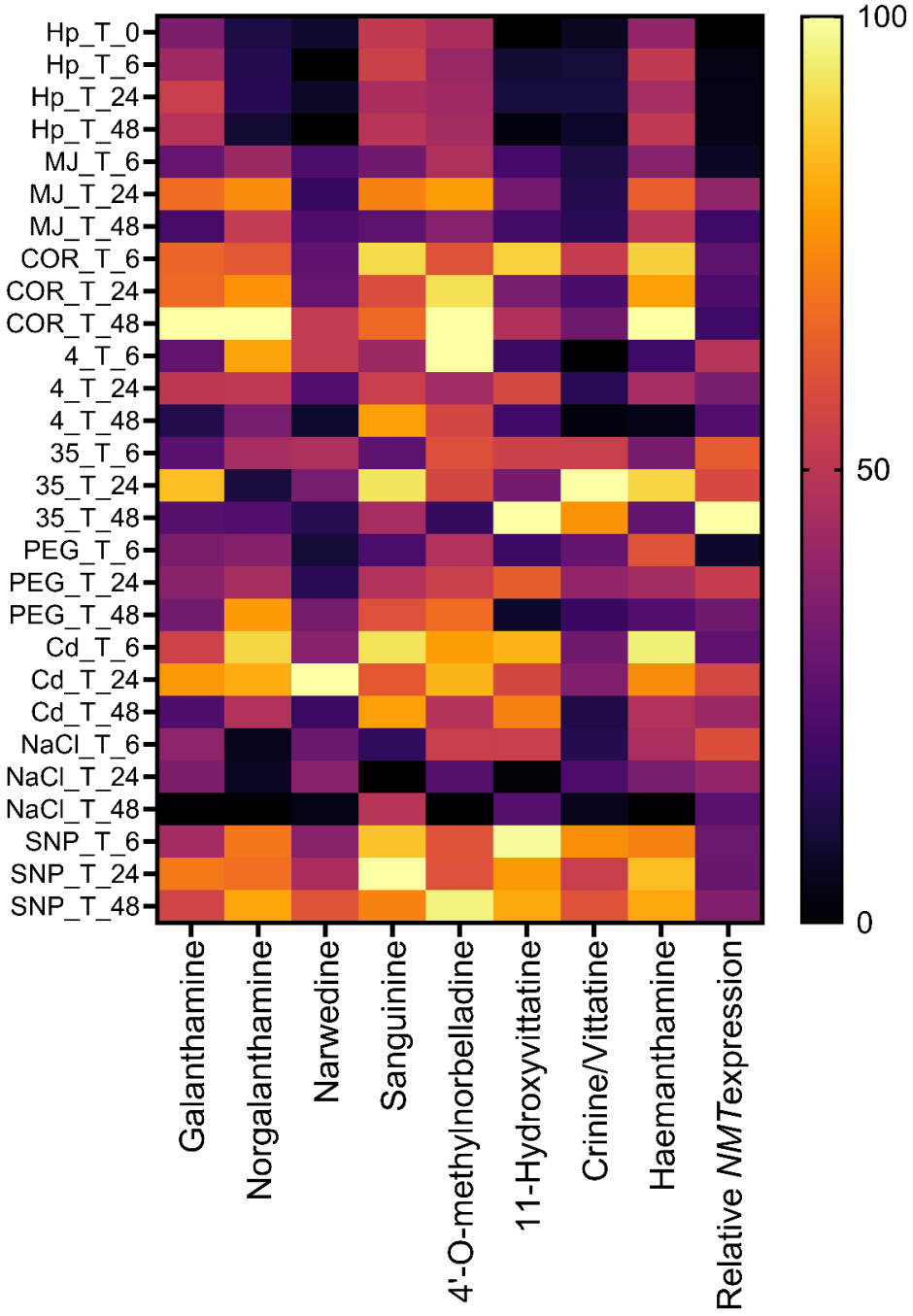

Figure 1.A16. Heat map showing the accumulation of alkaloids and relative *NMT* expression in *H. papilio* under different stress treatments. Relative abundance corresponds to the mean value of three independent replicates. Values were normalized to the sample with the highest level (100%) for each compound.

APPENDIX II

Supplementary Data of Chapter III

Table 2.A1. Overview of the localization of Amaryllidaceae alkaloids of *Hippeastrum papilio*.

		Leaf			***Bulbs***				***Root***		
		Tip	Mid	Base	O	Mid	AL	BP	Base	Mid	Tip
Norcraugsodine	Detection frequency	100	66	100	100	100	500	100	100	100	100
	outer epidermis layer	1	1	0	1	0	0	0	na	na	na
	Epidermis (higher/outter)	0	1	1	1	1	0	0	na	na	na
	Epidermis (Lower/inner)	0	1	1	1	0	0	0	na	na	na
	Exodermis	na	na	na	na	na	na	na	1	1	0
	Endodermis	na	na	na	na	na	na	na	0	0	0
	Vascular bundles	1	1	0	1	1	0	1	1	1	0
	Parenchyma	1	1	1	0	0	1	0	1	1	1
Norbelladine	Detection frequency	100	66	100	100	100	500	100	100	100	100
	outer epidermis layer	1	0	0	0	0	0	0	na	na	na
	Epidermis (higher)	0	1	1	1	1	0	0	na	na	na
	Epidermis (Lower)	0	1	1	1	0	0	1	na	na	na
	Exodermis	na	na	na	na	na	na	na	1	1	0
	Endodermis	na	na	na	na	na	na	na	1	0	0
	Vascular bundles	1	1	0	1	1	0	1	1	1	1
	Parenchyma	1	1	1	1	0	1	1	1	1	1
4'-*O*-Methylnorbelladin	Detection frequency	100	66	100	100	0	0	100	100	100	33

e (norgalanthamine, or normaritidine)	outer epidermis layer	1	1	1	1	0	0	0	na	na	na
	Epidermis (higher)	1	0	1	1	0	0	1	na	na	na
	Epidermis (Lower)	0	0	0	1	0	0	1	na	na	na
	Exodermis	na	na	na	na	na	na	na	1	1	1
	Endodermis	na	na	na	na	na	na	na	1	1	1
	Vascular bundles	1	1	1	1	0	0	1	1	1	1
	Parenchyma	1	1	1	1	0	0	1	1	1	1
Nornarwedine (Vittatine)	Detection frequency	100	66	100	100	100	50	100	100	100	100
	outer epidermis layer	1	1	1	1	1	0	0	Na	Na	na
	Epidermis (higher)	0	1	1	1	1	0	0	na	na	na
	Epidermis (Lower)	0	1	1	1	0	0	1	na	na	na
	Exodermis	na	na	na	na	na	na	na	1	1	1
	Endodermis	na	na	na	na	na	na	na	1	0	0
	Vascular bundles	1	1	0	1	1	0	1	1	1	0
	Parenchyma	1	1	1	1	0	1	0	1	1	1
Narwedine	Abundance	100	100	100	100	100	50	100	100	100	100
	outer epidermis layer	1	1	1	1	1	0	0	na	na	na
	Epidermis (higher)	0	1	1	1	0	0	0	na	na	na
	Epidermis (Lower)	0	1	1	+	-	0	1	na	na	na
	Exodermis	na	na	na	na	na	na	na	1	1	1
	Endodermis	na	na	na	na	na	na	na	1	0	0
	Vascular bundles	1	1	1	1	1	0	1	1	1	1
	Parenchyma	1	1	1	1	0	1	0	1	1	1
Galanthamine	Detection frequency	100	100	100	100	50	0	100	100	100	66
	outer epidermis layer	1	1	1	1	1	0	0	na	na	na
	Epidermis (higher)	1	1	1	1	1	0	1	na	na	na

	Epidermis (Lower)	1	1	1	1	0	0	1	na	na	na
	Exodermis	na	na	na	na	na	na	na	1	1	1
	Endodermis	na	na	na	na	na	na	na	1	1	1
	Vascular bundles	1	1	1	1	0	0	1	1	1	1
	Parenchyma	1	1	1	1	1	0	1	1	1	1
11β-Hydroxygalanthamine	Detection frequency	100	83	100	50	50	0	100	100	100	33
	outer epidermis layer	1	1	1	0	0	0	0	na	na	na
	Epidermis (higher)	1	1	1	1	1	0	0	na	na	na
	Epidermis (Lower)	1	1	1	1	0	0	1	na	na	na
	Exodermis	na	na	na	na	na	na	na	1	1	1
	Endodermis	na	na	na	na	na	na	na	1	1	1
	Vascular bundles	1	1	1	1	1	0	1	1	1	1
	Parenchyma	1	1	1	1	1	0	0	1	1	1
11-Hydroxyvittatine	Detection frequency	100	66	100	100	50	0	100	100	100	100
	outer epidermis layer	1	1	0	0	0	0	0	na	na	na
	Epidermis (higher)	0	1	1	1	1	0	0	na	na	na
	Epidermis (Lower)	0	1	1	1	1	0	1	na	na	na
	Exodermis	na	na	na	na	na	na	na	0	0	0
	Endodermis	na	na	na	na	na	na	na	0	1	1
	Vascular bundles	1	1	1	0	1	0	1	0	1	1
	Parenchyma	1	1	1	1	1	0	1	1	1	1
Haemanthamine	Detection frequency	100	66	100	100	100	50	100	100	100	33
	outer epidermis layer	1	1	1	0	0	0	0	na	na	na
	Epidermis (higher)	0	1	1	1	1	0	0	na	na	na
	Epidermis (Lower)	0	1	0	1	0	0	1	na	na	na
	Exodermis	na	na	na	na	na	na	na	1	1	1

	Endodermis	na	na	na	na	na	na	na	0	0	0
	Vascular bundles	1	1	0	1	1	0	1	1	0	0
	Parenchyma	1	1	1	0	0	1	0	1	1	1
3-O-Demethyl-3-O-(3-hydroxybutanoyl)-haemanthamine	Detection frequency	83	66	83	100	100	0	100	100	33	0
	outer epidermis layer	0	0	0	0	1	0	0	na	na	na
	Epidermis (higher)	0	0	1	0	1	0	0	na	na	na
	Epidermis (Lower)	0	0	0	0	0	0	0	na	na	na
	Exodermis	na	na	na	na	na	na	na	1	1	0
	Endodermis	na	na	na	na	na	na	na	1	1	0
	Vascular bundles	1	1	0	1	1	0	1	0	1	0
	Parenchyma	1	1	1	0	1	0	0	1	0	0
Papiline	Detection frequency	100	83	100	100	100	25	100	100	100	66
	outer epidermis layer	1	1	1	0	1	0	1	na	na	na
	Epidermis (higher)	0	0	1	1	1	1	1	na	na	na
	Epidermis (Lower)	0	0	0	0	0	1	1	na	na	na
	Exodermis	na	na	na	na	na	na	na	1	1	1
	Endodermis	na	na	na	na	na	na	na	0	1	1
	Vascular bundles	1	1	1	1	0	0	1	1	1	1
	Parenchyma	1	1	1	1	1	0	1	1	1	1
Hippapiline	Detection frequency	100	83	100	100	50	0	100	100	100	66
	outer epidermis layer	1	1	1	0	1	0	0	na	na	na
	Epidermis (higher)	0	0	1	1	1	0	1	na	na	na
	Epidermis (Lower)	0	1	0	0	0	0	1	na	na	na
	Exodermis	na	na	na	na	na	na	na	1	1	0
	Endodermis	na	1	na	na	na	na	na	0	1	1
	Vascular bundles	1	1	1	1	1	0	1	1	1	1

	Parenchyma	1	1	1	1	1	0	1	1	1	1

Legend: na: not applicable; 1 detected, 0 not detected; O: Outter part, Middle: Middle part, AL: apex leaf; BP: Basal plate;

Table 2.A2: Primers used in RT-qPCR analysis

Primer ID	***Primer sequence***	***Number of nucleotide***
qRTHpTYDC1-F	5'-GACATCCTTCAGCTTCAACG-3'	20
qRTHpTYDC1-R	5'-CGACGGCTGAGGGTGATCTG-3'	20
qRTHpTYDC2-F	5'-CAAACTATGCTCTTGTTCCG-3'	20
qRTHpTYDC2-R	5'-ATAAGGGATCAACAGCAGC-3'	21
qRTHpNBS-F	5'-CATTCCAGGCGTAAACTATC-'3	20
qRTHpNBS-R	5'-TGTAGGAGCTGAAACCAAG-'3	19
qRTHpNR-F	5'-CTGGGATCATAGCACTAAAG-'3	20
qRTHpNR-R	5'-CGTCATCTATAACAGACTGC-'3	20
qRTHpOMT-F	5'-GCATATCCAGAATATCCGGG-'3	20
qRTHpOMT-R	5'-GACGTCGACAAATAGTCAG-'3	19
qRTHpCYP96T1-F	5'-AGCTCAAAGCGACCAGAAAG-'3	20
qRTHpCYP96T1-R	5'-GTCCCTCAGGAATTTGTCATCC-'3	22
qRTHpNMT-F	5'-CTTGATGTAGGATGTGGATGG-'3	21
qRTHpNMT-R	5'-CTTCATGTGCTCAAACATCTCG-'3	22
Actin-F	5'-TGGATTTGCTGGAGATGATGCT-'3	22
Actin-R	5'-TGGTGCCAAATCTTCTCCATATCA-'3	24

Table 2.A3 : Compounds identified in *Hippeastrum papilio* by Metaspace annotations

Compound group	*Compound*	*m/z*	*Organ*	*Comment*
Amaryllidaceae Alkaloids	Isatinone A/anhydrolycorine	252.1019	Roots	
	Crinan/ Gamma Lycorane	258.1488	Bulbs	
	Anhydrolycorinone	266.0812	Leaves, bulbs, roots	
	Ungeremine	267.0890	Leaves, bulbs, roots	

	Assoanine	268.1332	Leaves, bulbs, roots
	Apohaemanthamine	270.1125	Leaves, bulbs, roots
	Oxoassoanine	282.1125	Bulbs
	Lycoramine	290.1751	Leaves, bulbs, roots
	9,10-Dimethoxy-1-methyllycorenan	302.1751	Leaves, roots
	N-allylnorgalanthamine	314.1751	Bulbs
	Hippeastrine	316.1179	Leaves, bulbs, roots
	Homolycorine/1-O-Acetylnorpluviine	316.1543	Leaves, bulbs, roots
	Belladine	316.1907	Bulbs,roots
	Crinamidine/Haemanthidine/9-O-Demethyl-2alpha-hydroxyhomolycorine	318.1336	Leaves
	Amaryllisine, Lycorenine,Papyramine	318.1700	Bulbs,roots
	O-methyllycorenine	332.1856	Bulbs
	Albomaculine	346.1649	Leaves,bulbs, roots
N-benzoyl-L-phenylalanine	O-demethyl-Galanthamine beta-D-glucuronide	450.1758	
	Galanthamine beta-D-glucuronide	464.1915	
Phenanthridine alkaloids	Trisphaeridine	224.0706	Roots
	Crinasiadine	240.0655	Roots
Beta-carboline alkaloids	Trichotamine	533.1455	Leaves, roots

Potential other Alkaloids	Reticuline	330.1700	Leaves, bulbs, roots	
	Acutumidine	384.1208	Bulbs	Halogenated alkaloid
Colchicine pathway	Trimethylcolchicinic acid; N-Deacetylcolchiceine	344.1492	Roots	
	Deacetylcolchicine	358.1649	Leaves, bulbs	
	Demecolchine/Androcymbine/Isoandrocymbine	372.1805	Leaves, Bulbs	
	N-Acetoacetyl-deacetylcolchicine	442.186	Roots	
Flavonoids	7,4'-Dihydroxyflavan, (4R)-4,2'-Dihydroxyisoflavan	243.1016	Bulbs	
	4'-Methoxyflavanone	255.1016	Bulbs	
	Luteolin/Kaempferol	287.055	Leaves	
	Quercetin/8-Hydroxykaempferol/6-Hydroxykaempferol/8-Hydroxyluteolin	303.0499	Leaves	
	Quercetin 3-O-glucoside/more	465.1028	Leaves	
	Kaempferol-3-O-rutinoside/ Kaempferol 3-O-rhamnoside-7-O-glucoside	595.1757	Leaves	
Anthranilate	Anthranilate	138.055	Leaves	Triptophane precursor
	Cinnamyl anthranilate	254.1176	Leaves, bulbs	
Amides	N-p-trans-Coumaroyltyramine	284.1281	Leaves,bulbs, roots	
	n-trans-caffeoyltyramine	300.1230	Leaves	
Lignans	Deoxypodophyllotoxin	399.1438	Leaves	A liganan
	1-Acetoxypinoresinol	417.1544	Leaves	A liganan, only in the leaf tips

Pigments	Pheophorbide a	593.2857	Leaves	Chlorophil breakdown compounds
	Echinenone	551.4247	Leaves	Xanthophyll
	Adonixanthin/Dinoxanthin/Didinoxanthin	583.4146	Leaves	beta catorine
	4-Ketomyxol	599.4095	Leaves	Xanthophyll
Other compounds	5-O-Feruloylquinic acid	369.1180	Leaves	in green coffee beans
	Risedronic acid	284.0084	Leaves	Phosphate containing
	Potassium dibasic phosphate	174.8959	Leaves, bulbs, roots	Phosphate containing
	ADP		Leaves	
	Humilixanthin/Dinobuton	327.1187	Leaves	non-proteinogenic alpha-amino acid
	4-Methylumbelliferone/ Herniarin	177.0546	Bulb	
	Adenine	136.0618	Bulb	
	Guanine	152.0567	Bulb	
	5-Methylcytosine	126.0662	Bulb	
	2',3'-Cyclic UMP	307.0326	Bulb, leaves	
	Flumetover	368.1468	Bulb	Fungicide
	6alpha-Hydroxycastasterone	467.3731	Leaves	Plant steroid

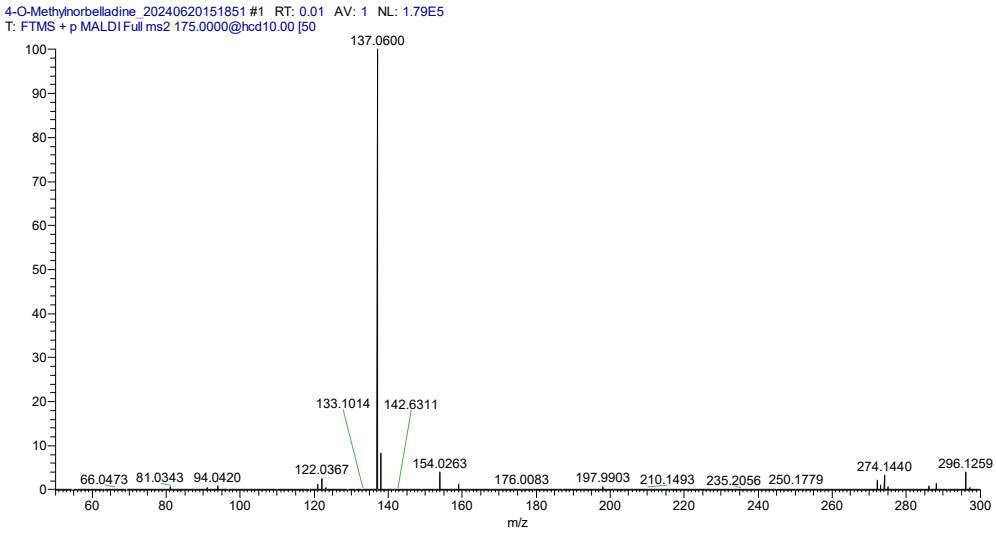

Figure 2.A1a: MS profile of the 4'-O-methylnorbelladine standard.

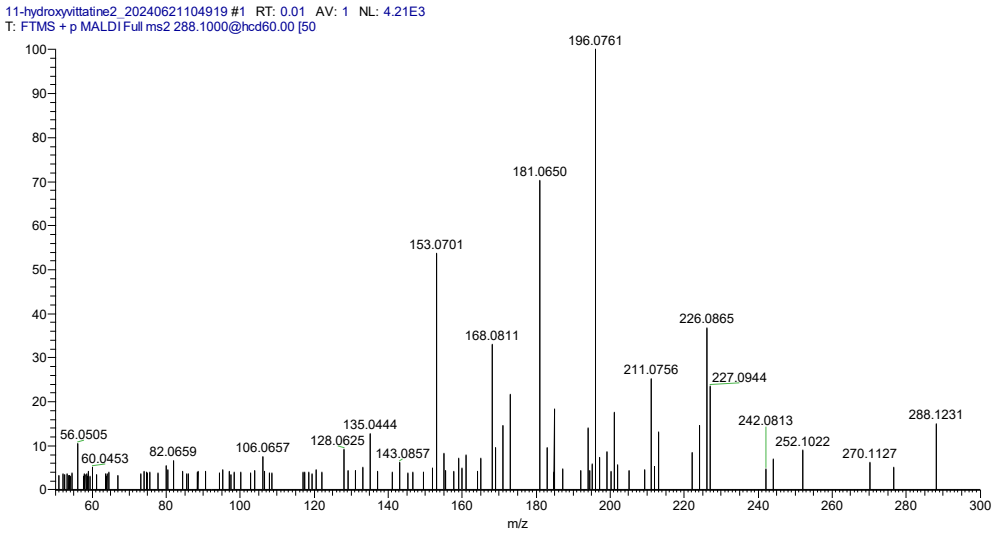

Figure 2.A1b: MS profile of the 11'-hydroxyvittatine standard.

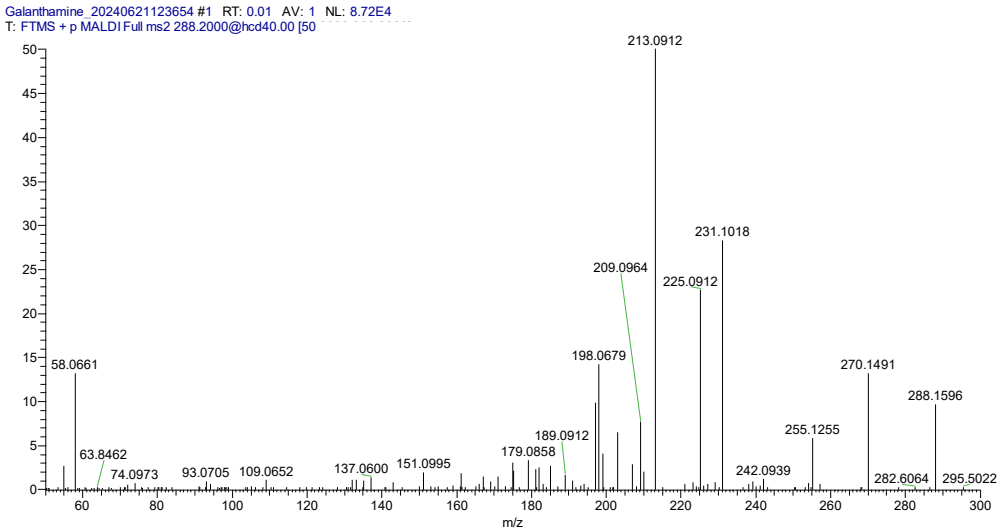

Figure 2.A1c: MS profile of the Galanthamine standard.

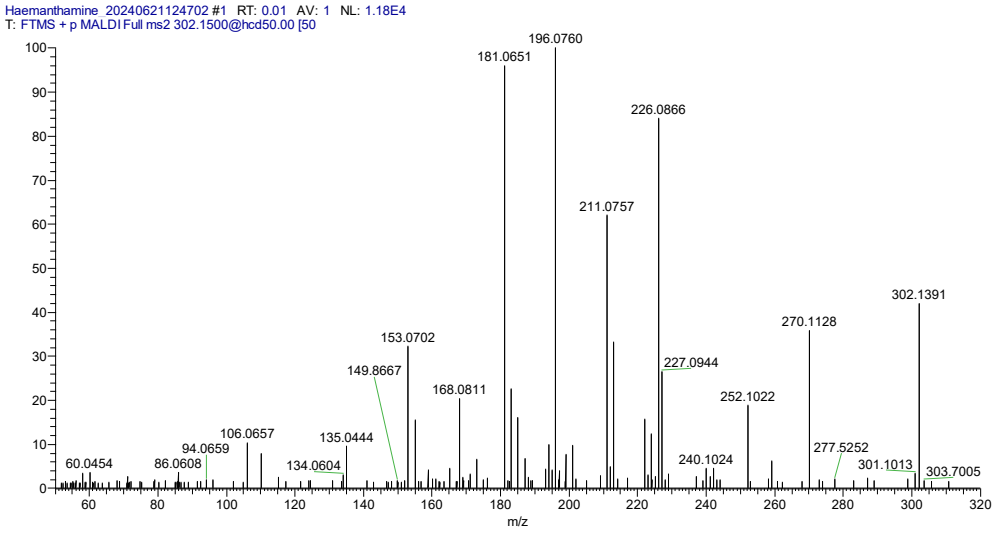

Figure 2.A1d: MS profile of the Heamanthamine standard.

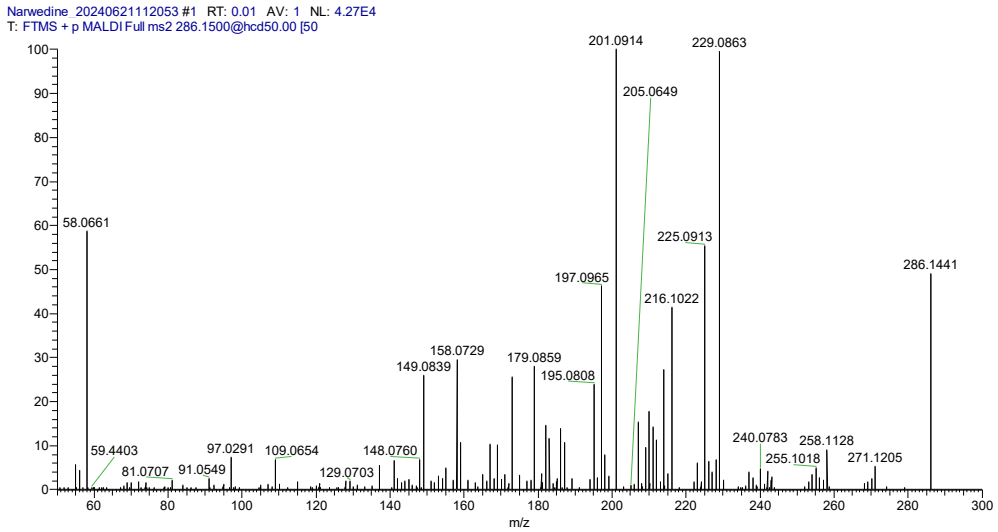

Figure 2.A1e: MS profile of the Narwedine standard.

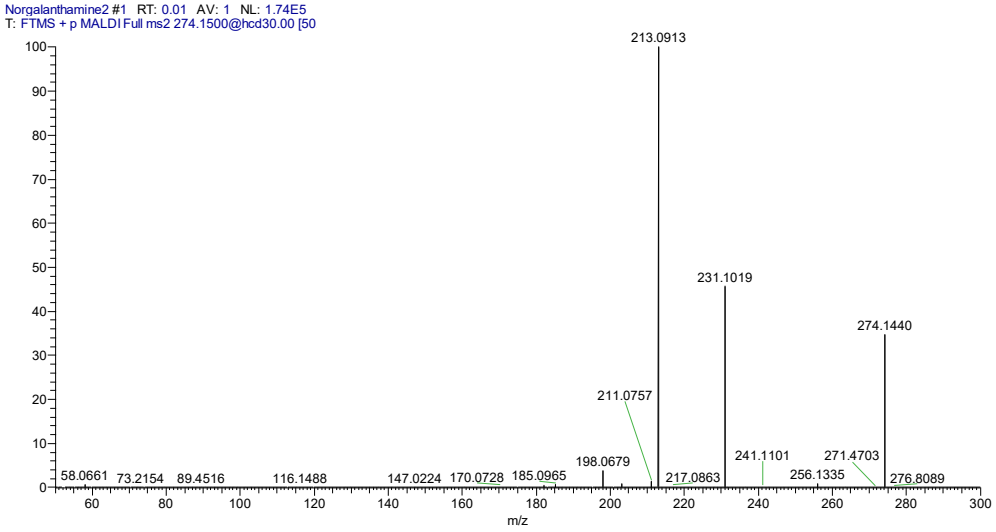

Figure 2.A1f: MS profile of the Norgalanthamine standard.

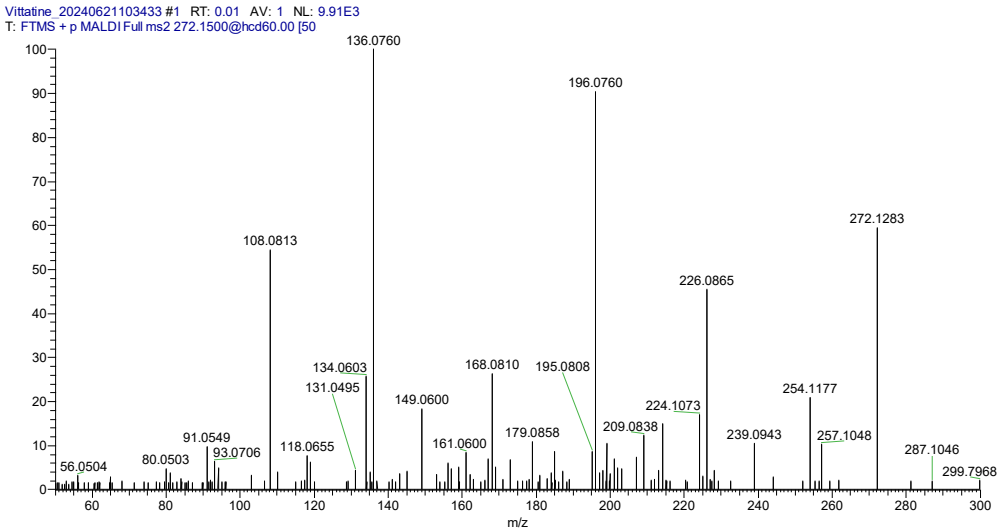

Figure 2.A1g: MS profile of the Vittatine standard.

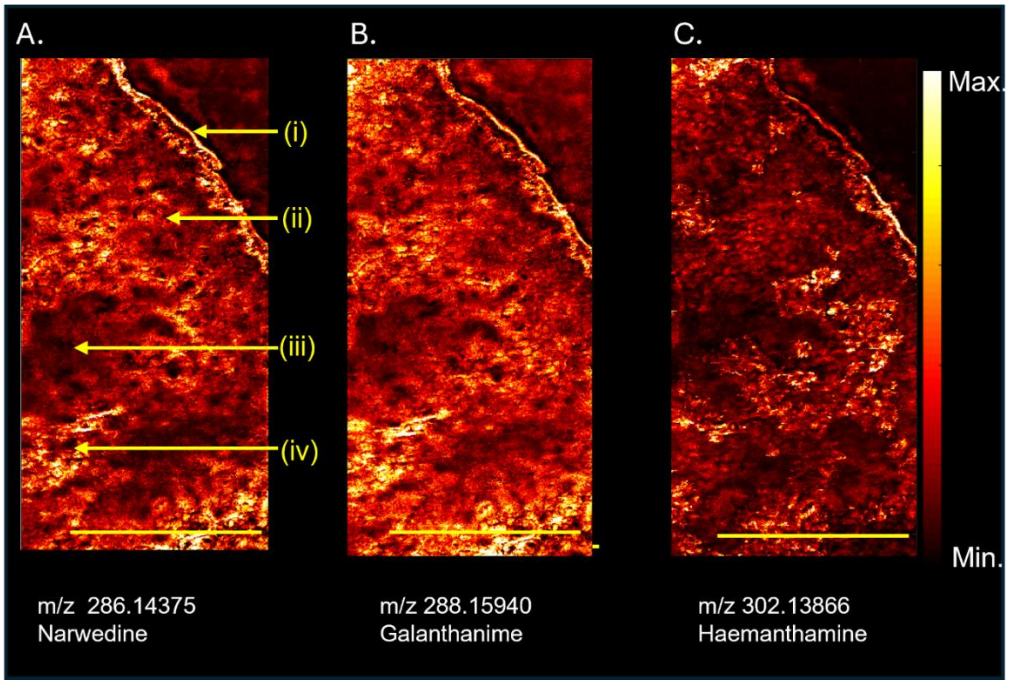

Supplementary figure 2.A2: MALDI-MS images a cross section of *Hippeastrum papilio* leaf tissue. (i) Epidermis, (ii) Parenchyma, (iii) Aerenchyma (iv) Vascular bundles. The pixel size is 5 µm. Scale bars: 1 mm. More details at https://metaspace2020.org/project/Hippeastrum_paplio_MALDI

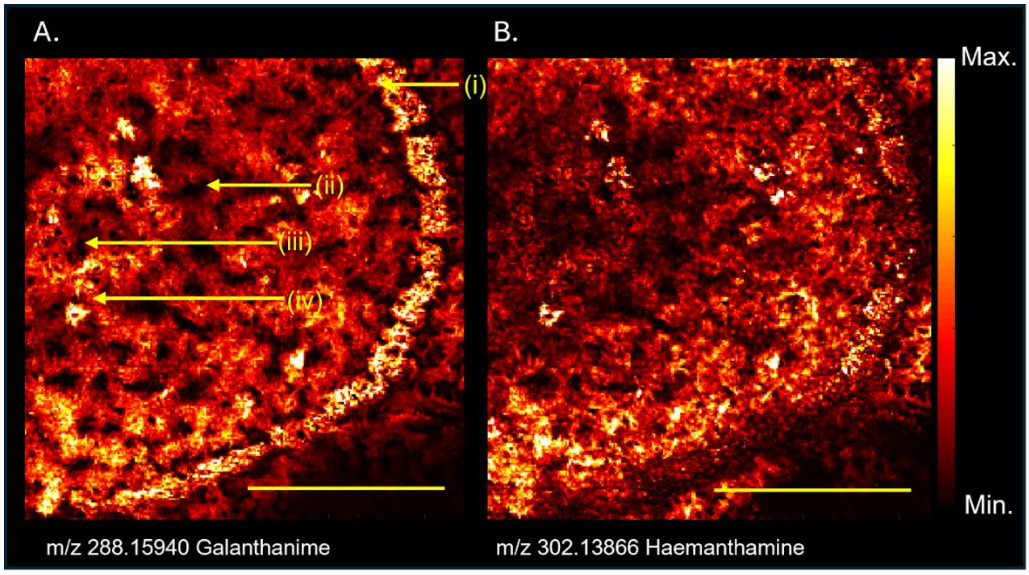

Supplementary figure 2.A3: MALDI-MS images a cross section of *Hippeastrum papilio* root tissue. (i) Exodermis, (ii) Cortex, (iii) Vascular bundles (iv) Endodermis. The pixel size is 10 µm. Scale bars: 1 mm. More details at https://metaspace2020.org/project/Hippeastrum_paplio_MALDI

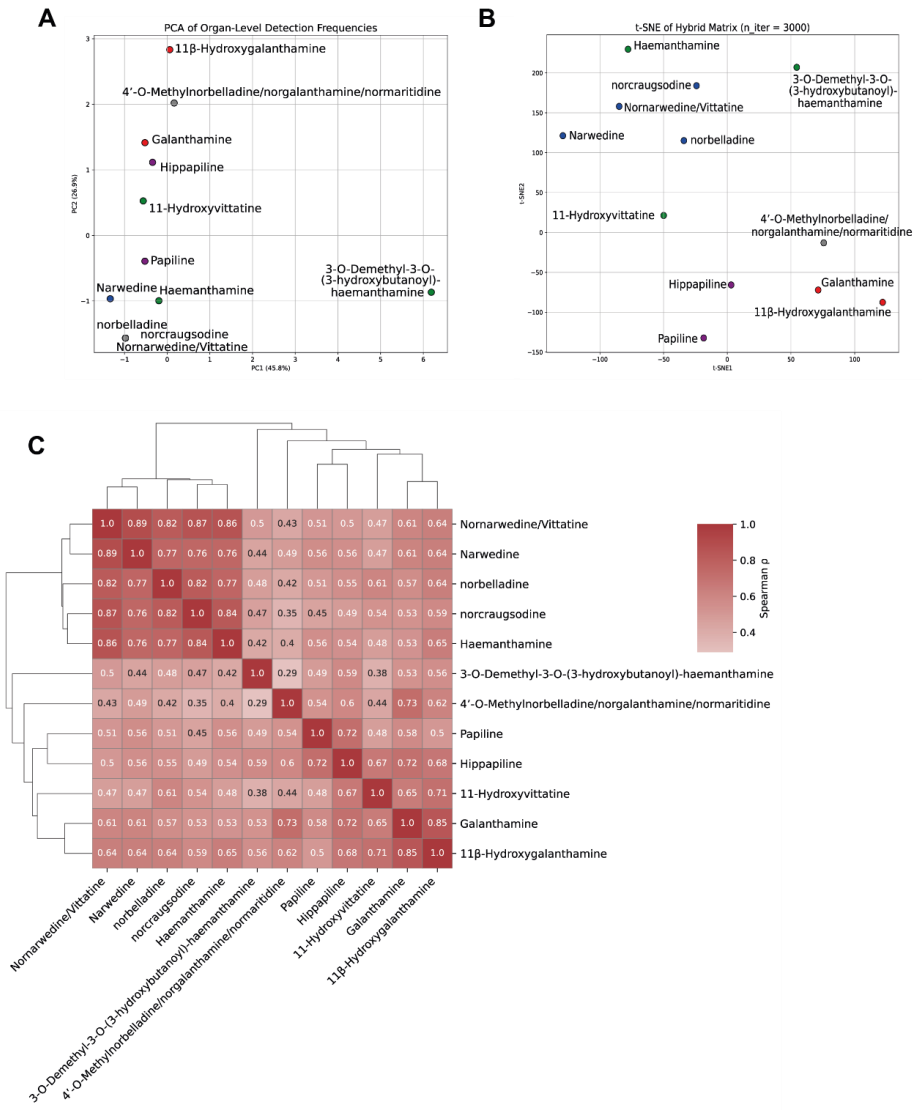

Supplementary Figure 2.A4: Integrated Analysis of Alkaloid Distribution in *Hippeastrum papilio* Tissues. (A) Principal Component Analysis (PCA) of normalized metabolite detection frequencies across major plant organs (leaves, bulbs, and roots). Each point represents a single alkaloid. Colors indicate chemical classification. **(B)** *t*-Distributed Stochastic Neighbor Embedding (*t*-SNE) projection of alkaloids based on the same hybrid matrix used in (A). Each point represents a metabolite. Spatial proximity reflects similarity in tissue-specific distribution patterns and organ-level accumulation. Axes (*t*-SNE 1 and *t*-SNE 2) are unitless and optimized to preserve local relationships in high-dimensional space. Compound names are indicated. **(C)** Clustered Spearman correlation heatmap based on the hybrid matrix. Hierarchical clustering groups metabolites based on their similarity in localization and accumulation profiles. Correlation coefficients (ρ) are shown within the heatmap cells.

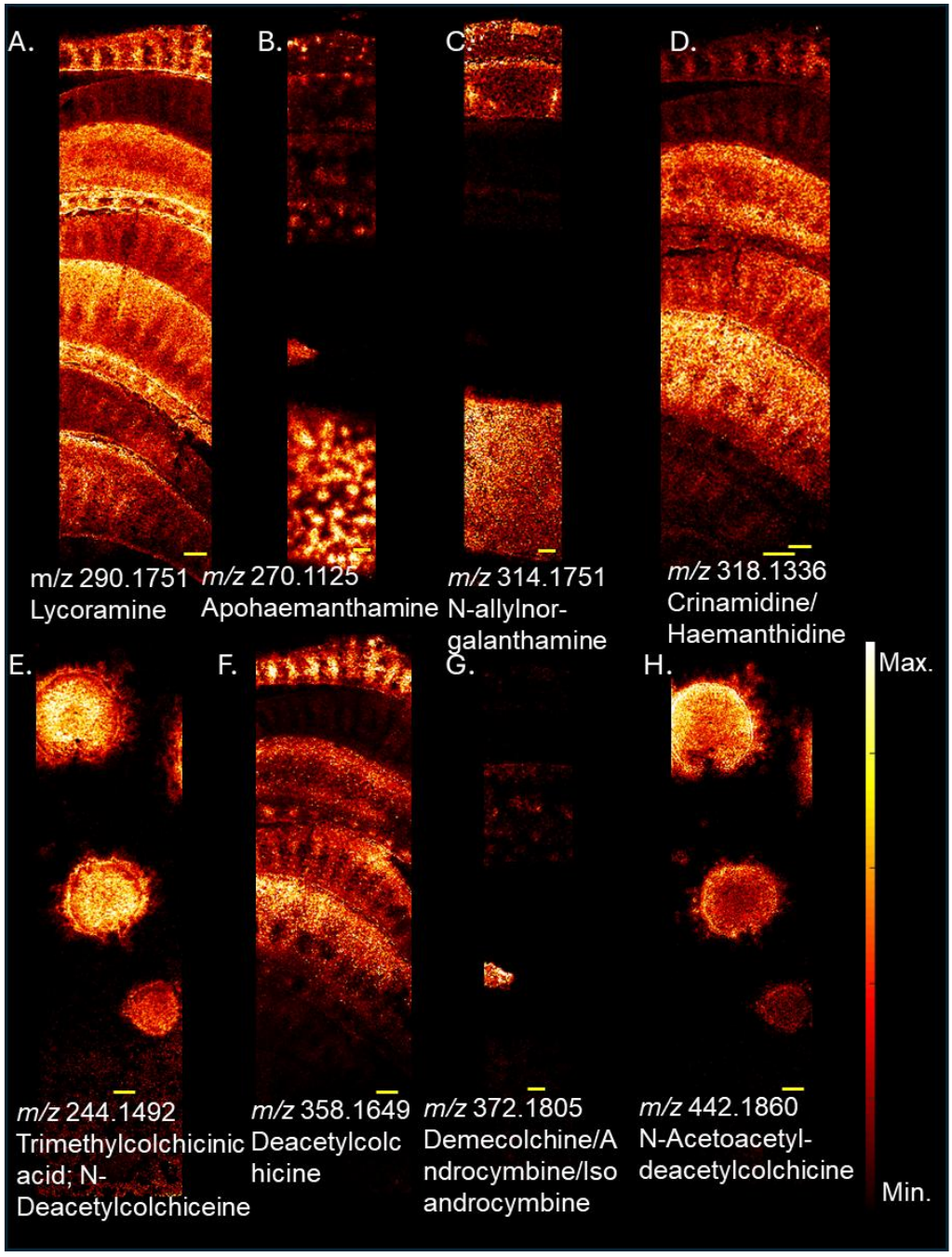

Supplementary figure 2.A5: MALDI-MS images of Metaspace annotated Amaryllidaceae alkaloids and Colchicine bioaynthetic steps in cross sections of *Hippeastrum papilio* tissues. A. D. F: Leaf sections (pixel size 40 µm), B. C. G: Bulb sections (pixel size 30 µm), E. H.: Root sections (pixel size 40 µm). Scale bars: 1 mm.

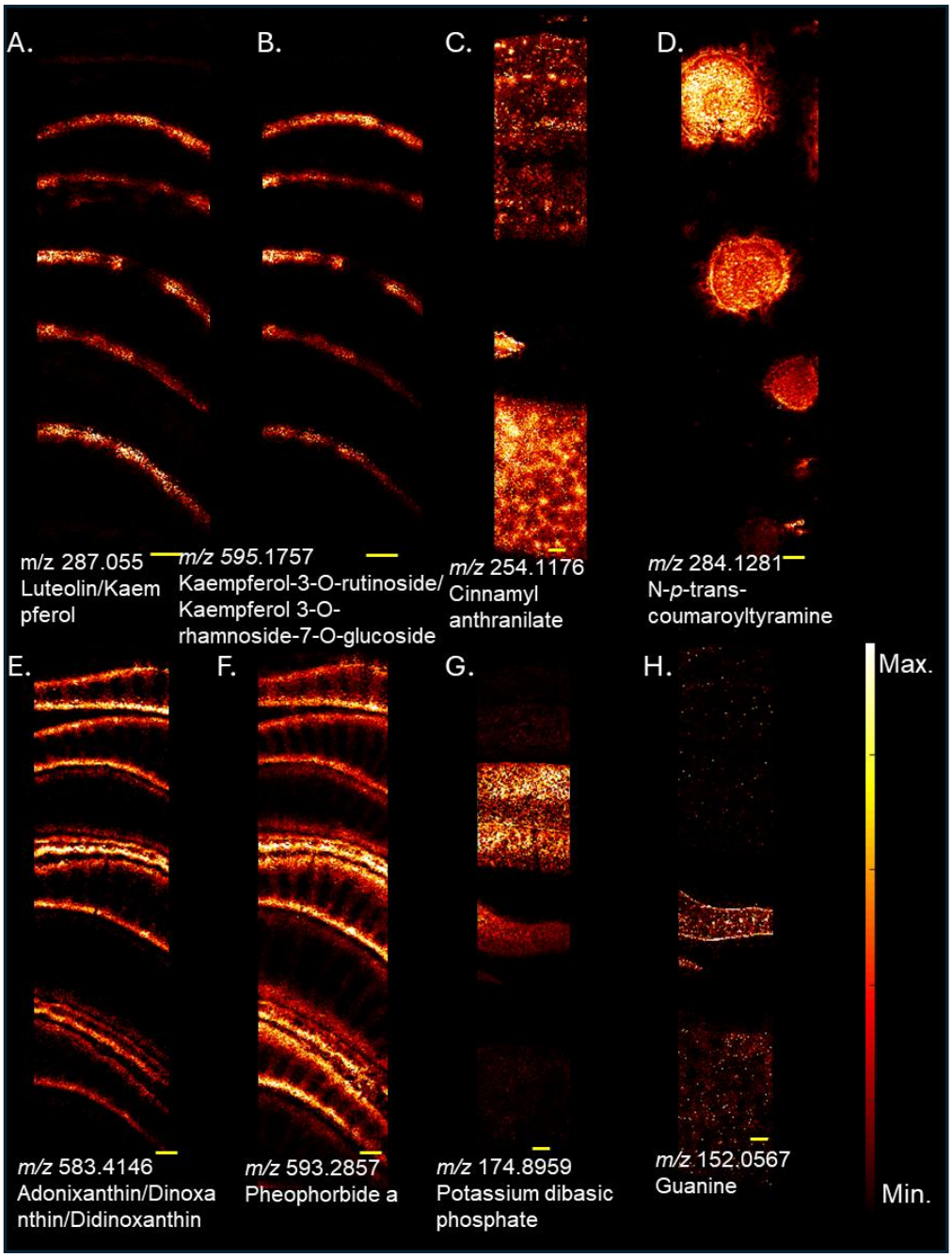

Supplementary figure 2.A6: MALDI-MS images of Metaspace annotated compounds in cross sections of *Hippeastrum papilio* tissues. A. B. E. F: Leaf sections (pixel size 40 µm), C. G. H.: Bulb sections (pixel size 30 µm), D.: Root sections (pixel size 40 µm)

APPENDIX III : Co-authored paper No.1

Biotechnological Approaches to Optimize the Production of Amaryllidaceae Alkaloids

Manoj Koirala [1], Vahid Karimzadegan [1], Nuwan Sameera Liyanage [1], Natacha Mérindol [1] and Isabel Desgagné-Penix [1,2,*]

[1]Department of Chemistry, Biochemistry and Physics, Université du Québec à Trois-Rivières, Trois-Rivières, QC G9A 5H7, Canada

[2]Groupe de Recherche en Biologie Végétale, Université du Québec à Trois-Rivières, Trois-Rivières, QC G9A 5H7, Canada

Biomolecules **2022**, *12*(7), 93; https://doi.org/10.3390/biom12070893

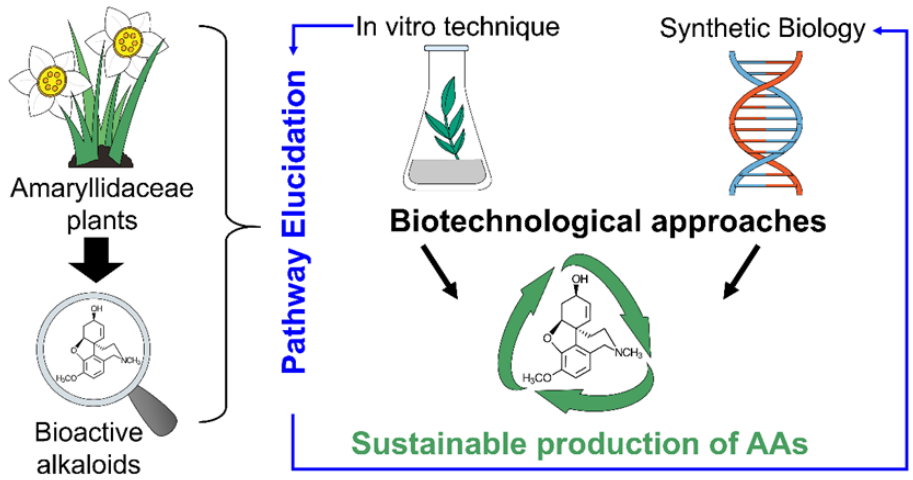

Abstract

Amaryllidaceae alkaloids (AAs) are plant specialized metabolites with therapeutic properties exclusively produced by the Amaryllidaceae plant family. The two most studied representatives of the family are galanthamine, an acetylcholinesterase inhibitor used as a treatment of Alzheimer's disease, and lycorine, displaying potent in vitro and in vivo

cytotoxic and antiviral properties. Unfortunately, the variable level of AAs' production *in planta* restricts most of the pharmaceutical applications. Several biotechnological alternatives, such as in vitro culture or synthetic biology, are being developed to enhance the production and fulfil the increasing demand for these AAs plant-derived drugs. In this review, current biotechnological approaches to produce different types of bioactive AAs are discussed.

Keywords

amaryllidaceae alkaloids; bioactive molecules; biotechnological approach; biosynthesis; in vitro cultures; synthetic biology

For this paper I wrote the section *In Vitro* Techniques to Produce Amaryllidaceae Alkaloids and prepared the graphics.

APPENDIX IV : Co-authored paper No.2

Auxin and light-mediated regulation of growth, morphogenesis, and alkaloid biosynthesis in *Crinum* x *powellii* 'Album' callus

Manoj Koirala [a], Karen Cristine Goncalves dos Santos [a], Sarah-Eve Gélinas [a], Simon Ricard [a], Vahid Karimzadegan [a], Basanta Lamichhane [a], Nuwan Sameera Liyanage [a], Natacha Merindol [a], Isabel Desgagné-Penix [a b]

[a]Department of Chemistry, Biochemistry and Physics, Université du Québec à Trois-Rivières, Trois-Rivières, QC, Canada

[b]Plant Biology Research Group, Trois-Rivières, Québec, Canada

https://doi.org/10.1016/j.phytochem.2023.113883

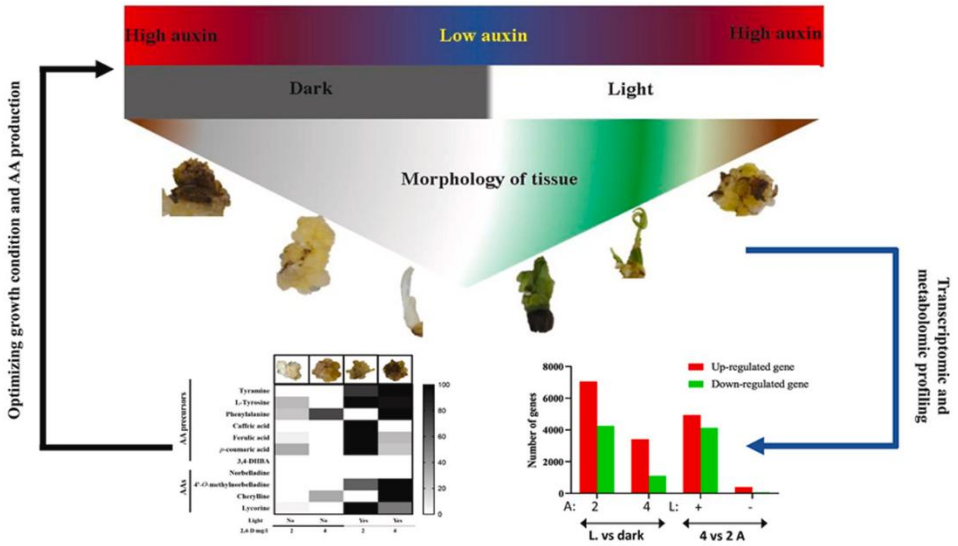

Targeted metabolomic and transcriptomic studies reveal the effect of auxin and light on the growth, morphogenesis, and alkaloid biosynthesis in *C.* x *powellii* "Album". An investigation of the effects of different growth factors on *in vitro* tissues helps to better understand the balance between stress and growth, and eventually, further fine-tune alkaloid production (L: light, A: auxin 2,4-D in mg/L).

Abstract

Crinum x *powellii* 'Album' belongs to the Amaryllidaceae medicinal plant family that produces a range of structurally diverse alkaloids with potential therapeutic properties. The optimal conditions for *in vitro* tissue

growth, morphogenesis, and alkaloid biosynthesis remain unclear. Auxin and light play critical roles in regulating plant growth, development, and alkaloid biosynthesis in several Amaryllidaceae plants. Here, we have succeeded in showing, for the first time, that the combination of auxin and light significantly influence *C.* x *powellii* “Album” *in vitro* tissue growth, survival, and morphogenesis compared to individual treatments. Furthermore, this combination also upregulates the expression of alkaloid biosynthetic genes and led to an increase in the content of certain alkaloids, suggesting a positive impact on the defense and therapeutic potential of the calli. Our findings provide insights into the regulation of genes involved in alkaloid biosynthesis in *C.* x *powellii* “Album” callus and underline the potential of auxin and light as tools for enhancing their production in plants. This study provides a foundation for further exploration of *C*. x *powellii* “Album” calli as a sustainable source of bioactive alkaloids for pharmaceutical and agricultural applications. Furthermore, this study paves the way to the discovery of the biosynthetic pathway of specialized metabolites from *C.* x *powellii* “Album”, such as cherylline and lycorine.

Keywords

Amaryllidaceae alkaloids, Stress, Transcriptomic study, AAs biosynthesis pathway, specialized metabolism, multi-omics

For this paper, I worked with the *in vitro* culture development.

APPENDIX V: Co-authored paper No.3

Unveiling Amaryllidaceae alkaloids: from biosynthesis to antiviral potential – a review

Thilina U. Jayawardena‡ [a], Natacha Merindol‡ [a], Nuwan Sameera Liyanage [a] and Isabel Desgagné-Penix *[ab]

[a]Department of Chemistry, Biochemistry, and Physics, Université du Québec à Trois-Rivières, Trois-Rivières, QC G8Z 4M3, Canada. E-mail: Isabel.Desgagne-Penix@uqtr.ca

[b]Plant Biology Research Group, Université du Québec à Trois-Rivières, Trois-Rivières, QC, Canada

DOI: 10.1039/D3NP00044C (Review Article) *Nat. Prod. Rep.*, 2024, **41**, 721-747

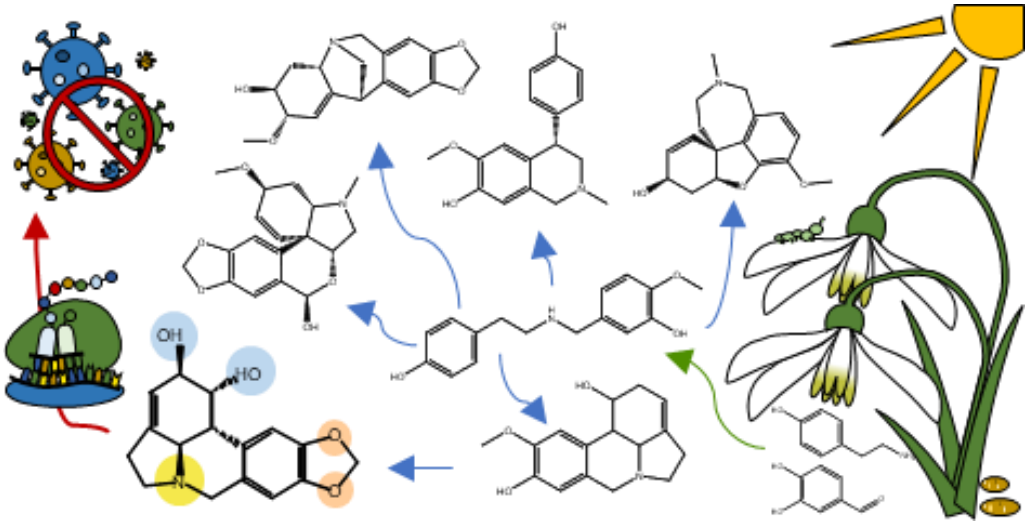

Abstract

Amaryllidaceae alkaloids (AAs) are a unique class of specialized metabolites containing heterocyclic nitrogen bridging that play a distinct role in higher plants. Irrespective of their diverse structures, most AAs are biosynthesized *via* intramolecular oxidative coupling. The complex

organization of biosynthetic pathways is constantly enlightened by new insights owing to the advancement of natural product chemistry, synthetic organic chemistry, biochemistry, systems and synthetic biology tools and applications. These promote novel compound identification, trace-level metabolite quantification, synthesis, and characterization of enzymes engaged in AA catalysis, enabling the recognition of biosynthetic pathways. A complete understanding of the pathway benefits biotechnological applications in the long run. This review emphasizes the structural diversity of the AA specialized metabolites involved in biogenesis although the process is not entirely defined yet. Moreover, this work underscores the pivotal role of synthetic and enantioselective studies in justifying biosynthetic conclusions. Their prospective candidacy as lead constituents for antiviral drug discovery has also been established. However, a complete understanding of the pathway requires further interdisciplinary efforts in which antiviral studies address the structure–activity relationship. This review presents current knowledge on the topic.

For this paper, I was involved in the writing of biosynthetic pathways, and the preparation of graphics and graphical abstracts.

APPENDIX VI: Co-authored paper No.4

Kinetic and *in silico* structural characterization of norbelladine *O*-methyltransferase of Amaryllidaceae alkaloids biosynthesis

Manoj Koirala[1] , Natacha Merindol[1] , Vahid Karimzadegan[1] , Sarah-Eve Gélinas[1] , Nuwan Sameera Liyanage[1] ·, Basanta Lamichhane[1] , Maria Camila García Tobón[1] , Patrick Lagüe[2] , Isabel Desgagné-Penix[1,3] DOI: 10.1016/j.jbc.2024.107649

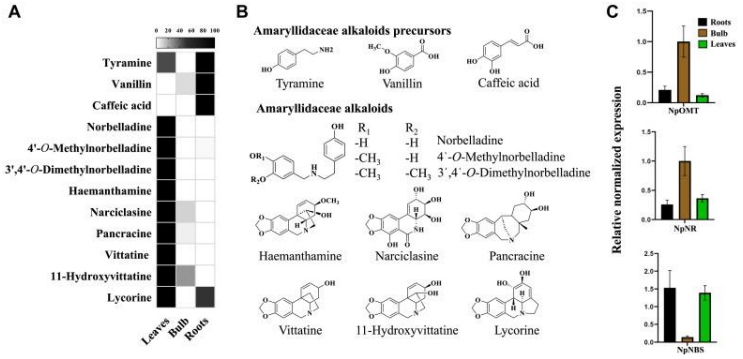

Abstract

Amaryllidaceae alkaloids are a diverse group of alkaloids exclusively reported from the Amaryllidaceae plant family. *In planta*, their biosynthesis is still not fully characterized; however, a labeling study established 4ˈ-*O*-methylnorbelladine as the key intermediate compound of the pathway. Previous reports have characterized *O*-methyltransferases from several Amaryllidaceae species. Nevertheless, the formation of the different *O*-methylnorbelladine derivatives (3ˈ-*O*-methylnorbelladine, 4ˈ-*O*-methylnorbelladine, and 3ˈ4ˈ-*O*-

dimethylnorbelladine), the role, and the preferred substrates of *O*-methyltransferases are not clearly understood. In this study, we performed the biochemical characterization of an *O*-methyltransferase candidate from *Narcissus papyraceus* (*Np*OMT) *in vitro* and *in vivo,* following biotransformation of norbelladine in *Nicotiana benthamiana* having transient expression of *NpOMT*. Docking analysis was further used to investigate substrate preferences, as well as key interacting residues of *Np*OMT. Our study shows that *Np*OMT methylates norbelladine preferentially at the 4′-OH position *in vitro* and *in planta.* Interestingly, *Np*OMT also catalyzed the synthesis of 3′,4′-*O*-dimethylnorbelladine from norbelladine and 4′-*O*-methylnorbelladine during *in vitro* enzymatic assay. Furthermore, we show that *Np*OMT methylates 3,4-dihydroxybenzylaldehyde and caffeic acid in a nonregiospecific manner to produce meta/para monomethylated products. This study reveals a novel catalytic potential of an Amaryllidaceae *O*-methyltransferase and its ability to regioselectively methylate norbelladine in the heterologous host *N. benthamiana*.

Keywords

Amaryllidaceae alkaloids, biosynthesis, O-methyltransferase, regio-selectivity, catalytic potential, molecular docking

For this paper, I supplied the plant material, and alkaloid extraction and qRT-PCR.

APPENDIX VII: Co-authored paper No.5

Marine specialized metabolites: Unveiling Nature's chemical treasures from the deep blue

Thilina U. Jayawardena [a], Natacha Merindol [a], Nuwan Sameera Liyanage [a], Fatima Awwad [a], Isabel Desgagné-Penix [a b]

https://doi.org/10.1016/j.trac.2024.118097

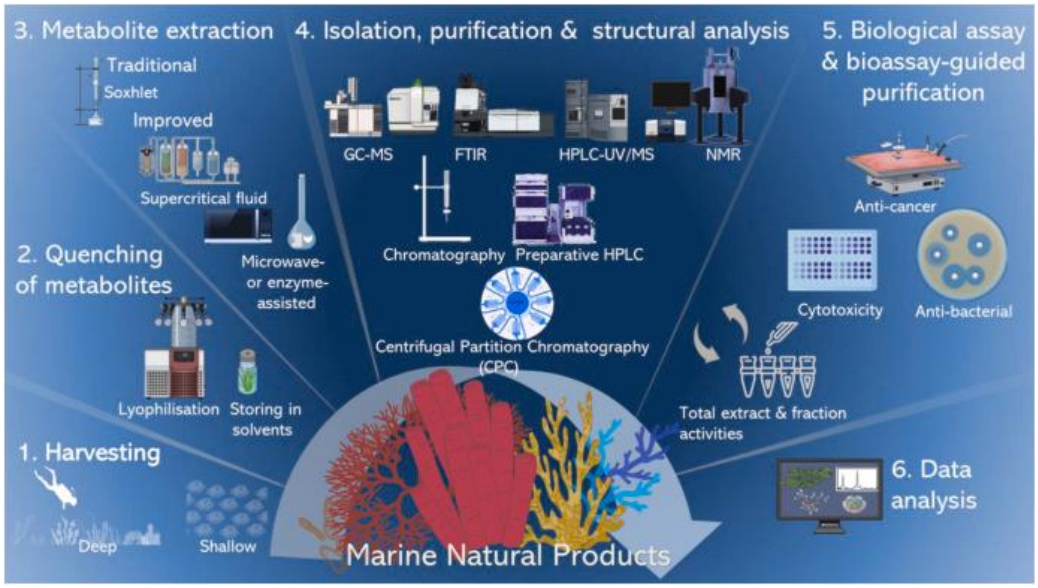

Abstract

Marine specialized metabolites (MSM) represent a fascinating realm of chemical diversity with multifaceted functions across the spectrum of life on Earth. These metabolites serve as weapons, metal transporters, regulatory agents, and more. The conservation of genes responsible for their production over extensive evolutionary timescales underscores

their selective advantage. Recent decades have witnessed an upsurge in MSM studies, driven by advancements in analytical techniques and the ever-growing accessibility of the aquatic environment. Marine macro and microorganisms offer a rich tapestry of specialized metabolites, some exhibiting potent activities in diverse domains, including medicine. The study of MSM presents several challenges, reflecting the need to separate complex mixtures into individual bioactive metabolites and utilize state-of-the-art extraction methods. Comprehensive structural analysis relies on advanced spectroscopic approaches, including nuclear magnetic resonance and mass spectrometry. These tools are instrumental in unravelling the chemical diversity of MSM and understanding their potential applications. While bioprospecting offers enormous potential, it raises critical challenges concerning sustainability, conservation, and equitable benefit-sharing. International protocols like the Nagoya Protocol seeks to regulate access to and share benefits from genetic resources, with considerable implications for marine bioprospecting. The convergence of advanced metabolomics, metagenomics, and synthetic biology offers promising avenues for accelerating the discovery and sustainable production of MSM, shaping the future of this field. This comprehensive review provides a deep dive into the challenges, methodologies, and emerging trends in studying marine-derived natural products, underscoring the immense potential of MSM for advancing chemical sciences and their transformative

applications in diverse areas such as food, medicine, biotechnology, and environmental conservation. By bridging multiple disciplines, the continued exploration and sustainable utilization of these metabolites hold the promise of unlocking new innovations for society's benefit.

Keywords

Natural products, Conservation, Bioprospecting, metabolomics, Biotechnology, Biosynthesis, Isolation and spectroscopic characterization

For this paper, I involved in the writing and preparation of the figures.

APPENDIX VIII: Co-authored paper No.6

Antiviral alkaloids from *Crinum jagus*: Extraction, synergistic effects, and activity against dengue virus and human coronavirus OC43

Thilina U. Jayawardena[a,b,1], Natacha Merindol[a,b,1], Nuwan Sameera Liyanage[a,b], Sarah-Eve Gélinas[a,b], Berthoux Lionel[c] · Ka Seydou[a,d], Matar Seck[d], Anto nio Evidente[e], Isabel Desgagné-Penix[a,b]

DOI: 10.1016/j.heliyon.2025.e42580

Abstract

Crinum jagus, a medicinal plant from the Amaryllidaceae family, possesses potent antiviral properties attributed to alkaloids such as cherylline and lycorine. This study evaluated various extraction methods--including continuous shaking, hot solvent, microwave-assisted, ultrasound-assisted, and liquid-liquid extraction using methanol, followed by ethyl acetate and subsequent acid-base to optimize the yield of bioactive compounds. The extraction method significantly influenced phenolic acid and alkaloid precursor content, with liquid-liquid extraction yielding the highest amounts. LC-MS/MS analyses confirmed the presence of major alkaloids in the extracts, notably cherylline and lycorine. The cytotoxic and antiviral properties of *C. jagus* extracts were

assessed using a reporter-encoding dengue virus (DENV) vector and the β-coronavirus HCoV-OC43. LLE_E (liquid-liquid extract), enriched in phenolic compounds, was the most cytotoxic extract at concentrations above 0.6 µg/mL. Acid-base fractions, enriched in alkaloids, exhibited higher cytotoxicity than the methanol extracts counterparts, with significant cell death at concentrations above 2.5 µg/mL Additionally, the acid-base and LLE_E extracts were also the most efficient in inhibiting the replication of both HCoV-OC43 and DENV, with EC_{50} values ranging from 1 to 2.5 µg/mL. The synergistic antiviral effect of cherylline with other *C. jagus* alkaloids was also evaluated, revealing that a combination of cherylline with gigantellinine strikingly reduced the flavivirus replication. These findings underscore the potential of *C. jagus* as a source of bioactive compounds with antiviral properties and highlight the importance of optimizing extraction methods to enhance specific applications.

Keywords

Antiviral agents, Amaryllidaceae alkaloids, Extraction methods, LC-MS/MS, Flavivirus, Cherylline, β-coronavirus, Synergism, Cytotoxicity.

For this paper, I worked in the alkaloid extractions.

APPENDIX IX: Cover graphics